1-1-2000

Polycarbodiimides at interfaces : polymer adsorption at solution-silica interfaces and thermal decomposition of an adsorbed thin polymer film.

Richard Jay Larson
University of Massachusetts Amherst

POLYCARBODIIMIDES AT INTERFACES: POLYMER ADSORPTION AT SOLUTION-SILICA INTERFACES AND THERMAL DECOMPOSITION OF AN ADSORBED THIN POLYMER FILM

A Dissertation Presented

by

RICHARD JAY LARSON JR.

Submitted to the Graduate School of the
University of Massachusetts Amherst in partial fulfillment
of the requirements for the degree of

DOCTOR OF PHILOSOPHY

May 2000

Polymer Science and Engineering

POLYCARBODIIMIDES AT INTERFACES: POLYMER ADSORPTION AT SOLUTION-SILICA INTERFACES AND THERMAL DECOMPOSITION OF AN ADSORBED THIN POLYMER FILM

A Dissertation Presented

by

RICHARD JAY LARSON JR.

Approved as to style and content by:

Thomas J. McCarthy, Co-Chair

Bruce M. Novak, Co-Chair

C. Peter Lillya, Member

Richard J. Farris, Department Head
Polymer Science and Engineering

To Sharon, Jessica,

and our families

ACKNOWLEDGEMENTS

I would like to thank professor Bruce Novak and professor Tom McCarthy for providing me with an invaluable educational experience. They are exceptional educators as well as mentors, and I have been most fortunate to have had the opportunity to learn and grow under their guidance. In addition, I thank professor Peter Lillya for participating as a member of my committee.

I am so grateful to Markem Corporation for providing me the opportunity to pursue a graduate level education. Furthermore, I cannot thank the Putnam family enough for having the confidence in my capabilities and for their company's support of my graduate studies. I was blessed with a very unique opportunity and this brief description of thanks does not do justice for the way I feel about what has occurred.

I would like to thank the faculty of the Polymer Science and Engineering Department for the initial education and preparation for performing research in the field of polymer science. Thank you also, to Jack for providing education, training, consultation, and maintenance on x-ray photoelectron spectroscopy.

I would like to thank the past and current Novak and McCarthy group members for their friendship and support throughout my graduate studies. A special thanks to Jeff and Jen, my lab partners, for all their help, support, and friendship. I also owe a special thanks to Alex for his time spent discussing my research and furthering my education on surface chemistry.

The opportunity for me to pursue graduate studies would not have been possible without strong family support. I thank my parents for their love and support and instilling in me at a young age the importance of an education. I thank Sharon's parents for their love and support. A special thanks to my mother and Sharon's mother for the numerous times their lives were disrupted in order to stay with my daughter so that I could spend every possible moment at PS&E.

My most important acknowledgements are to my wife Sharon and my daughter Jessica for enduring the vicissitudes of a husband/father in graduate school. To Jessica, thanks for always reminding me of what is truly important. To Sharon, thank you so much for your love, understanding, and emotional support throughout my stay in graduate school as well as our eleven years of marriage.

ABSTRACT

POLYCARBODIIMIDES AT INTERFACES: POLYMER ADSORPTION AT SOLUTION-SILICA INTERFACES AND THERMAL DECOMPOSITION OF AN ADSORBED THIN POLYMER FILM

MAY 2000

RICHARD JAY LARSON JR., B.Sc., KEENE STATE COLLEGE

M.S, UNIVERSTIY OF MASSACHUSETTS AMHERST

Ph.D., UNIVERSITY OF MASSACHUSETTS AMHERST

Directed by: Professor Thomas J. McCarthy and Professor Bruce M. Novak

Trends in the adsorption of poly(*N*-methyl-*N'*-((±)-α-phenylethyl)carbodiimide), poly-**R/S**, and poly(*N*-methyl-N'-((-)-α-phenylethyl)carbodiimide), poly-**S**, to native silicon oxide were shown to be influenced by the polymer's conformation in solution (worm-like and rigid, respectively), solvent quality, molecular weight, and process conditions. High affinity adsorption isotherms were measured for poly-**R/S** adsorbed from toluene to silica and the adsorbed amount increased with molecular weight. The adsorbed amount of poly-**R/S** and poly-**S** from THF was influenced by both solvent quality and the conformation of the polymer in solution. For both polymers, adsorbed from THF, the XPS and contact angle data indicated that the adsorbed amount decreased with molecular weight and the adsorbed amount, for equal molecular weights, of poly-**S** was greater than poly-**R/S**. Using AFM, the adsorbed films of both polymers were shown to dewet during the evaporation of solvent. The extent of dewetting is shown as a function of solvent quality, temperature, and experimental processes. The size and dimensions of the surface structures after dewetting were shown to increase with molecular weight.

Using organosilane chemistry, lyophobic silicon-supported monolayers of tris(trimethylsiloxy)chlorosilane (tris(TMS)), 10–(carbomethoxy)decyldimethyl-chlorosilane (CMDCS), diphenyldichlorosilane (DPDCS), and mixed binary monolayers

of tris(TMS) with CMDCS were prepared; followed by adsorption of poly-**R/S** and poly-**S** to the monolayers. Relative to silica, both polymers have little affinity to adsorb to surfaces composed mostly of methyl (tris(TMS)) or methylene (CMDCS) groups. Furthermore, the adsorbed amount increased with molecular weight but decreased with chain rigidity. In addition, the adsorbed films dewetted upon solvent evaporation. Vapor phase modification of silica with DPDCS was shown by AFM to form patchy surface structures. Both polymers were shown to have a higher affinity for the DPDCS modified surfaces compared to adsorptions performed on tris(TMS) and CMDCS surfaces. Adsorption experiments with poly-**R/S** and poly-**S** to surfaces composed of hydrolyzed CMDCS (H–CMDCS) indicated an increase in the adsorbed amount with increasing amount of H-CMDCS.

Adsorbed films of poly-**R/S** on native silicon oxide were prepared for studying the effect of thermal decomposition on the adsorbed polymer film. Using real-time FT–IR and TGA, the decomposition rates were measured, but experimental conditions are shown to influence the data. Topography analysis, by tapping mode AFM, of the decomposed adsorbed films indicated changes in the surface structure with thermal exposure. In addition, with thermal exposure the adsorbed film became weakly attached to the substrate. Nonetheless, thermal decomposition can be used to modify an adsorbed film of poly-**R/S**.

TABLE OF CONTENTS

LIST OF TABLES

LIST OF FIGURES

Figures

LIST OF SCHEMES

CHAPTER 1

THE ADSORPTION OF POLY(*N*-METHYL-*N*′-(α-PHENYLETHYL)CARBODIIMIDE) AT SOLUTION-SILICA INTERFACES

Introduction

The science of polymer adsorption at the solution-solid interface is of fundamental importance for developing technologies such as adhesives, lubricants, colloid stabilizers, biological membranes, and medicines.[1] We (McCarthy's research group) have been interested in controlling polymer adsorption by utilizing various techniques, such as surface modification,[2-5] specific polymer functionalization ("sticky-feet"),[6,7] controlled functionality of block copolymers,[8] and more recently, layer-by-layer deposition techniques.[9,10] All of these techniques modify the surface microstructure resulting in macroscopic property changes such as adhesion, friction, and wettability.

The work described here explores the macroscopic changes that occur when a polymer with a well-defined architecture is adsorbed to silica. Since there has been limited research on the adsorption of polymers with extended conformations,[1] we focused on assessing the tendency for the wormlike poly(*N*-methyl-*N*′-((±)-α-phenylethyl)carbodiimide), poly-**R/S**, and rodlike poly(*N*-methyl-N′-((-)-α-phenylethyl)carbodiimide), poly-**S**, to adsorb onto solid surfaces. In addition, we researched controlling the structure of adsorbed thin films of polycarbodiimide through surface modification of the silica substrate. We analyzed factors such as molecular weight and solvent quality while monitoring the effects by contact angle, x-ray photoelectron spectroscopy (XPS), and atomic force microscopy (AFM).

Homopolymer Adsorption

The adsorption of polymers is important to many technologies that are fundamentally based on interfacial interactions. There are texts which review adsorption physics of both small molecules[11] and polymers.[1] Adsorption is a thermodynamic process that requires the overall change in free energy to be negative. Consider a surface submerged in a polymer solution; the adsorbed layer is described as the increase in solute concentration (surface excess Γ) within the interfacial region. As polymer approaches the surface, three interactions become important: solvent-surface (χ_{1s}), segment-surface (χ_{2s}), and solvent-segment interactions (Flory-Huggins parameter χ_{FH}). Thus, polymer adsorption depends on the net adsorption energy experienced by the polymer segments. This net energy is described as the exchange free energy (χ_s) which is the difference between χ_{2s} and χ_{1s}. In terms of energy potentials, the adsorption energy

$$\chi_s = \left(u_1^a - u_2^a\right)/kT \tag{1.1}$$

of solvent molecule (u_1^a) must be less negative than that of the polymer segment (u_2^a), resulting in a positive χ_s for polymer adsorption to occur as defined by Equation 1.1. If χ_s is negative, depletion occurs. Since adsorption is a thermodynamic process, there is a critical exchange energy (χ_{sc}) which is the minimal amount of energy required for adsorption.

For a given polymer, each segment has an equal segmental adsorption energy which is independent of chain length. Thus, as the polymer chain length increases, there are a greater number of potential adsorbers.[12] For adsorption to occur, the polymer must undergo conformational changes as it approaches an impenetrable surface.[13] This loss in conformational entropy upon adsorption is another important factor controlling adsorption. Therefore, the unfavorable loss in translational entropy must be overcome by the energy change associated with numerous segmental attachments on the surface.

The adsorption rate is primarily determined by the mass transport through solution and attachment to the interface.[14] As the surface becomes saturated with a polymer layer, reorganization begins to take place. The shorter polymer chains (lower molecular weight) adsorb first and as longer chains enter the adsorbed layer, competition between chains results with the shorter chains being displaced by the longer ones. It is the small increase in translational entropy that drives the replacement of short adsorbed chains by longer ones.[15,16] The rate of segmental exchange is dependent on the interactions of the polymer, the surface, and the solvent. Recently, Santore et al.[17] measured the rate-limiting step of the exchange process between long and short chains of polyethyleneoxide (PEO) as being the increase in concentration of long chains in the adsorbed layer, and not the release of short chains from the surface. They concluded that for PEO, competitive adsorption between chains of different lengths is a transport-limited process. Dijt et al.[12] commented that the displacement rate may also depend on the rate of conformational changes in the adsorbed layer, and thus, on the dynamic stiffness of the polymer chain.

As the segmental density increases on the surface, crowding effects lead to repulsion and limit further adsorption.[18] This osmotic force (Π) may limit further segmental attachment, but the surface is not static. Segmental exchanges continue to occur between polymer chains in the adsorbed layer, thereby making the surface dynamic. Moreover, the energetics of segmental crowding must be overcome by the more favorable χ_{2s} interactions. Consequently, the osmotic force generated at the interface is influenced by differences between χ_{2s}, χ_{1s}, and χ_{FH}.

In general, the adsorption process is driven by favorable segment-surface interactions, but the loss in conformational entropy and increase in osmotic forces at the interface limit, (or prohibit) the process. Three main processes control the kinetics of adsorption: (1) mass transport from the bulk to the surface (by diffusion or convection),

(2) segmental attachment, and (3) equilibration to the thermodynamically favorable configuration of the chains.[19] Each of these processes could possibly be rate determining.

The final equilibrium structure of the adsorbed layer is influenced by the kinetics[12-14,20] and thermodynamics described above. Polymers are generally very surface-active due to the many potential segment attachment points, thus, the adsorbed layer is a function of the structure and composition of the monomer.[18] At very low surface coverage, a homopolymer molecule adsorbs with a flat conformation (lowers the energy the most), and as the concentration in the adsorbed layer increases, the competition becomes higher between segments and surface sites. This results in chains protruding into solution, forming loops and tails (Fig. 1.1), and segments anchored to the surface called trains.[21]

The Adsorption Isotherm

Adsorption isotherms are graphical representations of the changes in the excess amount of polymer at the interface (Γ^{ex}) with increasing polymer solution concentration.[1] A typical isotherm is shown in Figure 1.2 and its shape is classified as a high-affinity

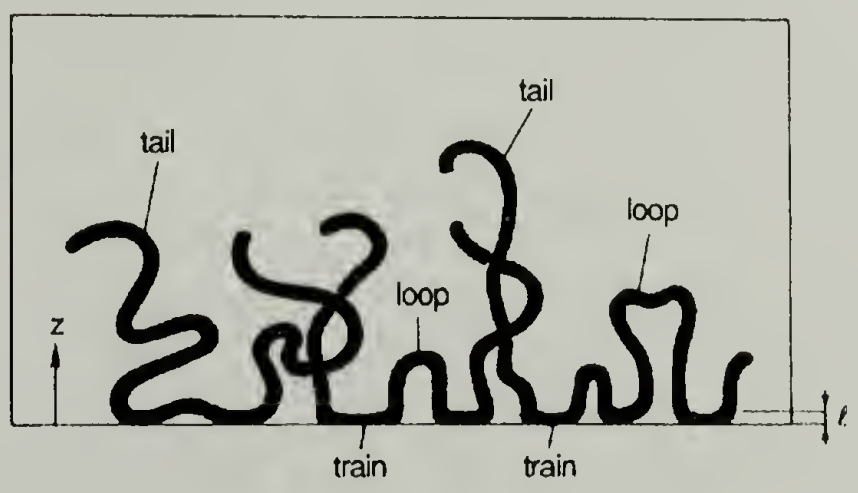

Figure 1.1. Pictorial representation of an adsorbed polymer layer. Loops, tails, and trains are indicated, where the thickness of the trains is represented by *l* and the distance from the interface is represented by z.[1] (with kind permission from Kluwer Academic Publishers)

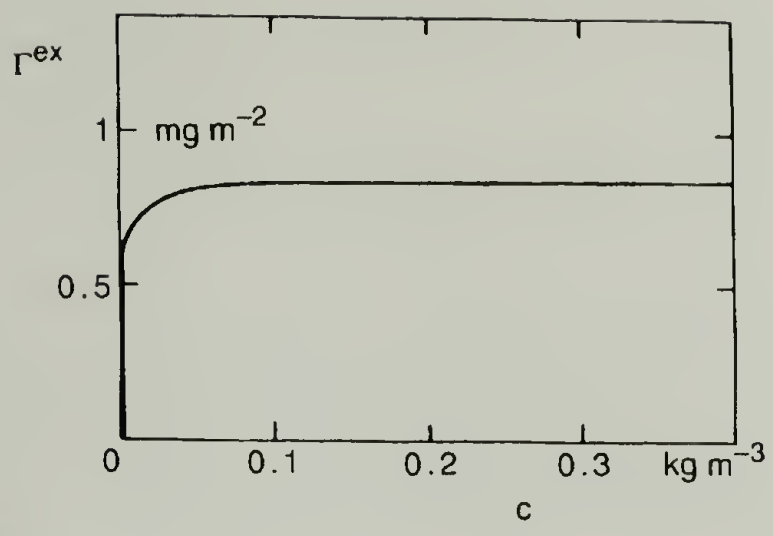

Figure 1.2. An example of a high-affinity polymer adsorption isotherm.[1] (with kind permission from Kluwer Academic Publishers)

isotherm. The high-affinity isotherm shown in Figure 1.2, indicates that polymer adsorption has occurred at very low concentrations, followed by saturation of the surface as indicated by the nearly horizontal part of the curve. This horizontal region is typically referred to as the plateau region. The shape of the isotherm is dependent on the polymer, solvent quality, and molecular weight.

Effects of Solvent Quality

Solvency plays a critical role in the adsorption of polymers as evidenced by the previously discussed interaction parameters. Generally, polymers adsorbed from theta (Θ) solvents generate higher adsorbed amounts than from good solvents, especially at high molecular weight.[1] In good solvents, the adsorbed amount steadily increases in the low molecular weight range, but for very high molecular weights, the plateau value becomes independent of chain length whereas under Θ conditions the adsorbed amount increases with chain length. Graphically this is represented in Figure 1.3 which shows theoretical isotherms describing the adsorption characteristics of polymers in good (dashed curve) and theta (bold curves) solvents. The mechanism by which a polymer at

different molecular weights and fixed concentration adsorbs is dependent on the solvent quality.

Generally, for rod-like polymers the solvent choice is limited to good solvents.[22] Rod-like polymers often gel in good solvents and due to limited configurational entropy, rods are even more sensitive to poor solvent conditions. These solvency issues became apparent in working with poly-**S**. For poly-**R/S**, adsorption experiments were first performed in toluene, but poly-**S** gelled in this solvent. For this reason, the polymers are isolated by different methods and adsorption experiments were limited to the best solvent-THF.

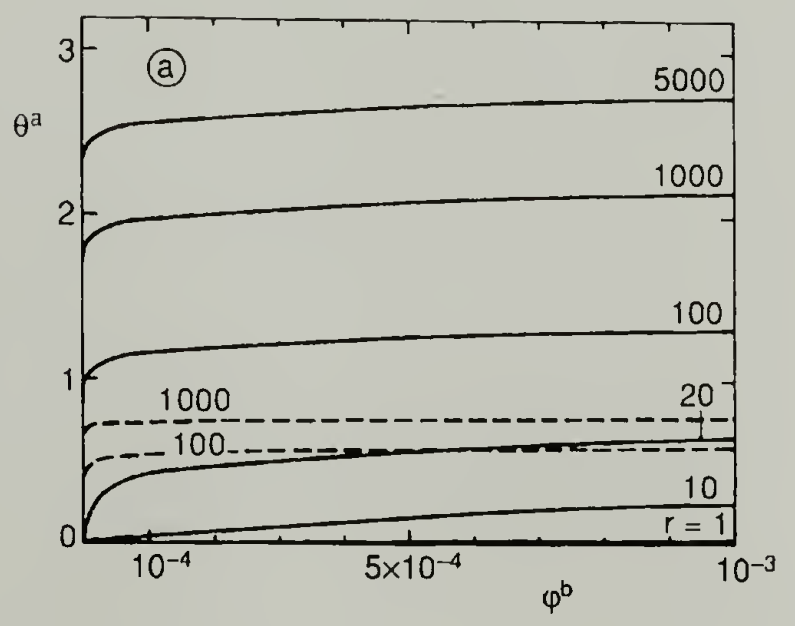

Figure 1.3. Theoretical adsorption isotherms for various chain lengths, r. Solid curves are for theta solvent ($\chi = 0.5$) conditions. Dashed curves are for good solvent conditions ($\chi = 0$). Where φ^b is the volume fraction in the bulk solution and θ^a is the adsorbed amount in monolayers (the amount of polymer in the system).[1] (with kind permission from Kluwer Academic Publishers)

Control of the solvent quality can be accomplished by changes in temperature or by varying the composition of the solvent.[19] Variations in temperature are advantageous when limited solvents are available. In addition, one-solvent systems generally result in a

more consistent polymer solution. The disadvantage with temperature variations is that molecular motions may change the adsorption kinetics. This would only appear to be an issue when comparing different adsorption systems. One goal of solvent blending is to decrease the solvent quality by the addition of a small amount of a nonsolvent. In selecting a nonsolvent, one must consider that it may change the effective adsorption energy of the polymer by interacting strongly with the segments. It may also limit adsorption due to strong interactions with the surface.

The effective segmental adsorption energy can be quantitatively controlled, as well as measured, by using a binary mixture of solvents in which one is a displacer. Experimental and theoretical reviews of displacer science have been reported.[6,7,16,19,23-27] Displacers are more strongly adsorbing solvent molecules that desorb polymer chains. When the concentration of displacer reaches a critical point, all the polymer chains are desorbed from the surface. The critical displacer concentration has been used to estimate the segmental adsorption energy of the polymer.[23,25]

The Effects of Molecular Weight and Polydispersity

There are general trends in the shape of adsorption isotherms that are associated with changes in molecular weight. Low molecular weight polymers tend to have a less high-affinity character, which results in a more rounded isotherm. Roefs et al.[28] modeled the adsorption of polydisperse polymers. High-affinity isotherms were predicted for polydispersities less than 1.1, but as the polydispersity became ≥ 1.1, the isotherms became more rounded. Adsorption experiments have been carried out using two polymers differing only in chain length.[15] The results for the competitive adsorption of a 9K and 3040K polystyrene (poly-1 and poly-2 respectively) are shown in Figure 1.4. Curves 1 and 2 are respectively the isotherms of neat poly-1 and poly-2. The curve 1 + 2 is the isotherm generated from a blend of poly-1 and poly-2. The isotherm shows a steep initial increase in adsorption, which indicates that both polymers are able to find a place

on the surface. After 40 seconds, a less steep region begins to form which is characteristic of a saturated surface. This is where adsorption is beginning to become preferential in poly-2. In this regime, each chain of poly-2 is fully adsorbed and the smaller chains of poly-1 can only adsorb in the sites not occupied by the larger ones. At 140 seconds, the plateau region begins to form as polymer 2 fully saturates the surface.

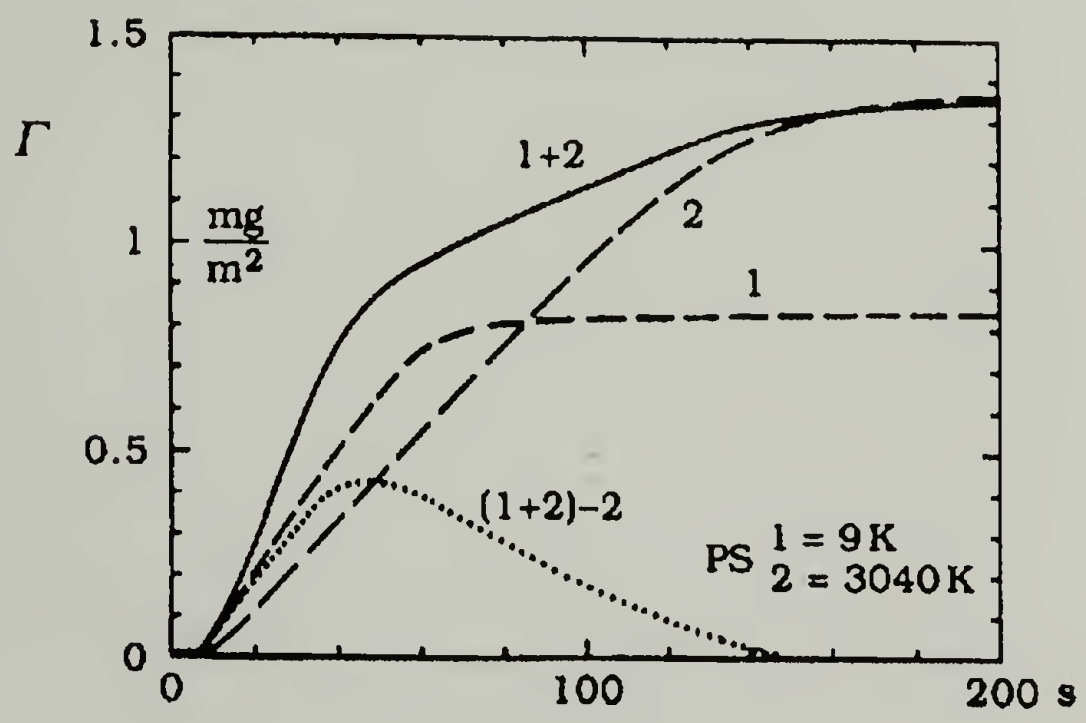

Figure 1.4. Exchange kinetics for the adsorption of polystyrene (PS) from solution in decalin onto silica.[15] Curve 1 and 2 represent the adsorption isotherm of 9K and 3040K PS respectively, onto silica. The plot of 1+2 represents the adsorption isotherm of a blend of 1 and 2. This plot shows the exchange between low molecular weight PS and high molecular weight PS with time. The initial steep slope of the 1+2 curve represents competition for adsorption of both 1 and 2. The next region of lesser slope represents the exchange of 1 by 2 and the plateau region at ~140 seconds indicates complete surface saturation by polymer 2.

Desorption of Polymers

Adsorption and desorption are processes requiring conformational changes in polymer structure.[15,16,19] Intuitively, a polymer does not desorb by the complete simultaneous release of all anchored segments, but most likely by a segment-by-segment

displacement. The release of a segment from the surface results in a small favorable increase in translational entropy. Nevertheless, this small amount of configurational freedom may not be enough to keep the polymer segments from initially adsorbing. It should however, not be concluded that polymer adsorption is irreversible. Under some conditions, desorption can occur, such as, when the adsorbed layer is exposed to several pure solvent exchanges. The desorption kinetics are usually very slow and only significant for those segments weakly adsorbed.

Adsorption of Stiff Polymers

Adsorption experiments on very long chain macromolecules that have rigid rod behavior in solution, have been limited, because there are few polymers with this characteristic.[1] Dimarzio and Bishop[29] have modeled the helix-random coil transitions of DNA attached to a surface. The central conclusion is that the presence of a plane surface sharpens the phase transition. The model also predicted that partial DNA helixes first form in solution and then the helical sections adsorb to the surface.

Murakami[30] used bending energies to model an isolated stiff chain polymer at low surface coverage near the adsorbing interface. They showed the desorption-adsorption transition (loops) become more acute due to higher bending energies associated with increases in polymer stiffness. Khokholv and Ternovsky[31] modeled the adsorption of a long ideal polymer chain with a variable degree of stiffness on a plane surface utilizing the methodology of a lattice model. They calculated the mean lengths of adsorbed segment and loop segment, the fraction of adsorbed repeating units, and the thickness of the adsorbed layer. When adsorbed, stiff chains were found to be more inclined to flatten out than flexible polymers. This is because desorption of the segments leads to a loss not only in the adsorption energy but also in the energy of chain bending. The adsorption was shown to be a second-order phase transition, where "trains" are relatively long and loop sections are relatively short compared to flexible chains. Train sections measured

thousands of Kuhn segments, and projections from the surface, which were found to be rare, occurred only in the form of small "hairpins".

Kuznetsov and Sung[32] used scaling theory to model semiflexible polymers near an attracting surface. These wormlike structures can be considered as an array of rigid rods and their properties are significantly different from those of flexible ones. These polymers near surfaces and interfaces can have liquid-crystalline (LC) properties. The LC ordering must take place near the attracting surface because the stiff segments tend to orient along the surface. They point out that very few studies have been devoted to stiffness effects on adsorption.

Unstable Thin Polymer Films

The demand for developing and understanding thin film technologies can be found in various applications including coatings, lubrication, dielectrics, nonlinear optics, miniaturization of biomedical devices, and numerous other fields.[33,34] Thin film thicknesses are on the order of 1 μm or less, whereas, thick films are greater than a micron.[35] In most cases, the preparation of thin films on solid surfaces can be accomplished through spin coating,[36,37] floatation,[33] grafting,[38] solvent casting,[39] Langmuir-Blodgett transfer techniques,[40,41] and polymer adsorption.[1] However, the above applications require films that remain homogeneous, stable, and of uniform thickness. Thus, several research groups have studied the stability of thin films against dimensional changes.[33-35,37-39,42-51] While thick films may be stable or metastable due to gravity,[52,53] in thinner films, intermolecular forces cause intrinsic instabilities.[54] The wetting and dewetting behaviors of thin polymer films on several substrates including silicon wafers have been studied both theoretically[55-60] and experimentally.[37,45,47,61-67]

The majority of the referenced experimental work followed similar procedures for studying polymer dewetting. Samples were prepared by methods previously described and then dewetting was initiated by annealing the polymer films above the glass

transition temperature. Whether the film wets or dewets can be described by the spreading parameter S:[45,51,68]

$$S = \gamma_B - (\gamma_A + \gamma_{AB}) \tag{1.2}$$

where γ_A and γ_B are the surface tension of liquid (A) and solid substrate (B), and γ_{AB} is the AB interfacial tension. If S is positive, A spreads on B, and when S is negative, dewetting occurs.

Dewetting of a thin liquid polymeric film on a solid substrate is mechanistically referred to as spinodal dewetting.[38] However, there are still debates about the actual destabilizing mechanism.[35,44,50] Nonetheless, the mechanism is based in antagonistic (attractive/repulsive) long- (van der Waals) and (relatively) short-range interactions that decay with thickness. For polymeric thin films above their T_g, thermal fluctuations result in surface undulations that can reach a critical height equal to the film thickness. When these length scales are reached, the depressions hit the substrate, and on nonwettable substrates, rupture the film. This results in the initiation of the dewetting process. For thicker films, dewetting is initiated by a process referred to as hole nucleation, which is not the result of thermal fluctuations.[35]

In the early stages of dewetting, holes are formed that eventually impinge on one another (Figure 1.5) forming ribbons. During the late stages, Rayleigh instabilities cause the ribbons to decay, resulting in the formation of droplets (Figure 1.6). The completely drained thin film resembles Voronoi tessellation patterns.[50] The dewetting process is influenced by film thickness, polymer-surface interactions, molecular weight, viscosity, and surface tension.[50]

Spinodal Dewetting

Although experimentally it has proved difficult to observe the dynamically unstable surface waves that are theoretically believed to initiate spinodal dewetting, Herminghaus et al.[44] have observed such dewetting in thin liquid crystal and liquid metal films from solid substrates. With spinodal dewetting, thermal fluctuations must reach an

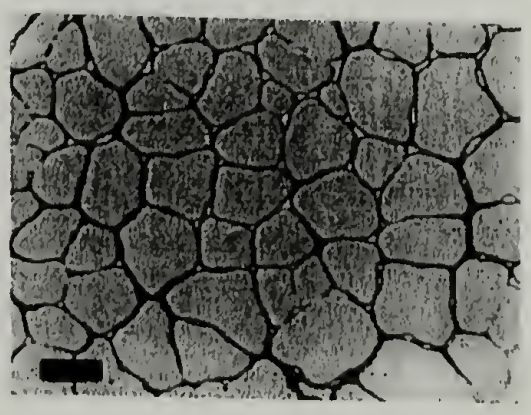

Figure 1.5. Polygonal patterns formed by a 10 nm thick dewetted polystyrene film on a silanized silicon wafer before Rayleigh instabilities led to the formation of droplets. The molecular weight of the polystyrene was 660K and the length of the bar is 10 μm.[35]

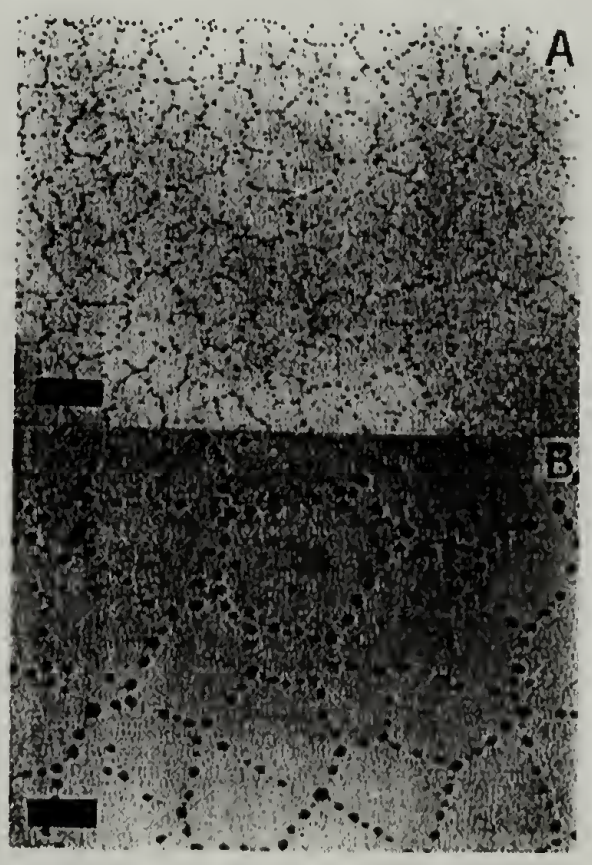

Figure 1.6. Micrographs of final patterns after dewetting of a 25 nm (A) and a 45 nm (B) thick polystyrene film on a silicon wafer. The ribbons have decayed to droplets (dark colored) due to Rayleigh instabilities. The length of the bar is 100 μm.[35]

amplitude where, in the valley of these fluctuations, the liquid reaches the substrate and develops a hole. Whether or not the critical amplitude of these fluctuations is reached depends on long-range forces, such as van der Waals forces. If wetting is favored, long-range forces stabilize lateral film fluctuation by acting as a restoring force. When wetting is not favored, these long-range forces do not stabilize surface fluctuations which can result in surface waves reaching the critical amplitude associated with initiation of dewetting. In their work, Herminghaus et al.[44] review how the stabilization of thin films by long-range forces is a function of the interaction between solid–liquid and liquid–air interfaces.

Herminghaus et al. studied the dewetting of liquid crystal (LC) films by floating a thin film of tris(trimethylsiloxy)silane-ethoxycyanobiphenyl ($5AB_4$) onto hydrophilized silicon wafers at 10 °C. $5AB_4$ undergoes a phase change from crystalline to isotropic at 18 °C. Immediately after transfer of the film onto the silicon wafer, holes began to grow. They observed different mechanisms of dewetting in which holes grew from both nucleation by defects and by an undulative mode associated with surface fluctuations that led to spinodal dewetting. The different mechanisms were observed by light microscopy where nucleated dewetting occurred almost immediately and gradually continued with time. Over time, they observed the formation of holes which were not visible initially, but upon appearing in the film, holes would grow rapidly in amplitude. They associated this behavior with an undulative (dynamically unstable) mode of dewetting.

Their observations were qualitatively described through the polarity differences between the solid-substrate interfaces. $5AB_4$ is strongly dipolar, therefore a strongly polar substrate would favor complete wetting. Without such a substrate, the film would dewet because of the long-range dipolar forces that give rise to the material's strong cohesion energy. For this reason, water was chosen as the substrate, and a Langmuir trough for the device for preparation of freestanding films. When the film is transferred to the hydrophilized silicon, there is a substantial decrease in the substrate polarizability,

resulting in a reduction of polar adhesion between $5AB_4$ and the substrate. This reduction in polar adhesion causes instabilities due to long-range cohesion forces. The result is a film that shows undulative mode (spinodal) dewetting.

Using scanning force microscopy, Herminghaus et al. concluded that the measured surface structures were representative of periods between undulations. The thickness of the film between the periods was indicative of a local (metastable) minimum between the critical interfacial interactions previously described. They also commented on how immediately after transfer of the film to the silicon wafer, the withdrawal of the water subphase might have initiated spinodal dewetting. However, it was pointed out that additional research was required to confirm the affect of water drainage on spinodal dewetting.

Müller-Buschbaum and Stamm,[37] studied the surface morphology of spin-cast homogeneous thin films of polystyrene on silicon wafers before and after dewetting of the film from the substrate. The characterization of the surface morphology right after sample preparation, in the melt, and in the final dewetted state was accomplished by using X-ray reflectivity. Using optical microscopy, they found that the solvent used for the spin-casting gave rise to different dewetting structures. Moreover, the initial in-plane surface morphology of the samples prior to heating was influenced by the solvent used. It was mentioned that homopolymer samples prepared by spin-casting usually exhibit smooth surfaces. However, initial surface structure right after spin-casting had been observed for polymer blends. These initial structures were the result of different rates of solvent volatility.

It was also shown that polystyrene thin films prepared by spin-casting from cyclohexane had radial structure indicating the material flow during rotation of the sample. Inhomogeneous thin films of polystyrene were prepared when spin-cast from THF, a result of the solvents high volatility, whereas, the samples spin-cast from toluene produced thin films that were smooth and featureless. Upon dewetting, only the thin film

prepared from toluene exhibited Voronoi tessellation patterns. For the thin film prepared from cyclohexane, the dewetting structure was a random arrangement of large drops. The dewetted thin film prepared from THF exhibited a random arrangement of various sized islands of polymer. Therefore, solvent choice has a dramatic effect on the initial thin film formation, which directly influences the dewetting structure.

The affect of solvent on polymer dewetting was further studied by Fondecave et al.[43] Part of this work focused on the dewetting of films of poly(dimethylsiloxane) in solution with an oligomer of dimethylsiloxane as the solvent. The substrate for these experiments was an oxidized silicon wafer modified with a monolayer of hexadecyltrichlorosilane (HTS) or octadecyltrichlorosilane (OTS). For both modifications, the oligomeric solvent wetted the substrate, and the polymer dewetted from the substrate. Instability studies were performed by placing a sessile microdroplet (nL) of polymer solution onto the substrate and using optical microscopy, observing dewetting.

During the study of microscopic droplet wetting, they observed the "leak out transition" associated with the droplet of solution being surrounded by a "halo" film of pure solvent. They referred to the appearance of this halo effect as the "fried egg" configuration. The leak out transition was also described as the phase separation of the two miscible liquids, where at high polymer concentration, the solvent preferentially interacts with the polymer. At low polymer concentration, the solvent interacts with the substrate and "leaks", forming a precursor film. Since the solvent likes the polymer and would also like to wet the substrate, critical interactions must come in play and control whether solvent "leaks" from solution or remains in the droplet.

Marangoni instabilities (see Fig. 1.7) of the droplet contour were observed for droplets of polymer solution below a critical polymer volume fraction. It was discussed how surface tension gradients due to solvent leakage with subsequent increases in polymer concentration at the wedge of the drop induced Marangoni instabilities. They

referred to several examples where these surface tension gradients can originate from either concentration gradients for binary mixtures or thermal gradients for volatile liquids. As an example, they described the Marangoni instabilities observed for volatile droplets where the drop rapidly spreads across a substrate becoming flat and surrounded by a rim. As the rim recedes, it decays into droplets and the process continues in a cascading fashion until all that remains is microdroplets dispersed on the substrate.

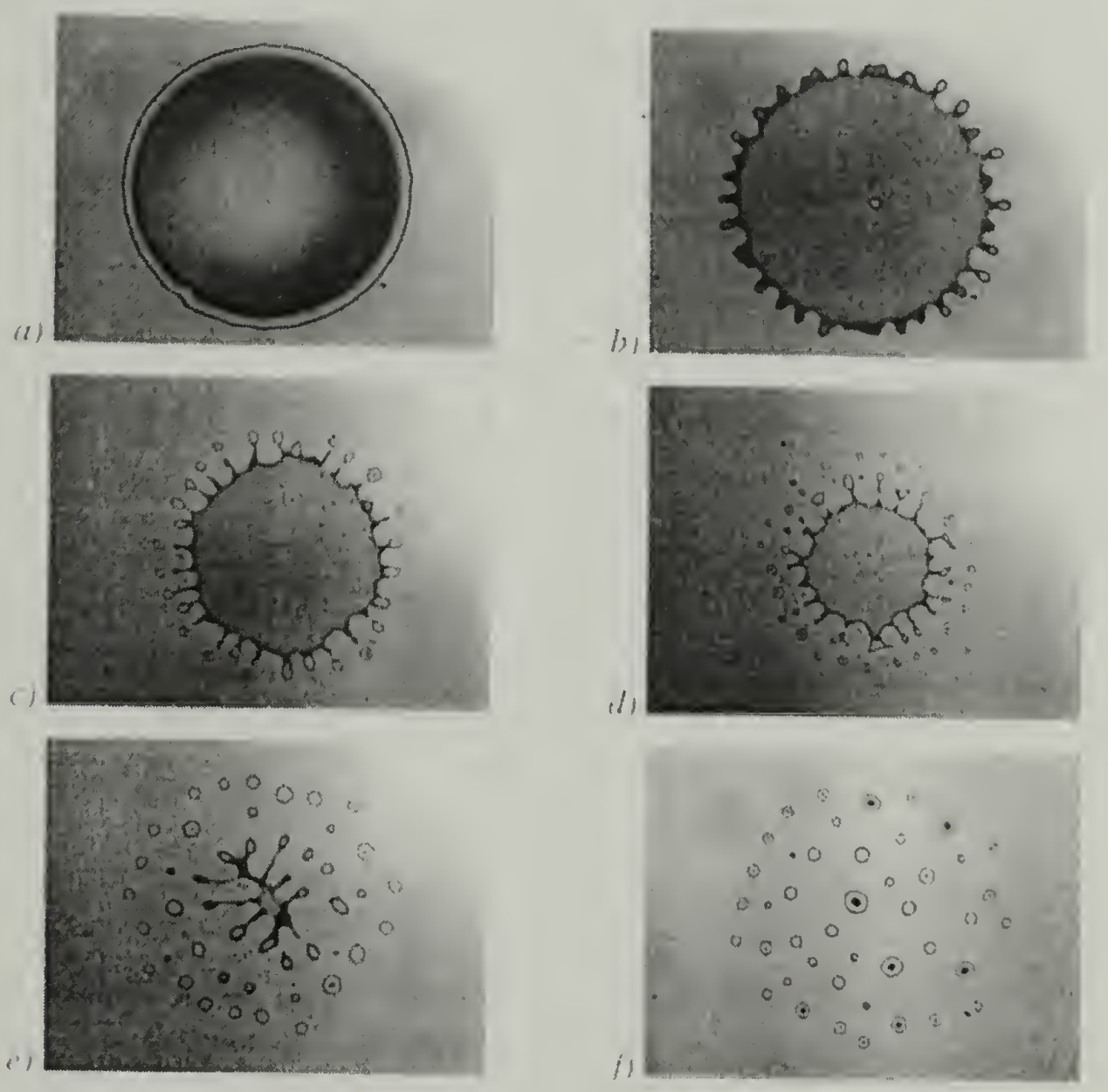

Figure 1.7. Marangoni instability of a dilute drop of PDMS in solution with its oligomer. (a) Rapid spreading of the drop (flattens out) induces surface tension gradients which result in undulations (b) at the drop rim (perimeter). The instabilities at the rim lead to the formation of digitation, while the rim simultaneously dewets. (c) Further dewetting results in the decay of the finger projections and the formation of a new rim, which continues to contract toward the center. (d,e) The process of rim formation, digitation, Rayleigh instabilities, and new rim formation continue until the drop completely dewets leaving a surface (e) of microdroplets.[43]

They questioned how the leak out transition would effect the stability of a thin film of polymer solution. For pure PDMS which dewetted from the substrate, the resulting surface structure resembles the classical polygonal geometry associated with Voronoi patterns. In addition, the surface between the decayed ribbons is "dry", thus, this is the name given to this type of dewetting. In the case of dewetting of the PDMS and oligomer solution, the Marangoni effect was the referred mechanism. While rims continually moved across the surface, fingering instabilities would form and decay into droplets. The result was a surface with Voronoi patterns where the polygons were full of droplets and between the droplets; this confirmed the existence of a thin film of pure solvent. Thus, "wet" dewetting is associated with the coexistence between a thin film of pure solvent and droplets of polymer solution. In conclusion, they stated that for a thin film of polymer solution, "wet" dewetting occurs if the polymer is depleted at both interfaces and the thickness correlation length of the depleted layer is larger than the thickness of the "leaked" film of pure solvent.

Extended and Rod-like Polymers

Overview

For polymers, three major types of molecular conformations exist: rigid rods, extended chains, and random coils.[69] Extended chains are associated with both those chains that are stiffer than usual, and those rod-shaped chains that contain flexible spacers. In addition, polymers with worm-like conformations fall under the extended chain classification. Unique properties such as liquid crystallinity[70] and high strength[71-73] are attainable because of the rod and extended chain architectures. There are new potential applications emerging that utilize the unique mechanical, morphological, and physical properties of these types of polymers.[22,74] An important limitation of polymers

with rigid rod conformations is that many are intractable in terms of processing and solubility.

Many of the polymers described as having rigid rod or worm-like character are polymerized by step-growth processes. This methodology results in low molecular weight and large polydispersities.[75] Examples of such polymers are biopolymers (e.g. DNA, xanthan), aromatic polyamides (e.g. Kevlar [poly(imino-1,4-phenyleneiminoterephthaloyl)], Nomex [poly(1,3-phenyleneiminoisophthaloyl)], and heterocyclic polymers (e.g. PBT (polybenzthiazoles), PBO (polybenzoxazoles)). Generally, it is accepted that to synthetically produce polymers with high molecular weight and low polydispersity, some form of living chain-growth polymerization methodology is required. A living polymerization results when there is an absence of chain termination and chain transfer.

In the Novak group, we have been interested in developing living polymerizations that produce polymers with well-defined helical conformations in both solution and solid state. These conformations are controlled by restricting the degrees of freedom along the polymer backbone which results in the macromolecule adopting an extended chain or rigid rod architecture. One such class of polymer that is being extensively studied in our group is the polycarbodiimides. Recent developments in transition metal complexes have made possible the polymerization of polycarbodiimides with well-defined architectures.[76-79] The research presented here focuses on the tendency of the rod and worm-like, poly-**S** and poly-**R/S** (see Fig. 1.9) to adsorb to solid surfaces. The chain architecture of these polymers is controlled by the stereochemistry of the monomer where enantiomeric pure or racemic monomer results in rod or worm-like conformations, respectively.[77,80-82] The synthesis of both poly-**S** and poly-**R/S** is well controlled and the polymer is soluble, to some degree, in common solvents.

Another effect of the extended chain architecture of poly-**R/S** and poly-**S** is that of liquid crystallinity. Goodwin et al.[82] performed intrinsic viscosity measurements and

reported on the LCP nature of poly-**R/S** and poly-**S**. Qualitatively, toluene solutions containing a few percent of polycarbodiimide formed viscous solutions, while solutions approaching 10 weight percent behaved like a gel. Reduced viscosity measurements showed decreasing shear dependence with successive runs of a particular solution, and would asymptotically approach a reproducible value. Furthermore, after 0.5 hour, during which time the polymer solution remained undisturbed, if the value that was first measured was measured again, a gradual decrease to a reproducible value would be measured. Goodwin explained how these results were consistent with the behavior of a liquid crystalline, rigid rod polymer being aligned by the shear forces within a flow field. Additional research in the Novak group has shown that these polycarbodiimides are lytropic liquid crystalline polymers.

Rod-shaped polymer chains are used to make strong fibers because of the ease in orienting the chains in the fiber direction, without folding.[69] This ability to order the chains is demonstrated by the intrinsic viscosity measurements, where viscosity increases with solution concentration, followed by an abrupt decrease. The increase in viscosity with concentration occurs while the liquid crystalline polymers are isotropic, and the sudden decrease is a result of increasing anisotropy.

Design of Polycarbodiimides

Initial work in the Novak group for developing living routes to polymers with well-defined helical conformations concentrated on the poly(isocyanides)[83-85] and poly(isocyanates) shown in Figure 1.8.[76,86-88] Both poly(isocyanides)[89-93] (with their bulky imine groups) and poly(isocyanates)[94-96] have been shown to adopt helical conformations in solution. Although both poly(isocyanides) and poly(isocyanates) adopt helical conformations, there are significant differences in their respective helix inversion barriers ($\geq$ 27 kcal/mol[97] vs 3-5 kcal/mol[98,99]) and persistence lengths (30 Å[100] and 600 Å[98,101-106]). It was desirable to develop a polymer with the high inversion barrier of the

poly(isocyanides) and the long persistence lengths of the poly(isocyanates). To accomplish this, the idea was to replace the carbonyl group in the poly(isocyanates) backbone with the more sterically demanding imine group of the poly(isocyanides). Using a retrosynthetic approach to assist in designing a polymer with an amidinate type repeat unit resulted in the scheme to polymerize the carbodiimide monomer.[107] The stiffness of the polycarbodiimides is still currently being studied.[108] Recently, the persistence length of a 750K poly-**R/S** was measured by light scattering and found to be among the stiffest of soluble synthetic polymers, with $L_p = 42 \pm 8$ nm.[109]

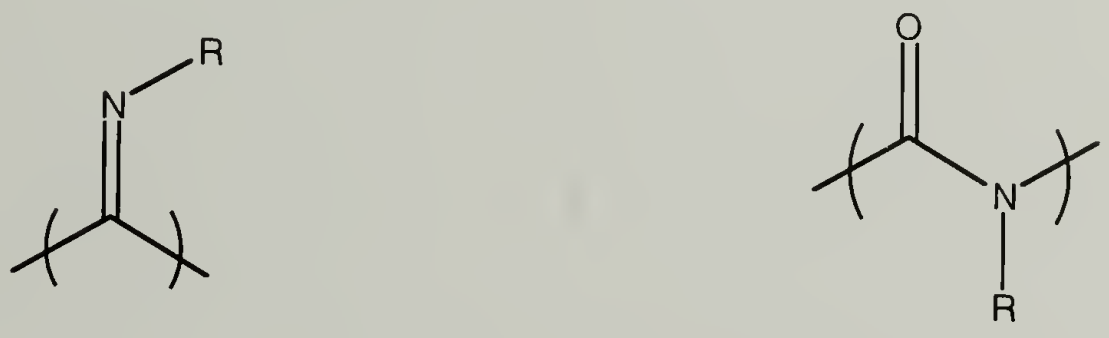

Figure 1.8. On the left is the structure of poly(isocyanides) and on the right is the structure of poly(isocyanates).

Polymer Surface Analytical Techniques

Adsorbed thin films of polycarbodiimide were analyzed by x-ray photoelectron spectroscopy (XPS), contact angle measurements (CA), ellipsometry, and tapping mode atomic force microscopy (AFM). The different surface techniques analyze various depths and provide different types of information that, when combined, give a quantitative and qualitative description of the surface. Ellipsometry was used to analyze a few spin-cast thin films and we chose to omit discussion of this technique.

X-ray Photoelectron Spectroscopy (XPS)

XPS, also referred to as Electron Spectroscopy for Chemical Analysis (ESCA), is an important technique for polymer surface analysis. Utilizing the photoelectric effect, XPS measures the atomic composition in the outer 10–100 Å of an object,[110] and with certain instruments, analyses at depths of 200 Å,[111] have been obtained. Besides the quantitative aspects, XPS also gives qualitative information about the chemical states at the surface. One limitation of XPS for polymer analysis is the lack of molecular specificity.[112] For example, polyethylene and polypropylene can not be differentiated by XPS. The next few paragraphs briefly describe the main principles behind XPS, and several texts have chapters devoted to the topic.[111-113]

During an XPS experiment, a sample is irradiated with soft x-rays (usually Al K_α or Mg K_α) under ultra high vacuum conditions. The photon energy is transferred to the core electrons, thereby pumping up the energy of the electrons to a level that allows them to escape the atom. The kinetic energy, E_k, of the photoelectron is measured at a detector and since the X-ray photon energy $h\nu$ is known, the binding energy, E_b of that inner-shell electron can be calculated by the following equation:

$$E_b = h\nu - E_k \tag{1.3}$$

The binding energy of the electron is specific for each atomic orbital of the source element, and the XPS measures the number of these electrons from each element present. The atomic composition is calculated from peak areas and atomic sensitivity factors that take into consideration the varying photoelectric cross-sections of atoms. For this reason, atomic composition based on peak sizes cannot be compared directly. The sensitivity factors, obtained from samples with known composition, compensate for the photoelectron flux produced from a specific core level of an atom. Sensitivity factors are

dependent on the photon energy, the atomic number, and the orientation of the sample with respect to the X-ray beam and the analyzer.[112]

The surface sensitivity of XPS is a result of ejected core electrons which at certain depths below a surface experience inelastic interactions, thereby losing kinetic energy that limits the no-loss emission to a mean depth of only a few atomic layers.[112] These inelastic interactions limit ejected core photoelectrons to finite escape depths, which result in the exponential decrease in XPS sensitivity with depth. Equation 1.4 describes the relationship between the number of electrons detected (N) to the number of electrons ejected (N_o) at sampling depth t and where λ is the electron mean free path and θ is the

$$N = N_o e^{-\left(\frac{t}{\lambda \sin\theta}\right)} \tag{1.4}$$

angle to the detector from the plane of the sample surface.[111] This exponential decrease in sensitivity indicates that XPS data can be biased high by functionality concentrated in the outermost surface layers. The measurement of mean free paths for organic polymers is somewhat controversial.[111] Ashley et al.[114] have addressed the problem theoretically by calculating the mean free paths based on the kinetic energy of the electron, bulk density, and molecular structure. For XPS analysis of film samples carried out in this dissertation, the Al K_α anode was used.

According to Equation 1.4, an atomic composition depth profile of a surface can be obtained by varying the angle between the sample surface and the detector. Scheme 1.1 shows the sample/detector geometry. At shallow take-off angles, electrons have to travel a greater distance through the solid before emitting towards the detector so only those ejected photoelectrons from the outermost surface are analyzed. Therefore, XPS is more surface-selective at smaller take-off angles. All samples in this dissertation were analyzed at 15° and 75° take-off angles (between the plane of the sample surface and detector). Equation 1.4 indicates that 95% of detected photoelectrons originate in the

outermost $3\lambda\sin\theta$. For example, if we use $\lambda = 14$ Å (for C_{1s} electrons[110]), 15° and 75° take-off angles assay the outer ~ 10 Å and ~ 40 Å, respectively. Approximately 54% of the photoelectrons measured at 75°, originate from the top 10 Å. For this reason, data exhibiting large variations in take-off angle can reveal information about the distribution of functionality in the surface of a sample.

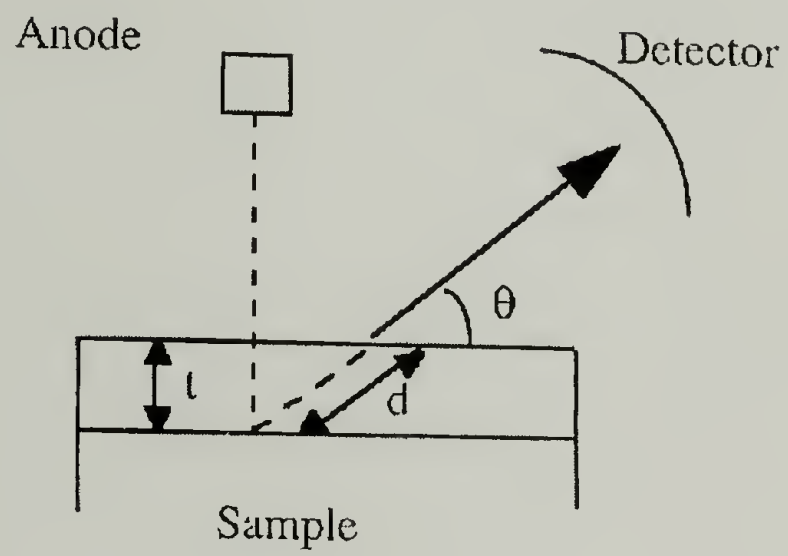

Scheme 1.1. Sample/detector geometry in variable angle XPS.

Contact Angle Analysis

Contact angle is the most surface-sensitive analytical technique because it measures the wettability of the outermost few angstroms of a surface. The physics of contact angle analysis are discussed in more detail in chapter 2. The contact angle (θ) is

$$\gamma_{lv}\cos\theta = \gamma_{sv} - \gamma_{sl} \qquad (1.5)$$

governed by the equilibrium between the surface tensions in the region of the solid/liquid/vapor three-phase boundary as described by Young's equation (Eq. 1.5). The

variables are defined as: γ_{lv} is the surface tension of the liquid in equilibrium with its saturated vapor, γ_{sv} is the surface tension of the solid in equilibrium with the saturated vapor of the liquid, and γ_{sl} is the solid-liquid interfacial tension, as shown in Scheme 1.2.

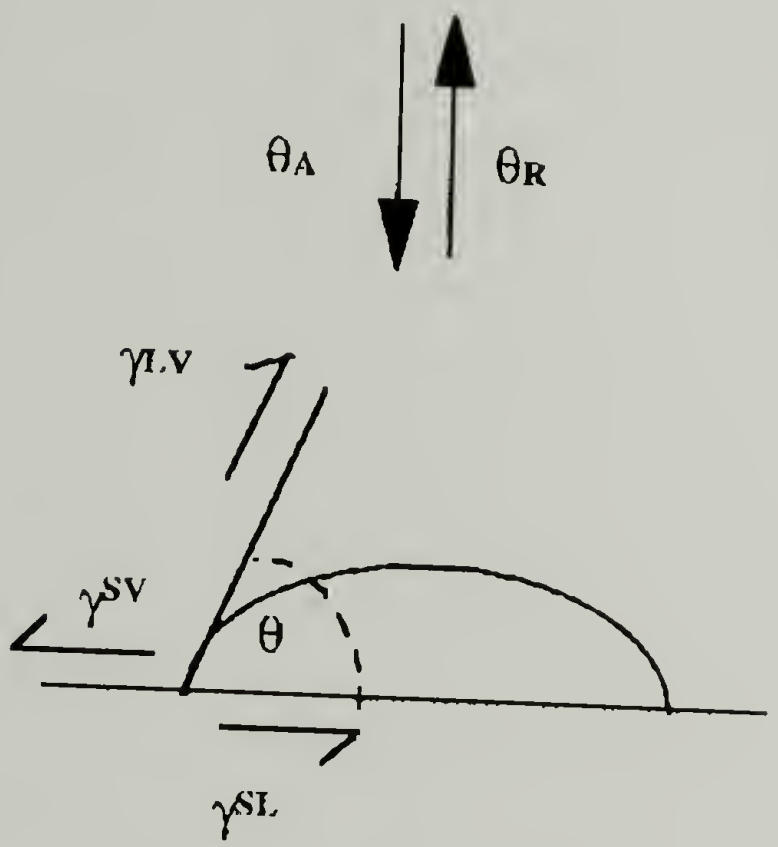

Scheme 1.2. Dynamic contact angle measurement.

Young's equation is based on the following assumptions: that the surface is rigid, immobile, nondeforming and smooth; the composition is chemically homogeneous and the solid does not interact with the probe fluid.[111] If all of these conditions are met, then there is an equilibrium contact angle. However, in most practical systems, not all the above criteria are met, resulting in contact angle hysteresis. In the research presented here, water was used as the probe fluid. We measured both advancing contact angles (θ_A) and receding contact angles (θ_R) as probe fluid, was added to or withdrawn from the drop. The difference between θ_A and θ_R is termed contact angle hysteresis.

Atomic Force Microscopy

Atomic force microscopy (AFM) was developed in 1986 by Binnig, Quate, and Gerber[115] in a collaboration between IBM and Stanford University. The technique was developed to exploit contact and non-contact forces for imaging surface topography and to study new physical phenomena at microscopic dimensions. Three modes of AFM presently available are contact, non-contact, and tapping.[116] Several other techniques are reviewed in the Digital Instrument Nanoscope III manual, including Lateral Force Microscopy (LFM), Force Modulation Microscopy, Magnetic Force Microscopy (MFM), Electric Force Microscopy (EFM), Surface Potential Microscopy, and others.[117] The Nanoscope III is the instrument used in the research presented here with all work performed using the TappingMode™ method.

Imaging surfaces with the atomic force microscope is analogous to a stylus profilimeter, where the contact force of a commercial profilimeter (~ 10^{-4} N) is reduced to 10^{-9} N, which is less than most interatomic forces.[118] The extremely small load on the surface by the stylus limits tip-induced surface deformations. However, in contact mode, even these small forces can damage polymer surfaces. In response to analyzing polymer surfaces, Zhong et al.[119] developed tapping mode AFM that achieves high resolution without inducing destructive frictional forces.

The probe used in AFM is a silicon cantilever with an integral silicon tip. With the tapping mode method, shown in Scheme 1.3, the cantilever is oscillated near its resonant frequency as it is scanned in a raster pattern across the sample surface. The probe is brought closer to the sample surface until it begins to intermittently contact ("tap") on the surface. This contact with the sample causes the oscillation amplitude to be reduced. A laser is reflected off the back of the probe and detected by a photodiode that measures changes in the amplitude of the reflected laser. These changes in amplitude are fed back to a x-y-z piezo that moves the cantilever in the z-direction an amount necessary to restore the resonant frequency. The numerous changes in amplitude

are compiled as series of sine waves that are then transformed by Fourier processes that convert the data to an image of the surface.

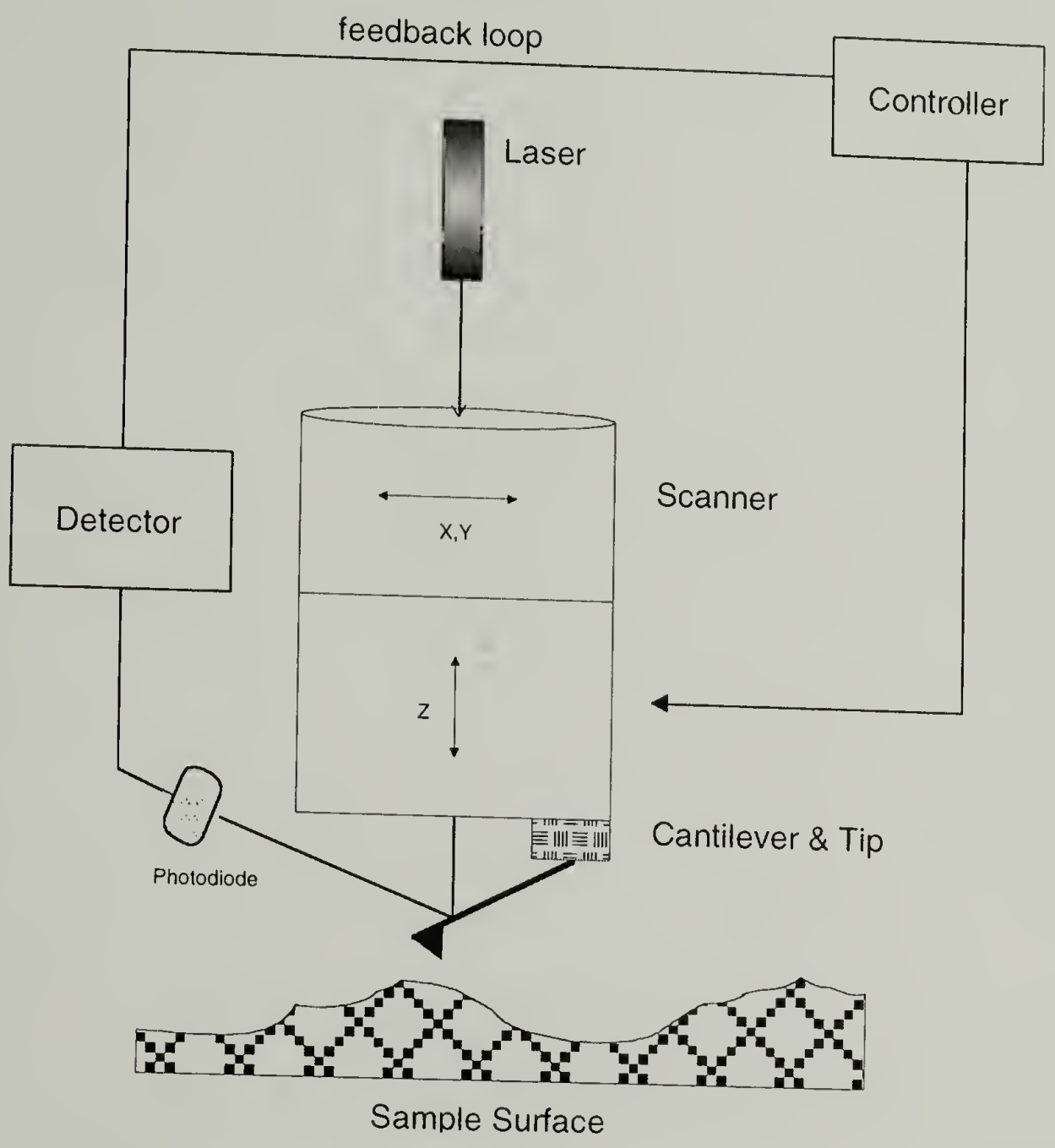

Scheme 1.3. General diagram of TappingMode™ AFM.

In addition to height analysis, there are other algorithms such as phase imaging that give information about modulus differences on the sample surface. This is accomplished by the computer measuring the phase lag in the laser as the tip strikes a hard or soft part of the surface. The imaged produced appears three dimensional, similar to a scanning electron micrograph. However, care must be taken in interpreting the

results from phase imaging, because the image is strongly affected by the force at which the tip probes the surface. The reader is referred to the Nanoscope Manual for a more complete overview of phase imaging.[117]

With the various AFM modes, researchers have characterized the surface structure of homopolymers,[120-129] block copolymers,[130-134] graft copolymers,[135] as well as polymer blends.[136] AFM has been used to study self-assembly,[137-142] map the growth of monolayers,[143,144] and measure the viscoelastic response of polymer surfaces.[137,145-152] Surface roughness and its effect on the wetting behavior of polymer thin films has also been explored by AFM.[153,154] Besides mapping the topography of a surface, the AFM can be used as a nanoscale surface force apparatus to measure adhesion between materials and measure indentation/deformation properties of surfaces under very small loads.[155] The AFM analyses presented here, focus on imaging the surface characteristics of adsorbed thin films on native silicon oxide.

Mentioned above are several applications for AFM. Two areas of research with AFM pertinent to our work are the visualization of single-chain conformations[39,48,50,74,156-160] and the dewetting dynamics of polymers at interfaces.[45,161,162] Quist et al.[157] used tapping mode scanning force microscopy to analyze the lateral sizes and height of human serum albumin adsorbed on mica. Qualitatively, they estimated the profile of adsorbed molecules, but concluded that quantitative height information needed careful evaluation. The lateral dimensions of the adsorbed molecules were calculated from subtracting the tip radius from the measured length. For example, they estimated that a probe with a radius of 10 nm traversing a 2 nm high object results in an increase in the lateral dimension of approximately 14 nm. It was also discussed as to how the height measurements might have been affected by deformation of the polymer by the tapping probe. Researchers have studied how artifacts effect size measurements by quantifying the dimensions of the probe prior to analysis and then subtracting the tip effects.[163,164]

Kumaki et al.[156] used TappingMode AFM to observe individual copolymer chains that were transferred from water onto mica. The measured dimensions of the polymer agreed with values expected for the molecular weights studied. Ebihara et al.[158] used AFM in the noncontact mode to measure the helical nanostructure of poly(n-decyl-(S)-2-methlybutylsilane) cast onto a sapphire plate. Rigid rod like segments and helical kinks were observed for the polymer casted from a very dilute toluene solution of about 10^{-10} (Si-unit)/L, but for polymer casted from 10^{-8} (Si-unit)/L toluene solution, a network-like image was observed. Without description here, both works mentioned above made debatable assumptions in supporting the measured profiles.

Experimental Section

Materials

Unless otherwise noted, materials were obtained from commercial suppliers and used without further purification. Methylene chloride was stored over 3 or 4 Å molecular sieves for 48 hours immediately prior to use. Benzene and toluene used in air- and water-sensitive procedures was dried over LaRoche A-2 activated alumina and Engelhard CU–0226S (formally known as Q-5 reactant; a supported copper redox catalyst) following the process described by Pangborn et al.[165] Bis(cyclopentadienyl)titanium dichloride, titanium (IV) chloride, *N*,*N*-dimethyltrimethylsilylamine, and toluene were freeze-pump-thawed three times immediately prior to vacuum transfer in the gas phase to their appropriate reaction vessel. Purification of triphenylphosphine was accomplished by recrystallization from hexane.

General Procedures

Air- and moisture-sensitive procedures were carried out using standard Schlenk techniques and a mBraun Lab Master 100 recycling inert atmosphere box (N_2). Thermal characterization was carried out with a Perkin Elmer System 7 DSC and TGA. Unless otherwise noted, DSC measurements were acquired at a ramp rate of 10 °C per minute. Melting point temperature was recorded by taking the maximum peak temperature of the endotherm. For TGA, the degradation temperature is reported using the trigger point routine of Perkin Elmer 7 series/UNIX thermal analysis software, version 4.0. Refractive index increments for GPC/LS were obtained with a Photal (Otsuka Electronics) RM-102A Differential Refractometer with 632.8 nm wavelength source. Tandem Gel Permeation Chromatography/Light Scattering (GPC/LS) was performed using a Hewlett Packard 1050 series liquid chromatography pump, a Wyatt Technologies Dawn DSP-F light scattering instrument equipped with a K5 flow cell at 632.8 nm, and a Wyatt Technologies Optilab 903 refractive index detector equipped with a P-10 flow cell thermostated at 25.0 °C. A set of two size exclusion columns (PLGel, mixed C, 5 μm particle size, Polymer Laboratories) was used with HPLC grade THF mobile phase at 1.0 mL/min. Evaporative mass detection was performed at Polymer Labs using their EMD unit connected to a HPLC pump via a single PLGel mixed B, using a 5 μm particle size column. Unless otherwise noted, solutions for GPC/LS were prepared at ~ 3 mg/mL. FTIR spectra were of thin films on NaCl plates. The ^{1}H NMR was measured at 200 MHz with samples solvated in $CDCl_3$ that was transferred through the gas phase following three Schlenk-freeze-pump-thaw cycles. ^{1}H NMR spectra are referenced to the solvent used ($CDCl_3$ singlet at 7.26 ppm) and reported as δ (ppm) downfield from TMS.

Preparation of *N,N'*-di-n-hexylurea

A 500-mL round-bottomed flask was charged with 200 mL of reagent grade chloroform, a magnetic stir bar, and 10 mL of *n*-hexylisocyanate (8.76 g, 68.9 mmol).

The flask was covered with a septum, purged with N_2 , immersed in an ice bath and cooled while stirring. Over a period of 30 minutes, 9.10 mL of *n*–hexylamine (6.97 g, 68.9 mmol), diluted with 5.0 mL $CHCl_3$, was added dropwise by temporary removal of the septum and at a rate that avoided reflux. The resulting solution was stirred for one hour at which point the ice bath was removed and the solution was stirred for an additional hour at room temperature. Solvent was removed with a rotary evaporator at 30 °C yielding a white solid. The product of this reaction was of such purity that no further purification was necessary. Yield: 15.32 g (67.1 mmol, 97%), mp = 78.42 °C; FTIR (KBr pellet) and ^{1}H NMR (200 MHz, $CDCl_3$) results matched the literature spectra.[82]

Preparation of *N*-methyl-*N'*-(α-phenylethyl)urea

The same procedure for the preparation of *N,N'*-di-*n*-hexylurea was employed. The quantities of reagents used were 4.00 mL of methylisocyanate (3.87 g, 67.8 mmol), 8.74 mL of neat α-phenylethylamine (8.22 g, 67.8 mmol), and 200 mL $CHCl_3$. CAUTION: methylisocyanate is highly toxic and volatile. Do not freeze. All procedures were carried out in a certified fume hood. Yield: 11.29 g (63.3 mmol, 93%), mp = 94.4 °C - 95.8 °C.

Preparation of *N*-methyl-*N'*-(α-phenylethyl)carbodiimide

Unless otherwise noted, carbodiimides were all prepared in a similar manner with slight modification of literature procedures.[166] A dry 500-mL round bottom flask was charged with 22.08 g of triphenylphosphine (84.2 mmol, 50% excess to the urea), an egg–shaped magnetic stir bar, 200 mL of dried methylene chloride, was then sealed with a septum, and purged with dry N_2 gas. The flask was cooled by immersion in an ice bath and stirred vigorously with a magnetic stir plate. A 10 mL graduated cylinder was charged with 4.34 mL of bromine (13.46 g, 84.2 mmol, 50% excess to the urea) diluted to 10 mL with dry methylene chloride. The bromine solution was added drop–wise to the

flask, over a 30-minute period, avoiding reflux by temporary removal of the septum. The suspension of dibromotriphenylphosphorane (beige color) was stirred for 30 minutes and then 24.67 mL of triethylamine (17.91 g, 177 mmol, 110% excess to bromine-solution turned yellow) was added by temporary removal of the septum. Over a one hour period, 10.0 g of *N*-methyl-*N'*-(α-phenylethyl)urea (56.1 mmol, suspension turned brown) was added to the flask by temporary removal of the septum, avoiding reflux. The suspension was stirred for an additional hour and 0.159 g of suspension was removed to check for carbodiimide by IR (thin film, 2125 (vs)).[167-169] The suspension was transferred to a 500-mL separatory funnel to which 100 mL of H_2O was added in order to extract the triethylammonium hydrobromide. The suspension was shaken and the organic phase was separated from the aqueous phase (pale red color). The procedure was repeated until the pale red color of the aqueous phase had turned a light beige color. The resulting dichloromethane solution was dried by stepwise addition of magnesium sulfate and then filtered into a dry 500-mL round bottom flask. The volatile material was removed with a rotary evaporator at aspirator pressure. The resulting brown solid was washed with approximately 30 mL of hexane, until most of the brown color was removed, leaving beige colored solid. The suspension was filtered into a dry 50-mL round bottom flask in order to remove the solids. The volatile material was removed from the remaining solution by a rotary evaporator. To the white oily film remaining in the flask was added a micro stir bar and approximately 0.1 g of CaH_2. The mixture was stirred for 24 hours at room temperature. Distillation of the extracts from CaH_2 using a short path distillation head at 40 °C and 110 torr into a 50-mL Schlenk flask afforded *N*-methyl-*N'*-(α-phenylethyl)carbodiimide as a clear, colorless liquid. Yield 5.51 g (34.4 mmol, 61%), ^{1}H NMR (200 MHz, $CDCl_3$) δ (ppm) 1.48 (d, 3H, CH_3), 2.85 (s, 3H, CH_3N), 4.51 (q, 1H, benzylic H), 7.25 (m, 4H, aromatic). Several preparations were performed with yields of approximately 80%.

Preparation of *N,N'*-di-*n*-hexylcarbodiimide

The preparation for this monomer is described here because in this chapter the refractive index increment was calculated. The same procedure for the preparation of *N*-methyl-*N'*-(α-phenylethyl)carbodiimide was employed, and the quantities of reagent used were 15.88 g of *N, N'*-di-*n*-hexylurea (75.5 mmol), 27.17 g of triphenylphosphine (103.6 mmol), 5.34 mL of bromine (16.56 g, 103.6 mmol), 31.8 mL of triethylamine (23.09 g, 228.2 mmol). Distillation of extracts from CaH_2 at 55 °C and 100 torr yielded 10.44 g (49.6 mmol, 67%) of monomer.

Preparation of Cyclopentadienyltitanium trichloride

Following procedures described in the general section, 13 mL of titanium (IV) chloride ($TiCl_4$, 22.5 g, 119 mmol, note; excess is not necessary) was transferred through the gas phase into a 25-mL storage tube. In a recycling inert atmosphere dry box (N_2 gas), a 25-mL reaction flask containing a stir bar was charged with 10.03 g of bis(cyclopentadienyl)titanium dichloride (Cp_2TiCl_2, 40.3 mmol), removed from the dry box, and charged with 100 mL of dry toluene by vacuum transfer techniques. The $TiCl_4$ was transferred through the gas phase into the 25-mL reaction flask, the reaction flask purged with Ar gas, and then placed into a hot oil bath at 140 °C. The mixture was heated at reflux for 15 hours and then was allowed to stand at room temperature for 96 hours. During this period, the cyclopentadienyltitanium trichloride ($CpTiCl_3$) precipitated from solution. Volatile materials were removed through the gas phase by vacuum transfer techniques. The reaction flask was returned to the dry box, and 3 ~ 5 g of orange $CpTiCl_3$ powder was charged to a sublimator. The sublimator was placed into a 100 °C oil bath and sublimation under dynamic vacuum yielded orange crystals. Multiple sublimations were required to obtain purity. ^{1}H NMR (200 MHz, $CDCl_3$) δ (ppm) 7.04 (s, 5H, Cp).

Preparation of Bischloro-η^5-cyclopentadienyl-dimethylamido titanium(IV)

A modification of the procedure of Patten[170] and Goodwin[82] was employed. In a recycling inert atmosphere dry box (N_2) a 50-mL storage tube was charged with 6.77 g of $CpTiCl_3$ (33.5 mmol), 25 mL of dry benzene, and a stir bar. Transferred through the gas phase to the storage tube was 5.76 g of *N,N'*-dimethyl-trimethylsilylamine (49.11 mmol, 47% excess). Under static vacuum, the storage tube was placed in an oil bath at 40 °C for 40 minutes and vigorously stirred. The dark red solution was removed from the heat and stirred at room temperature for 64 hours, where upon the volatile material was removed under reduced pressure leaving a red powder (6.56 g, 93% crude yield). Sublimation at 90 °C (0.005 torr) yielded (6.33 g, 90%) of orange/red crystals. ^{1}H NMR (200 MHz, $CDCl_3$) δ (ppm) 3.84 (s, 6H, $N(CH_3)_2$), 6.63 (s, 5H, Cp).

Preparation of Poly(*N,N'*-di-*n*-hexylcarbodiimide), (poly-**HC**)

A modification of the procedure of Goodwin[82] was employed and all polymerizations in the bulk state were performed in a similar manner. In an inert recycling atmosphere dry box, a 10-mL scintillation vial was charged with 7.5 mg of bischloro-η^5-cyclopentadienyl-dimethylamido titanium(IV) ($CpCl_2TiN(CH_3)_2$, 0.033 mmol) catalyst and approximately 0.5 mL of dry toluene. A 1000 μL syringe was used to quickly inject the catalyst solution into a 20-mL scintillation vial that was charged with 1.0 g of *N,N'*-di-*n*-hexylcarbodiimide (4.75 mmol, monomer : catalyst = 144 : 1) and a vigorously stirring micro stir bar. The mixture stirred for 3.75 hours, at which point the solution had gelled. The gel was removed from the dry box and approximately 15 mL of toluene was added to solubilize the gel. In order to precipitate (ppt) the poly-**HC**, as well as remove residual monomer and/or catalyst, a 150 mL beaker was charged with 100 mL of methanol and a stir bar. To the rapidly stirring methanol, the solubilized gel was added dropwise and a white rope-like poly-**HC** ppt was observed. The poly-**HC** was filtered through Whatman #1 filter paper and dried at room temperature for 15 minutes.

A 100-mL round bottom flask was charged with the dried poly-**HC**, 50 mL of reagent grade benzene, and a stir bar. The poly-**HC** went into solution after 24 hours of stirring at room temperature. The solution was lyophilized yielding the poly-**HC** as a fluffy, solid white plug. The FTIR spectral data for poly-**HC** agreed with the literature[82] (KBr pellet) 2958 (s), 2873 (s), 2858 (s), 2929 (s), 1647 (s), 1467 (m), 1353 (m), 1285 (m), 1248 (m), 1210 (m), 1180 (m), 1106 (m).

Preparation of Poly(*N*-methyl-*N'*-(α-phenylethyl)carbodiimide)

A modification of the procedure of Goodwin[82] was employed and serves as a typical example of polymerizations carried out in scintillation vials. In an inert recycling atmosphere dry box (N_2), a micro stir bar was charged to a 4 ml scintillation vial containing 3.1 mL of *N*-methyl-*N'*-(α-phenylethyl)carbodiimide monomer (3 g, 18.7 mmol) and 1.0 mL of dry toluene. A 1.0 mL volumetric flask was charged with 40 mg of $CpCl_2TiN(CH_3)_2$ catalyst (175 μmol) and ~ 1 mL of toluene. To the rapidly stirring monomer solution, 350 μL of catalyst (14 mg, 61.4 μmol) solution was quickly injected from a 500 μL syringe (monomer:catalyst = 312:1, red solution). The rust red colored solution in the vial remained under rapid stirring at room temperature and gelled in 42 hours. The polymer was isolated from the viscous solution by charging ~ 15 mL of reagent grade THF and stirred for 24 hours. The mixture was precipitated in rapidly stirring methanol (70 mL). The polymer was dried under vacuum. Yield 2.87 g (93 %) FTIR spectral data and ^{1}H NMR agreed with literature.[82] Several molecular weights were prepared with yields of 72 - 98% obtained.

Measurement of the refractive index increment (dn/dc) of Poly(*N,N'*-di-*n*-hexylcarbodiimide) in THF

Five different concentrations of poly-**HC** (unknown molecular weight) in HPLC grade THF were prepared in 20-mL scintillation vials. Vial one was charged with 16.9 mg of poly-**HC** and 15.178 g of THF (17.07 mL) = 0.99 mg/mL. Vial two was charged

mg of poly-**HC** and 15.178 g of THF (17.07 mL) = 0.99 mg/mL. Vial two was charged with 22.4 mg of poly-**HC** and 13.357 g of THF (15.02 mL) = 1.49 mg/mL. Vial three was charged with 25.7 mg of poly-**HC** and 11.504 g of THF (12.94 mL) = 1.99 mg/mL. Vial four was charged with 37.0 mg of poly-**HC** and 13.329 g of THF (14.99 mL) = 2.47 mg/mL. Vial five was charged with 43.5 mg of poly-**HC** and 12.993 g of THF (14.61 mL) = 2.98 mg/mL. A micro stir bar was added to each vial and prior to taking measurements, the samples were stirred for 48 hours at approximately 30 °C. A Hakke water circulator thermostated to 25.0 °C ± 0.2 °C was connected to the Photal instrument's sample chamber. The Photal instrument's cuvette has two chambers; one reference and the other sample. Material was charged and removed from the cuvette with a long neck Pasteur pipette. One cycle equals a charge and removal of the sample. The cuvette was first washed with ten cycles in each chamber with THF. The Photal was zeroed with THF in both chambers. The left chamber was used for poly-**HC** solutions, while the right retained the THF reference. A poly-**HC** solution sample was charged to the left chamber for five cycles and the sample was allowed to equilibrate to temperature for ten minutes, at which point the dial measurement was taken. The remaining concentrations were measured following the five cycles/10 minute equilibrate procedure. The Photal calibration number was written on the instrument and used for all calculations; 4.9222×10^{-4} dn/ddial.

Measurement of the refractive index increment (dn/dc) of Poly(*N,N'*-di-*n*-hexylcarbodiimide) in toluene

The same procedure described for poly-**HC** in THF was used for determining the dn/dc for poly-**HC** in toluene. The concentration of the samples prepared were as follows: vial one was charged with 11.1 mg of poly-**HC** and 8.3132 g of toluene (9.611 mL) = 1.15 mg/mL; vial two was charged with 20.7 mg of poly-**HC** and 8.5343 g of toluene (9.866 mL) = 2.10 mg/mL; vial three was charged with 31.1 mg of poly-**HC** and 8.5945 g of toluene(9.936 mL) = 3.13 mg/mL; vial four was charged with 40.1 mg of

poly-**HC** and 8.4328 g of toluene (9.749 mL) = 4.11 mg/mL; vial five was charged with 55.5 mg of poly-**HC** and 8.6558 g of toluene (10.001 mL) = 5.55 mg/mL.

Measurements by Thin Layer Chromatography (TLC)

All measurements were performed using silica gel plates (20 cm x 20 cm) from Merck. The plates were 250 μm thick silica gel with 60 Å pore size and pre-treated with a fluorescing (λ=254 cm) material. All plates were dried for a minimum of 2 hours at 177 °C prior to analysis. All solvents were HPLC grade and used as received. The method of Iyengar et al.[6] was followed for measuring R_f values.

Measurement of Adsorption Isotherms and Kinetics

Silicon Wafers were obtained from International Wafer Service, 1" diameter, single sided polished/etched, 500-550 μm thick, and N-doped. The root-mean–square (rms) roughness was measured by tapping mode AFM to be 2 Å. The wafers were prepared by immersion in a volumetric blend of 30% H_2O_2 (30% v/v) and 70% concentrated H_2SO_4 for 45 minutes and rinsed vigorously three times in Milli-Q water. The preparation of Milli-Q water involves reverse osmosis, ion-exchange, and filtration steps (10^{18} Ω/cm). Prior to use, the silicon wafers for toluene adsorptions were dried in an oven (150 °C, 2 hours) and then allowed to cool to room temperature before submersion into the polymer solution. For adsorptions performed in THF, the silicon wafers were removed directly from water and immersed twice in Methanol followed by three immersions into anhydrous THF (distilled from sodium benzophenone dianion), each lasting 30 seconds. The samples were then vigorously shaken, dried by nitrogen jet, and placed into the polymer solution. All adsorptions for isotherm data were carried out for 24 hours in jacketed, Schlenk flasks attached to a water bath circulator set at 25.0 °C. All adsorption kinetics experiments were performed at room temperature in sealed Pyrex jars (number 1395) purchased from VWR. Post adsorption, all samples were vigorously

rinsed three times in their respective adsorption solvent, placed in a Schlenk pot, and vacuum dried for 12 h prior to XPS and contact angle measurements.

Spin Casting

Spin casting polymer solutions onto silicon wafers was performed on a Headway Research Inc., Photo-resist Spinner model 1-EC101D-R79 using a speed controller model EC102-NRD.

Results and Discussion

Preparation and Characterization of Polycarbodiimides

Two chemically equivalent polymers with different stereochemistries were chosen to study how changes in architecture affect their adsorption onto solid surfaces.

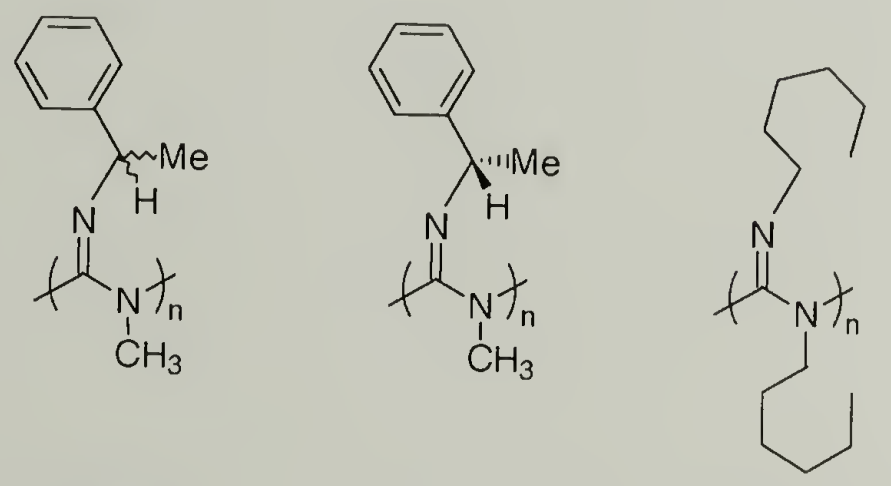

Poly-**R/S** Poly-**S** Poly-**HC**

Figure 1.9. The structure of racemic (poly-**R/S**), enantiomerically pure (poly-**S**) poly(*N*-methyl-*N'*-(α-phenylethyl)carbodiimide and poly(*N*,*N'*-di-*n*-hexylcarbodiimide) (poly–**HC**).

Goodwin[82] found by light scattering measurements that poly-**R/S** and poly-**S** (Fig. 1.9) formed worm-like and rigid rod conformations respectively. We also measured the refractive index increment for poly-**HC**. Adsorption experiments in the work presented here focused on poly-**R/S** and poly-**S**.

As previously mentioned, the polymerizations of poly-**R/S**, poly-**S**, and poly-**HC** were well controlled and gave high yields when the catalyst and monomer were purified just prior to polymerization. Lower yields were found for polymerizations carried out days after the purification of the catalyst and monomer. Prior to all polymerizations, the purity of monomer was checked by GC/MS while the catalyst was checked by ^{1}H NMR. The polymerizations were especially sensitive of any catalyst impurity. The impurities would poison the catalyst giving low polymer yields. The general polymerization scheme is shown in Scheme 1.4.

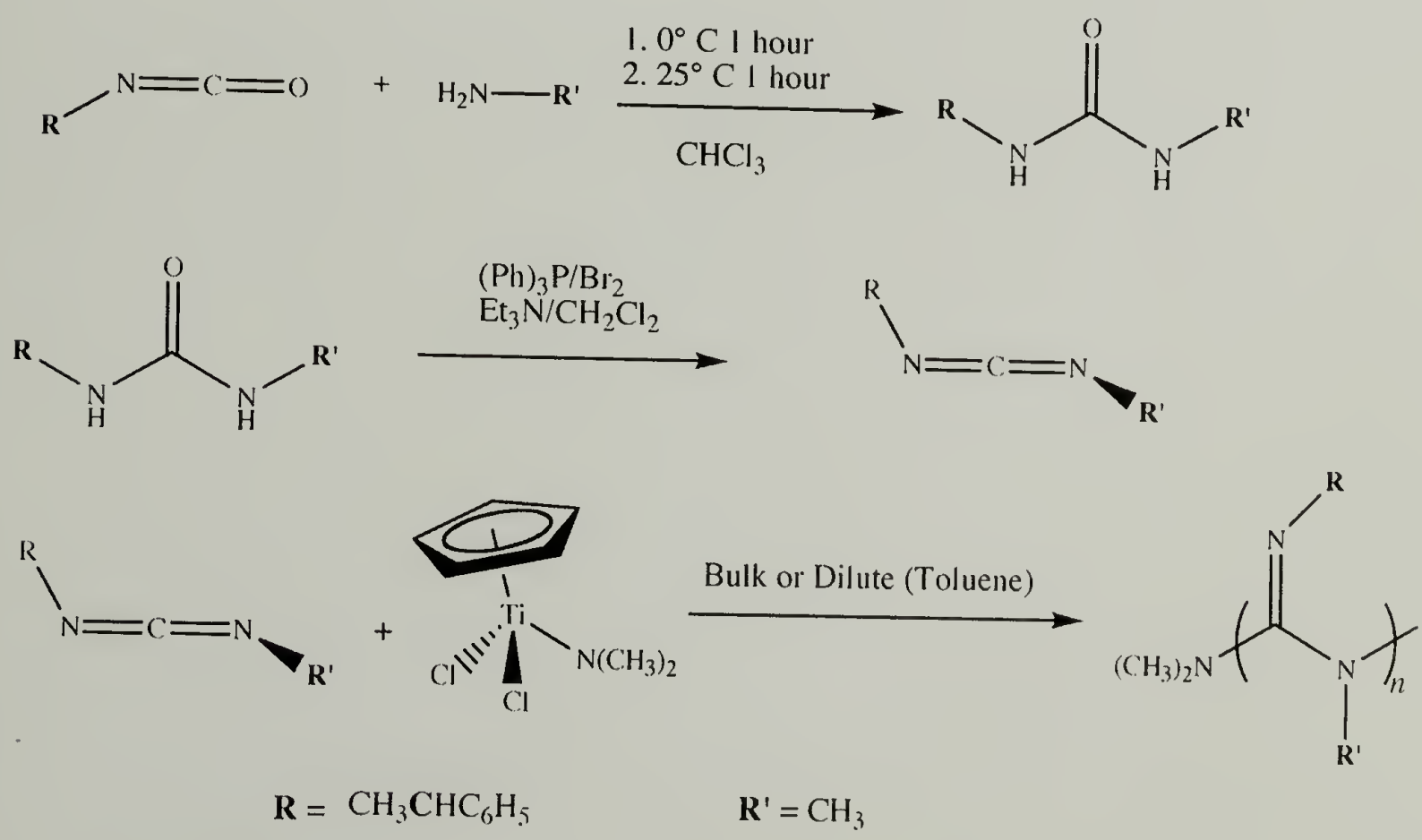

Scheme 1.4. General synthetic pathway to polycarbodiimides (example: Poly(*N*-methyl-*N'*-(α-phenylethyl)carbodiimide)

Analysis of the polymers by gel permeation chromatography (GPC) (relative to polystyrene standards) results in inflated polydispersities (Mw/Mn > 15).[77] Tandem GPC/LS has been used to determine molecular weights of these polymers as they elute over unusually large elution volumes as shown in Figures 1.10-1.12. Furthermore, this large elution volume is indicative of an interaction between the polymer and the column packing. To overcome these interactions, displacing solvents blended with THF were

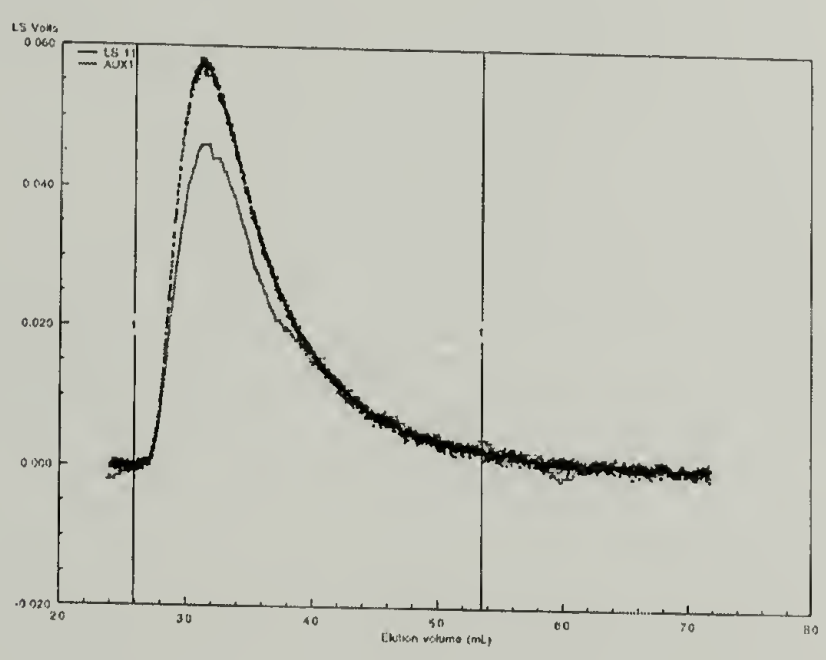

Figure 1.10. GPC/LS chromatogram of monomer:catalyst = 469:1 poly-**HC**. The bold curve is the chromatogram generated from the light scattering detector and the light curve is the chromatogram generated from the refractive index detector.

evaluated. It is difficult to perform GPC/LS on mixed solvent solutions.[171] Only recently has a technique been developed that demonstrates the use of a LS detector in mixed solvent HPLC.[172] Another technique that reduces solvent effects is evaporative light scattering. In this technique (also called evaporative mass detection, EMD), the eluent is nebulized and then passed through a heated tube to vaporize the mobile phase. Analytes less volatile than the mobile phase intersect a collimated light beam and the output is proportional to the amount of solute present over a wide concentration range. A

1 mg/mL solution of 250K poly-**R/S** in acetonitrile-THF (20:80) was resolved to a sharp unimodal peak over a short elution volume, as shown in Figure 1.13 and a Mw/Mn of 1.06 was determined.

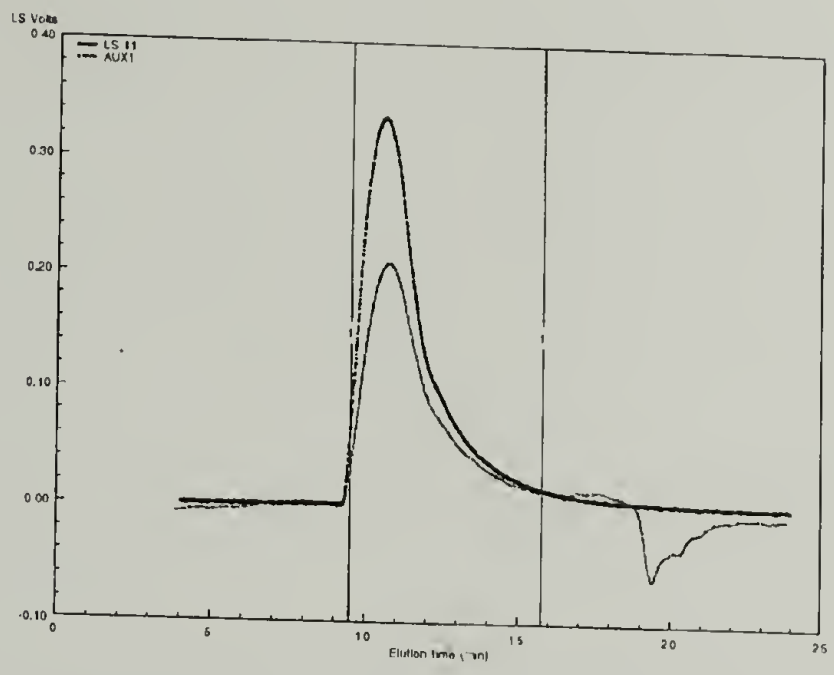

Figure 1.11. GPC/LS chromatogram of 3121:1 poly-**R/S**. The bold curve is the chromatogram generated from the light scattering detector and the light curve is the chromatogram generated from the refractive index detector.

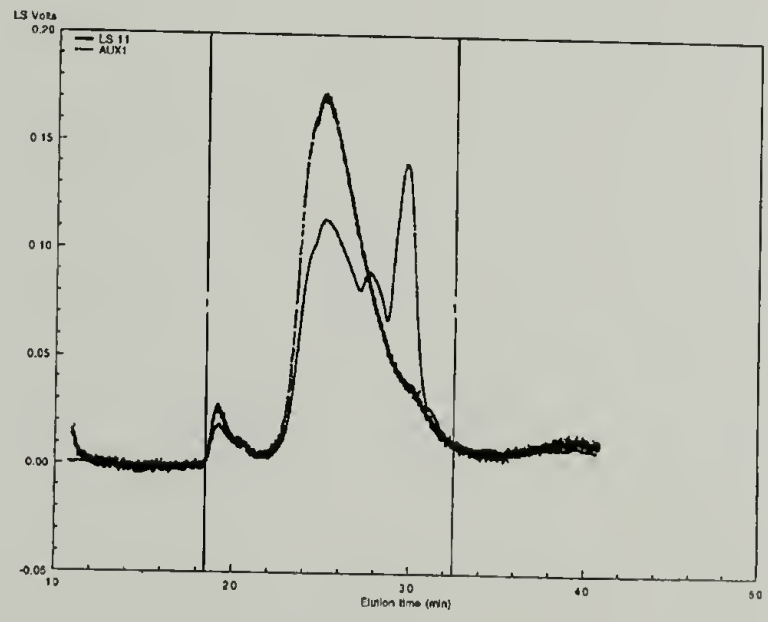

Figure 1.12. GPC/LS chromatogram of 1560:1 poly-**R/S**. The bold curve is the chromatogram generated from the light scattering detector and the light curve is the chromatogram generated from the refractive index detector.

Based on the results of GPC-EMD, we assumed that all polymerizations that follow the procedure used to synthesize the 250K poly-**R/S** would result in polymers with narrow polydispersities. Therefore, throughout this dissertation, the molecular weight of each polymer is reported using the monomer:catalyst ratio for example; 496:1 poly-**HC**.

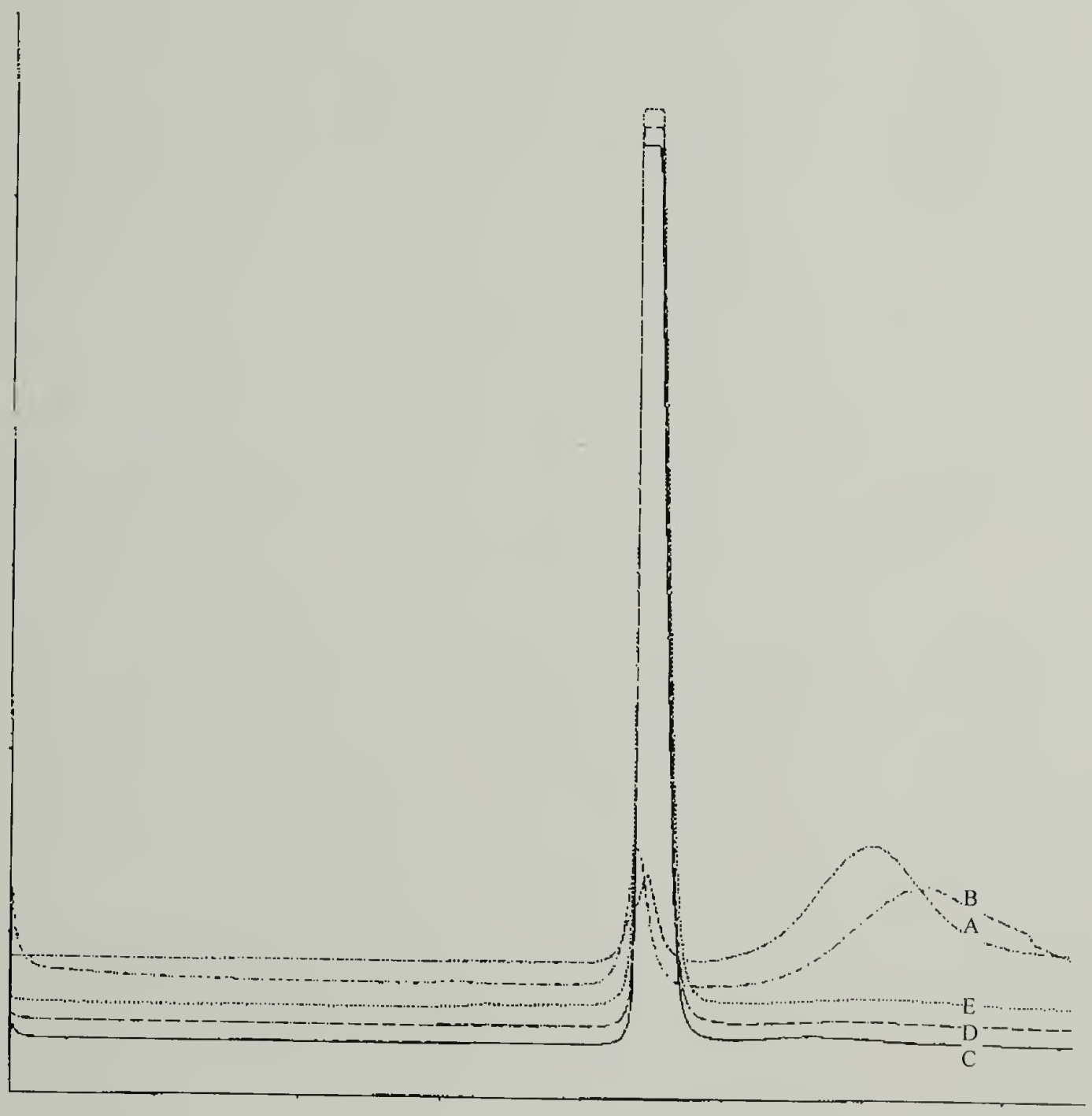

Figure 1.13. Evaporative Mass Detection chromatograms of 1560:1 poly-**R/S**; mobile phase ratio of solvent (THF)/displacer (acetonitrile), (A) 90/10 injection #1, (B) 90/10 injection #2, (C) 80/20 injection #1, (D) 80/20 injection #2, (E) 80/20 injection #3.

Prior to performing GPC/LS on 496:1 poly-**HC**, the refractive index increment (dn/dc) was determined using the Photal Refractometer. The results of two trials performed from THF at 25 °C can be found listed in Table 1.1. Certain data points were determined to be outlier points (*), and were not included in calculating the dn/dc value. These outlier data points were most likely the result of concentration fluctuations from either solvent evaporation and/or incomplete flushing of the previous sample. Linear regression analysis of the data (Fig. 1.14) resulted in a dn/dc value of 0.0992 mL/g at 25 °C and 632.8 nm. The recommended linear correlation, r, for the data was $r \geq 0.9995$ ($r^2 \geq 0.9990$) and the result for trial one was r = 0.99997 and trial two was r = 0.99963. Therefore, the results show nearly perfect linear correlation.[173] The average of trial one, 0.0992 mL/g, and trial two, 0.0979 mL/g, gave a dn/dc for poly-**HC** of 0.0986 mL/g. In toluene, poly-**HC** was iso-refractive because no change in refractive index was measured with change in concentration.

Table 1.1. Data generated from measuring the change in refractive index with concentration using the Photal Refractometer. The data are plotted in Figure 1.14.

Dial reading	Dial reading multiplied by constant 0.00049222 dn/ddial	Conc. g/mL dc
Trial One		
0	0	0*
0.221	1.088E-4	9.9E-4
0.32	1.578E-4	1.49E-3
0.42	2.067E-4	1.99E-3
0.495	2.437E-4	2.47E-3*
0.622	3.062E-4	2.98E-3
Trial Two		
0	0	0
0.228	1.122E-4	9.9E-4*
0.31	1.526E-4	1.49E-3
0.398	1.959E-4	1.99E-3
0.489	2.407E-4	2.47E-3
0.597	2.939E-4	2.98E-3

Thin Film Chromatography

Prior to performing adsorption experiments with poly-**R/S**, several solvents were evaluated for their solvation quality. This was accomplished by thin film chromatography following procedures described in the doctoral thesis of Iyengar.[174] The

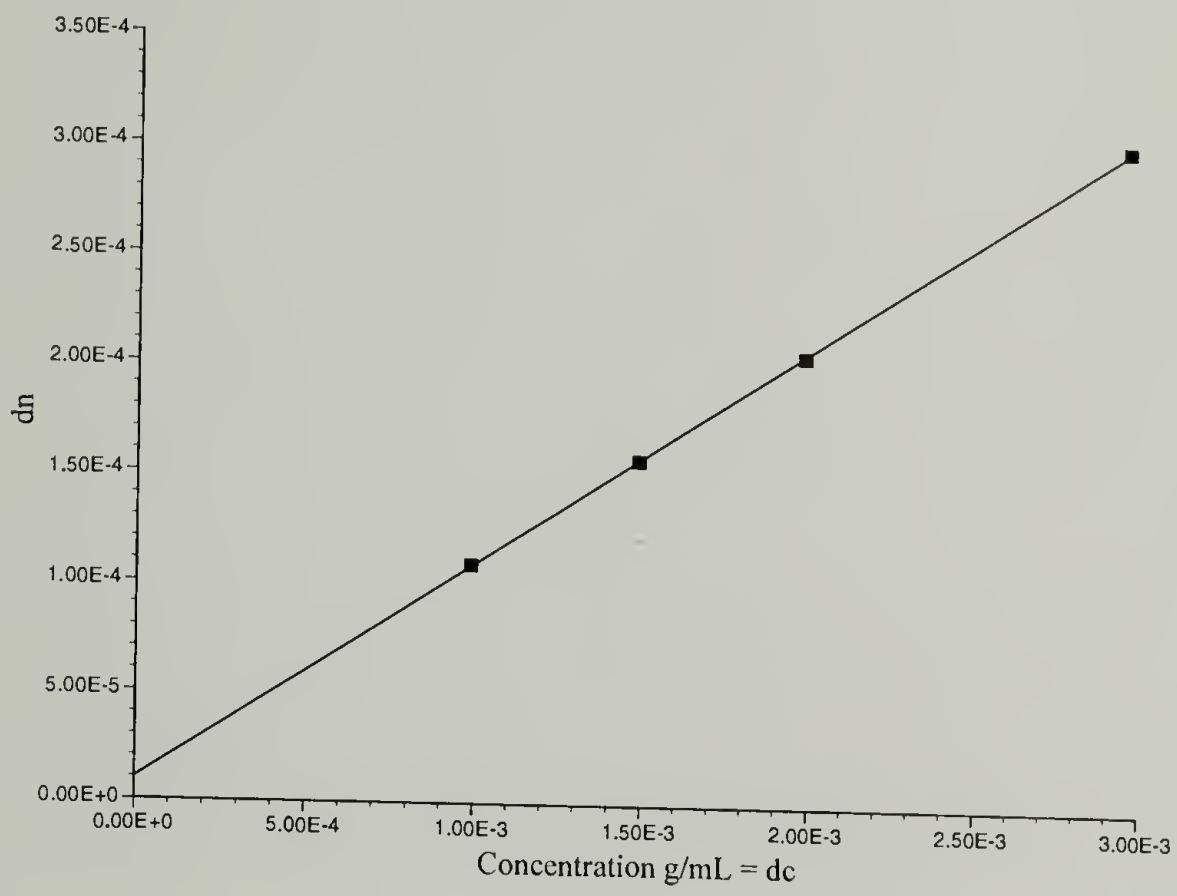

Figure 1.14. Trial one, refractive index increment (dn/dc) plot of the change in refractive index, dn, with concentration, dc (g/mL), for poly-HC 469:1 at 25 °C and λ = 632.8 nm. The slope gives a dn/dc value of 0.992 mL/g.

R_f values were measured for several molecular weights on both neutral silica and alumina plates with the results shown in Table 1.2. Only THF resulted in a measurable R_f value because the solvation kinetics of poly-**R/S** in THF was on the time scale of the experiment. The polycarbodiimides were found soluble in all the solvents tested except hexane. Because of the slow solvation kinetics, most of the solvents resulted in R_f values of zero. Interestingly, the THF results on silica show a greater independence between

solvent quality and molecular weight than measured for alumina. From the TLC results, we concluded that initial adsorption experiments for poly-**R/S** were to be performed from

Table 1.2. The results from screening solvent quality effects on different molecular weights of poly-**R/S** by thin film chromatography.

Solvent (Plate)	Monomer: catalyst	Rf	Solvent (Plate)	Monomer: catalyst	Rf
THF (silica)	292:1	0.78	Ethyl acetate (silica)	292:1	-
	335:1	0.79		335:1	-
	400:1	0.78		400:1	-
	715:1	0.79		715:1	-
	1340:1	0.74		1340:1	-
	4767:1	0.63		4767:1	-
THF (alumina)	292:1	0.89	Ethyl acetate (alumina)	292:1	-
	335:1	0.89		335:1	-
	400:1	0.90		400:1	-
	715:1	0.91		715:1	-
	1340:1	0.78		1340:1	-
	4767:1	0.70		4767:1	-
Toluene (silica)	292:1	0	Methylene chloride (silica)	292:1	0
	335:1	0		335:1	0
	400:1	0		400:1	0
	715:1	0		715:1	0
	1340:1	0		1340:1	0
	4767:1	0		4767:1	0
Toluene (alumina)	292:1	0	Benzene (silica)	292:1	0
	335:1	0		335:1	0
	400:1	0		400:1	0
	715:1	0		715:1	0
	1340:1	0		1340:1	0
	4767:1	0		4767:1	0
Chloroform (silica)	292:1	0	Hexane's (insoluble)	292:1	-
	335:1	0		335:1	-
	400:1	0		400:1	-
	715:1	0		715:1	-
	1340:1	0		1340:1	-
	4767:1	0		4767:1	-

toluene. Generally, the poorer solvent condition has been shown to increase the adsorbed amount of most polymers.[1,175] Since one of the objectives of the research presented here was to study how chain architecture affects adsorption, the poorer solvent condition was favored.

Polymer Adsorption: Base Line

Prior to measuring the adsorption isotherms, bulk films prepared by spin casting were characterized. With these samples, the objective was to characterize a homogeneous thin film of polycarbodiimide by the techniques to be used to analyze adsorbed thin films. Ellipsometry was used to measure the relative film thickness of 4681:1 poly-**R/S** spin-cast on cleaned silicon oxide. An iterative algorithm was used to calculate the thickness of approximately 300 Å (Table 1.3) and refractive indices between 1.61 and 1.63. The molecular weight dependent contact angle hysteresis shown in Table 1.4 suggests differences in surface roughness. In addition, the water contact angle data indicate substantial differences between the hydrophilic native silicon oxide and the hydrophobic poly-**R/S**.

Table 1.3. Thickness measurements by Ellipsometry of a thin film prepared by spin–casting a solution of 4681:1 poly-**R/S** in toluene onto native silicon oxide. Note, RI is refractive index.

Sample #	Delta	Psi	Thickness	RI
1000 rpm	111.84	16.52	278 A	1.613
	111.96	16.44	275 A	1.626
	109.80	17.08	297 A	1.594
	111.00	16.80	288 A	1.593
AVG			285 A	1.607
500→2000 rpm	94.52	21.16	411 A	1.636
	97.20	20.28	387 A	1.623
	98.80	19.84	374 A	1.630
	96.56	20.60	396 A	1.623
	98.52	19.92	376 A	1.630
AVG			389 A	1.628

Table 1.4. Water contact angle measurements performed on a thin film prepared by spin–casting a solution of 4681:1 poly-**R/S** in toluene onto native silicon oxide.

Sample Monomer:catalyst	θ_A H_2O	θ_R H_2O
Native Silicon Oxide	32°	14°
399:1	112°	87°
4681:1	110°	61°

Analysis by XPS of these spin-cast films resulted in the survey spectrum shown in Figure 1.15. The chemical composition of the polycarbodiimides used for this research contained only carbon, hydrogen, and nitrogen. Thus, the survey spectrum (at 75° take-off angle) for the spin-cast thin film of poly-**R/S** (from solution in toluene) shows the presence of nitrogen and carbon from the polymer as well as a small amount of oxygen. At 15° take-off angle, there was no oxygen detected and it is difficult to determine if the oxygen is from the silica surface, since no silicon was detected. Measurements of the atomic concentration for each element was performed by angle dependent XPS.

Shown in Figure 1.16, is the multiplex spectrum for carbon at 75° take-off angle. The carbon 1s is the most intense peak at the binding energy of 284.3 eV. In addition, there is a shoulder at 285.5 eV and a more pronounced shoulder between 286.3 eV and 288.3 eV. Also evident is the π-π^* interaction (called a shakeup peak) of the phenyl rings as indicated by the weak intensity at 290.3 eV. The various binding energies are associated with the different electronic states of carbon and the ratio of carbons in different electronic states was determined by a curve-fitting algorithm as demonstrated in Figure 1.17. As the environment around carbon becomes more electronegative, the binding energy increases. This is revealed by the three different electronic states for carbon as shown by the letters A and B, with C referring to the remaining carbons.

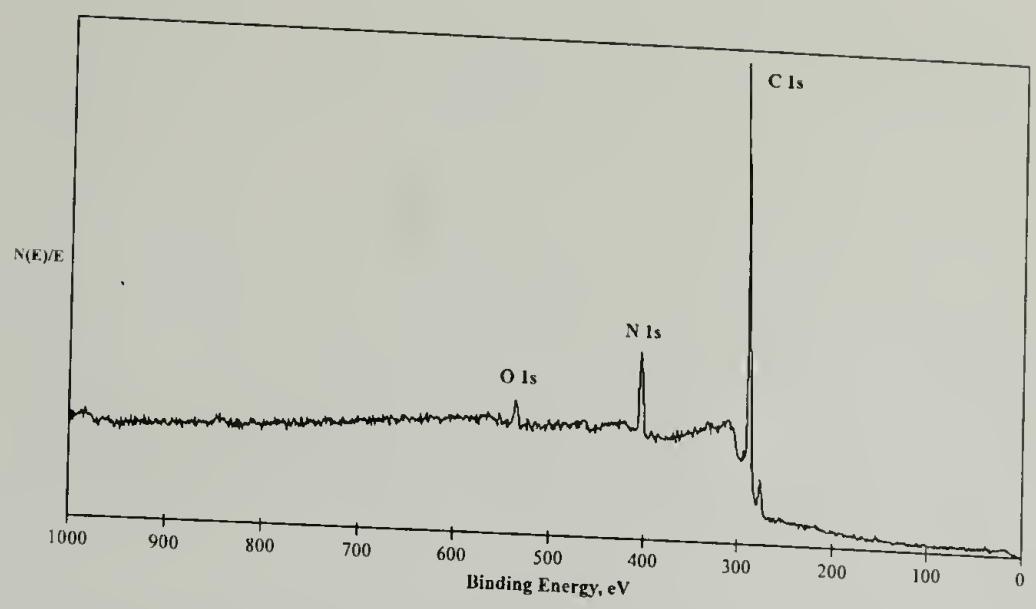

Figure 1.15. XPS survey spectrum (75° take-off angle) of a thin film prepared by spin–casting a solution of 4681:1 poly-**R/S** in toluene onto native silicon oxide.

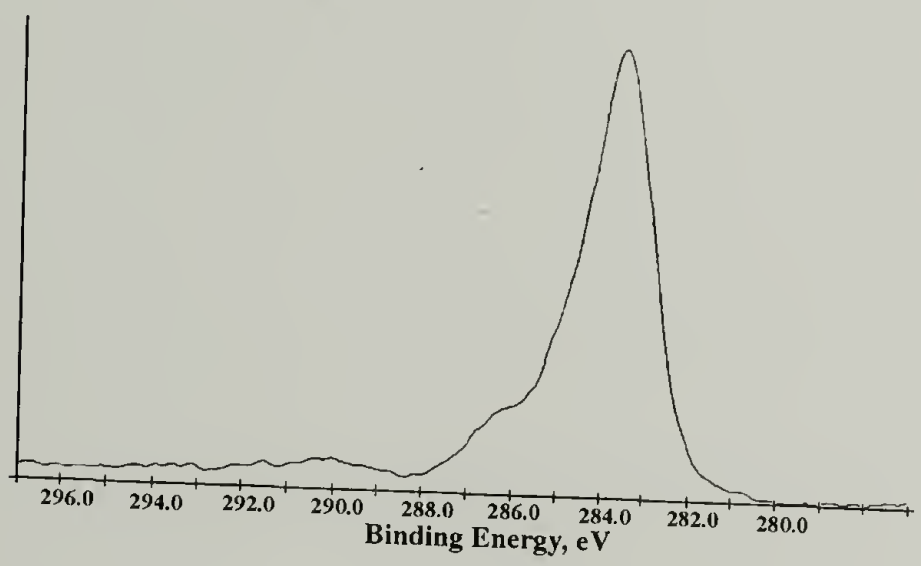

Figure 1.16. XPS multiplex spectrum (75° take-off angle) of the [C_{1s}] region of a thin film prepared by spin-casting a solution of 4681:1 poly-**R/S** in toluene onto native silicon oxide.

The nitrogen 1s region multiplex spectrum at 75° take-off angle is shown in Figure 1.18, with the spectrum showing two peaks due to the different electronic states of the two nitrogen's in poly-**R/S**. The peak assignments were determined by comparing spectra between poly-**R/S** and poly(isocyanides), with these results indicating that the binding energy for the two nitrogen's are 399.4 eV for the imine and 401.2 eV for the tertiary amine functionality.

Reported in Table 1.5 are the atomic concentrations calculated from angle–dependent XPS measurements of the spin-cast samples. The results confirmed the presence of poly-**R/S** on the spin-cast substrates due to the presence of nitrogen. Furthermore, for the repeat unit for poly-**R/S** and poly-**S**, the ratio of carbon to nitrogen should approach 5:1. Included with the ratio of carbon to nitrogen is that of silicon to nitrogen, which was used to indicate complete coverage of the substrate as the ratio approached zero. However, the complete attenuation of the Si 2p at both 15° and 75° take-off angles indicated that the films prepared with the higher molecular weight polymer were thicker. As previously mentioned, since the mean free path for poly-**R/S** was not available, we assumed that a 15° and 75° take-off angles measured the surface's

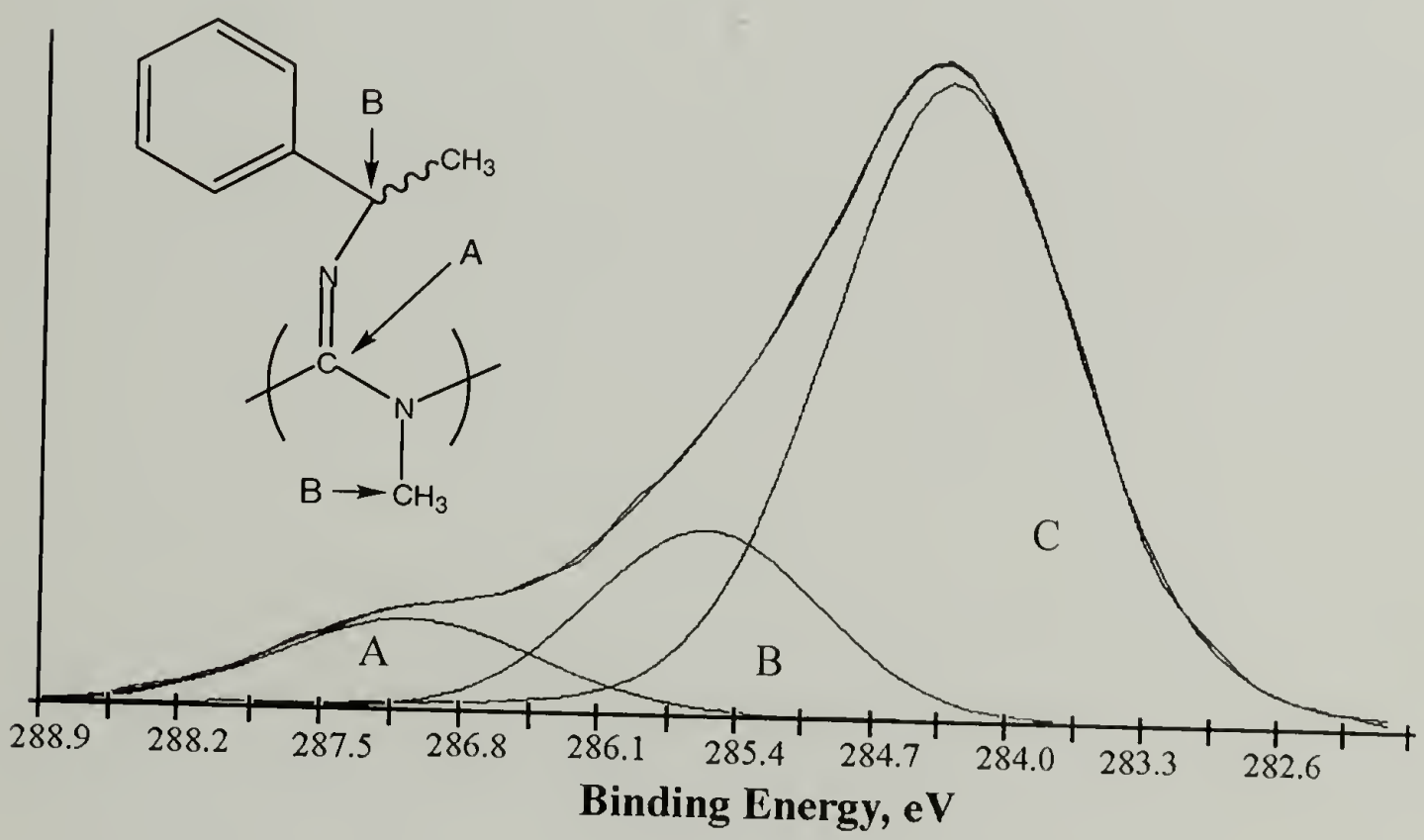

Figure 1.17. XPS curve fit of the C_{1s} region for 4681:1 poly–**R/S** where region A is the imine carbon (9.74%), region B is the *N* and *N'* carbons (18.12%), and region C is the phenyl and 1-methyl carbons (72.14%).

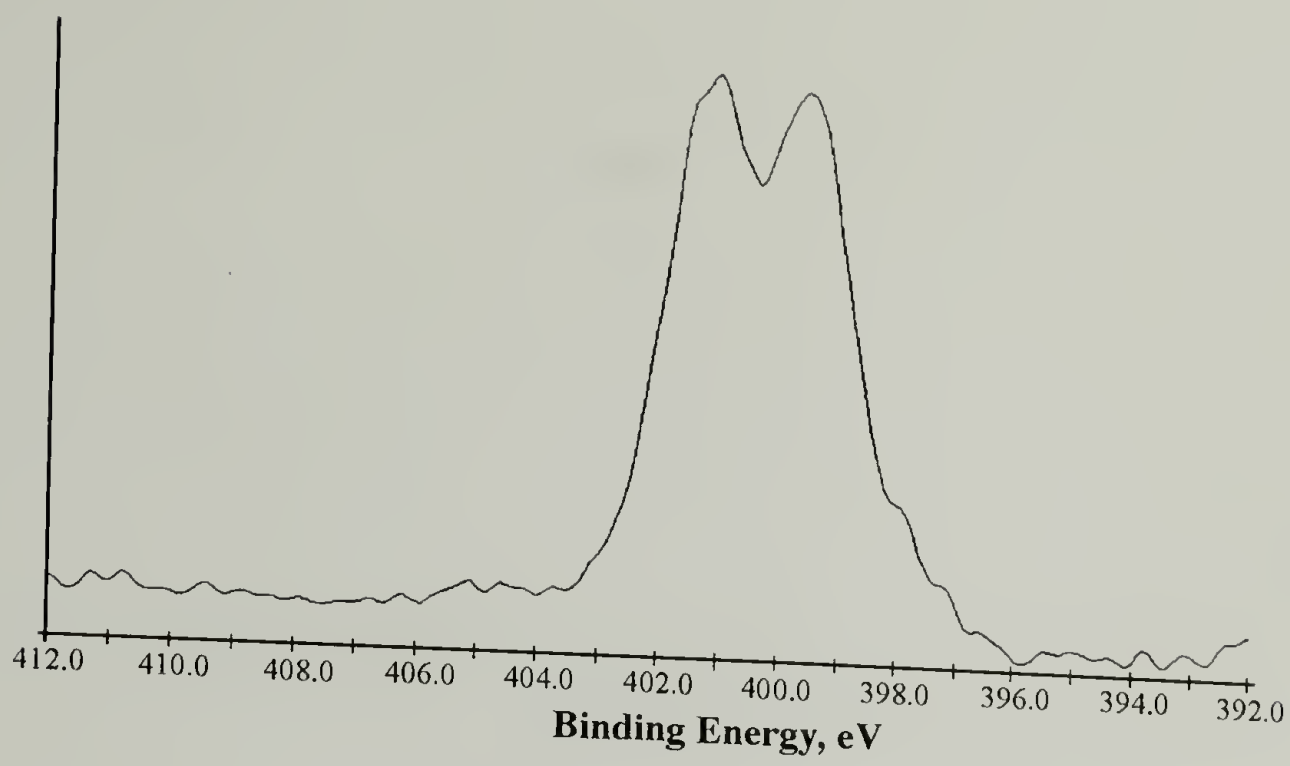

Figure 1.18. XPS multiplex spectrum (75° take-off angle) of the N_{1s} region of a thin film prepared by spin-casting a solution of 4681:1 poly-**R/S** in toluene onto native silicon oxide.

Table 1.5. XPS atomic concentration results of thin films prepared from solution of poly–**R/S** in toluene spin-casted onto native silicon oxide.

Sample Monomer:catalyst	$C_{15°}$	$N_{15°}$	$O_{15°}$	$Si_{15°}$	C:N	Si:N
Native Silicon Oxide	13.50	-	66.45	20.05	-	-
399:1	68.66	8.18	14.71	8.45	8.39	1.03
4681:1	85.66	14.34	-	-	5.97	-

Sample Monomer:catalyst	$C_{75°}$	$N_{75°}$	$O_{75°}$	$Si_{75°}$	C:N	Si:N
Native Silicon Oxide	4.41	-	53.58	42.01	-	-
399:1	74.12	13.65	8.77	3.45	5.43	0.25
4681:1	83.62	16.38	-	-	5.11	-

outer 10 Å and 40 Å, respectively. With this qualification, an estimation of film thickness was possible. However, this assumption was later found to be flawed due to dewetting of the polymer thin film (vide infra). The dewetting was not discovered until

later in this research, therefore, it was assumed that adsorption experiments could be accurately characterized by contact angle and XPS.

Adsorption Isotherm Measurements for poly-**R/S** and poly-**S**

The first experiments carried out were to evaluate the tendency for poly-**R/S** and poly-**S** to adsorb on native silicon oxide. This was accomplished by measuring the adsorption isotherm for each polymer spanning an order of magnitude in molecular weights. We first determined the affinity for poly-**R/S** to adsorb onto native silicon oxide by measuring the concentration dependence on adsorption. The adsorbed amount was measured by XPS and using the atomic concentration of $[N_{1s}]$, adsorption isotherms where generated. The methodology used measured the adsorbed amount of polymer at the substrate interface as a function of concentration for 24 hours at 25 °C. In addition to XPS, water contact angle analysis was performed on each sample.

Two molecular weights were analyzed and the results for the 4681:1 poly-**R/S** are found in Tables 1.6 and 1.7, and for the 312:1 poly-**R/S** in Tables 1.8 and 1.9. The data indicate that the adsorption for both molecular weight samples of poly-**R/S** from solution in toluene onto native silicon oxide has high affinity character. This is supported by the rapid increase in the adsorbed amount with solution concentration and by the quick generation of a plateau region in the adsorption isotherms shown in Figure 1.19. At 15° take-off angle, the $C_{15°}$:$N_{15°}$ data (Tables 1.6 and 1.8) does not indicate a significant difference (except at the lowest solution concentration) in the adsorbed amount between the two molecular weights, however differences were evident at 75° take-off angle. These differences suggest that a thinner adsorbed layer formed with the 312:1 poly-**R/S**. Contact angle results indicate differences in film structure, because the lower θ_A/θ_R measured (Table 1.9) for the 312:1 poly-**R/S** is a result of interaction between the probe fluid, polymer, and the silicon surface. As for the 4681:1 poly-**R/S**, these interactions with silica were not observed.

During the synthesis of poly-**S,** it became apparent that the purification process was limited to THF due to slow solvation kinetics in toluene. Over a period of two weeks, the poly-**S** did not completely dissolve in toluene. Therefore, lyophilization from

Table 1.6. XPS atomic concentration results of thin films of 4681:1 poly-**R/S**, adsorbed from toluene, on native silicon oxide. The adsorptions were performed at the concentrations listed.

Conc. mg/mL	$C_{15°}$	$N_{15°}$	$O_{15°}$	$Si_{15°}$	C:N	Si:N
0.0005	69.45	9.17	12.18	9.20	7.6:1	1.0:1
0.002	78.73	12.24	4.96	4.06	6.4:1	0.3:1
0.005	81.90	12.58	2.87	2.65	6.5:1	0.2:1
0.008	76.62	11.26	6.55	5.57	6.8:1	0.5:1
0.02	82.81	13.52	2.08	1.59	6.1:1	0.1:1
0.06	82.06	12.67	2.65	2.62	6.5:1	0.2:1
0.20	86.55	13.45	-	-	6.4:1	-
0.60	85.81	14.19	-	-	6.0:1	-

Conc. mg/mL	$C_{75°}$	$N_{75°}$	$O_{75°}$	$Si_{75°}$	C:N	Si:N
0.0005	30.10	5.38	35.68	28.83	5.6:1	5.4:1
0.002	42.94	8.49	26.54	22.03	5.1:1	2.6:1
0.005	48.57	9.31	22.20	19.93	5.2:1	2.1:1
0.008	39.45	7.67	28.29	24.59	5.1:1	3.2:1
0.02	56.00	10.83	18.28	14.89	5.2:1	1.4:1
0.06	48.64	9.95	22.88	18.53	4.9:1	1.9:1
0.20	58.91	11.89	15.22	13.98	5.0:1	1.2:1
0.60	56.07	10.97	16.52	15.22	5.1:1	1.4:1

Table 1.7. Contact angle (probe fluid, H_2O) measurements of thin films of 4681:1 poly–**R/S**, adsorbed from toluene, on native silicon oxide. The adsorptions were performed at the concentrations listed.

Conc. mg/mL	θ_A H_2O	θ_R H_2O
0.0005	92°	66°
0.002	91°	78°
0.005	91°	76°
0.008	93°	74°
0.02	93°	69°
0.06	92°	73°
0.2	92°	76°
0.6	93°	76°

Table 1.8. XPS atomic concentration results of thin films of 312:1 poly-**R/S**, adsorbed from toluene, on native silicon oxide. The adsorptions were performed at the concentrations listed.

Conc. mg/mL	$C_{15°}$	$N_{15°}$	$O_{15°}$	$Si_{15°}$	C:N	Si:N
0.0005	40.82	-	40.11	19.07	-	-
0.002	78.17	10.87	6.88	4.08	7.2:1	0.4:1
0.008	80.20	13.76	3.66	2.38	5.8:1	0.2: 1
0.02	73.76	9.24	11.16	5.84	8.0:1	0.6:1
0.2	85.29	12.08	2.63	0	7.1:1	-
0.4	84.63	11.84	2.83	0.7	7.1:1	0.06:1
0.8	83.99	11.58	3.30	1.14	7.3:1	0.1:1
1.2	82.61	12.34	3.66	1.39	6.7:1	0.1:1

Conc. mg/mL	$C_{75°}$	$N_{75°}$	$O_{75°}$	$Si_{75°}$	C:N	Si:N
0.0005	12.24	0.61	50.82	36.34	20:1	60:1
0.002	38.68	6.79	30.75	23.78	5.7:1	3.5:1
0.008	49.20	9.25	22.66	18.89	5.3:1	2.0:1
0.02	38.91	5.51	25.36	30.21	7.1:1	5.5:1
0.2	70.64	13.79	8.67	6.90	5.1:1	0.5:1
0.4	75.03	11.90	5.95	7.12	6.3:1	0.6:1
0.8	72.14	10.42	7.13	10.31	6.9:1	1.0:1
1.2	69.24	11.00	9.11	10.66	6.3:1	1.0:1

Table 1.9. Contact angle (probe fluid, H_2O) measurements of thin films of 312:1 poly–**R/S**, adsorbed from toluene, on native silicon oxide. The adsorptions were performed at the concentrations listed.

Conc. mg/mL	$\theta_{A\ Water}$	$\theta_{R\ Water}$
0.0005	46°	15°
0.002	84°	52°
0.008	78°	47°
0.02	95°	59°
0.2	61°	22°
0.4	95°	73°
0.8	95°	71°
1.2	96°	73°

benzene was not performed, and the poly-**S** and poly-**R/S** were purified by several precipitations in methanol. Since the objective was to characterize the adsorption of two chemically identical polymers that were different in solution conformation, we changed the solvent for adsorption experiments from toluene to THF.

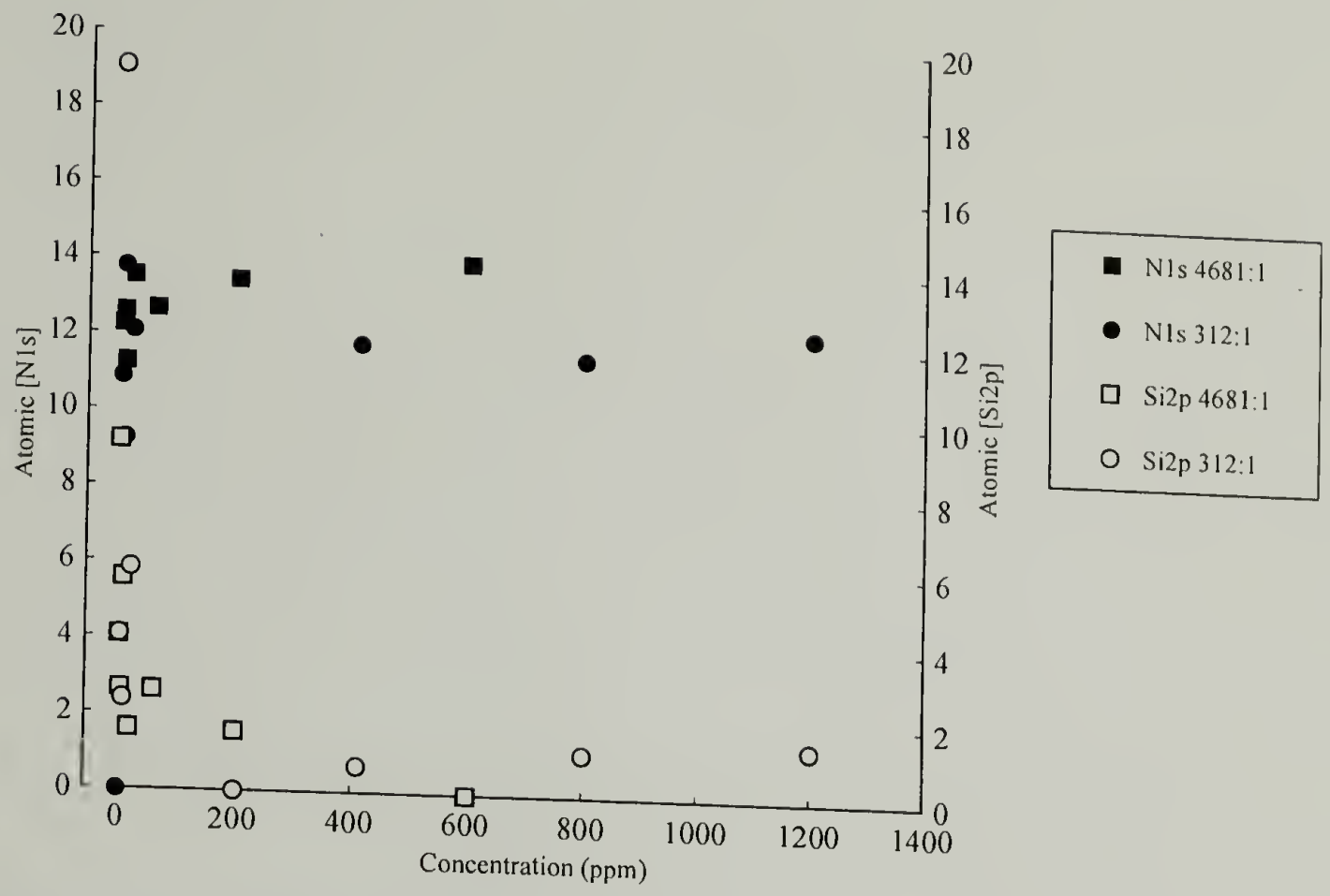

Figure 1.19. Combined adsorption isotherms for 4681:1 poly-**R/S** and 312:1 poly–**R/S** showing the gain in N_{1s} concentration with the subsequent attenuation of Si_{2p} concentration. The atomic concentrations were determined by XPS at 15° take-off angles of adsorbed films prepared by adsorbing poly-**R/S** from solution in toluene onto native silicon oxide for 24 hours at T=25 °C. Concentration is in ppm = mg/mL x 10^3

The study of molecular weight effects on adsorption were performed using poly–**R/S** and poly-**S** that differed in molecular weight (monomer:catalyst; 312:1 and 3121:1) by an order of magnitude. In addition, for both poly-**R/S** and poly-**S** a molecular weight (monomer:catalyst; 936:1) between the extremes was prepared. Adsorption isotherms for each molecular weight of poly-**R/S** and poly-**S** were measured and the data is shown in Tables 1.10 through 1.15 and Figures 1.20 through 1.22.

The adsorption isotherms (Fig. 1.20-1.22) indicate that poly-**S** has a higher affinity for the surface than poly-**R/S**. Though both polymers are chemically equivalent, the segment-surface interaction parameter is influenced by the conformation and stereochemistry of adjacent segments along the polymer chain. For example, intuitively the poly-**S** should contain fewer variations in local segmental stereochemistry whereas

more variations are possible for poly-**R/S**. It is these small ill-regularities in the form of enantiomeric side chains that introduce kinks into the polymer backbone and distorts the conformation of poly-**R/S** from rods to worms.[80] In addition, the segment-solvent interaction may be influence by the above mentioned local segmental variations.

Table 1.10. Adsorption isotherm data for the adsorption of 312:1 poly-**R/S** from THF to native silicon oxide for 24 hours at 25 °C. Listed are the atomic concentration data from XPS analysis at 15° and 75° take-off angles and the contact angle (probe fluid, H_2O) results where θ_A is the advancing contact angle and θ_R the receding angle. The solution concentration is in both mg/mL and ppm which equals mg/mL x 10^3. The data are plotted in the adsorption isotherm shown in Figure 1.20.

312:1 POLY-**R/S** mg/mL THF (ppm)	$C_{15°}$	$N_{15°}$	$O_{15°}$	$Si_{15°}$	C:N	Si:N	θ_A	θ_R
Control	30.06	-	55.27	14.67	-	-	13°	9°
0.0005 (0.5)	29.97	2.12	54.17	13.74	14.1 : 1	6.5 : 1	38°	16°
0.02 (20)	45.35	3.90	40.79	9.96	11.6 : 1	2.6 : 1	49°	16°
0.04 (40)	55.74	5.69	30.34	8.23	9.8 : 1	1.4 : 1	52°	17°
0.08 (80)	49.79	6.96	34.16	9.10	7.2 : 1	1.3 : 1	47°	19°
0.20 (200)	49.85	6.41	34.59	9.15	7.8 : 1	1.4 : 1	74°	23°
0.43 (430)	56.83	9.47	26.59	7.11	6.0 : 1	0.8 : 1	80°	23°
0.80 (800)	55.68	9.61	27.33	7.38	5.8 : 1	0.8 : 1	71°	16°
1.20 (1200)	58.98	11.25	23.35	6.41	5.2 : 1	0.6 : 1	68°	23°

312:1 POLY-**R/S** mg/mL THF (ppm)	$C_{75°}$	$N_{75°}$	$O_{75°}$	$Si_{75°}$	C:N	Si:N
Control	8.36	-	47.52	44.12	-	-
0.0005 (0.5)	9.21	0.70	44.34	45.74	13.0 : 1	65 : 1
0.02 (20)	15.98	2.14	39.80	42.00	7.5 : 1	20 : 1
0.04 (40)	19.57	2.33	42.45	35.64	8.3 : 1	15 : 1
0.08 (80)	13.95	2.98	44.28	38.78	4.7 : 1	13 : 1
0.20 (200)	20.10	3.57	40.67	35.67	5.6 : 1	10 : 1
0.43 (430)	23.53	4.13	38.92	33.42	5.7 : 1	8.1 : 1
0.80 (800)	21.59	4.63	38.87	34.92	4.7 : 1	7.5 : 1
1.20 (1200)	25.90	5.08	35.73	33.29	5.1 : 1	6.6 : 1

Therefore, the difference in the adsorbed amounts may be due to both the conformation of the solvent-swollen polymer and the influence of the conformation of local segments adjacent to the adsorbed segment. Earlier in this chapter, it was described that THF is a

much better solvent than toluene for both polymers. In THF, poly-**R/S** dissolved within minutes, whereas, the poly-**S** went into solution within 24 hours which indicates the solvating quality of THF is better for poly-**R/S** than poly-**S**. This suggests that in THF the hydrodynamic size of poly-**R/S** is larger than poly-**S**. Assuming equal molecular weight, the surface area covered by adsorbed poly-**R/S** would be less than poly-**S**, resulting in more poly-**S** adsorbing than poly-**R/S**.

Table 1.11. Adsorption isotherm data for the adsorption of 312:1 poly-**S** from THF to native silicon oxide for 24 hours at 25 °C. Listed are the atomic concentration data from XPS analysis at 15° and 75° take-off angles and the contact angle (probe fluid, H_2O) results where θ_A is the advancing contact angle and θ_R the receding angle. The solution concentration is in both mg/mL and ppm which equals mg/mL x 10^3. The data are plotted in the adsorption isotherm shown in Figure 1.20.

312:1 POLY-**S** mg/mL THF (ppm)	$C_{15°}$	$N_{15°}$	$O_{15°}$	$Si_{15°}$	C:N	Si:N	θ_A	θ_R
0.0005 (0.5)	24.34	0.50	58.39	16.76	48.7 : 1	34 : 1	30°	11°
0.005 (5)	28.72	0.91	55.89	14.47	31.6 : 1	16 : 1	32°	12°
0.01 (10)	26.81	1.24	57.50	14.45	21.6 : 1	12 : 1	34°	12°
0.05 (50)	31.29	2.64	53.12	12.95	11.9 : 1	5.0 : 1	37°	7°
0.11 (110)	54.79	9.61	27.94	7.66	5.7 : 1	0.8 : 1	38°	12°
0.52 (520)	59.02	10.32	25.44	5.22	5.7 : 1	0.5 : 1	43°	6°
1.03 (1030)	63.82	10.28	20.85	5.06	6.2 : 1	0.5 : 1	46°	8°
1.53 (1530)	60.24	9.13	23.99	6.64	6.6 : 1	0.7 : 1	46°	7°

312:1 POLY-**S** mg/mL THF (ppm)	$C_{75°}$	$N_{75°}$	$O_{75°}$	$Si_{75°}$	C:N	Si:N
0.0005 (0.5)	6.59	0.05	48.04	45.31	132 : 1	906 : 1
0.005 (5)	7.63	0.13	47.74	44.51	58.7 : 1	342 : 1
0.01 (10)	7.82	0.27	48.33	43.58	29.0 : 1	161 : 1
0.05 (50)	12.11	1.12	46.82	39.95	10.8 : 1	36 : 1
0.11 (110)	24.96	3.98	38.63	32.43	6.3 : 1	8.1 : 1
0.52 (520)	36.00	6.02	30.01	27.97	6.0 : 1	4.6 : 1
1.03 (1030)	33.66	6.10	33.51	26.73	5.5 : 1	4.4 : 1
1.53 (1530)	28.79	5.22	35.87	30.13	5.5 : 1	5.8 : 1

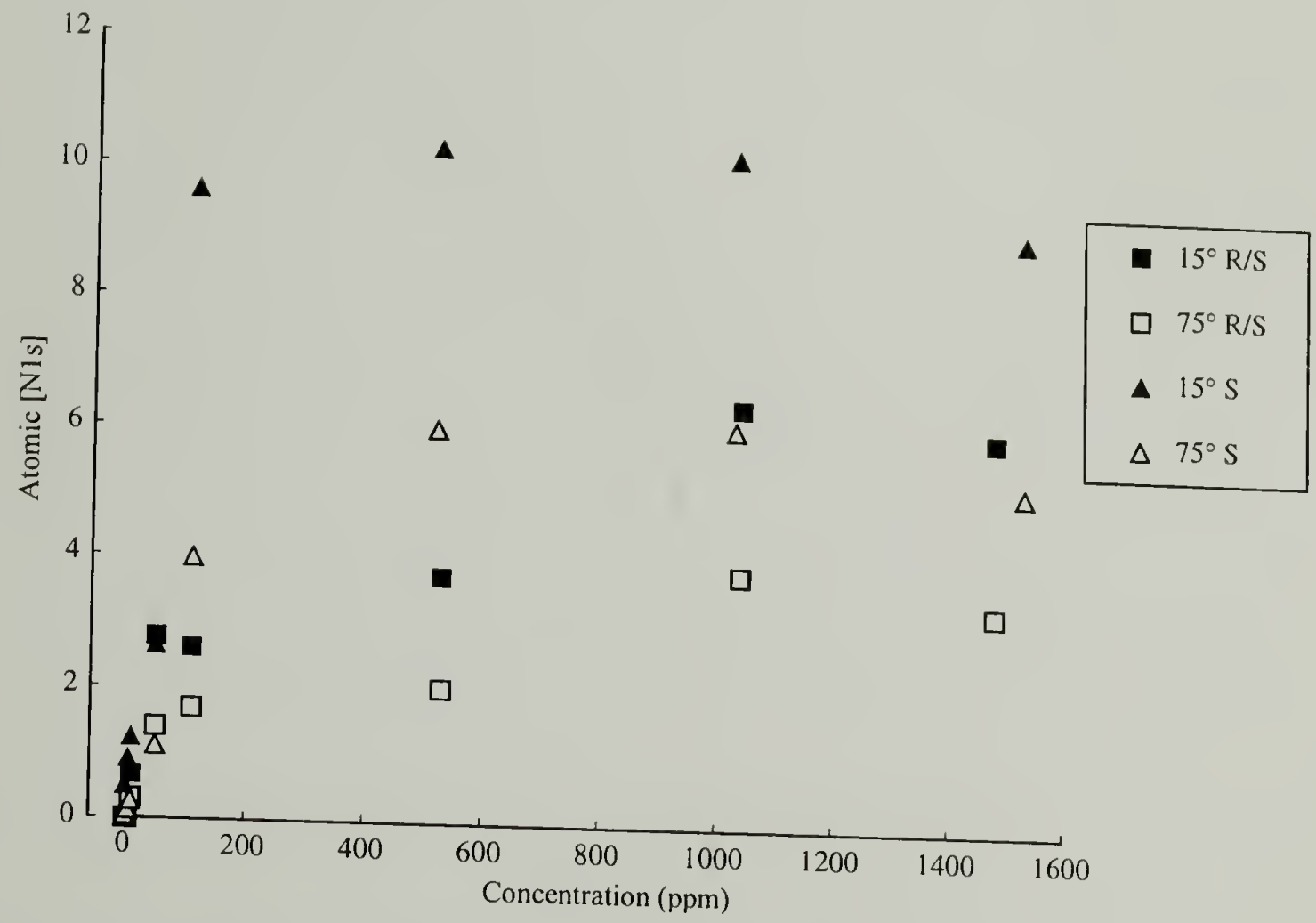

Figure 1.20. Combination of adsorption isotherms (24 hr at 25 °C) generated from the XPS data (Tables 1.10-1.11) for 312:1 poly-**R/S** and 312:1 poly-S showing the gain in N_{1s} concentration with increasing concentration of polymer in THF. Concentration is in ppm = mg/mL x 10^3

Table 1.12. Adsorption isotherm data for the adsorption of 936:1 poly-**R/S** from THF to native silicon oxide THF for 24 hours at 25 °C. Listed are the atomic concentration data from XPS analysis at 15° and 75° take-off angles. The solution concentration is in both mg/mL and ppm which equals mg/mL x 10^3. The data are plotted in the adsorption isotherm shown in Figure 1.21.

936:1 POLY-**R/S** mg/mL THF (ppm)	$C_{15°}$	$N_{15°}$	$O_{15°}$	$Si_{15°}$	C:N	Si:N
0.0005 (0.5)	44.34	1.02	42.47	12.17	43.5 : 1	12 : 1
0.005 (5)	44.69	1.69	36.76	16.85	26.4 : 1	10 : 1
0.01 (10)	48.47	2.54	37.41	11.58	19.1 : 1	4.6 : 1
0.05 (50)	48.01	3.41	32.67	15.91	14.1 : 1	4.7 : 1
0.10 (100)	34.14	3.00	44.56	18.30	11.4 : 1	6.1 : 1
0.58 (580)	44.84	4.41	37.53	13.22	10.2 : 1	3.0 : 1
1.11 (1110)	48.57	8.07	34.29	9.08	6.0 : 1	1.1 : 1
1.50 (1500)	54.02	8.71	30.06	7.21	6.2 : 1	0.8 : 1

936:1 POLY-**R/S** mg/mL THF (ppm)	$C_{75°}$	$N_{75°}$	$O_{75°}$	$Si_{75°}$	C:N	Si:N
0.0005 (0.5)	10.12	0.74	40.22	48.93	13.7 : 1	66 : 1
0.005 (5)	12.94	0.65	39.46	46.95	19.9 : 1	72 : 1
0.01 (10)	17.16	1.07	41.63	40.14	16.0 : 1	38 : 1
0.05 (50)	17.14	1.45	36.84	44.57	11.8 : 1	31 : 1
0.10 (100)	14.10	2.08	41.65	42.18	6.8 : 1	20 : 1
0.58 (580)	14.85	2.55	42.21	40.39	5.8 : 1	16 : 1
1.11 (1110)	24.27	4.24	38.06	33.42	5.7 : 1	7.9 : 1
1.50 (1500)	25.52	4.60	35.29	34.59	5.5 : 1	7.5 : 1

Table 1.13. Adsorption isotherm data for the adsorption of 936:1 poly-**S** from THF to native silicon oxide for 24 hours at 25 °C. Listed are the atomic concentration data from XPS analysis at 15° and 75° take-off angles and the contact angle (probe fluid, H_2O) results where θ_A is the advancing contact angle and θ_R the receding angle. The solution concentration is in both mg/mL and ppm which equals mg/mL x 10^3. The data are plotted in the adsorption isotherm shown in Figure 1.21.

936:1 POLY-**S** mg/mL THF (ppm)	$C_{15°}$	$N_{15°}$	$O_{15°}$	$Si_{15°}$	C:N	Si:N	θ_A	θ_R
0.0005 (0.5)	45.87	1.52	35.48	17.13	30.2 : 1	11 : 1	24°	5°
0.005 (5)	43.30	1.25	35.92	19.53	34.6 : 1	16 : 1	29°	7°
0.01 (10)	33.70	1.67	42.57	22.06	20.2 : 1	13 : 1	32°	7°
0.05 (50)	45.86	2.68	34.57	16.90	17.1 : 1	6.3 : 1	39°	6°
0.12 (120)	40.35	2.21	37.71	19.73	18.3 : 1	8.9 : 1	39°	10°
0.54 (540)	42.53	3.47	36.14	17.86	12.3 : 1	5.1 : 1	42°	13°
1.02 (1020)	41.08	3.84	36.78	18.31	10.7 : 1	4.8 : 1	49°	13°
1.52 (1520)	44.58	3.88	33.39	18.16	11.4 : 1	4.7 : 1	64°	16°

936:1 POLY-**S** mg/mL THF (ppm)	$C_{75°}$	$N_{75°}$	$O_{75°}$	$Si_{75°}$	C:N	Si:N
0.0005 (0.5)	12.65	0.42	28.10	58.83	30.1 : 1	140 : 1
0.005 (5)	14.04	0.59	29.92	55.45	23.8 : 1	94 : 1
0.01 (10)	12.16	0.72	31.38	55.75	16.9 : 1	77 : 1
0.05 (50)	14.06	0.96	30.72	54.26	14.6 : 1	57 : 1
0.12 (120)	12.70	1.51	32.82	52.98	8.4 : 1	35 : 1
0.54 (540)	14.70	1.40	33.83	50.06	10.5 : 1	36 : 1
1.02 (1020)	15.38	1.64	29.90	53.08	9.4 : 1	32 : 1
1.52 (1520)	12.96	1.52	31.33	54.19	8.5 : 1	36 : 1

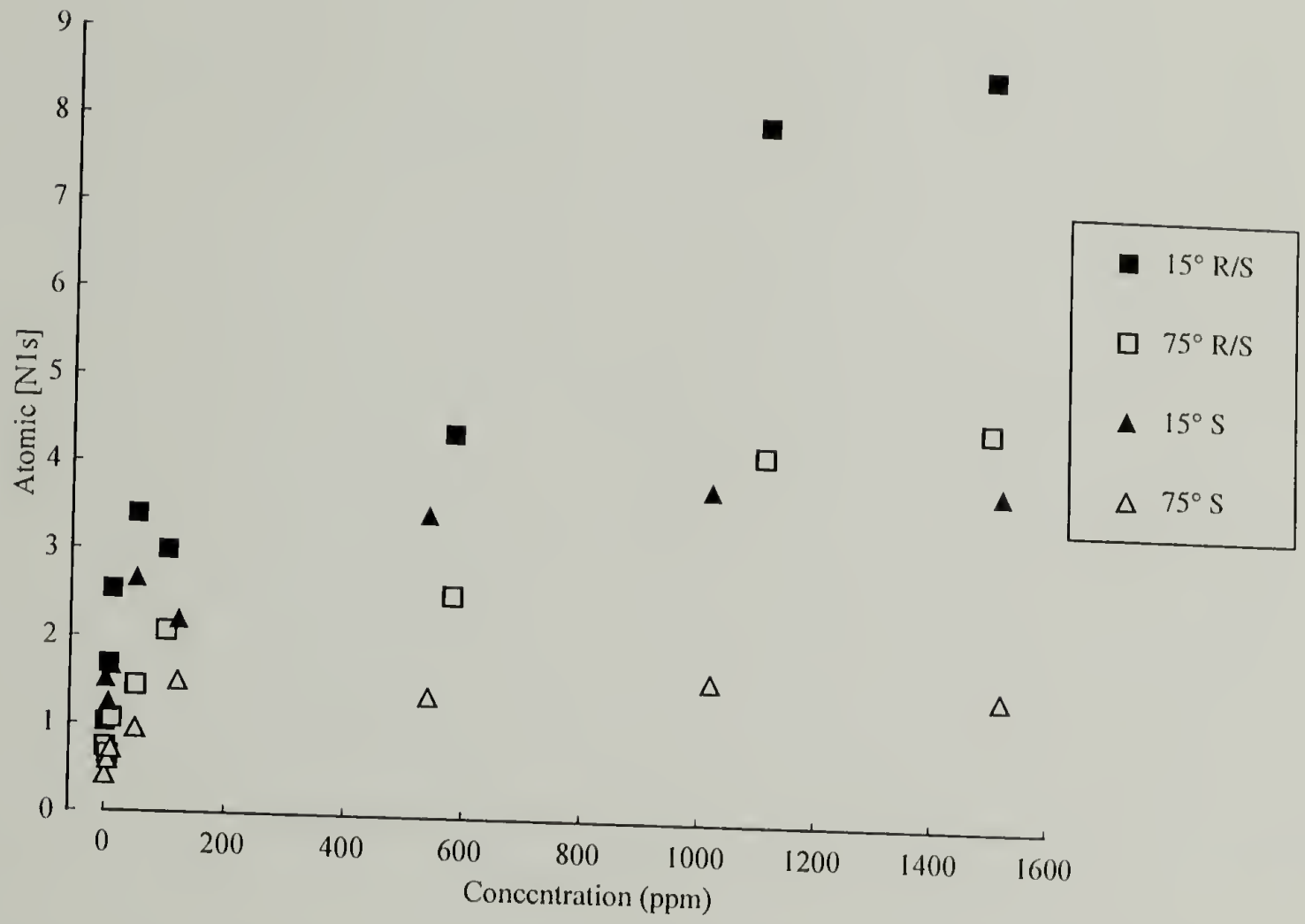

Figure 1.21. Combination of adsorption isotherms (24 hr at 25 °C) generated from the XPS data (Tables 1.12-1.13) for 936:1 poly-**R/S** and 936:1 poly-**S** showing the gain in N_{1s} concentration with increasing concentration of polymer in THF. Concentration is in ppm = mg/mL x 10^3

Table 1.14. Adsorption isotherm data for the adsorption of 3121:1 poly-**R/S** from THF to native silicon oxide for 24 hours at 25 °C. Listed are the atomic concentration data from XPS analysis at 15° and 75° take-off angles and the contact angle (probe fluid, H_2O) results where θ_A is the advancing contact angle and θ_R the receding angle. The solution concentration is in both mg/mL and ppm which equals mg/mL x 10^3. The data are plotted in the adsorption isotherm shown in Figure 1.22.

3121:1 POLY-**R/S** mg/mL THF (ppm)	$C_{15°}$	$N_{15°}$	$O_{15°}$	$Si_{15°}$	C : N	Si :N	θ_A	θ_R
0.0005 (0.5)	33.97	-	41.58	24.00	-	-	40°	14°
0.005 (5)	39.92	0.33	44.54	15.21	121 : 1	46 : 1	39°	16°
0.01 (10)	36.37	0.04	41.83	21.76	909 : 1	544 : 1	39°	17°
0.05 (50)	33.71	0.82	41.78	23.70	41 : 1	29 : 1	40°	17°
0.11 (110)	32.44	1.75	43.78	22.04	19 : 1	13 : 1	46°	16°
0.50 (500)	35.56	2.26	45.05	17.12	16 : 1	7.6 : 1	46°	19°
1.10 (1100)	37.36	3.11	43.90	15.64	12 : 1	5.0 : 1	47°	18°
1.50 (1500)	34.09	2.26	47.85	15.81	15 : 1	7.0 : 1	49°	20°

3121:1 POLY-**R/S** mg/mL THF (ppm)	$C_{75°}$	$N_{75°}$	$O_{75°}$	$Si_{75°}$	C:N	Si :N
0.0005 (0.5)	9.97	-	37.82	52.22	-	-
0.005 (5)	14.07	0.08	48.37	37.47	179 : 1	468 : 1
0.01 (10)	9.59	-	40.69	49.72	-	-
0.05 (50)	9.38	0.40	40.78	49.43	24 : 1	124 : 1
0.11 (110)	10.11	0.88	39.46	49.55	12 : 1	56 : 1
0.50 (500)	11.50	1.33	43.71	43.45	8.6 : 1	33 : 1
1.10 (1100)	14.62	1.51	45.82	38.05	9.7 : 1	25 : 1
1.50 (1500)	11.45	1.17	46.00	41.39	9.8 : 1	35 : 1

Table 1.15. Adsorption isotherm data for the adsorption of 3121:1 poly-**S** from THF to native silicon for 24 hours at 25 °C. Listed are the atomic concentration data from XPS analysis at 15° and 75° take-off angles and the contact angle (probe fluid, H_2O) results where θ_A is the advancing contact angle and θ_R the receding angle. The solution concentration is in both mg/mL and ppm which equals mg/mL x 10^3. The data are plotted in the adsorption isotherm shown in Figure 1.22.

936:1 POLY-**S** mg/mL THF (ppm)	$C_{15°}$	$N_{15°}$	$O_{15°}$	$Si_{15°}$	C:N	Si : N	θ_A	θ_R
0.0005 (0.5)	48.37	2.04	36.21	13.37	23.7 : 1	6.6 : 1	15°	6°
0.005 (5)	31.31	1.16	53.24	14.30	27.0 : 1	12 : 1	19°	9°
0.01 (10)	39.45	1.75	44.71	14.09	22.5 : 1	8.1 : 1	34°	6°
0.05 (50)	39.38	2.97	41.46	16.19	13.3 : 1	5.5 : 1	31°	12°
0.10 (100)	68.00	8.12	17.33	6.55	8.4 : 1	0.8 : 1	46°	16°
0.46 (460)	66.45	9.72	15.20	8.63	6.8 : 1	0.9 : 1	65°	22°
1.01 (1010)	58.31	9.17	24.39	8.13	6.4 : 1	0.9 : 1	47°	18°
1.62 (1620)	58.03	8.63	22.58	10.75	6.7 : 1	1.2 : 1	95°	27°

936:1 POLY-**S** mg/mL THF (ppm)	$C_{75°}$	$N_{75°}$	$O_{75°}$	$Si_{75°}$	C : N	Si : N
0.0005 (0.5)	13.47	0.81	43.64	42.09	16.6 : 1	52 : 1
0.005 (5)	10.41	0.64	46.07	42.89	16.3 : 1	67 : 1
0.01 (10)	13.21	0.97	46.48	39.34	13.6 : 1	41 : 1
0.05 (50)	11.54	1.73	35.96	50.77	6.7 : 1	29 : 1
0.10 (100)	20.87	3.11	37.60	38.43	6.7 : 1	12 : 1
0.46 (460)	27.83	4.58	32.91	34.68	6.1 : 1	7.8 : 1
1.01 (1010)	22.03	3.66	35.21	39.10	6.0 : 1	11 : 1
1.62 (1620)	28.50	4.08	33.34	34.08	7.0 : 1	8.4 : 1

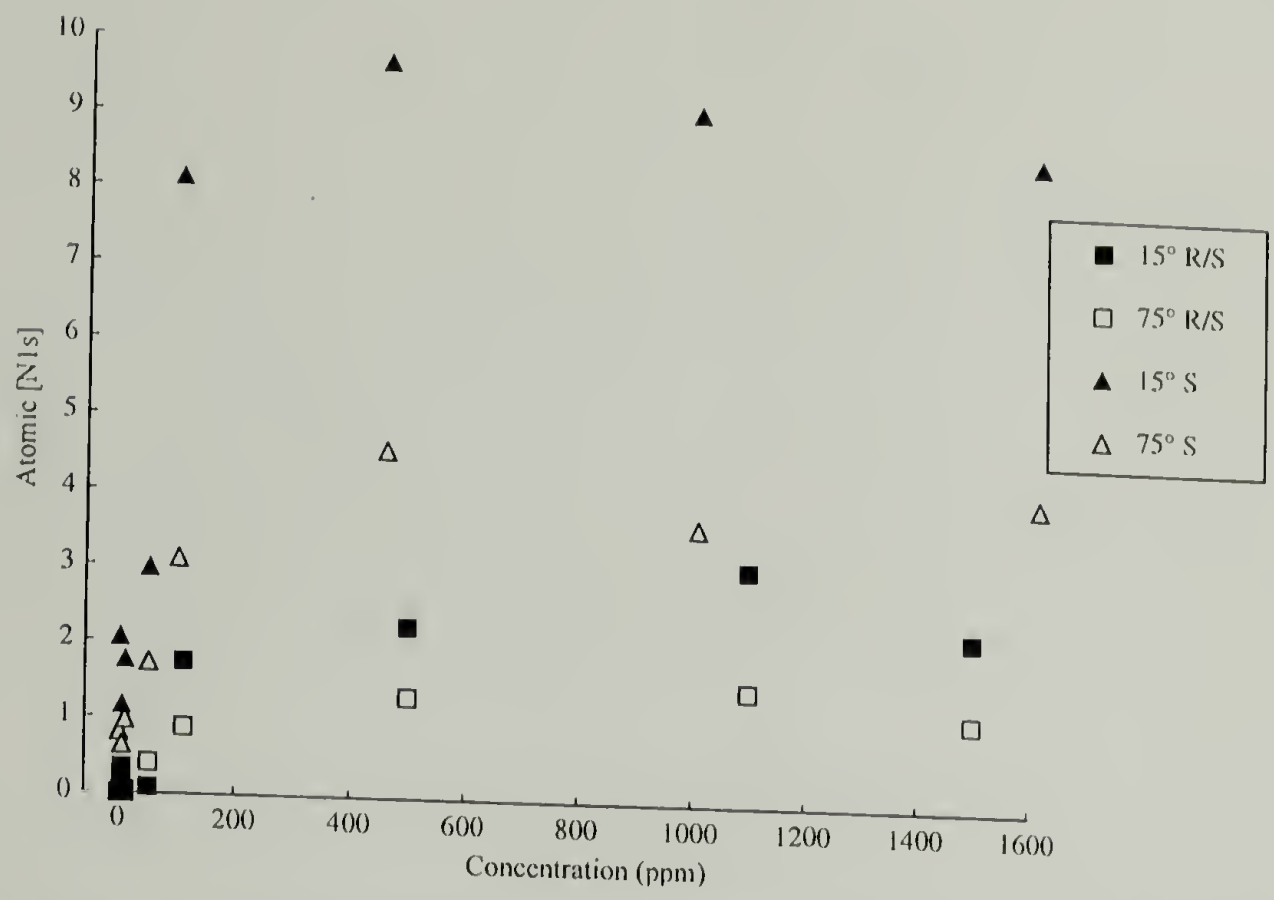

Figure 1.22. Combination of adsorption isotherms (24 hr at 25 °C) generated from the XPS data (Tables 1.14-1.15) for both 3121:1 poly-**R/S** and 3121:1 poly-**S** showing the gain in N_{1s} concentration with increasing concentration of polymer in THF. Concentration is in ppm = mg/mL x 10^3

Adsorptions of poly-**R/S** from toluene solution resulted in higher adsorbed amounts than similar experiments performed using THF. This result was expected since adsorptions from poor solvents usually result in higher adsorbed amounts. Nevertheless, interesting is the difference in contact angle between adsorptions from toluene and THF. The lower advancing and receding contact angles for adsorptions from THF suggest a much larger surface area of the silicon surface present than adsorptions from toluene. In addition, the greater hysteresis for adsorptions from THF suggests that the topography of these adsorbed films was rougher than adsorbed films from toluene. We initially believed that this was a result of less polymer adsorbing from THF than toluene during the time frame of the experiment. This led us to perform adsorption kinetics with the goal of determining the maximum amount of polymer that could adsorb from THF.

As can be seen from the data in Tables 1.11, 1.12, and Figure 1.21, the results for the 936:1 polymers did not correlate with the other two samples. Careful analysis of the polymer samples and the repeat of data points confirmed the scatter in the results. These results were explainable only after we started characterizing the topography of the adsorbed layers by atomic force microscopy. By AFM analysis, it was shown that the adsorbed layers dewetted resulting in a rough surface, thereby causing scatter in the XPS data (vide infra).

Adsorption kinetics were measured for all three molecular weight samples of poly–**R/S** and poly-**S**. The objective was to determine the maximum amount of polymer that would adsorb to native silicon oxide. The first kinetics experiments were performed for 48 hours. However, as seen in Tables 1.16 through 1.21 and Figures 1.23 through 1.27, there was difficulty in determining the plateau region because the XPS results for several of the samples indicated that the adsorbed amounts still increased with time. Therefore, a second set of kinetics was performed from a period of 72 hours to 20 days.

As with the adsorption isotherm data, the kinetics data indicated that larger amounts of poly-**S** adsorbed than poly-**R/S** of equivalent molecular weight. In addition, the kinetics data for the 936:1 poly-**R/S** and poly-**S** indicated the same reversal in the above trend as was seen with the adsorption isotherms. Although these same trends were generally shown in the kinetic experiments results, the scatter in the data between the two periods of 0-48 hours and 3-20 days was hypothesized to be the result of differences in substrate surface. The kinetics plots (Figures 1.23 through 1.28) show the varying degree of scatter between the two different experimental time frames. However, the data did suggest that for both 312:1 and 3121:1 polymers, the adsorbed amount reached a maximum between 48 and 72 hours. Still, the underlining issue with the data was the amount of scatter.

Table 1.16. Adsorption kinetics data from the adsorption of 312:1 poly-**R/S** from THF to native silicon oxide at 1 mg/mL and 25 °C. Listed are the atomic concentration data from XPS analysis at 15° and 75° take-off angles. The data are plotted in Figure 1.23.

312:1 POLY-**R/S** Day	$C_{15°}$	$N_{15°}$	$O_{15°}$	$Si_{15°}$	$C_{15°}$:$N_{15°}$	$Si_{15°}$:$N_{15°}$
4hr	34.42	2.65	47.62	15.31	13.0 : 1	5.8 : 1
10hr	42.44	4.70	40.61	12.25	9.0 : 1	2.6 : 1
1	44.37	4.86	39.67	11.10	9.1 : 1	2.3 : 1
34hr	42.83	5.65	38.25	13.27	7.6 : 1	2.3 : 1
2	51.24	6.83	30.98	10.95	7.5 : 1	1.6 : 1
3	39.99	4.67	43.77	11.56	8.6 : 1	2.5 : 1
7	44.50	5.24	39.96	10.30	8.5 : 1	2.0 : 1
11	48.86	5.35	35.15	10.64	9.1 : 1	2.0 : 1
14	49.02	5.10	36.03	9.84	9.6 : 1	1.9 : 1
20	49.56	5.89	35.10	9.46	8.4 : 1	1.6 : 1

312:1 POLY-**R/S** Day	$C_{75°}$	$N_{75°}$	$O_{75°}$	$Si_{75°}$	$C_{75°}$:$N_{75°}$	$Si_{75°}$:$N_{75°}$
4hr	16.42	1.93	44.45	37.20	8.5 : 1	19.3 : 1
10hr	20.91	3.25	40.49	35.35	6.4 : 1	10.9 : 1
1	21.75	3.79	40.16	34.30	5.7 : 1	9.1 : 1
34hr	19.66	3.38	42.23	34.73	5.8 : 1	10.3 : 1
2	25.77	4.48	36.53	33.22	5.8 : 1	7.4 : 1
3	21.35	3.30	41.47	33.88	6.5 : 1	10.3 : 1
7	21.47	3.26	41.59	33.68	6.6 : 1	10.3 : 1
11	20.68	3.42	41.39	34.50	6.0 : 1	10.1 : 1
14	24.34	2.58	47.44	25.64	9.4 : 1	9.9 : 1
20	24.00	3.39	39.50	33.11	7.1 : 1	9.8 : 1

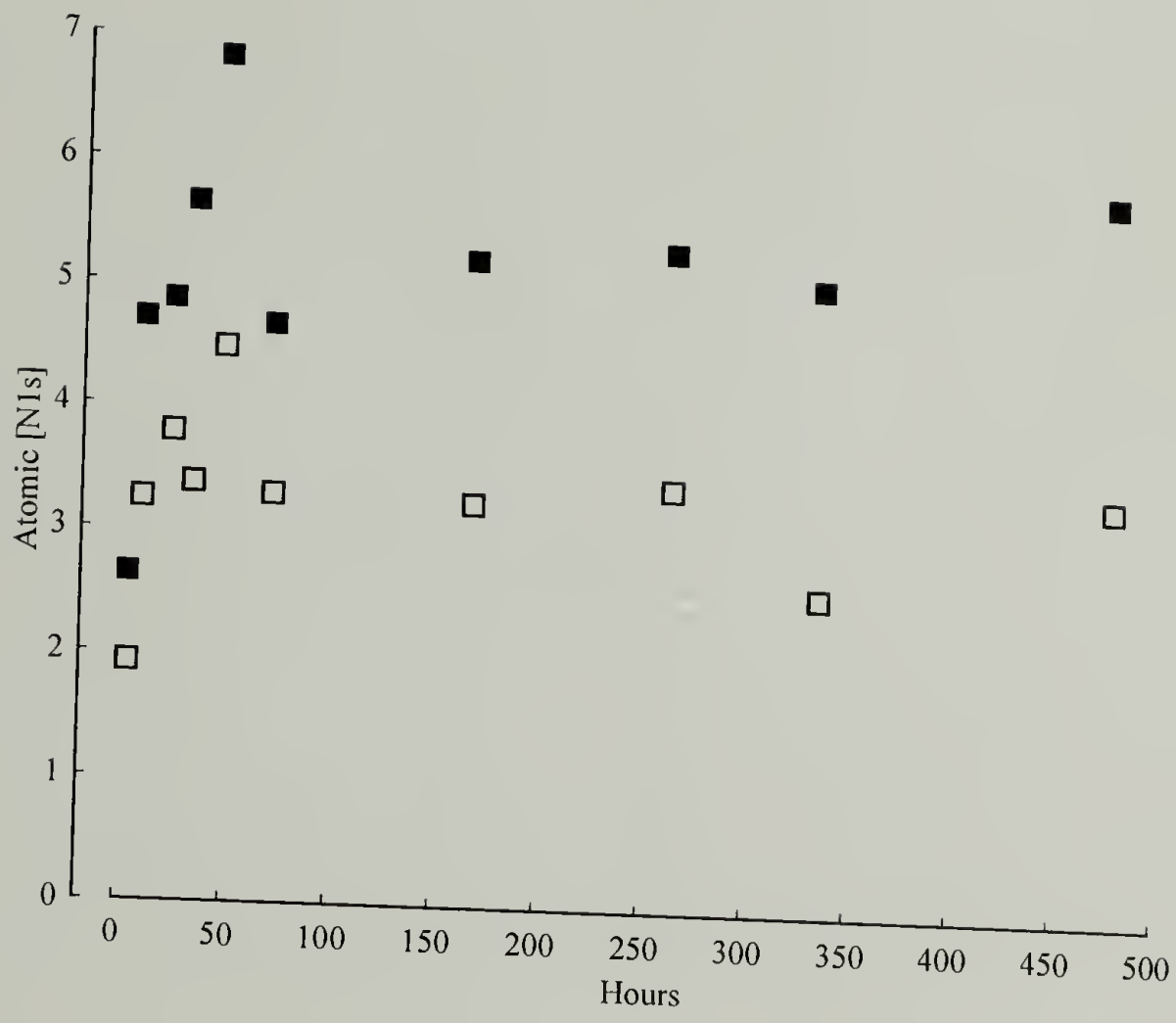

Figure 1.23. Plot of atomic concentration data generated from XPS of 312:1 poly-**R/S** adsorbed films on native silicon oxide. Plotted are both the 15° (■) and 75° (□) take-off angle XPS data (Table 1.16) showing the change in N_{1s} concentration with increasing adsorption time. The adsorption of poly-**R/S** was performed from solution in THF at a concentration of 1 mg/mL.

Table 1.17. Adsorption kinetics data from the adsorption of 312:1 poly-S from THF to native silicon oxide at 1 mg/mL and 25 °C. Listed are the atomic concentration data from XPS analysis at 15° and 75° take-off angles. The data are plotted in Figure 1.24.

312:1 POLY-S Day	$C_{15°}$	$N_{15°}$	$O_{15°}$	$Si_{15°}$	$C_{15°}:N_{15°}$	$Si_{15°}:N_{15°}$
4hr	53.18	7.44	30.79	8.59	7.1 : 1	1.2 : 1
10hr	59.79	9.56	23.99	6.66	6.3 : 1	0.7 : 1
1	62.38	11.55	20.19	5.88	5.4 : 1	0.5 : 1
34hr	71.51	12.47	12.18	3.84	5.7 : 1	0.3 : 1
2	75.74	14.02	8.60	1.64	5.4 : 1	0.1 : 1
3	49.20	6.15	34.98	9.67	8.0 : 1	1.6 : 1
7	48.66	6.86	35.70	8.78	7.1 : 1	1.3 : 1
11	56.58	6.60	28.20	8.62	8.6 : 1	1.3 : 1
14	53.86	7.55	30.73	7.87	7.1 : 1	1.0 : 1
20	57.03	8.18	27.77	7.02	7.0 : 1	1.0 : 1

312:1 POLY-S Day	$C_{75°}$	$N_{75°}$	$O_{75°}$	$Si_{75°}$	$C_{75°}:N_{75°}$	$Si_{75°}:N_{75°}$
4hr	29.16	5.12	37.26	28.47	5.7 : 1	5.6 : 1
10hr	36.29	5.74	32.13	25.83	6.3 : 1	4.5 : 1
1	42.65	8.97	24.94	23.44	4.8 : 1	2.6 : 1
34hr	50.07	10.33	21.25	18.36	4.8 : 1	1.8 : 1
2	53.27	11.26	18.97	16.51	4.7 : 1	1.5 : 1
3	24.11	3.53	39.06	33.29	6.8 : 1	9.4 : 1
7	23.64	3.94	40.62	31.80	6.0 : 1	8.1 : 1
11	26.94	3.97	39.66	29.43	6.8 : 1	7.4 : 1
14	23.83	4.77	39.67	31.72	5.0 : 1	6.6 : 1
20	31.57	4.98	36.82	26.63	6.3 : 1	5.3 : 1

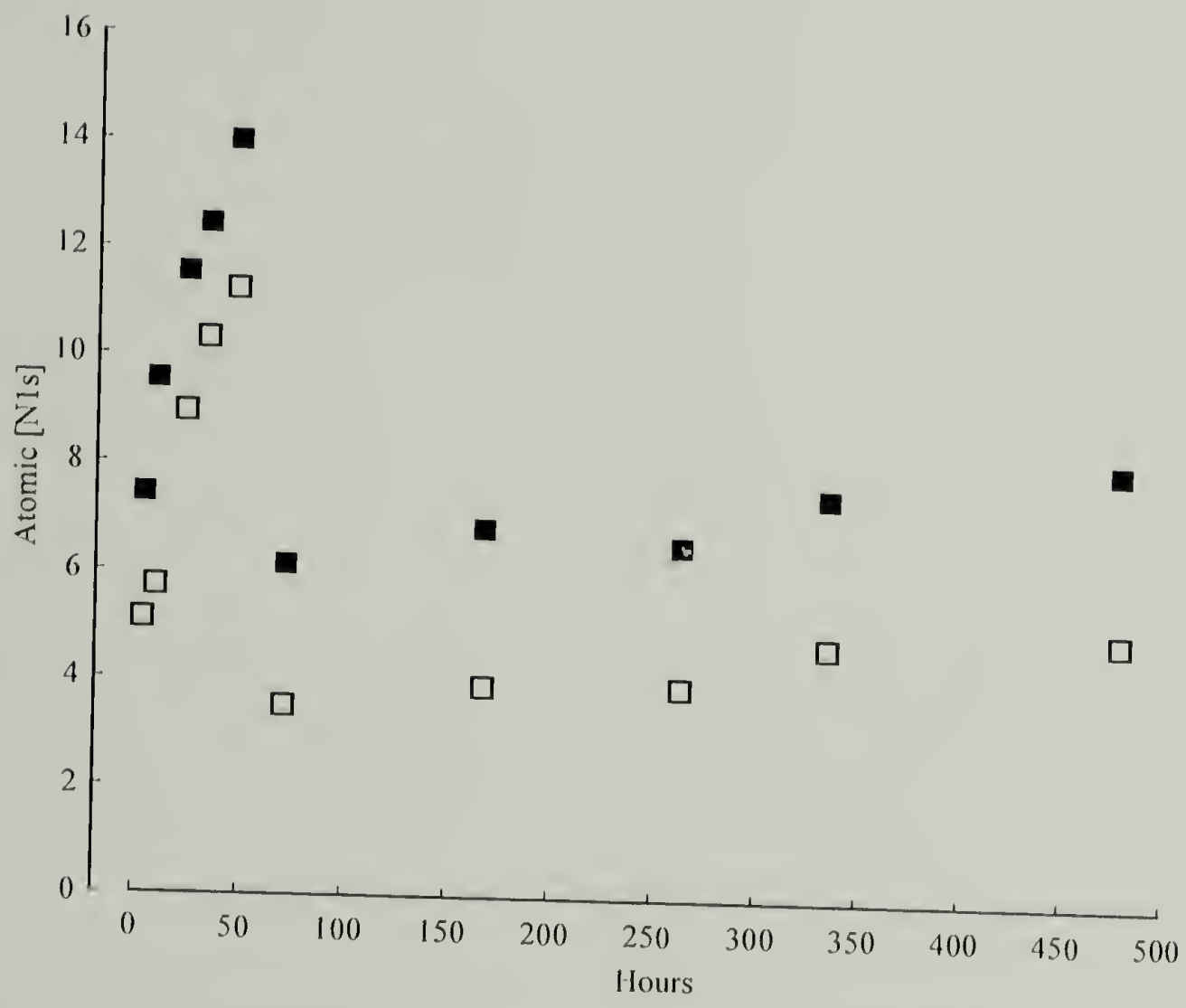

Figure 1.24. Plot of atomic concentration data generated from XPS of 312:1 poly-S adsorbed films on native silicon oxide. Plotted are both the 15° (■) and 75° (□) take-off angle XPS data (Table 1.17) showing the change in N_{1s} concentration with increasing adsorption time. The adsorption of poly-S was performed from solution in THF at a concentration of 1 mg/mL.

Table 1.18. Adsorption kinetics data for the adsorption of 936:1 poly-**R/S** from THF to native silicon oxide at 1 mg/mL and 25 °C. Listed are the atomic concentration data from XPS analysis at 15° and 75° take-off angles. The data are plotted in Figure 1.25.

936:1 POLY-**R/S** Day	$C_{15°}$	$N_{15°}$	$O_{15°}$	$Si_{15°}$	$C_{15°}:N_{15°}$	$Si_{15°}:N_{15°}$
4hr	36.22	2.75	46.30	14.72	13.2 : 1	5.4 : 1
10hr	33.45	2.65	49.76	14.14	12.6 : 1	5.3 : 1
1	34.72	3.11	48.01	14.16	11.2 : 1	4.6 : 1
34hr	38.08	3.76	43.66	14.49	10.1 : 1	3.9 : 1
2	48.72	4.72	34.61	11.95	10.3 :1	2.5 : 1
3	50.40	8.08	32.31	9.20	6.2 : 1	1.1 : 1
7	59.06	9.74	23.46	7.73	6.1 : 1	0.8 : 1
11	60.87	9.36	22.83	6.94	6.5 : 1	0.7 : 1
14	61.81	9.59	22.37	6.24	6.4 : 1	0.7 : 1
20	60.89	9.82	23.21	6.07	6.2 : 1	0.6 : 1

936:1 POLY-**R/S** Day	$C_{75°}$	$N_{75°}$	$O_{75°}$	$Si_{75°}$	$C_{75°}:N_{75°}$	$Si_{75°}:N_{75°}$
4hr	13.79	2.26	42.50	41.46	6.1 : 1	18.3 : 1
10hr	16.27	1.59	43.31	38.83	10.2 : 1	24.4 : 1
1	18.65	2.31	42.55	36.49	8.1 : 1	8.1 : 1
34hr	17.66	2.51	43.54	36.30	7.0 : 1	14.5 : 1
2	25.63	4.28	36.89	33.20	6.0 : 1	7.8 : 1
3	31.50	5.44	34.82	28.24	5.8 : 1	5.2 : 1
7	29.79	6.09	37.57	26.55	4.9 : 1	4.4 : 1
11	27.32	5.52	37.59	29.57	4.9 : 1	5.4 : 1
14	30.48	5.62	35.38	28.52	5.4 : 1	5.1 : 1
20	34.76	7.27	35.89	22.08	4.8 : 1	3.0 : 1

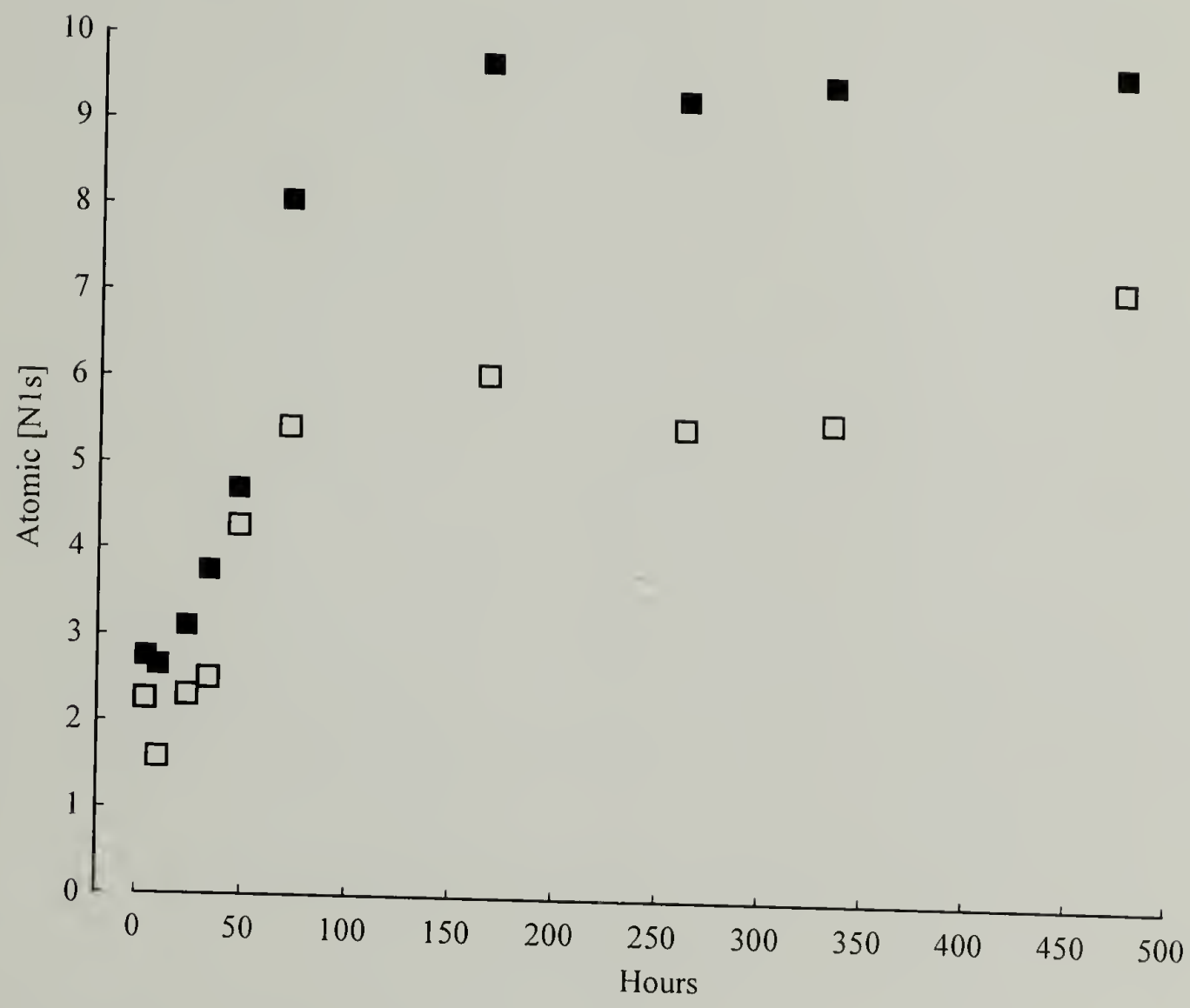

Figure 1.25. Plot of atomic concentration data generated from XPS of 936:1 poly-**R/S** adsorbed films on native silicon oxide. Plotted are both the 15° (■) and 75° (□) take-off angle XPS data (Table 1.18) showing the change in N_{1s} concentration with increasing adsorption time. The adsorption of poly-**R/S** was performed from solution in THF at a concentration of 1 mg/mL.

Table 1.19. Adsorption kinetics data from the adsorption of 936:1 poly-**S** from THF to native silicon oxide at 1 mg/mL and 25 °C. Listed are the atomic concentration data from XPS analysis at 15° and 75° take-off angles. The data are plotted in Figure 1.26.

936:1 POLY-**R/S** Day	$C_{15°}$	$N_{15°}$	$O_{15°}$	$Si_{15°}$	$C_{15°} : N_{15°}$	$Si_{15°} : N_{15°}$
4hr	40.04	3.67	43.25	13.04	10.9 : 1	3.6 : 1
10hr	44.08	4.52	38.51	12.89	9.8 : 1	2.9 : 1
1	34.53	4.24	47.81	13.42	8.1 : 1	3.2 : 1
34hr	47.26	5.38	36.34	11.02	8.8 : 1	2.0 : 1
2	53.94	8.52	28.46	9.08	6.3 : 1	5.9 : 1
3	42.87	5.67	41.49	9.97	7.6 : 1	1.8 : 1
7	51.29	6.48	32.11	10.13	7.9 : 1	1.6 : 1
11	52.71	7.34	30.29	9.65	7.2 : 1	1.3 : 1
14	52.05	6.70	31.92	9.33	7.8 : 1	1.4 : 1
20	53.76	6.66	30.36	9.21	8.1 : 1	1.4 : 1

936:1 POLY-**R/S** Day	$C_{75°}$	$N_{75°}$	$O_{75°}$	$Si_{75°}$	$C_{75°} : N_{75°}$	$Si_{75°} : N_{75°}$
4hr	17.86	2.56	42.93	36.65	7.0 : 1	14.3 : 1
10hr	20.87	3.37	41.23	34.53	6.2 : 1	10.2 : 1
1	18.73	3.48	43.21	34.57	5.4 : 1	9.9 : 1
34hr	21.78	3.31	41.09	33.82	6.6 : 1	10.2 : 1
2	22.02	4.53	39.38	34.06	4.9 : 1	7.5 : 1
3	21.21	3.34	39.92	35.53	6.4 : 1	1.1 : 1
7	23.25	4.43	39.41	32.90	5.2 : 1	7.4 : 1
11	22.98	4.04	39.00	33.98	5.7 : 1	8.4 : 1
14	24.97	4.12	39.39	31.51	6.1 : 1	7.6 : 1
20	23.60	3.83	38.17	34.40	6.2 : 1	9.0 : 1

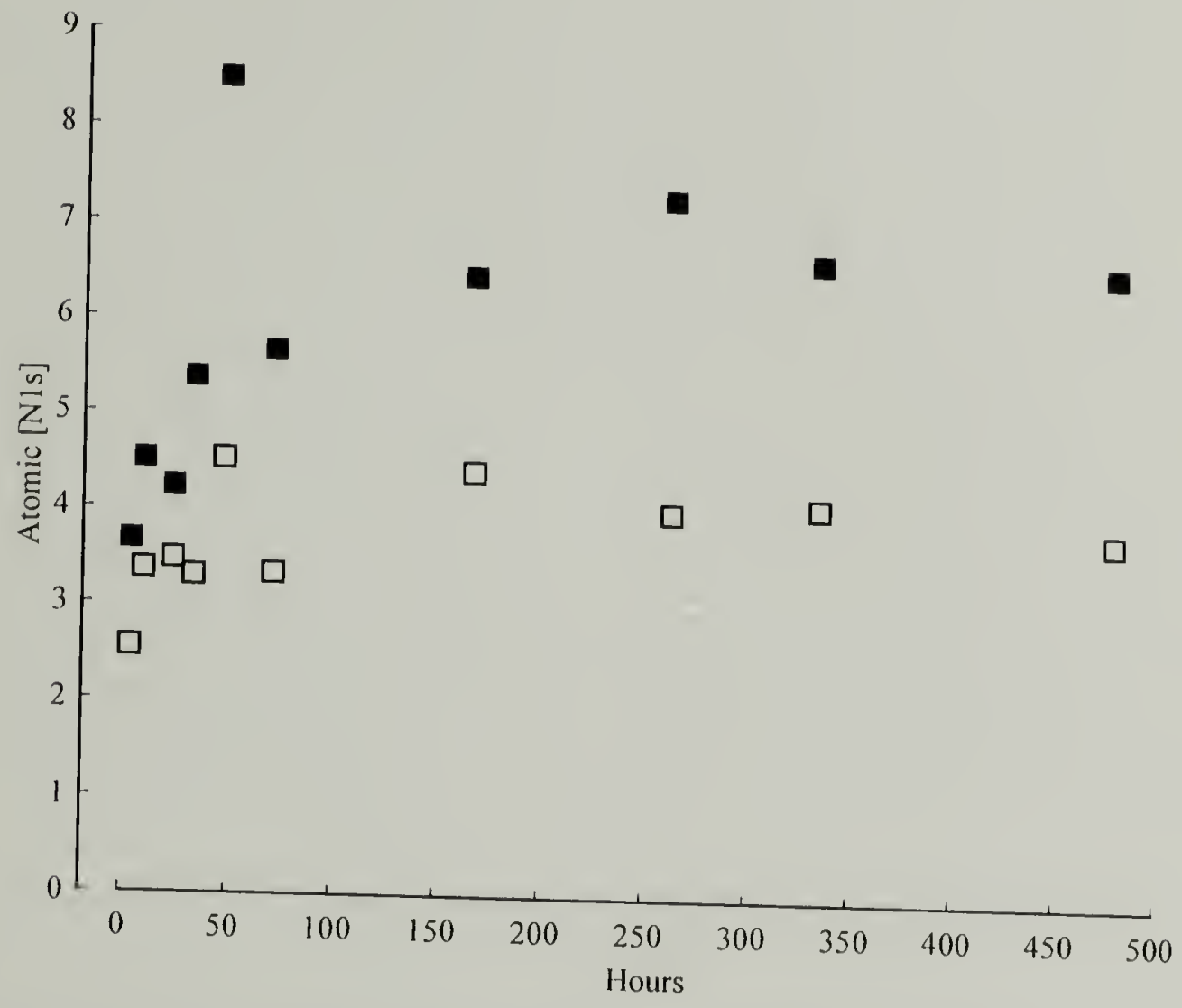

Figure 1.26. Plot of atomic concentration data generated from XPS of 936:1 poly-S adsorbed films on native silicon oxide. Plotted are both the 15° (■) and 75° (□) take-off angle XPS data (Table 1.19) showing the change in N_{1s} concentration with increasing adsorption time. The adsorption of poly-S was performed from solution in THF at a concentration of 1 mg/mL.

Table 1.20. Adsorption kinetics data from the adsorption of 3121:1 poly-**R/S** from THF to native silicon oxide at 1 mg/mL and 25 °C. Listed are the atomic concentration data from XPS analysis at 15° and 75° take-off angles. The data are plotted in Figure 1.27.

3121:1 POLY-**R/S** Day	$C_{15°}$	$N_{15°}$	$O_{15°}$	$Si_{15°}$	$C_{15°} : N_{15°}$	$Si_{15°} : N_{15°}$
4hr	41.29	1.26	41.14	16.30	32.8 : 1	12.9 : 1
8.5 hr	43.04	2.69	39.62	14.65	16.0 : 1	5.4 : 1
1	36.40	1.95	45.78	15.87	18.7 : 1	8.1 : 1
36 hr	45.81	2.90	36.54	14.75	15.8 : 1	5.1 : 1
3	51.97	4.58	30.89	12.55	11.3 : 1	2.7 : 1
4	46.71	4.80	34.30	14.19	9.7 : 1	3.0 : 1
7	39.57	3.34	41.07	16.01	11.8 : 1	4.8 : 1
12	39.56	2.12	43.21	15.11	18.7 : 1	7.1 : 1
16	42.21	2.51	38.98	16.30	16.8 : 1	6.5 : 1

3121:1 POLY-**R/S** Day	$C_{75°}$	$N_{75°}$	$O_{75°}$	$Si_{75°}$	$C_{75°} : N_{75°}$	$Si_{75°} : N_{75°}$
4hr	13.09	1.04	49.87	35.99	12.6 : 1	34.6 : 1
8.5 hr	17.54	1.05	48.34	33.08	16.7 : 1	31.5 : 1
1	14.80	0.88	50.74	33.58	16.8 : 1	38.2 : 1
36 hr	16.82	1.39	51.36	30.43	12.1 : 1	21.9 : 1
3	22.80	2.56	46.46	28.19	8.9 : 1	11.0 : 1
4	19.18	2.22	45.64	32.96	8.6 : 1	14.8 : 1
7	15.28	0.74	48.53	35.45	20.6 : 1	47.9 : 1
12	15.76	0.91	49.73	33.60	17.3 : 1	36.9 : 1
16	15.87	1.76	50.05	32.33	9.0 : 1	18.4 : 1

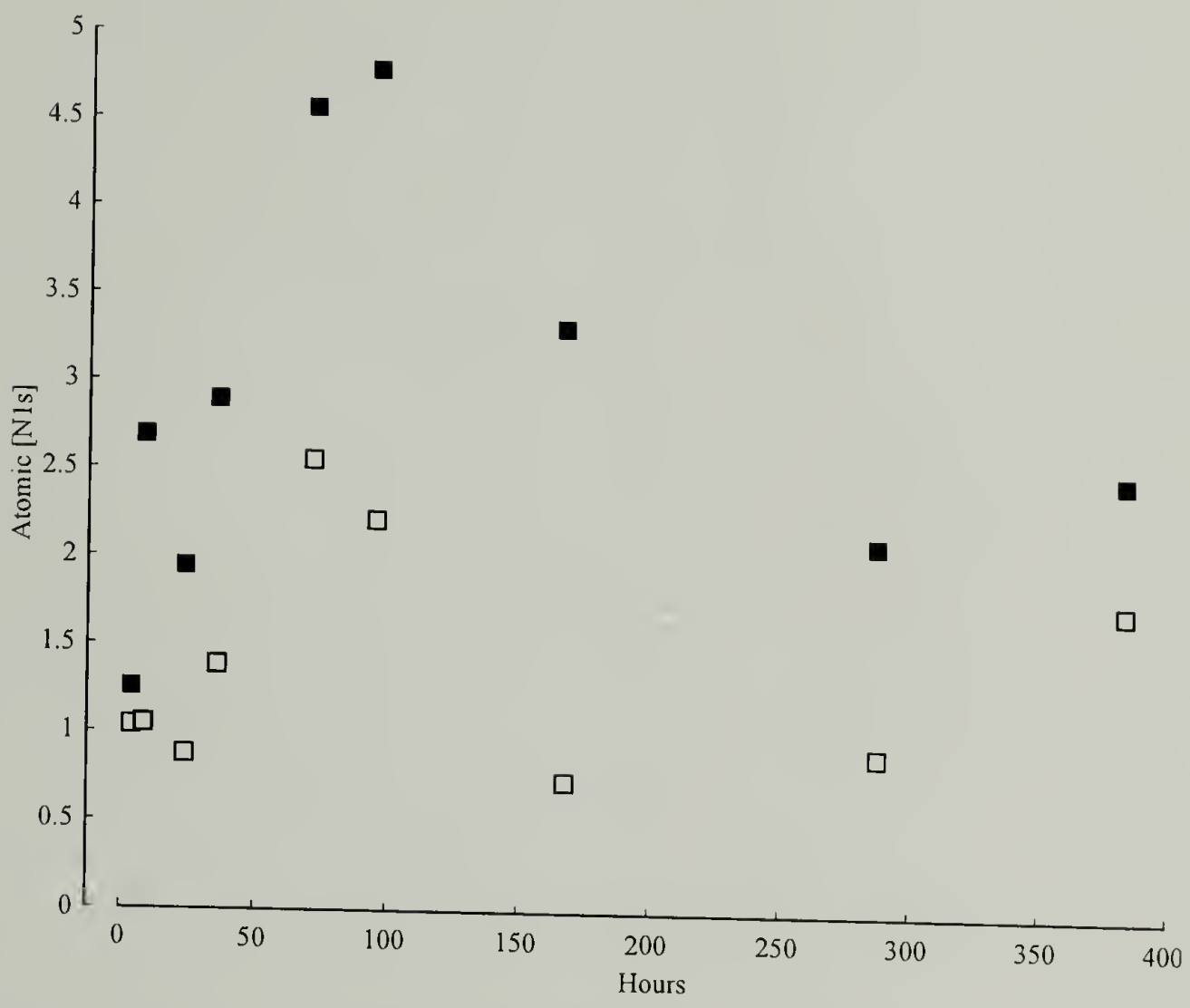

Figure 1.27. Plot of atomic concentration data generated from XPS of 3121:1 poly-**R/S** adsorbed films on native silicon oxide. Plotted are both the 15° (■) and 75° (□) take-off angle XPS data (Table 1.20) showing the change in N_{1s} concentration with increasing adsorption time. The adsorption of poly-**R/S** was performed from solution in THF at a concentration of 1 mg/mL.

Table 1.21. Adsorption kinetics data for the adsorption of 3121:1 poly-**S** from THF to native silicon oxide at 1 mg/mL and 25 °C. Listed are the atomic concentration data from XPS analysis at 15° and 75° take-off angles. The data are plotted in Figure 1.28.

3121:1 POLY-**S** Day	$C_{15°}$	$N_{15°}$	$O_{15°}$	$Si_{15°}$	$C_{15°} : N_{15°}$	$Si_{15°} : N_{15°}$
4hr	36.17	3.04	46.37	14.42	11.9 : 1	4.7 : 1
10hr	38.30	3.78	45.88	12.03	10.1 : 1	3.2 : 1
1	37.92	3.95	45.03	13.10	9.6 : 1	3.3 : 1
34hr	35.81	4.47	46.14	13.59	8.0 : 1	3.0 : 1
2	51.82	7.80	30.50	9.89	6.6 : 1	1.3 : 1
3	43.17	5.29	39.48	12.06	8.2 : 1	2.3 : 1
7	43.92	4.77	39.35	11.96	9.2 : 1	2.5 : 1
11	43.39	4.56	40.53	11.53	9.5 : 1	2.5 : 1
14	42.58	4.28	41.44	11.70	9.9 : 1	2.7 : 1
20	42.12	4.33	42.75	10.80	9.7 : 1	2.5 : 1

3121:1 POLY-**S** Day	$C_{75°}$	$N_{75°}$	$O_{75°}$	$Si_{75°}$	$C_{75°} : N_{75°}$	$Si_{75°} : N_{75°}$
4hr	15.60	2.32	42.68	39.41	6.7 : 1	17.0 : 1
10hr	21.48	2.81	42.09	33.62	7.6 : 1	12.0 : 1
1	16.83	2.83	43.37	36.97	5.9 : 1	13.1 : 1
34hr	17.30	2.88	41.66	38.16	6.0 : 1	13.3 : 1
2	22.12	3.55	40.73	33.60	6.2 : 1	9.5 : 1
3	20.35	2.63	40.04	36.98	7.7 : 1	14.1 : 1
7	18.58	3.60	43.33	34.49	5.2 : 1	9.6 : 1
11	19.67	2.55	42.51	35.27	7.7 : 1	13.8 : 1
14	18.62	2.74	43.34	35.30	6.8 : 1	12.9 : 1
20	17.02	2.70	41.42	38.87	6.3 : 1	14.4 : 1

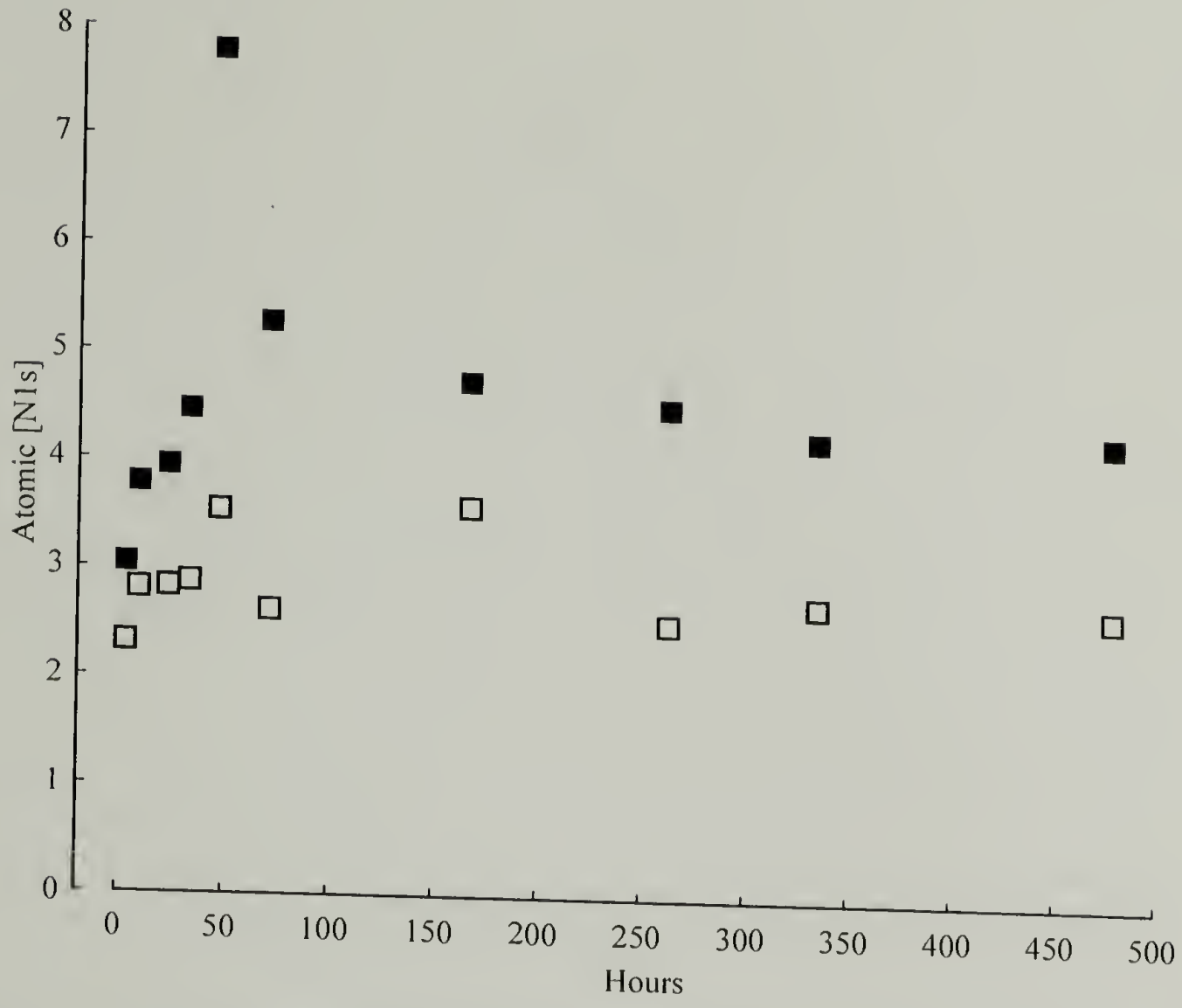

Figure 1.28. Plot of atomic concentration data generated from XPS of 3121:1 poly-S adsorbed films on native silicon oxide. Plotted are both the 15° (■) and 75° (□) take-off angle XPS data (Table 1.21) showing the change in N_{1s} concentration with increasing adsorption time. The adsorption of poly-S was performed from solution in THF at a concentration of 1 mg/mL.

Combining the contact angle results from the adsorption isotherm measurements with the XPS results from the kinetics analysis, we concluded that variations in the native silicon oxide surface could potentially cause differences in the adsorbed amount. To understand the scatter in the data we chose two research paths. The first was to study the topography of the surface by atomic force microscopy, and the second was to perform adsorption experiments on surfaces with known composition. The second path was accomplished by surface modification of the native silicon oxide by silane coupling agents, and the results from this research are presented in chapter two.

The XPS results from the adsorption kinetics experiments indicated that a maximum in the adsorbed amount of polymer occurred between 48 and 72 hours. With this in mind, thin films of poly-**R/S** and poly-**S** were prepared by adsorption from THF for 53 hours. The results are shown in Table 1.20 and interestingly, the adsorbed amount was greater for all molecular weights of poly-**S** than equivalent poly-**R/S**. Previous experiments resulted in higher adsorbed amounts of 936:1 poly-**R/S**. In addition, the data show how the adsorbed amount decreased with increasing molecular weight. As previously mentioned, this is most likely a result of increasing hydrodynamic radius with molecular weight where upon fewer molecules can occupy the adsorbed layer. By XPS, the adsorbed amounts are significantly lower than similar adsorption experiments performed from toluene with both the XPS data and the contact angle data indicating exposed silicon surface. Using atomic force microscopy, we explored the topography of these surfaces in an attempt to understand the XPS and contact angle results.

Table 1.22. XPS atomic concentration results and contact angle data (probe fluid, H_2O) of adsorbed films of both poly-**R/S** and poly-**S** on native silicon oxide. Adsorptions were performed for 53 hours, T = 25 °C, and at solution concentrations of 1 mg/mL in THF.

Sample	$C_{15°}$	$N_{15°}$	$O_{15°}$	$Si_{15°}$	C:N	Si:N	θ_A	θ_R
312:1 POLY-**R/S**	44.37	4.61	36.31	14.72	9.6:1	3.2:1	46°	22°
312:1 POLY-**S**	61.88	9.62	20.72	7.77	6.4:1	0.8:1	76°	29°
936:1 POLY-**R/S**	41.55	3.41	39.82	15.22	12.2:1	4.5:1	59°	22°
936:1 POLY-**S**	51.15	7.29	29.85	11.71	7.0:1	1.6:1	61°	18°
3121:1 POLY-**R/S**	36.34	2.54	46.03	15.09	14.3:1	5.9:1	38°	14°
3121:1 POLY-**S**	46.87	5.39	35.44	12.30	8.7:1	2.3:1	47°	17°

Sample	$C_{75°}$	$N_{75°}$	$O_{75°}$	$Si_{75°}$	C:N	Si:N
312:1 POLY-**R/S**	17.27	1.39	49.75	31.60	12.4:1	22.7:1
312:1 POLY-**S**	31.76	5.73	33.15	29.37	5.5:1	5.1:1
936:1 POLY-**R/S**	17.28	1.59	45.29	35.84	10.8:1	22.5:1
936:1 POLY-**S**	20.63	4.02	43.67	31.68	5.1:1	7.9:1
3121:1 POLY-**R/S**	14.41	1.20	48.06	36.34	12.0:1	30.2:1
3121:1 POLY-**S**	19.32	3.07	43.21	34.40	6.3:1	11.2:1

Cleaned native silicon oxide was examined by tapping mode AFM (Fig. 1.29) and was shown to have a root mean square roughness of 2 Å. The roughness was calculated by an algorithm used in the Nanoscope III system software and the results indicate the silicon wafer surface is smooth. All adsorption experiments were performed on substrates of this type.

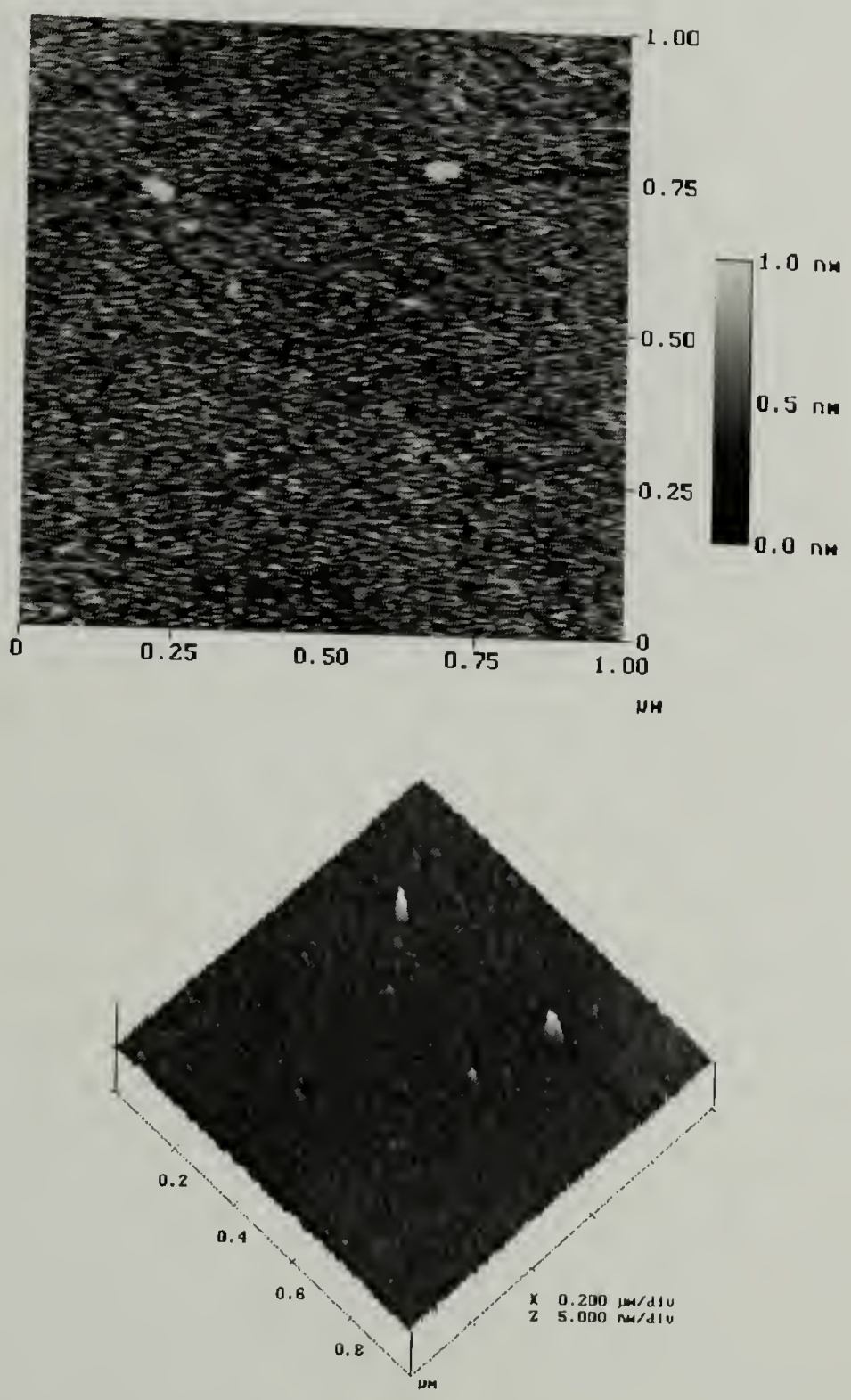

Figure 1.29. Tapping mode AFM height (top) and surface (bottom) image of cleaned native silicon oxide surface of the type used for all adsorption experiments performed in this dissertation.

Characterization of the topography of adsorbed thin films was accomplished by tapping mode AFM. The first image produced, Figure 1.30, was of poly-**R/S** adsorbed to native silicon oxide from toluene. The other AFM images shown in Figures 1.31 through 1.44 were acquired from both poly-**R/S** and poly-**S** adsorbed from THF onto native silicon oxide. The choice of molecular weights is insignificant, because the samples were prepared with the idea of quickly generating adsorbed films and to use these films to obtain a general idea of why the XPS and contact angle results were so different than adsorptions from toluene.

Atomic force microscopy of an adsorbed film of poly-**R/S** from toluene (see Fig. 1.30) resulted in a surface that appeared homogeneous with a root mean square roughness of approximately 50 Å. Contact angle results of $\theta_A/\theta_R = 93°/76°$ indicate complete coverage of the substrate. The film has the appearance of foam-like structure with the darkest spots associated with voids. Film thickness could not be determined by AFM because the analysis occurs only on the outer surface of the film.

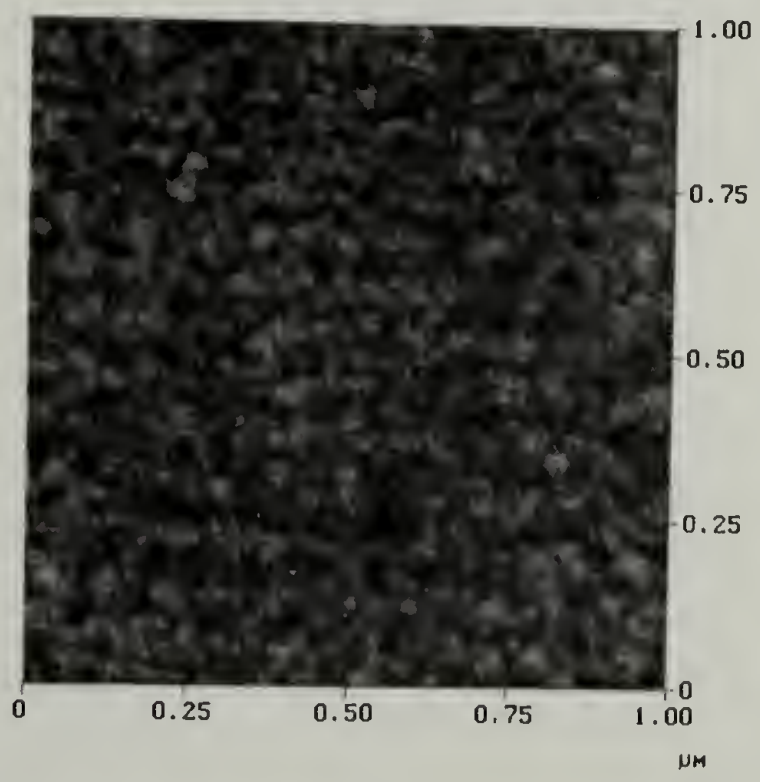

Figure 1.30. Tapping mode AFM height image from an adsorbed thin film of 4681:1 poly–**R/S** adsorbed from toluene to native silicon oxide at 1 mg/mL for 24 hours at 25 °C.

Atomic force microscopy images of adsorbed thin films of poly-**R/S** and poly-**S** show a different surface structure than the adsorbed films prepared from toluene. The height image shown in Figure 1.31 for the 312:1 poly-**S** suggests a surface with discontinuous structure. Section analysis, Figure 1.31, characterizes the surface as rough, and composed of numerous valleys, ridges, and knolls. The brightest areas indicate the high points which appear to be interconnected by ridges. Figure 1.32 shows the same surface viewed over an area of 50 μm^2 and also shown in Figure 1.32, is the phase image of that same area. The surface structure described for Figure 1.31 is also observed in the larger area image (Fig. 1.32). Surface structures greater than 10 nm were observed, for both measured length scales.

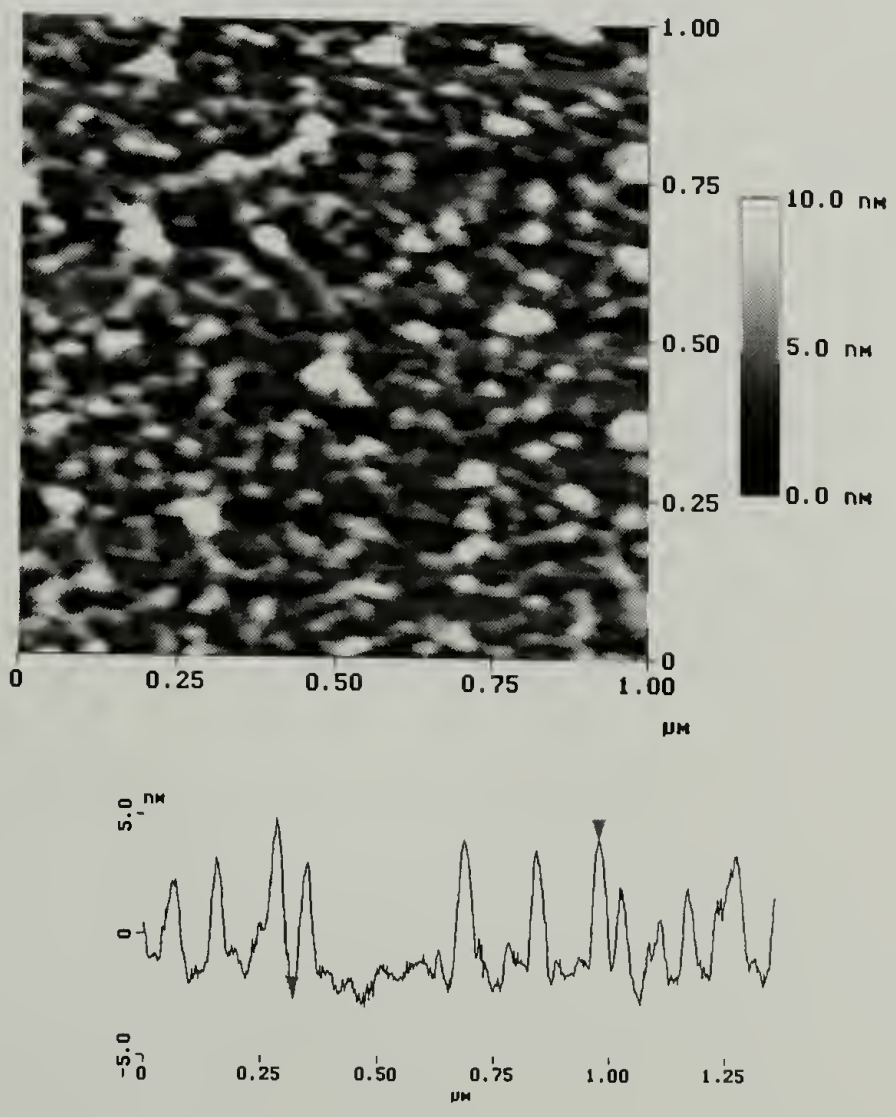

Figure 1.31. Tapping mode AFM height (left image) and section analysis (right image) of an adsorbed thin film of 312:1 poly–**S** adsorbed from THF to native silicon oxide at 1 mg/mL for 53 hours at 25 °C. Surface roughness calculations were performed on the area between the diamond symbols shown in the section analysis plot.

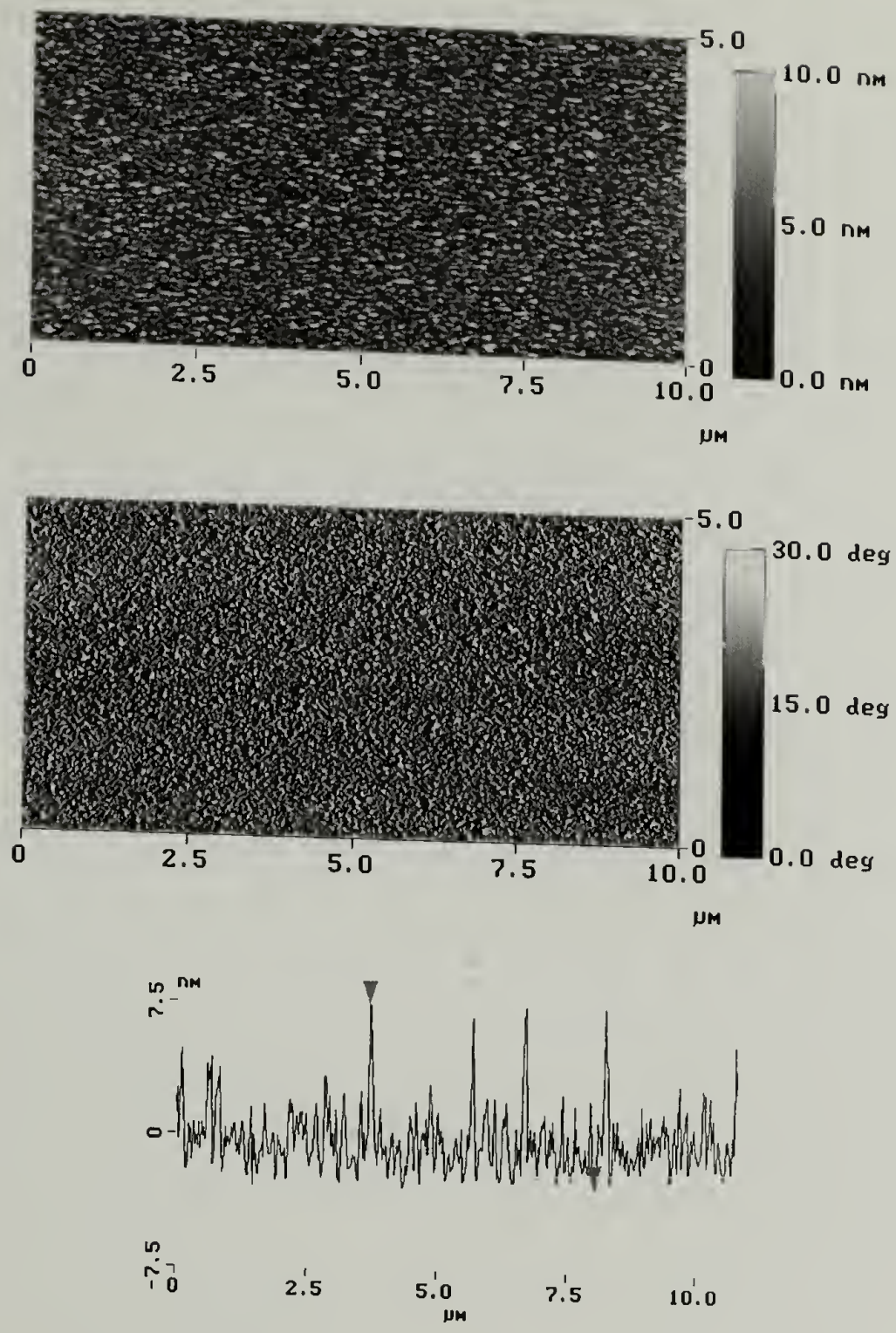

Figure 1.32. Tapping mode AFM height (upper image), phase image (middle), and section analysis (lower image) of an adsorbed thin film of 312:1 poly–**S** adsorbed from THF to native silicon oxide at 1 mg/mL for 53 hours at 25 °C. Surface roughness calculations were performed on the area between the diamond symbols shown in the section analysis plot.

Characterization of the surface topography by tapping mode AFM for the 936:1 poly-**R/S** sample (Figure 1.33) resulted with an apparent different structure than the 312:1 poly-**S**. However, close examination suggested similarities with the poly-**R/S** adsorbed film displaying thicker and longer ridges and less structure between the ridges. The length scales of the surface structures are greater for the 936:1 poly-**R/S** than the

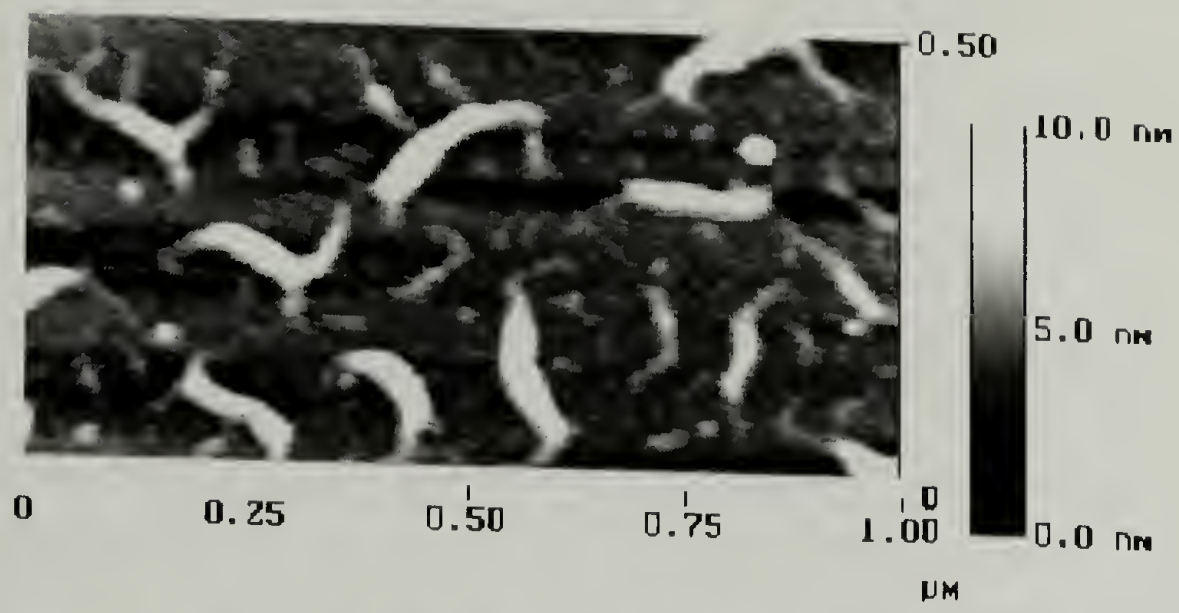

Figure 1.33. Tapping mode AFM height images (upper and middle image) and section analysis (lower image) of an adsorbed thin film of 936:1 poly–**R/S** adsorbed from THF to native silicon oxide at 1 mg/mL for 53 hours at 25 °C. Surface roughness calculations were performed on the area between the diamond symbols shown in the section analysis plot.

312:1 poly-**S**. This is further supported by the 50 μm^2 image that when compared to Figure 1.32 shows much larger structure. We explored the direct relationship between Mw and stereochemistry by comparing the surface structure of adsorbed films of the 3121:1 poly-**R/S** and 3121:1 poly-**S**. The surface structure for the high Mw poly-**R/S**

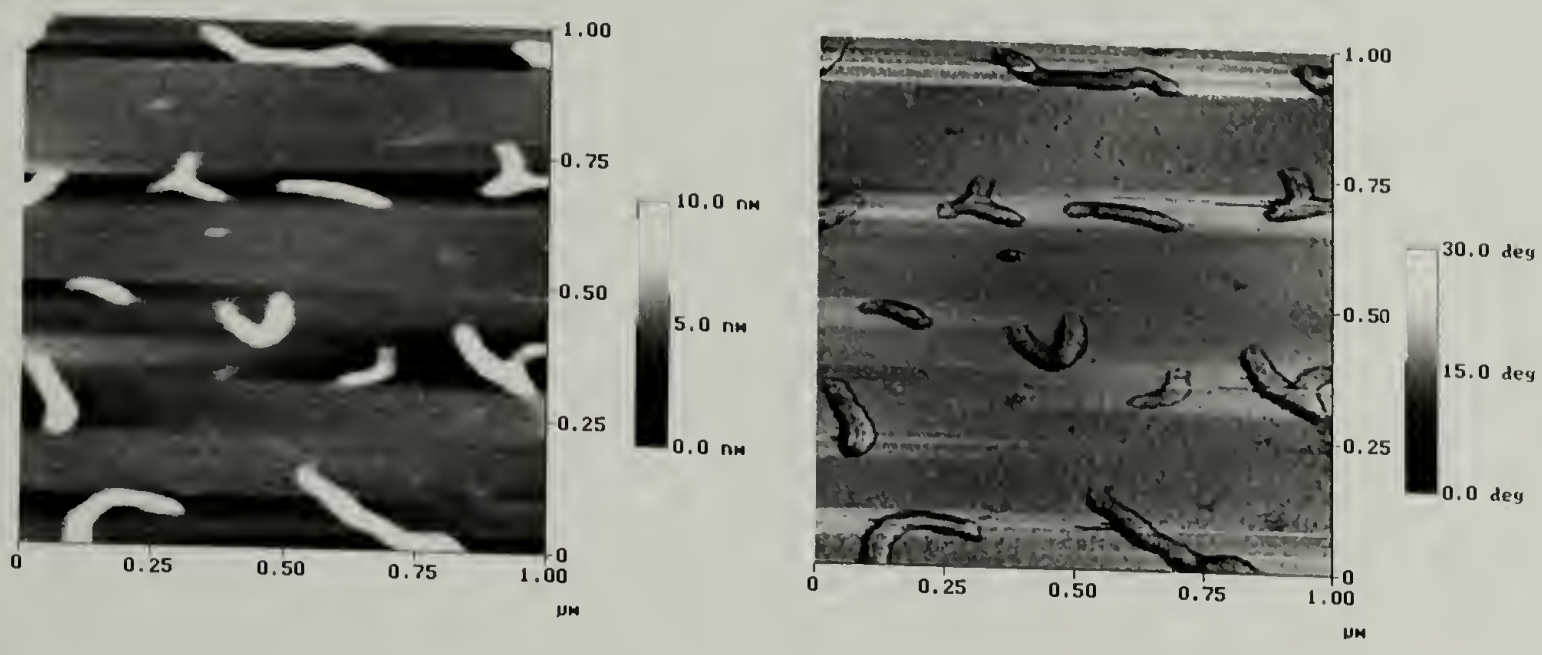

Figure 1.34. Tapping mode AFM height image (left image), phase (right image) and section analysis (lower image) of an adsorbed thin film of 3121:1 poly–**R/S** adsorbed from THF to native silicon oxide at 1 mg/mL for 53 hours at 25 °C. Surface roughness calculations were performed on the area between the diamond symbols shown in the section analysis plot.

sample (seen in Figure 1.34), shows a discontinuous surface composed of large structures that are thick, wide, and long. Very little structure was observed between the ridges suggesting the areas between the surface structures may be the silica substrate. In addition, no fine ribbons were evident between the larger structures, yet small droplets were observed. The surface structure of the 3121:1 poly-**S** is shown in Figures 1.35-1.36.

Compared to the 3121:1 poly-**R/S**, it indicates more finger protrusions with longer ridges of comparable height. Moreover, small droplets are seen between the smaller finger regions. All the images indicate that with increasing Mw, the aspect ratio of the surface structures increased and the complexity decreased. The phase images are included to help assist in viewing the images. However, since the phase mode indicates differences in surface modulus this technique can be used to differentiate between polymer and silicon surface.

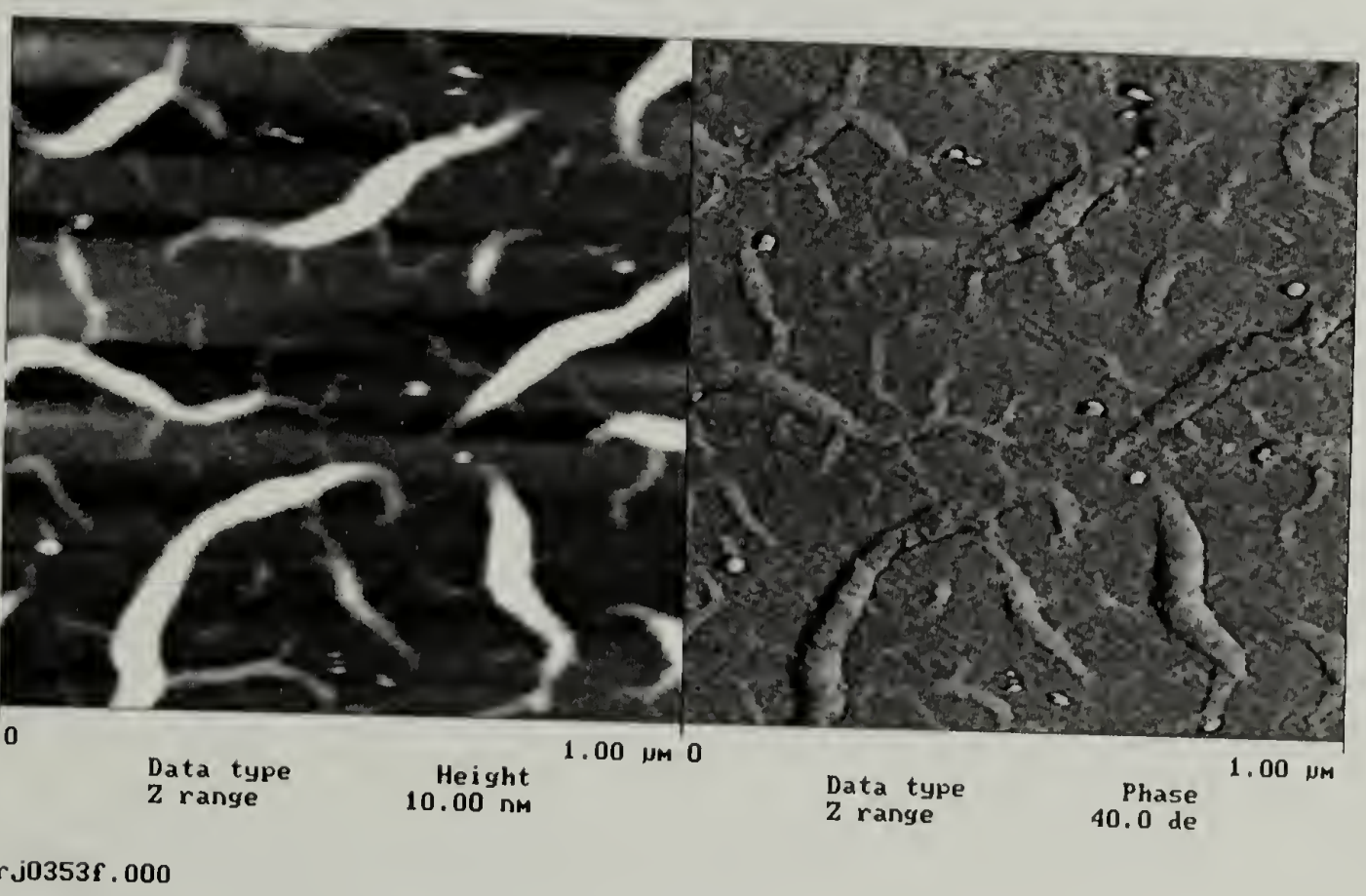

Figure 1.35. Tapping mode AFM height image (left image) and phase (right image) of an adsorbed thin film of 3121:1 poly–**S** adsorbed from THF to native silicon oxide from at 1 mg/mL for 53 hours at 25 °C.

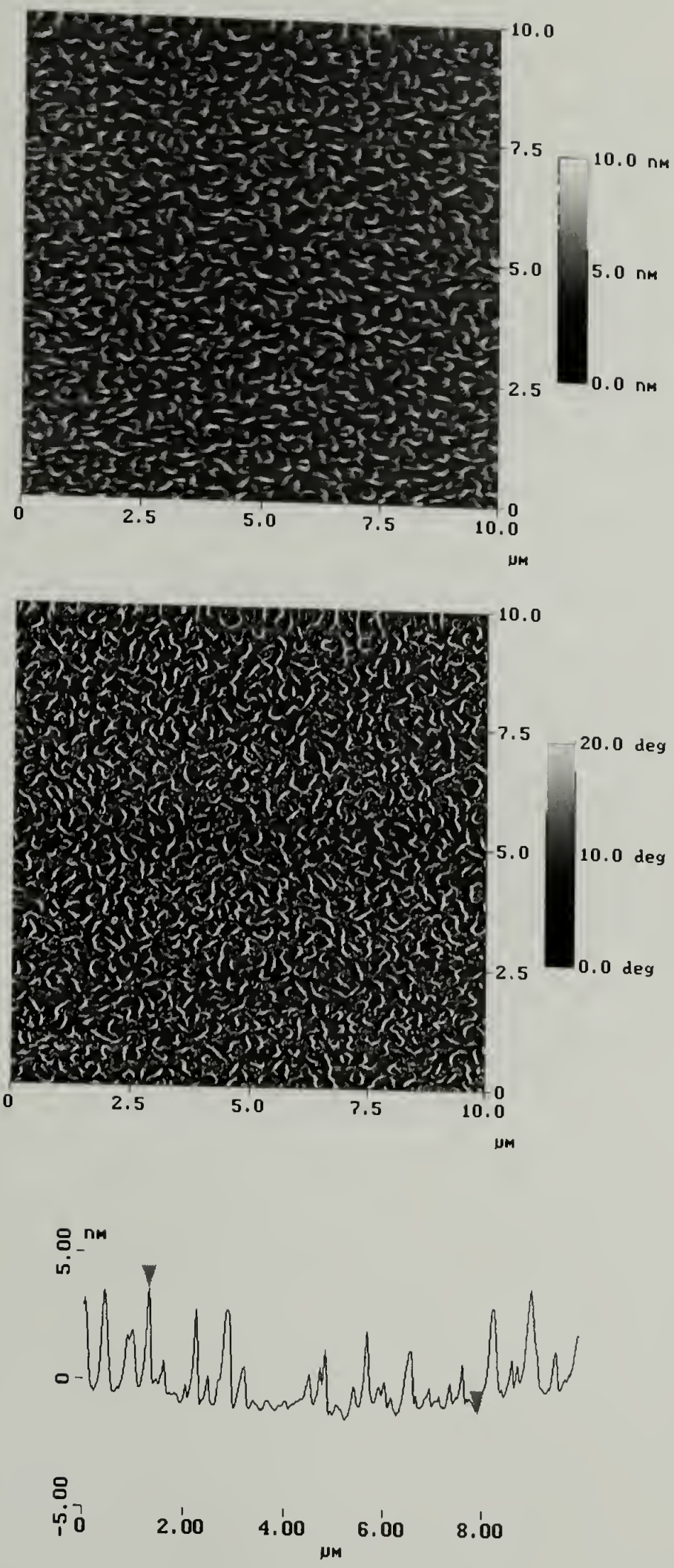

Figure 1.36. Tapping mode AFM height images (upper image), phase (middle image) and section analysis (lower image) of an adsorbed thin film of 3121:1 poly–**S** adsorbed from THF to native silicon oxide at 1 mg/mL for 53 hours at 25 °C. Surface roughness calculations were performed on the area between the diamond symbols shown in the section analysis plot.

The differences in the surface structure of adsorbed poly-**R/S** and poly-**S** were shown to be dependent on the solvent. We wanted to know why the complexity with the better solvent THF occurred. In addition, why did adsorbed films from toluene have continuous surface structure? The AFM images helped explain the scatter in the XPS and contact angle results. The thin films adsorbed from THF were rough with heights greater than 100 Å and phase imaging indicating large distances of silica surface between the peaks. Since XPS is angle dependent (i.e. line-of-sight), the actual area of polymer analyzed was small because only the highest regions were detected. Another indication of surface roughness was the large signal-to-noise ratio at short acquire times. To overcome the noise, long acquisition times of 30 minutes were necessary. The contact angle results suggested a rough surface with exposed silicon surface due to the hysteresis and low receding contact angles. Nonetheless, what role did solvent quality have in the formation of the observed surface structures? Along with solvent, what effects did temperature and kinetics of evaporation have on the final surface structure?

Effects of Solvent Quality

To explore the mechanism by which the previously shown surface structures formed, we choose to perform standard adsorption experiments, but added one last rinse in a non-solvent. Close examination of the data suggested a mechanism where the adsorbed film may be dewetting with solvent evaporation. Through rinsing with a nonsolvent, the idea was to partition the THF out of the polymer and frustrate the dewetting process, locking in its structure.

The choice of non-solvents was based not only on their poor solvating qualities but also on their vapor pressure at room temperature, because the formation of the observed surface structures is likely related to the evaporation rate of the solvent.[37] The rinsing of adsorbed films from toluene induced drying at a noticeably slower rate than adsorptions performed from THF. This obviously would be anticipated due to the lower

vapor pressure for toluene than THF. The faster evaporation rate would result in a rapid increase in viscosity, therefore reducing flow across the surface and producing a more homogeneous film. This is analogous to what Reiter et al.[35] observed for the dewetting of 660K polystyrene just above the polymers glass transition temperature, where the rate of dewetting was very slow due to viscosity effects. However, this was not observed for the poly-**R/S** and poly-**S**, since THF was the faster evaporating solvent and generated adsorbed films with more complex surface structure. Based on the better solvent quality of THF, as the concentration increased with solvent evaporation, the polymer/THF solution viscosity would remain lower than similar polymer/toluene solutions. To explore both theories, the following three non-solvents with a range of vapor pressures were researched: ether, methanol, and water. In addition, the adsorptions from THF were performed with the 3121:1 poly–**S**. We reasoned that the previous tapping mode AFM images indicated that this polymer formed surface structures with more detail than poly–**R/S** and the other molecular weight polymers.

The results from XPS and contact angle are shown in Table 1.23 and Table 1.24. Both the nitrogen and silicon atomic concentration data indicate thin film formation of poly-**S** adsorbed from THF to native silica. Recall that for poly(*N*-methyl-*N'*-(α-phenylethyl)carbodiimide), the carbon to nitrogen ratio is ~5:1. As seen in Table 1.23, the C:N ratio of 5:1 is not observed, where previously only adsorption from toluene generated $C_{75°}$:$N_{75°}$ ratios of ~5:1. Receding contact angle results listed in Table 1.24 indicate that the silica surface is exposed to the water probe fluid. The contact angle data for the control native silicon oxide surface were shown to be $\theta_A/\theta_R = 8°/0°$ for surfaces dried in an oven at 130° C for 2 hours prior to measurement and $\theta_A/\theta_R = 30°/13°$ for surfaces dried in vacuum for 12 hours. Thus, the advancing angles are larger than those measured previously for native silicon oxide and indicate the presence of polymer.

Table 1.23. XPS atomic concentration results from the analysis of adsorbed thin films of 3121:1 poly-**S** adsorbed from THF to native silicon at 1 mg/mL for 93 hours at 25 °C. Post adsorption the samples were rinsed three times with THF followed by one final rinse in the listed non-solvent.

Final Rinse Solvent	$C_{15°}$	$N_{15°}$	$O_{15°}$	$Si_{15°}$	$C_{15°} : N_{15°}$	$Si_{15°} : N_{15°}$
THF	45.48	4.81	36.88	12.83	9.5 : 1	2.7 : 1
Ether	45.99	3.05	37.19	13.77	15.1 : 1	4.5 : 1
Methanol	43.53	3.82	38.73	13.92	11.4 : 1	3.6 : 1
Water	34.90	2.75	45.19	17.17	12.7 : 1	6.2 : 1

Final Rinse Solvent	$C_{75°}$	$N_{75°}$	$O_{75°}$	$Si_{75°}$	$C_{75°} : N_{75°}$	$Si_{75°} : N_{75°}$
THF	17.86	1.99	50.64	29.51	9.0 : 1	14.8 : 1
Ether	15.91	2.02	48.45	33.62	7.9 : 1	16.6 : 1
Methanol	16.61	2.18	46.93	34.29	7.6 : 1	15.7 : 1
Water	16.01	1.14	50.37	32.47	14.0 : 1	28.4 : 1

Table 1.24. Water contact angle results from the analysis of adsorbed thin films of 3121:1 poly-**S** adsorbed from THF to native silicon at 1 mg/mL for 93 hours at 25 °C. Post adsorption the samples were rinsed three times with THF followed by one final rinse in the listed non-solvent.

Final Rinse Solvent	θ_A	θ_R
THF	44° ± 1°	13° ± 1°
Ether	47° ± 2°	16° ± 2°
Methanol	59° ± 3°	19° ± 3°
Water	48° ± 6°	20° ± 3°

Atomic force microscopy of the surfaces prepared with a final rinse in a non-solvent indicated that dewetting was occurring. As seen in the AFM images in Figures 1.37 and 1.38, the adsorption quenched in ether showed evidence of structures associated with dewetting such as droplets, holes, rims, and ribbons. Polymer dewetting is initiated with the formation of holes, which grow in size, with the leading wall of the hole referred to as the rim.[35] As the holes impinge on one another, the rims coalesce to form ribbons. Further decay (i.e. dewetting or drainage of the polymer) of the ribbons results in the formation of droplets. Shown in Figures 1.37 and 1.38 is evidence that late stage of dewetting has occurred because mixed between the ribbons are droplets. Some of the

droplet volumes were calculated by using the Bearing algorithm from the Nanoscope software package. From the volume, calculations were performed to determine the number of polymer molecules that compose the droplet. By assuming the polymer density to be 1 gm/cm^3 and the molecular weight of the polymer samples to be 50K and 500K respectively for the 312:1 and 3121:1 monomer:catalyst polymerization conditions, the number of moles of polymer in the droplet was calculated followed by multiplication by Avogadro's number. In Figure 1.37, the smaller droplets were on the order of 195 nm^3 which calculates to 0.2 molecules. Droplets on the order of 464 nm^3 to 2021 nm^3 were measured and calculated to be composed of 0.6 to 2.4 molecules respectively.

Early stages of dewetting are evident in the AFM images of poly-**S** adsorption quenched in methanol (Figures 1.39 and 1.40). Observed are holes with large ribbons and finger-like projections off the ribbons that extend out to what appears to be the early stages of droplet formation. Upon further dewetting, it appears droplets of various sizes remain. Reiter et al.[35] found in their work with polystyrene, that ribbons decay to droplets of size equal to the width of the ribbons. Thus, the size of the droplets may indicate the size scale of the ribbons from which they were formed. Volume calculations by the Bearing algorithm for a few droplets result in volumes between 308 nm^3 to 419 nm^3 which corresponds to 0.4 to 0.5 molecules respectively. The AFM images shown in Figures 1.41 and 1.42 are of water-quenched adsorption of poly-**S** from THF. In these images, the ribbons are thick with numerous small droplets dispersed between much larger droplets. A few of the droplets were measured to have volumes ranging from 2553 nm^3 (3.1 molecules) to 10,708 nm^3 (12.9 molecules) and very few finger projections were observed emerging from the walls of the ribbons.

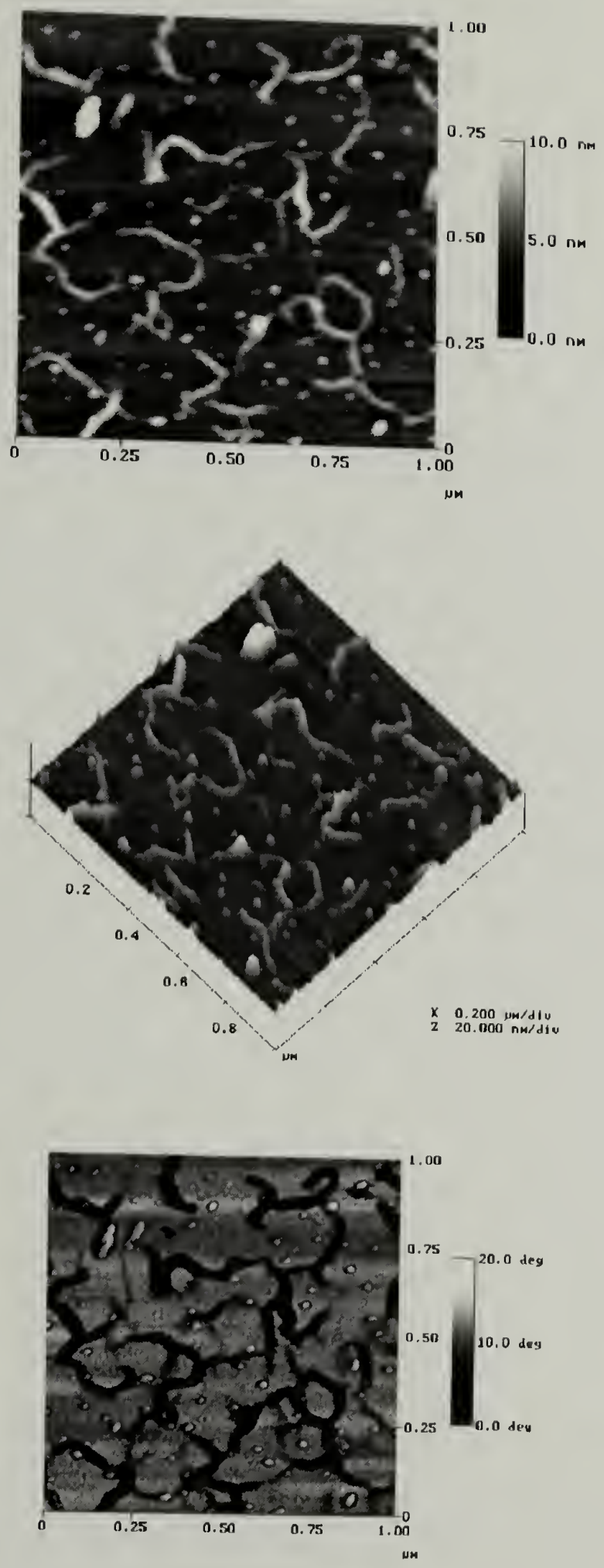

Figure 1.37. Tapping mode AFM (1 μm^2) height (top), surface(middle), and phase (bottom) images of adsorbed 3121:1 poly-**S** from THF to native silicon oxide at 1 mg/mL for 93 hours at 25 °C. Post adsorption the sample was rinsed three times with THF followed by one final rinse in ether.

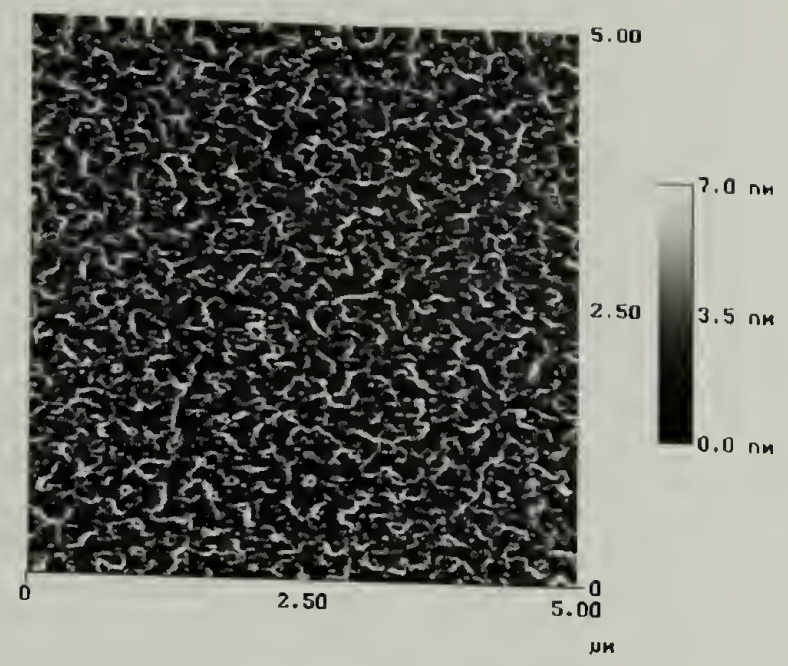

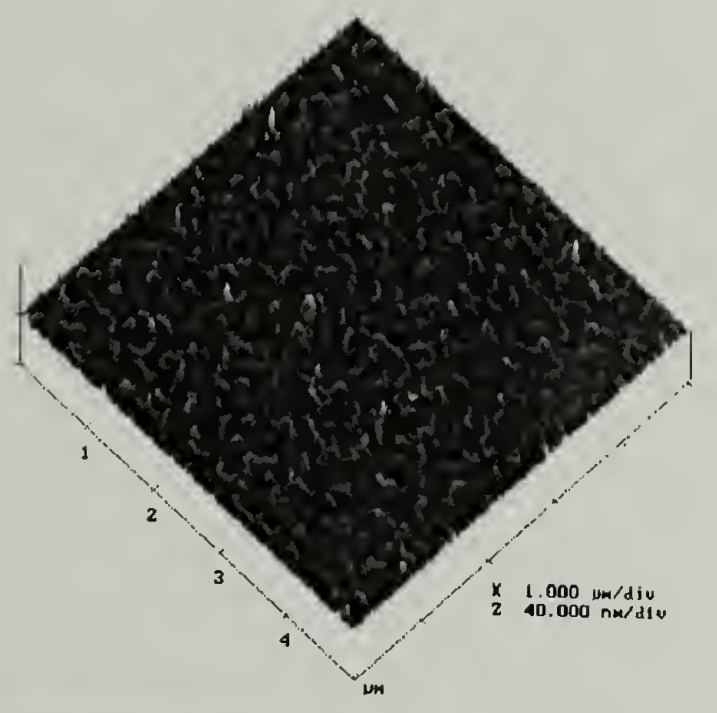

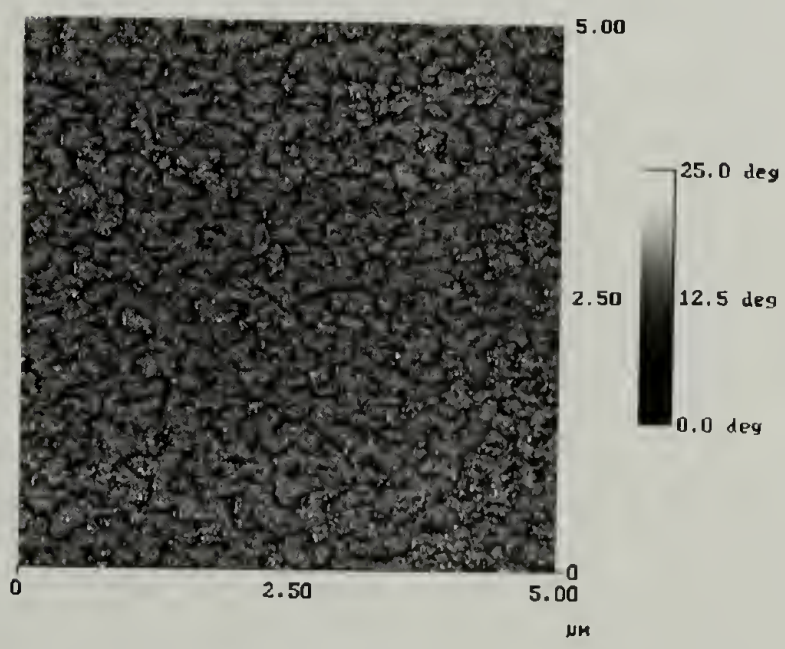

Figure 1.38. Tapping mode AFM (25 μm2) height (top), surface(middle), and phase (bottom) images of adsorbed 3121:1 poly-**S** from THF to native silicon oxide at 1 mg/mL for 93 hours at 25 °C. Post adsorption the sample was rinsed three times with THF followed by one final rinse in ether.

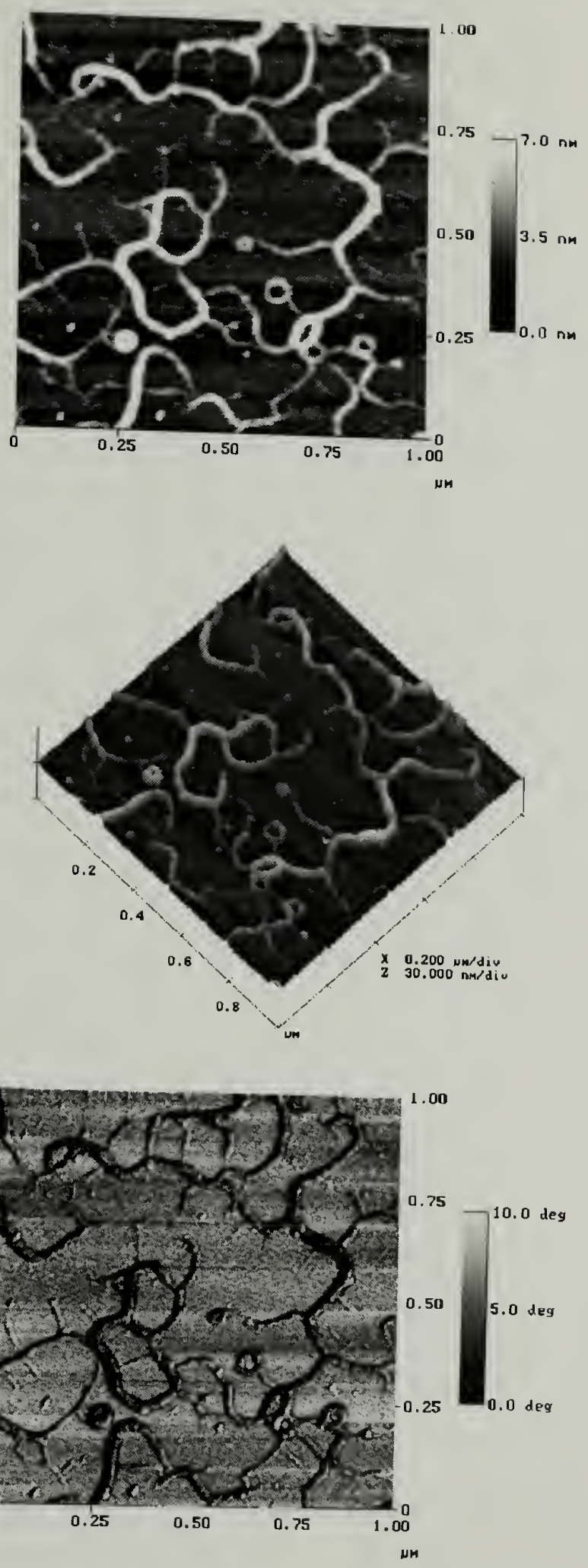

Figure 1.39. Tapping mode AFM (1 μm^2) height (top), surface(middle), and phase (bottom) images of adsorbed 3121:1 poly-**S** from THF to native silicon oxide at 1 mg/mL for 93 hours at 25 °C. Post adsorption the sample was rinsed three times with THF followed by one final rinse in methanol.

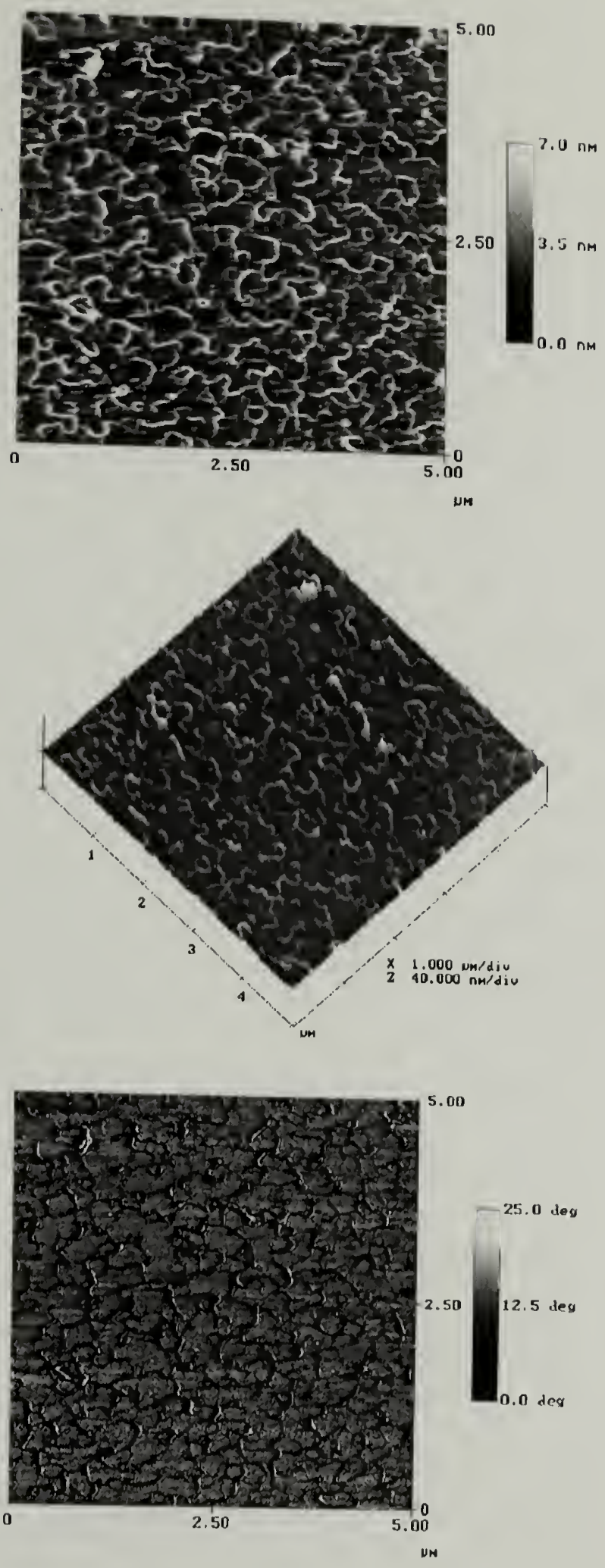

Figure 1.40. Tapping mode AFM (25 μm^2) height (top), surface(middle), and phase (bottom) images of adsorbed 3121:1 poly-**S** from THF to native silicon oxide at 1 mg/mL for 93 hours at 25 °C. Post adsorption the sample was rinsed three times with THF followed by one final rinse in methanol.

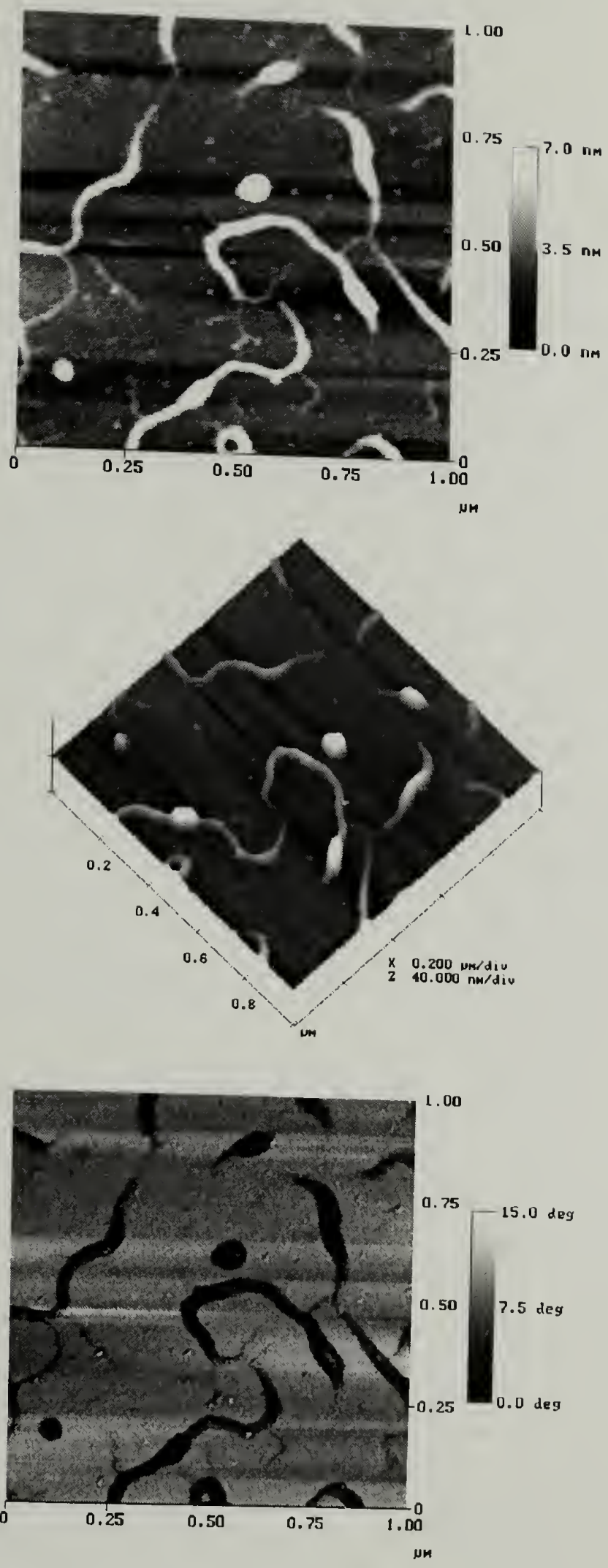

Figure 1.41. Tapping mode AFM (1 μm^2) height (top), surface (middle), and phase (bottom) images of adsorbed 3121:1 poly-**S** from THF at 1 mg/mL for 93 hours at 25 °C. Post adsorption the sample was rinsed three times with THF followed by one final rinse in water.

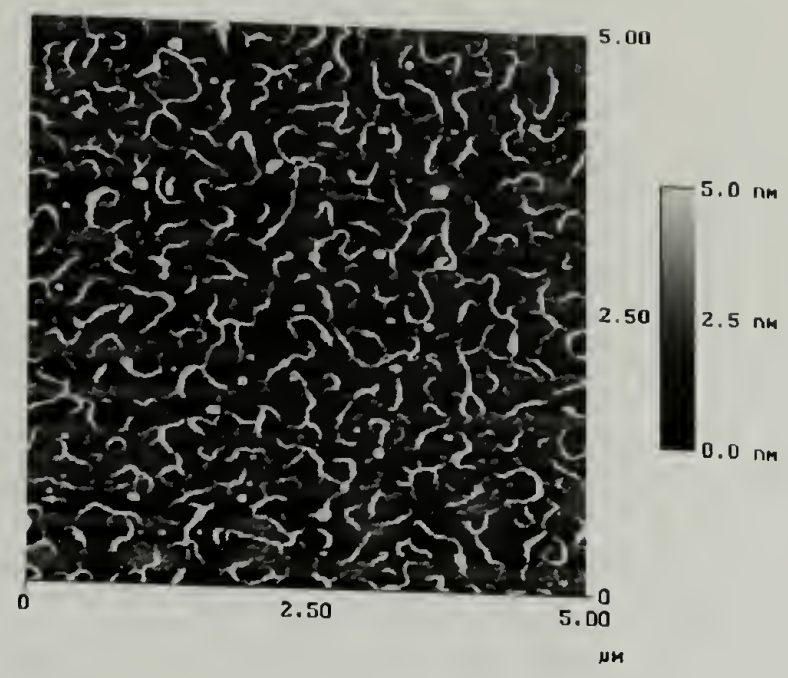

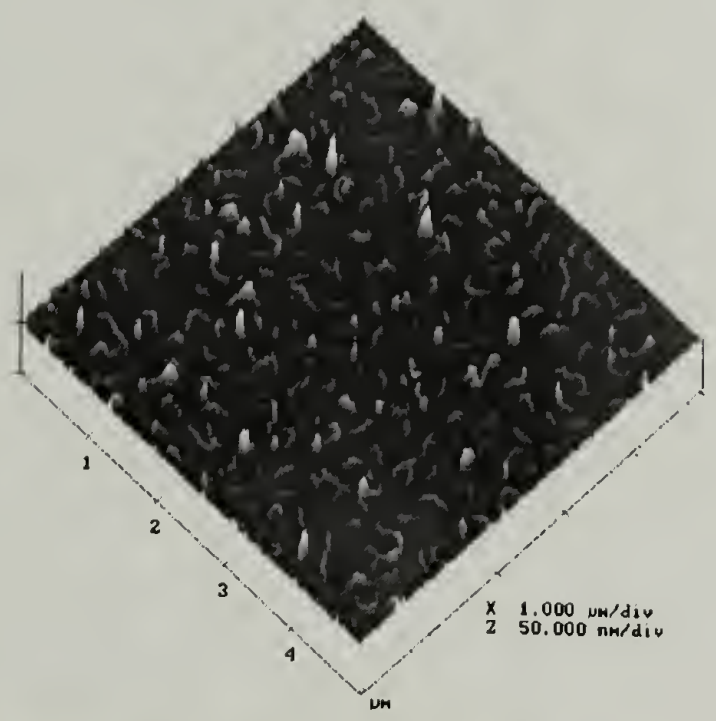

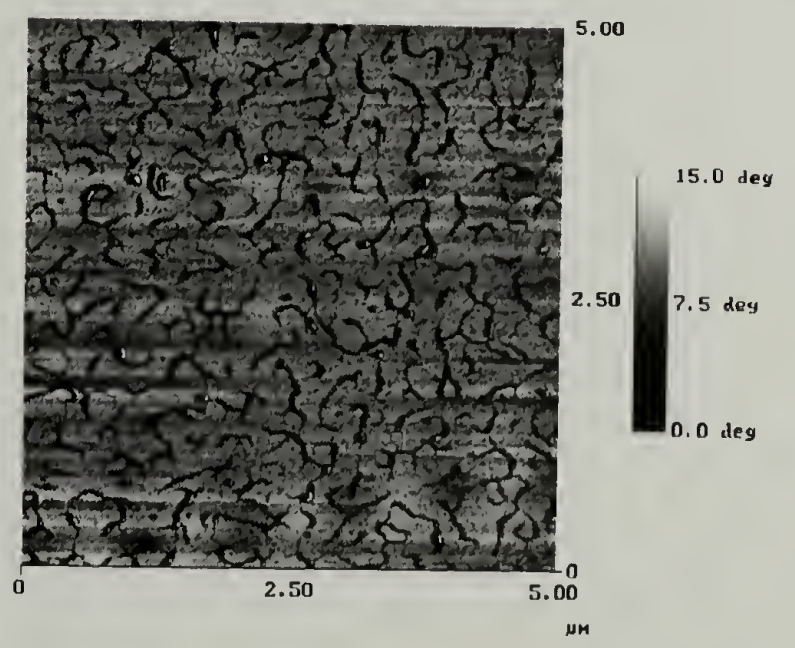

Figure 1.42. Tapping mode AFM (25 μm^2) height (top), surface(middle), and phase (bottom) images of adsorbed 3121:1 poly-**S** from THF to native silicon oxide at 1 mg/mL for 93 hours at 25 °C. Post adsorption the sample was rinsed three times with THF followed by one final rinse in water.

Comparing the AFM images from all three non-solvent conditions, we observed a few trends. The number of droplets appeared to decrease and the ribbon structures became thicker as the non-solvent rinse condition was modified from ether, to methanol, and then water. In addition, the adsorption quenched in methanol showed the highest level of finger protrusion formation. We postulated why the observed stages of dewetting were dependent on the non-solvent. The trend of surface structure complexity with increasing solvent evaporation (ether, methanol, and water respectively) suggested that the degree of dewetting could possibly be due to entrapment. However, the surface structures indicated that solvent partitioning might also be a critical factor. To better understand the mechanisms involved in the formation of the observed degrees of dewetting, we performed kinetics studies by adsorbing polymer from both toluene and THF.

As previously shown in the AFM images, various degrees of the dewetting process were indicated by differences in ribbon, hole, and droplet formations. We wanted to understand the mechanism differences by which adsorptions from THF produced complex surfaces and adsorptions from toluene produced relatively uniform surfaces. One of the possible mechanisms for this variation in surface structure was directly related to the adsorbed amount. Adsorptions of poly-**R/S** from toluene are fast (as indicated by the adsorption isotherm data), and we questioned whether the film uniformity was directly related to film thickness, because thickness had been shown to directly influence the mechanism of dewetting.[34,35,45,46,48,50] For adsorptions of poly-**R/S** from THF, the isotherm data indicated a relatively slower rate of adsorption, therefore, potentially producing thinner adsorbed films. However, the adsorption isotherms were generated using XPS results, and these results were suspect because of the differences in surface roughness as shown by AFM. Recall how the XPS analysis is performed: the surface is flooded with soft X-rays and only the ejected photoelectrons that escape at an angle equivalent to that of the detector are analyzed. For a uniform and smooth surface,

the ejected photoelectrons represent the entire surface but if the surface is rough, the actual surface the detector analyzes is biased. Therefore, this led to the question, do equivalent amounts of poly-**R/S** adsorb from toluene and THF? In addition, during adsorptions from THF does the initial adsorption of polymer produce uniform films that begin to dewet as polymer begins to saturate the surface?

Experimentally, these questions were addressed by performing adsorption kinetics of 3121:1 poly-**R/S** from toluene and THF both at 1.0 mg/mL. The XPS results are listed in Table 1.25 and contact angle results are listed in Table 1.26. The adsorptions

Table 1.25. XPS atomic concentration results of thin films of adsorbed 3121:1 poly-**R/S** to native silicon oxide from THF or toluene at 1 mg/mL at 25 °C for the time indicated. The data describes the affect of solvent and time of adsorption, on the dried surface structure of the adsorbed film.

Condition	$C_{15°}$	$N_{15°}$	$O_{15°}$	$Si_{15°}$	$C_{15°} : N_{15°}$	$Si_{15°} : N_{15°}$
30 min THF	37.92	1.72	44.95	15.41	22 : 1	9.0 : 1
30 min TOL	83.69	13.83	0.72	1.76	6.1 : 1	0.1 : 1
1 hr THF	42.64	3.95	38.89	14.51	11 : 1	3.7 : 1
1 hr TOL	83.61	14.84	0.92	0.63	5.6 : 1	0.04 : 1
2hr THF	39.90	3.01	42.05	15.04	13 : 1	5.0 : 1
2 hr TOL	83.99	14.53	0.73	0.76	5.8 : 1	0.05 : 1
4 hr THF	45.01	4.41	37.75	12.84	10 : 1	2.9 : 1
4 hr TOL	84.02	14.71	1.28	0.00	5.7 : 1	0
6 hr THF	44.49	4.44	36.23	14.85	10 : 1	3.3 : 1
6 hr TOL	83.30	15.26	0.84	0.60	5.5 : 1	0.04 : 1

Condition	$C_{75°}$	$N_{75°}$	$O_{75°}$	$Si_{75°}$	$C_{75°} : N_{75°}$	$Si_{75°} : N_{75°}$
30 min THF	12,67	1.38	51.34	34.61	9.2 : 1	25 : 1
30 min TOL	57.55	12.51	15.99	13.96	4.6 : 1	1.1 : 1
1 hr THF	15.21	1.19	52.46	31.14	13 : 1	26 : 1
1 hr TOL	53.31	10.54	18.88	17.26	5.1 : 1	1.6 : 1
2hr THF	13.24	1.02	51.91	33.83	13 : 1	33 : 1
2 hr TOL	58.24	12.30	15.24	14.22	4.7 : 1	1.2 : 1
4 hr THF	15.17	1.71	49.20	33.92	8.9 : 1	20 : 1
4 hr TOL	57.60	11.65	16.07	14.67	4.9 : 1	1.3 : 1
6 hr THF	17.00	1.39	45.56	36.05	12 : 1	26 : 1
6 hr TOL	55.97	12.68	17.06	14.29	4.4 : 1	1.1 : 1

were performed over a period of 30 minutes to 6 hours following previously described standard adsorption procedures. The XPS ([N_{1s}]) and water contact angle results for 30 minutes to 2 hours indicate that adsorptions from toluene are faster than from THF. Intuitively, this was anticipated based on solvent quality, where toluene is the poorer of the two solvents. Therefore by theory[1], more polymer should adsorb from toluene than THF as long as the adsorption is performed for an equivalent period. However, comparing the two solvent conditions of the poly-**R/S** adsorptions, the data indicate very different surface structures formed during short adsorption periods. During these short adsorption times, the XPS and contact angle data were comparable to adsorptions performed over much longer times. Nevertheless, previous results have shown that caution should be applied in interpreting adsorption results by only XPS and contact angle data. Therefore, the study of adsorbed films should include characterization of surface topography by, for example, AFM.

Table 1.26. Water contact angle of thin films of adsorbed 3121:1 poly-**R/S** to native silicon oxide from THF or toluene at 1 mg/mL at 25 °C for the time indicated. The data describes the affect of solvent and time of adsorption, on the dried surface structure of the adsorbed film.

Condition	θ_A	θ_R
30 min THF	37° ± 1°	18° ± 1°
30 min TOL	94° ± 3°	81° ± 3°
1 hr THF	36° ± 1°	21° ± 2°
1 hr TOL	91° ± 2°	79° ± 1°
2hr THF	35° ± 1°	18° ± 1°
2 hr TOL	93° ± 1°	80° ± 1°
4 hr THF	39° ± 2°	19° ± 1°
4 hr TOL	93° ± 1°	80° ± 1°
6 hr THF	40° ± 2°	19° ± 2°
6 hr TOL	93° ± 1°	82° ± 2°

Characterization of surface topography of the samples prepared during the kinetics experiment was performed using tapping mode AFM. The results for one hour

and four hour adsorptions from THF and toluene are shown in Figures 1.43 and 1.45 and Figures 1.44 and 1.46, respectively. The image for the one-hour adsorption from THF (Fig. 1.43), shows a surface composed of dispersed polymer droplets with heights greater than 20 Å. Further, the area between the drops was shown by phase mode AFM to be

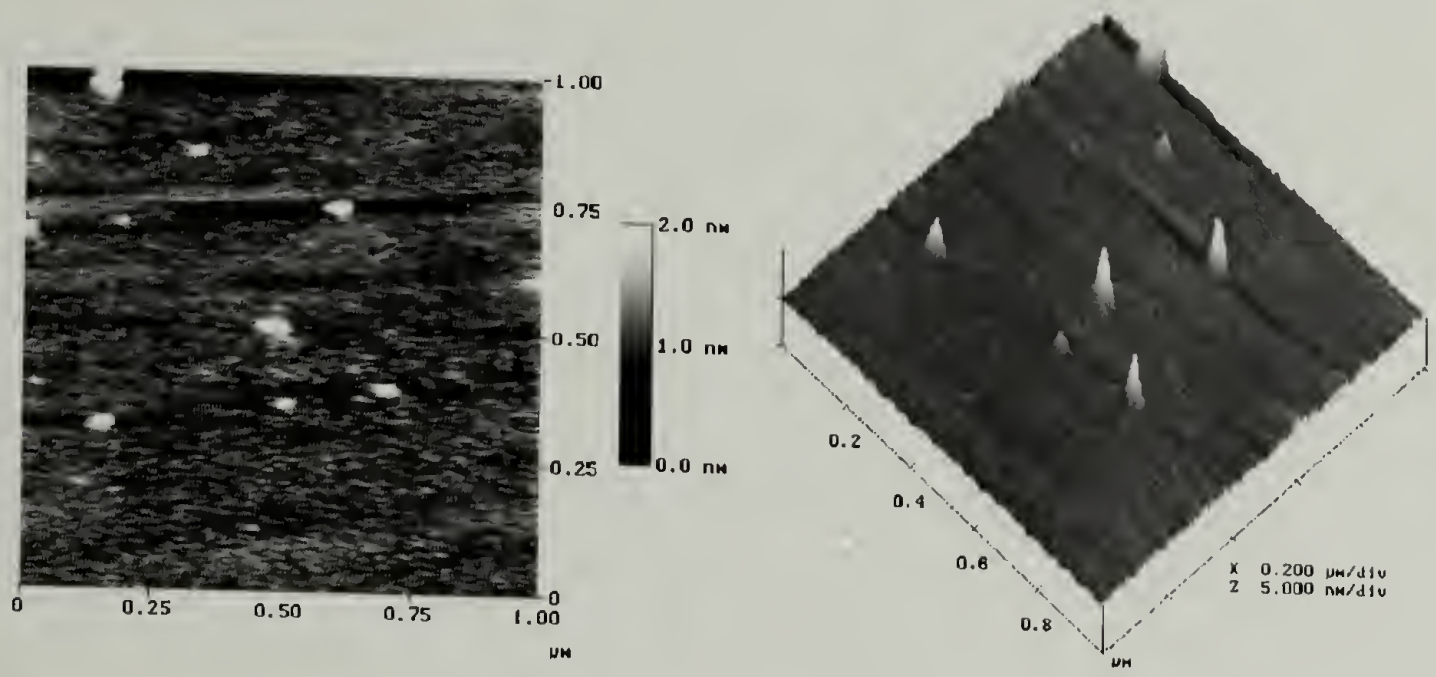

Figure 1.43. Tapping mode AFM height (left) and surface (right) images of adsorbed 3121:1 poly-**R/S** from THF to native silicon oxide at 1 mg/mL for 1 hour at 25 °C.

native silicon oxide. The receding water contact angle data indicate interactions between the probe fluid, water and the silica substrate. Comparable results were also found for the 30 minute and the 2 hour adsorbed films from THF. For the adsorptions from toluene, at all adsorption times, AFM showed (Fig. 1.44 and 1.46) no significant differences in surface structure. Contact angle results indicated the adsorbed films from toluene were uniform and thick enough to shield the water probe fluid, from the native silicon oxide substrate. The AFM results for the four-hour adsorption from THF (Figure 1.45) show dewetting and structures similar to those previously analyzed. However, the heights of the ribbons were significantly smaller than shown by AFM for comparable adsorptions at

longer times. This suggests that fewer polymer chains had adsorbed during this short period. Therefore, this indicates that the degree of dewetting and the size scale of the surface structures during dewetting is related to the adsorbed amount. This is supported by the observed complexity of the surface structure for this molecular weight of poly-**R/S** is much finer than previously observed. Therefore, the surface structure may be a kinetic

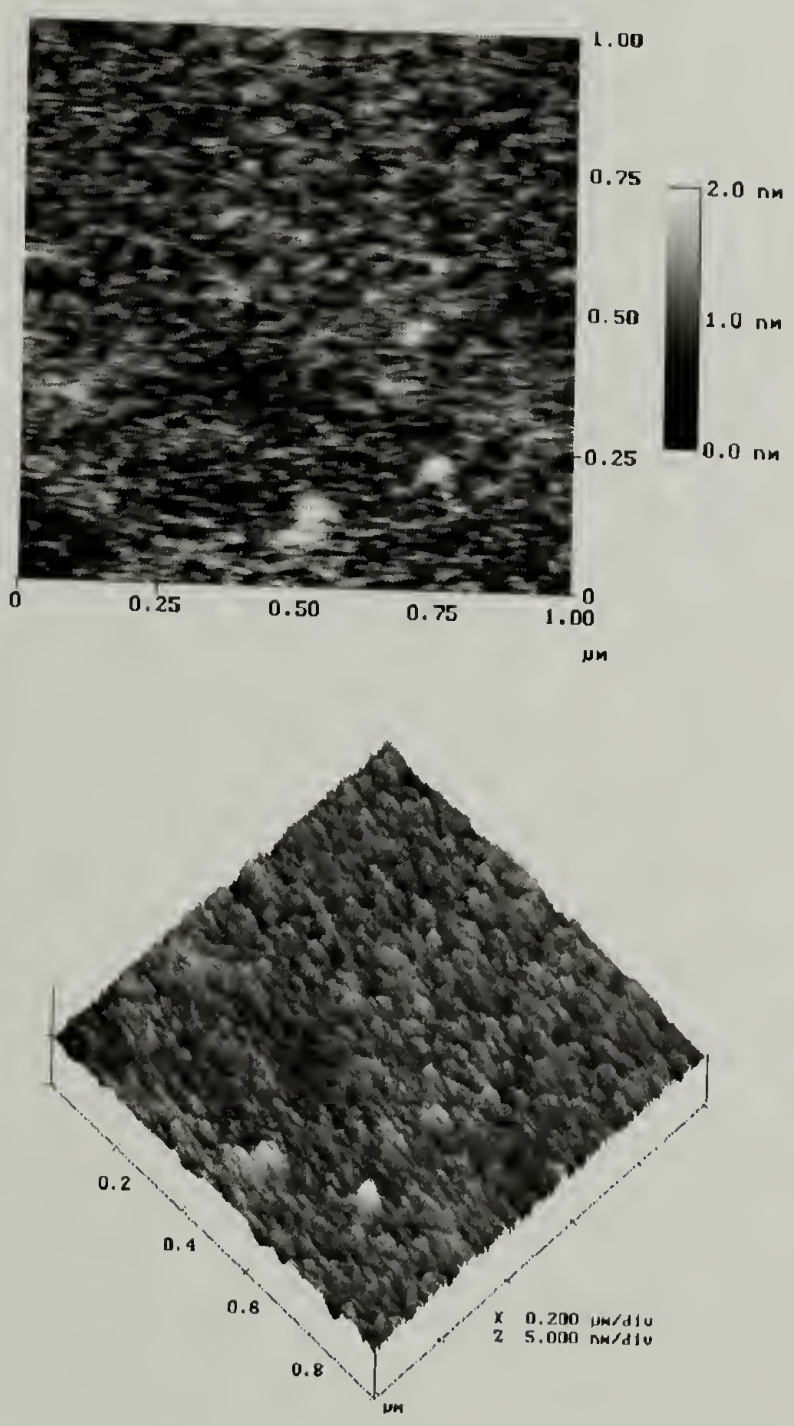

Figure 1.44. Tapping mode AFM height (top) and surface (bottom) images of an adsorbed thin film of 3121:1 poly-**R/S** on native silicon oxide from toluene for 1 hour at 25 °C and a solution concentration of 1 mg/mL.

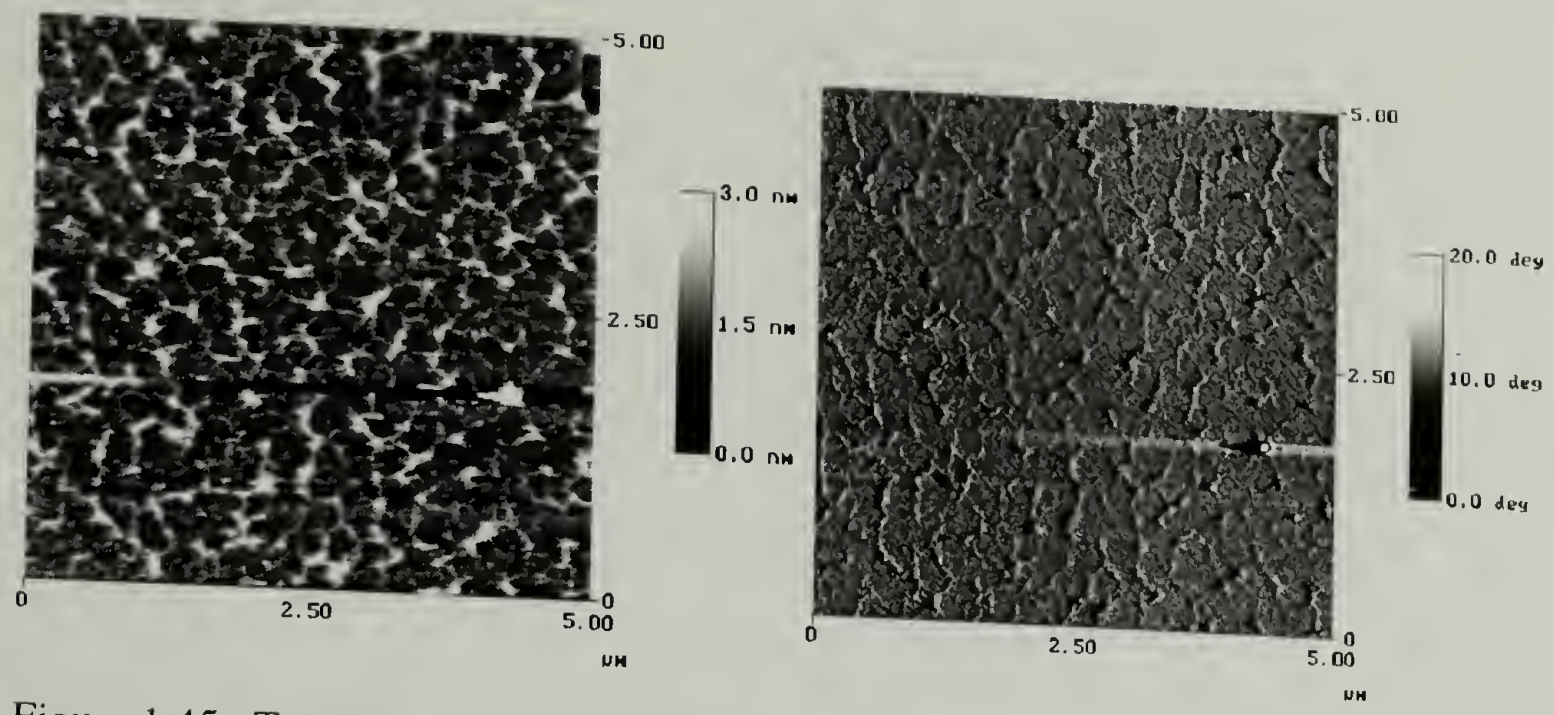

Figure 1.45. Tapping mode AFM height (upper) and phase (lower) images of adsorbed 3121:1 poly-**R/S** from THF to native silicon oxide at 1 mg/mL for 4 hours at 25 °C.

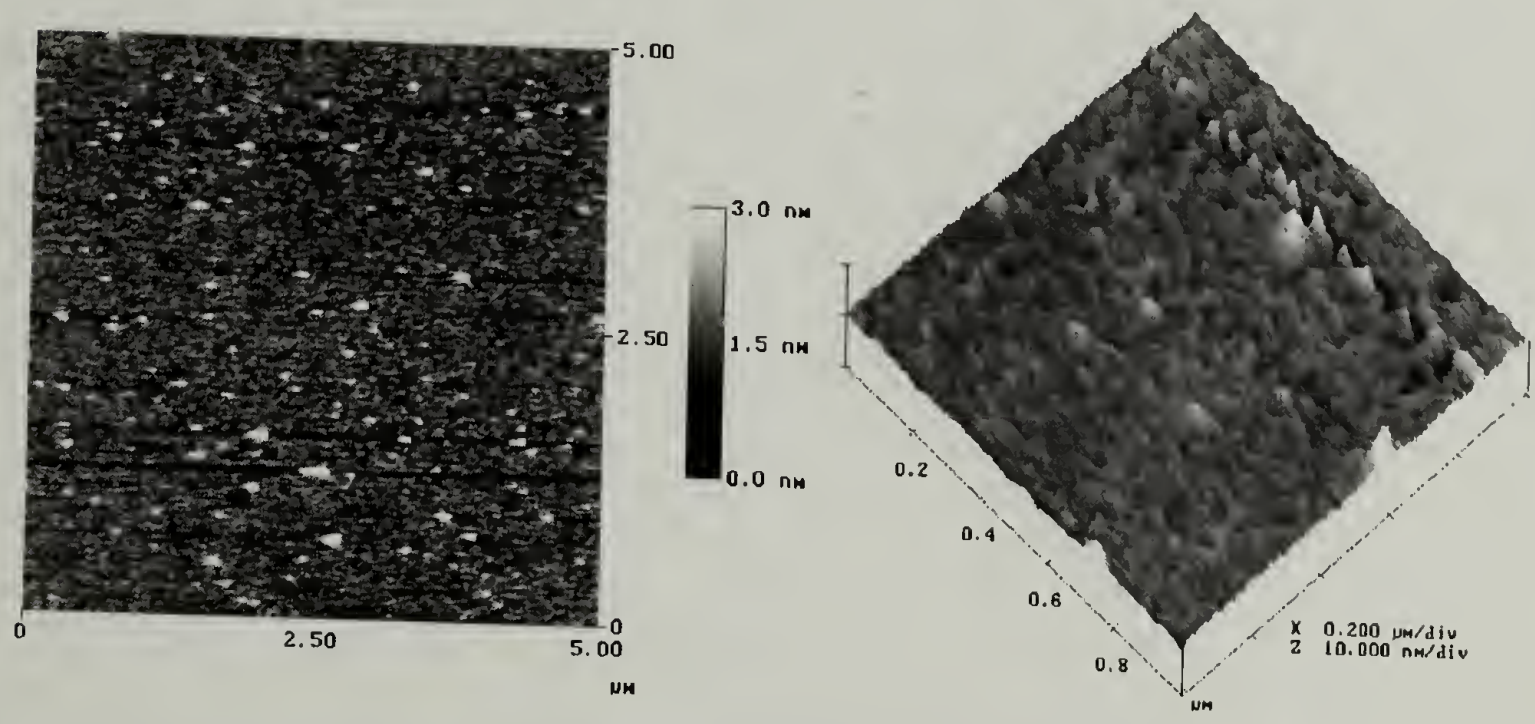

Figure 1.46. Tapping mode AFM height (upper) and surface (lower) images of an adsorbed thin film of 3121:1 poly-**R/S** adsorbed from toluene to native silicon oxide at 1 mg/mL for 4 hours at 25 °C.

trapping of the early stages of dewetting where potentially over a longer period of time the surface would further dewet and form larger as well as less complex structures. Thus, the data suggest that kinetic trapping of the surface structure was feasible, so we next investigated how to research this.

Kinetic Trapping

Kinetic trapping of the surface structures was researched by performing adsorption experiments from toluene and THF using 3121:1 poly-**R/S**. Two adsorbed films from toluene were prepared with one rinsed in toluene and the other rinsed in THF. In addition, an adsorbed film from THF was rinsed in toluene. All adsorptions were performed at solution concentrations of 1.0 mg/mL, and the films were analyzed by XPS, contact angle, as well as tapping mode AFM.

Atomic concentration data for all three adsorption conditions described above are listed in Table 1.27. The data for the adsorption from toluene and rinsed from toluene is comparable with previous results. However, the most interesting results were of the other adsorption conditions. For instance, the atomic concentration data for the THF/toluene (adsorption solvent/rinse solvent) adsorption method were identical to the results for the toluene/toluene adsorption condition. The atomic concentration data for the toluene/THF adsorption protocol were similar to previous results shown for adsorptions from THF followed by rinsing in THF. The data in Table 1.27 indicate that adsorptions performed from either THF or toluene result in comparable amounts of 3121:1 poly-**R/S** saturating the surface. Therefore, the observed surface structures must be directly related to solvent quality.

The adsorbed films were further studied by performing contact angle measurements with the results listed in Table 1.28. Concurrent with the XPS results, the contact angle data for the toluene/toluene condition had been previously observed for adsorption of 3121:1 poly-**R/S** under similar methods. Although the XPS results for the toluene/toluene and THF/toluene were similar, the contact angle results were very different. The advancing contact angle for the THF/toluene adsorption condition was on average 23° higher then for the toluene/toluene adsorption condition, and yet the receding contact angles were equivalent. For the THF/toluene condition, the advancing contact angle was very difficult to obtain because of rapid instabilities in the water drop upon

contact with the adsorbed polymer layer. This was indicative of the water drop removing or displacing the adsorbed film. When the instability stopped, the measured advancing and receding contact angles (listed in Table 1.28 in parenthesis) approached values comparable with those previously measured for contaminated native silicon oxide substrate. The contact angle results for the toluene/THF condition were comparable to the angles measured for adsorptions performed from THF then rinsed in THF. Generally, the contact angle results concurred with the XPS results except for the THF/toluene data that indicates a different surface structure. To explore these differences, tapping mode AFM was performed.

Table 1.27. XPS atomic concentration results from the analyses of adsorbed thin films of 3121:1 poly-**R/S** adsorbed from the first solvent listed in the solvent pairs, to native silicon oxide. The second solvent listed is the solvent used to rinse the adsorbed layer after the polymer adsorbed for 96 hours. The results describe the affect of adsorption solvent (Tol = toluene) and rinse solvent on the surface structure of the adsorbed dry film.

Condition	$C_{15°}$	$N_{15°}$	$O_{15°}$	$Si_{15°}$	$C_{15°} : N_{15°}$	$Si_{15°} : N_{15°}$
Tol / Tol	83.62	14.46	0.72	1.20	5.8 : 1	0.08 : 1
THF / Tol	82.56	14.78	1.06	1.61	5.6 : 1	0.11 : 1
Tol / THF	43.31	4.48	37.64	14.57	9.7 : 1	3.3 : 1

Condition	$C_{75°}$	$N_{75°}$	$O_{75°}$	$Si_{75°}$	$C_{75°} : N_{75°}$	$Si_{75°} : N_{75°}$
Tol / Tol	58.21	12.11	15.67	14.01	4.8 : 1	1.2 : 1
THF / Tol	52.76	11.30	18.88	17.06	4.7 : 1	1.5 : 1
Tol / THF	16.85	1.94	49.68	31.52	8.7 : 1	16.2 : 1

The XPS and contact angle data suggested that solvent quality was the critical factor affecting the surface structure of an adsorbed film of 3121:1 poly-**R/S**. However, the data also indicated that the surface structure of the adsorbed film could be controlled by varying the rinse solvent. To confirm the previous assessments, the surface topography of the above three samples prepared under different adsorption conditions

Table 1.28. Contact angle results from the analyses of adsorbed thin films of 3121:1 poly-**R/S** adsorbed from the first solvent listed in the solvent pairs, to native silicon oxide. The second solvent listed is the solvent used to rinse the adsorbed layer after the polymer adsorbed for 96 hours. The results describe the affect of adsorption solvent (Tol = toluene) and rinse solvent on the surface structure of the adsorbed dry film.

Condition	θ_A	θ_R
Tol / Tol	94° ± 1°	77° ± 1°
THF / Tol	117° ± 4°	79° ± 2°
	(37° ± 2°)	(11° ± 3°)
Tol / THF	59° ± 7°	14° ± 5°

were analyzed by tapping mode AFM, and the results are shown in Figures 1.47 through 1.49. The surface structure of the adsorbed film of 3121:1 poly-**R/S** from toluene followed by rinsing in toluene is shown in Figure 1.47 and the images are comparable to previous AFM images of samples prepared under similar conditions. Despite the contact angle data, the same similarities in surface structure were observed for the adsorbed film of 3121:1 poly-**R/S** from THF followed by rinsing in toluene (Figure 1.48). In addition, the adsorption of 3121:1 poly-**R/S** from toluene followed by rinsing in THF resulted in a dewetted surface (Figure 1.49) comparable to surface structures shown previously for adsorptions from THF followed by rinsing in THF.

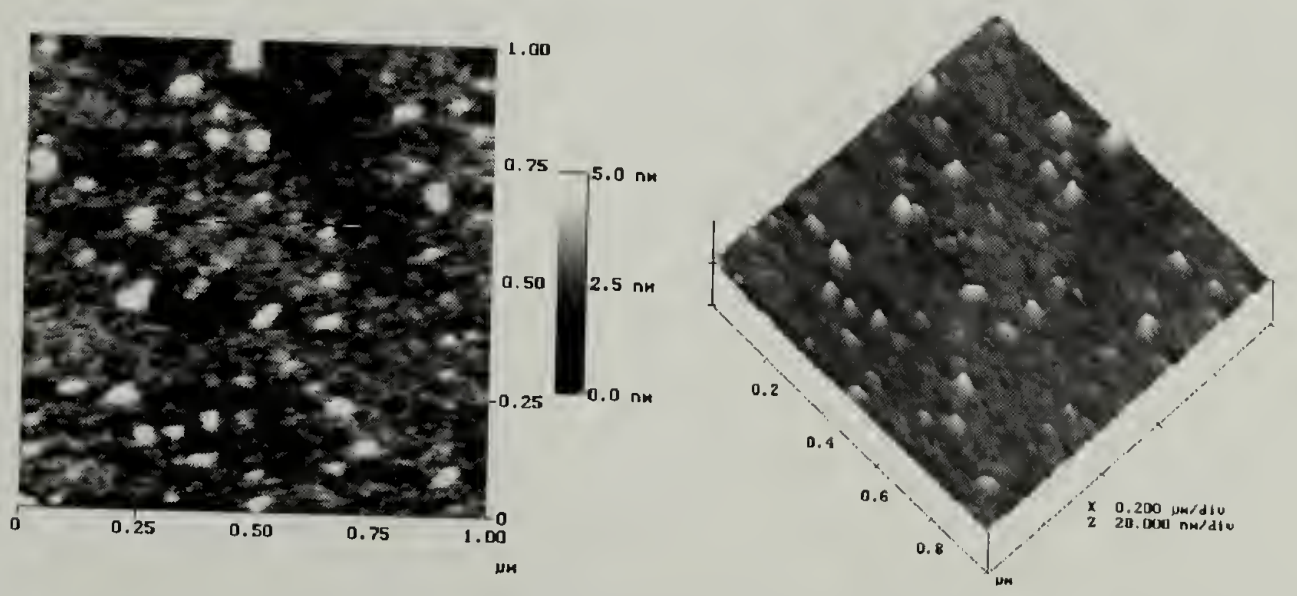

Figure 1.47. Tapping mode AFM height (left) and surface (right) images of an adsorbed thin film of 3121:1 poly-**R/S** from toluene to native silicon oxide for 96 hours followed by rinsing of the adsorbed film in toluene.

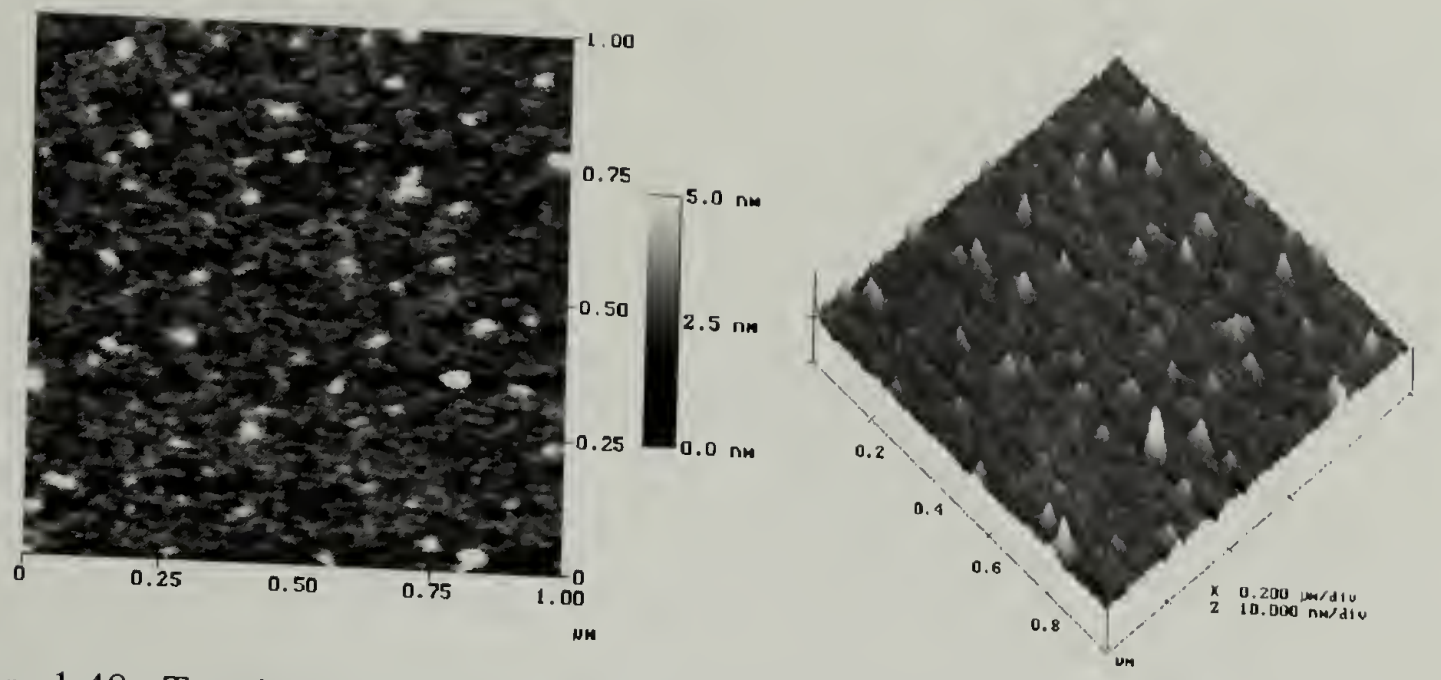

Figure 1.48. Tapping mode AFM height and surface images of an adsorbed thin film of 3121:1 poly-**R/S** from THF to native silicon oxide for 96 hours followed by rinsing of the adsorbed film in toluene.

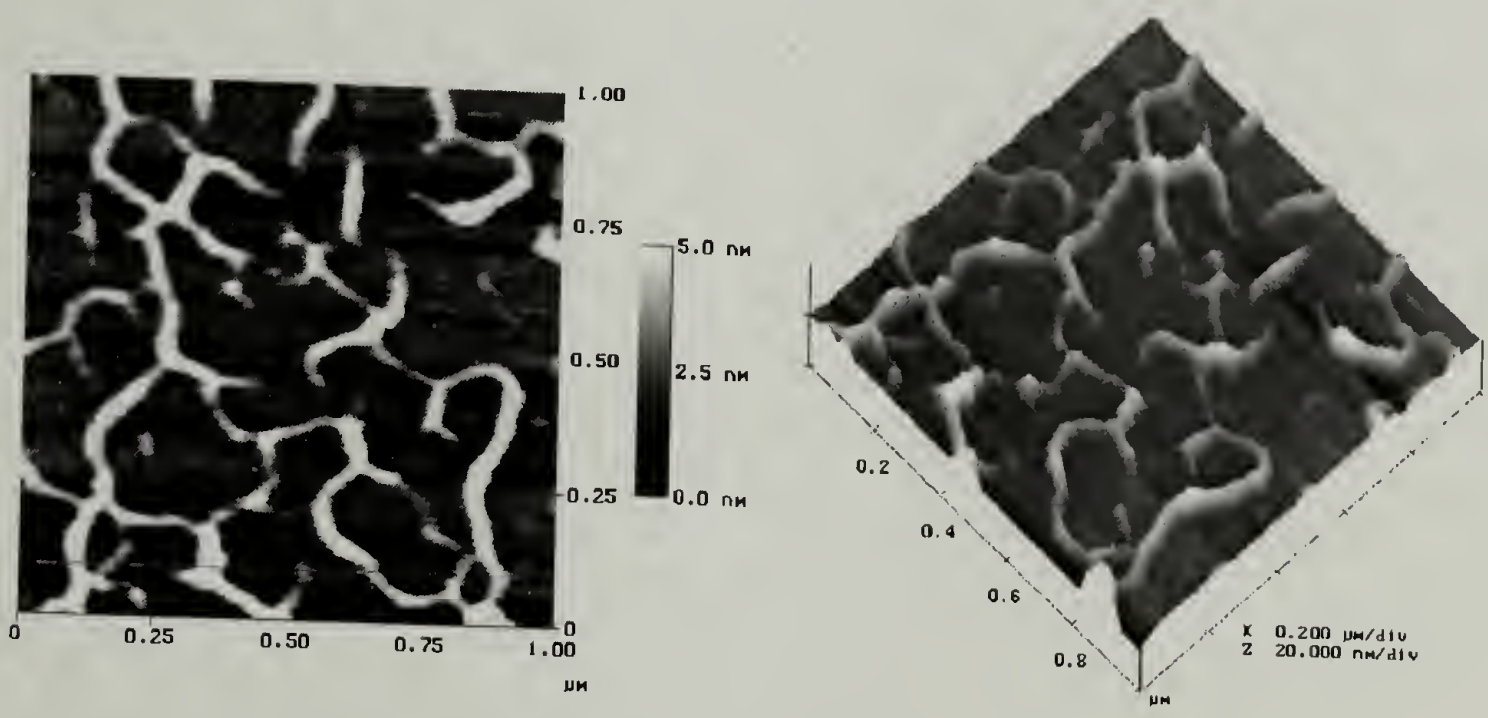

Figure 1.49. Tapping mode AFM height and surface images of an adsorbed thin film of 3121:1 poly-**R/S** from toluene to native silicon oxide for 96 hours followed by rinsing of the adsorbed film in THF.

The AFM results in combination with the XPS and contact angle results suggested that solvent quality was critical to the type of surface structure formed. In addition, from XPS and AFM data, it appeared the resulting surface structure was independent of

adsorption solvent but dependent on the rinse condition. Furthermore, contact angle data indicated a more complex picture existed for the adsorption from THF followed by rinsing in toluene. This surface was mobile due to the instabilities in the sessile drop. Since the AFM results are comparable between the THF/toluene surface and toluene/toluene surface, the images suggests that dewetting may have occurred at the polymer-substrate interface. This dewetting may have been concealed by a thin film of polymer with structure comparable to toluene/toluene conditions, because of the direct contact with toluene.

Solvent quality was shown to be a factor in the surface structure of the resulting film, nonetheless we needed to explore the kinetics of the dewetting process. Earlier we hypothesized that the evaporation rate of the rinse solvent must be contributing to the extent of dewetting. We researched the effects of evaporation by performing adsorptions of 3121:1 poly-**R/S** in THF (1.0 mg/mL) followed by rinsing in cold and room temperature THF. Contact angle data for the samples are listed in Table 1.29 and the

Table 1.29. Water contact angle results of adsorbed thin films of 3121:1 poly-**R/S** adsorbed from THF to native silicon oxide at the temperature reported. The results suggest that the temperature of the rinse solvent has little affect on the dried surface structured of the adsorbed film.

Rinse Conditions	θ_A	θ_R
7 °C THF	43° ± 2°	12 ° ± 2°
22 °C THF	41° ± 3°	13° ± 4°

results suggest little difference between the two conditions. However, the tapping mode AFM results shown in Figure 1.50 indicate differences between the two conditions. As expected, the colder rinse condition was observed to evaporate much slower than the

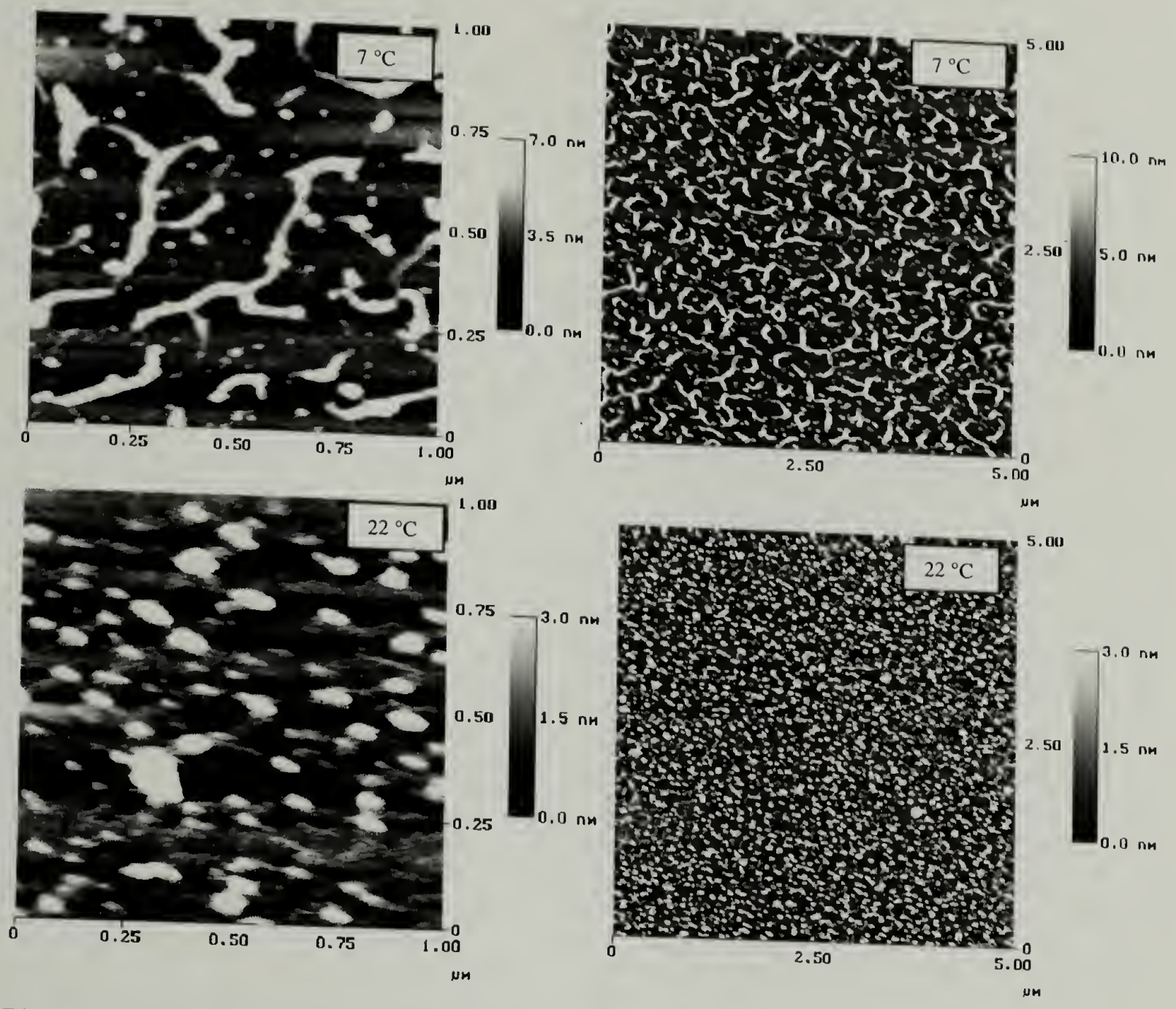

Figure 1.50. AFM tapping mode height images of adsorbed thin films of 3121:1 poly–**R/S** adsorbed from THF to native silicon oxide, where one set of adsorbed films were rinsed in 7 °C THF (top images) and the other set of adsorbed films were rinsed in 22 °C THF (bottom images). From these images it appears that the temperature of the rinse solvent has an affect on the extent of dewetting of the adsorbed film.

room temperature rinse. The 22 °C rinse conditions initially appeared to have dewetted to an extent associated with the classical late stages of dewetting where ribbons are further dewetting to droplets. However, close examination of the several images, including those shown in Figure 1.50, show fine ribbons between the droplet like structures indicating early stages of dewetting. But, the opposite argument could be made that the 22 °C rinse condition caused a greater degree of dewetting because of the numerous droplet like structures observed. Thus, it was difficult to confirm whether

early or late stages of dewetting occurred for the 22 °C rinse. Furthermore, we have shown many examples of dewetted adsorbed films formed during rinsing with solvent at room temperature. In comparison, the AFM image of the cold rinse condition shows late stage dewetting. The image indicates thick ribbons with bulges along their length, which are possibly the sites of growing droplets. In addition, dispersed between the ribbons are droplets that are most likely remnants of finger–like protrusions that earlier in the dewetting process, projected off the thick ribbons. What became apparent from the data was that kinetic trapping of the dewetting process was possible and that this could be accomplished by slowing the evaporation rate of the rinse solvent.

Since the evaporation rate of the rinse solvent was shown to contribute to the extent of dewetting, we controlled the evaporation rate as a means to kinetically trap the different phases of dewetting. This was accomplished by performing adsorption experiments with 3121:1 poly-**R/S** from toluene and THF, followed by special rinse conditions. For example, a seventy-two hour adsorption from toluene was rinsed twice in toluene and immediately followed by a 30-second partial (30% total area) submersion in THF at 5 °C. For comparison, a seventy-two hour adsorption from THF was rinsed twice in THF followed by 30% submersion in 22 °C toluene for thirty seconds. In addition, all the samples of post 30-second submersions were held horizontally during solvent evaporation. It should be noted that for all previous adsorption experiments the evaporation of solvent occurred on samples held vertically. The reason for allowing the rinse solvent to evaporate from a horizontally held sample position was to eliminate the affect of gravity on solution run off. On vertical samples, the solvent evaporation front was very noticeable and AFM analysis of these samples showed variation in the surface topography correlated with the rate of solvent loss. The following scheme shows the experimental method described above and the points to the locations on the sample surface of the acquired AFM images.

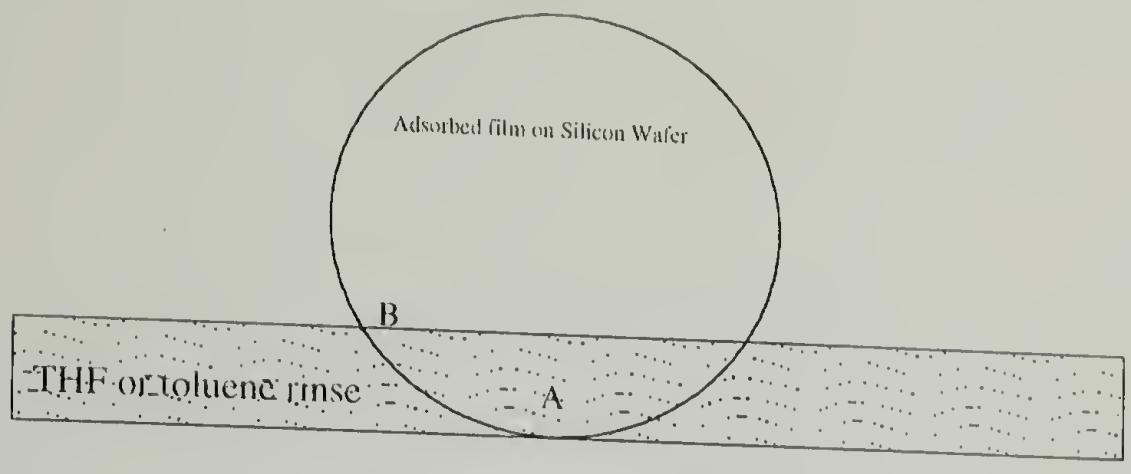

Scheme 1.5. Diagram of a submerged wafer (~ 30%) in the final rinse solvent, where A, refers to the location the AFM images shown in Figure 1.51 were acquired. Location B refers to the location of Figure 1.52 images.

Tapping mode AFM images for the adsorption of 3121:1 poly-**R/S** from THF to native silica followed by a 30% submersion in toluene showed uniform surface structures that were comparable to surfaces (shown in Figure.1.48) generated under similar conditions. For the adsorption performed in toluene followed by a 30% submersion in cold THF (5 °C), the AFM images (Figure 1.51-1.52) show a surface indicating very early stages of dewetting. Referring to Scheme 1.5, the images shown in Figure 1.51 were acquired in region A and Figure 1.52 in region B. The images show capillary growth of holes with finger like protrusions extending from the circular shaped rim. Reiter[35] described similar surface architecture for 40 nm thick films of 660K Mw polystyrene. Their study focused on the instabilities in thin (thickness < 100 nm) polystyrene films at and above the glass transition temperature. The observed finger instabilities for the 660K Mw polystyrene were believed to be due to the higher viscosity and entanglements of the polymer molecule. Eventually, the fingers became unstable and decomposed to droplets with a size proportional to the initial film thickness. Nevertheless, the final stage of the dewetted film exhibited polygon patterns. In Figure 1.52, these finger instabilities were shown to form during the early stages of dewetting of the 3121:1 poly-**R/S** sample. The two triangle markers on the section analysis, the

bottom right image in Figure 1.52, measure the rim height of the growing holes at approximately 6 nm for the mid-size hole and 9.5 nm for the largest hole. Phase mode AFM indicated that the region between the digitation was the silica substrate.

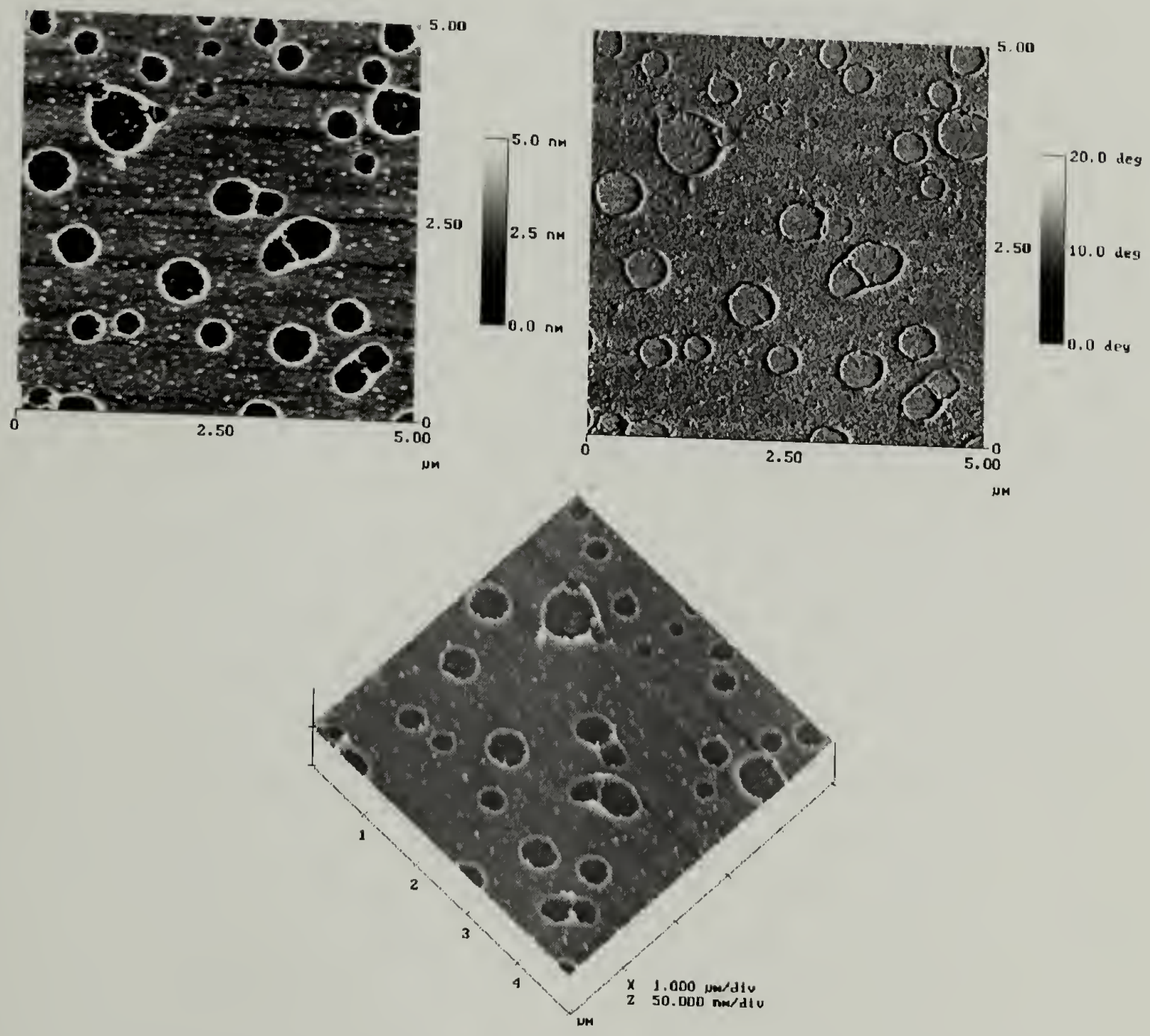

Figure 1.51. Tapping mode AFM height (top), phase (middle), and surface (bottom) images from the analysis of an adsorbed thin film of 3121:1 poly-**R/S** adsorbed from toluene to native silicon oxide for 72 hours at 25 °C followed by rinsing of the adsorbed layer in toluene, and then followed by an additional 30% surface area (see Scheme 1.5) rinse in cold (5 °C) THF. The sample was held horizontally while the solvent evaporated.

We were curious whether a thick film of poly-**R/S** would show the same dewetting instabilities as shown for thin films. For this experiment, a thick film of poly–**R/S** was produced by adsorbing 3121:1 poly-**R/S** from THF to silica for 72 hours followed by no rinse. Tapping mode AFM imaging of the air-dried sample is shown in Figure 1.53. The architecture resembles dewetting with very large ribbons of over one micron in height and possible finger instabilities evident in the upper right region of the image.

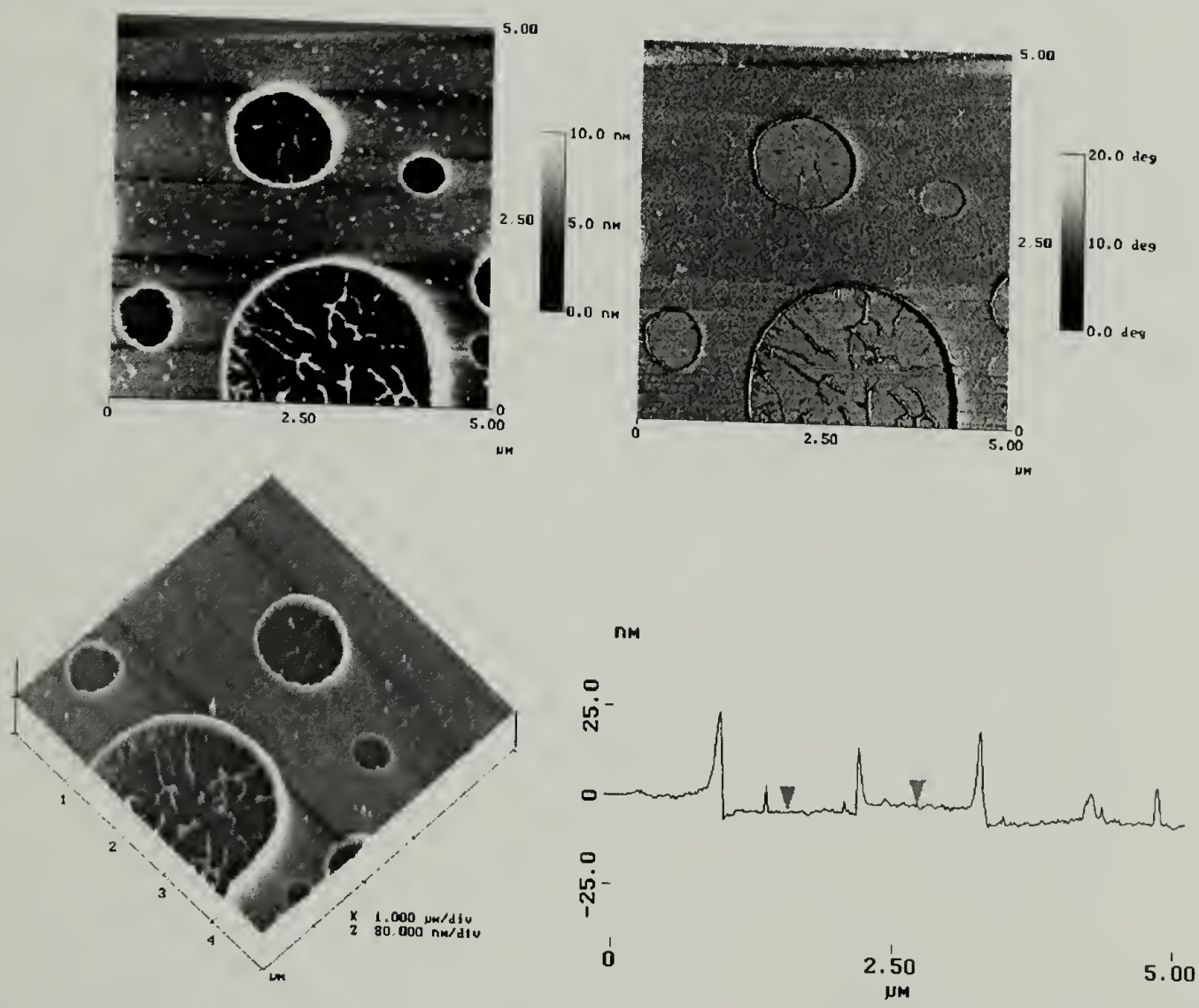

Figure 1.52. Tapping mode AFM height (top left), phase (top right), surface (bottom left), and section analysis (bottom right) images from the analysis of an adsorbed thin film of 3121:1 poly-**R/S** adsorbed from toluene to native silicon oxide for 72 hours at 25 °C followed by rinsing of the adsorbed layer in toluene, and then followed by an additional 30% surface area (see Scheme 1.5) rinse in cold (5 °C) THF. The sample was held horizontally while the solvent evaporated.

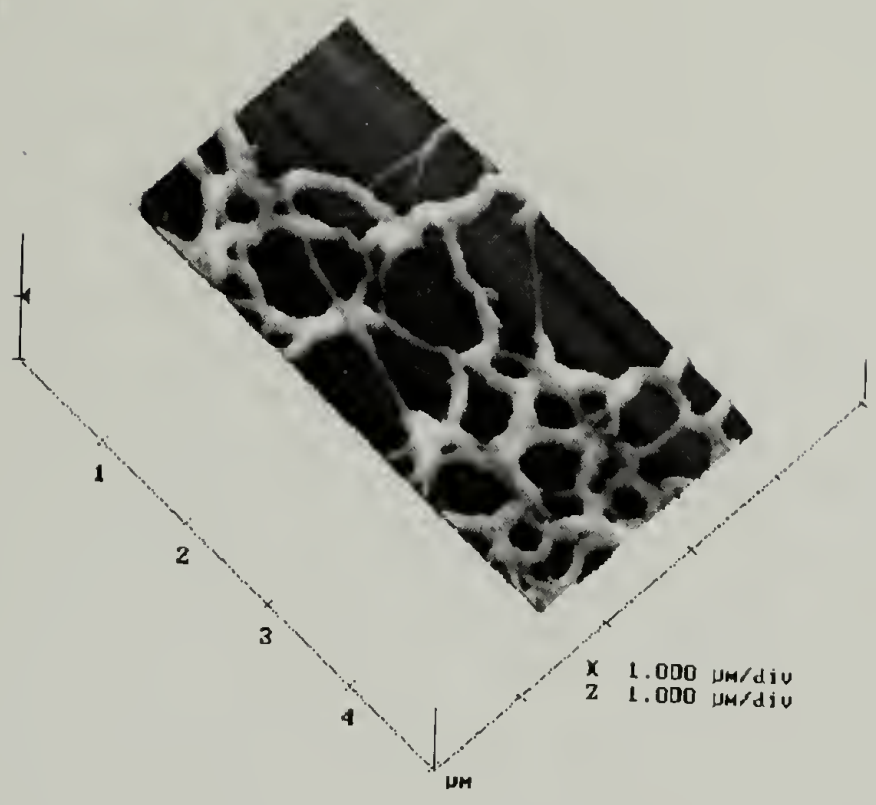

Figure 1.53. Tapping mode AFM surface image of adsorbed 3121:1 poly–**R/S** from THF to native silicon oxide for 72 hour followed by no rinsing. The adsorbed film was allowed to air dry while being held horizontally.

The data supported dewetting as the mechanism responsible for the various architectures of the adsorbed films. However, we wanted to confirm whether there was a molecular weight dependence on the degree of dewetting. In addition, we researched whether the stereochemistry of the polymer has an affect on the extent of dewetting. To accomplish these research objectives, adsorptions were performed with 312:1 and 3121:1 samples of poly-**S** and poly-**R/S**. The adsorption conditions are outlined in the XPS results shown in Table 1.30, and in the contact angle results shown in Table 1.31. The atomic concentration data for the adsorbed films of poly-**R/S** and poly-**S** concurred with earlier assessments. Generally, the atomic concentration data indicate that for the adsorptions performed from THF, followed by toluene rinse, and for the adsorptions of poly-**R/S** from toluene were for the most part independent of the polymer's stereochemistry and molecular weight. The contact angle data in Table 1.31 show the

same trends as the XPS results except for the adsorption of the 312:1 poly-**R/S** sample from toluene. Further, the adsorption of 312:1 poly-**R/S** from THF followed by toluene rinse resulted in contact angles typically associated with adsorptions from toluene, but the adsorption from toluene resulted in 25° lower contact angles. This suggested that molecular weight might have an affect on the surface structure of adsorbed films of poly–**R/S**. Therefore, tapping mode AFM was used to study the surface architecture differences of the adsorbed film.

Atomic force microscopy was used to characterize the surface topography of the samples described in Tables 1.30 and 1.31. The samples were first characterized by tapping mode AFM and then used to measure contact angle. Figure 1.54 shows the surface topography for the adsorption of 312:1 poly-**R/S** from THF to native silicon oxide followed by THF rinse at 3 °C. The image indicates the late stages of dewetting because only droplets remain and the receding contact angle data suggests that between the droplets is silica substrate. The tapping mode AFM images for the adsorption of 312:1 poly-**R/S** from toluene followed by THF rinse at 22 °C are shown in Figure 1.55. An early stage of dewetting is indicated due to the fine ribbon structures on the surface suggesting early growth of holes. The results of 3 °C and 22 °C rinse conditions concur with previous observations for the similar experiment performed with 3121:1 poly-**R/S** (see Fig. 1.50). In addition, the receding contact angle data indicates that the substrate is still partially shielded. Surface topography for the adsorption of 312:1 poly-**R/S** from THF followed by rinsing in toluene is shown in Figure 1.56. The image indicates a surface consistent with previous AFM images, atomic concentration data, and contact angle results for samples of various Mw of poly-**R/S** and poly-**S** adsorbed under similar conditions. However, the contact angle results for the adsorption of 312:1 poly-**R/S** from toluene followed by toluene rinse were not consistent with previous results for similar adsorptions. Figure 1.57 shows the tapping mode AFM image of adsorbed 312:1 poly–**R/S** and areas of dewetting are indicated by the appearance of ribbons and droplets.

Table 1.30. XPS atomic concentration results from adsorbed films of poly–**R/S** and poly–**S** on native silicon oxide and the affect on the surface structure as a function of the adsorption solvent and rinse solvent. The conditions are defined in the first column of the table.

Adsorption Solvent$_{rinse}$	$C_{15°}$	$N_{15°}$	$O_{15°}$	$Si_{15°}$	$C_{15°}$: $N_{15°}$	$Si_{15°}$: $N_{15°}$
312:1 POLY-**R/S**						
THF	51.37	5.84	30.81	11.98	8.8 : 1	2.1 : 1
THF_{RTOL}	82.40	14.62	1.31	1.67	5.6 : 1	0.1 : 1
Tol_{RTHF}	44.40	0.74	38.67	16.19	60 : 1	22 : 1
Toluene	83.27	12.60	2.81	1.32	6.6 : 1	0.1 : 1
312:1 POLY-**S**						
THF	46.94	3.03	32.62	17.42	16 : 1	5.7 : 1
THF_{RTOL}	83.43	12.94	1.64	1.99	6.4 : 1	0.2 : 1
3121:1 POLY-**R/S**						
THF	42.91	3.67	38.49	14.92	12 : 1	4.1 : 1
THF_{RTOL}	86.84	13.16	-	-	6.6 : 1	-
Tol_{RTHF}	58.26	5.81	24.48	11.45	10 : 1	2.0 : 1
Toluene	85.69	12.75	0.79	0.77	6.7 : 1	0.06 : 1
3121:1 POLY-**S**						
THF	39.68	2.29	38.92	19.10	17 : 1	8.3 : 1
THF_{RTOL}	84.51	14.44	0.60	0.45	5.9 : 1	0.03 : 1

Adsorption Solvent$_{rinse}$	$C_{75°}$	$N_{75°}$	$O_{75°}$	$Si_{75°}$	$C_{75°}$: $N_{75°}$	$Si_{75°}$: $N_{75°}$
312:1 POLY-**R/S**						
THF	26.55	3.11	33.17	37.17	8.5 : 1	12 : 1
THF_{RTOL}	58.51	10.74	15.89	14.85	5.4 : 1	1.4 : 1
Tol_{RTHF}	22.84	0.35	38.21	38.61	65 : 1	110 : 1
Toluene	50.87	9.21	16.99	22.93	5.5 : 1	2.5 : 1
312:1 POLY-**S**						
THF	18.53	1.17	37.82	42.49	16 : 1	36 : 1
THF_{RTOL}	53.73	8.78	15.84	21.65	6.1 : 1	2.5 : 1
3121:1 POLY-**R/S**						
THF	15.92	1.76	50.21	32.11	9.0 : 1	18 : 1
THF_{RTOL}	67.75	10.99	8.94	12.33	6.2 : 1	1.1 : 1
Tol_{RTHF}	23.08	2.38	35.11	39.43	9.7 : 1	17 : 1
Toluene	62.19	9.98	11.09	16.73	6.2 : 1	1.7 : 1
3121:1 POLY-**S**						
THF	14.85	1.15	39.73	44.27	13 : 1	39 : 1
THF_{RTOL}	57.31	11.16	15.23	16.30	5.1 : 1	1.5 : 1

Table 1.31. Water contact angle results of adsorbed thin films of poly-**R/S** and poly-**S** on native silicon oxide and the affect on surface structure as a function of the adsorption solvent as well as the temperature and/or chemistry of the rinse solvent. The conditions are defined in the first column of the table.

Conditions	θ_A	θ_R
312:1 POLY-**R/S**		
$THF_{3\,°C}$	46° ± 1°	17° ± 2°
$THF_{22\,°C}$	44° ± 1°	19° ± 1°
THF_{RTOL}	92° ± 0.5°	83° ± 1°
$Toluene_{RTHF}$	67° ± 1°	40° ± 1.5°
Toluene	66° ± 0.5°	41° ± 1.5°
312:1 POLY-**S**		
$THF_{3\,°C}$	45° ± 1.5°	20° ± 1.5°
$THF_{22°C}$	43° ± 2°	17° ± 3°
THF_{RTOL}	93° ± 1°	83° ± 1°
3121:1 POLY-**R/S**		
$THF_{3°C}$	44° ± 1°	17° ± 1.5°
$THF_{22°C}$	42° ± 0.5°	15° ± 1.5°
THF_{RTOL}	93° ± 1°	82° ± 0.5°
$Toluene_{RTHF}$	44° ± 2°	16° ± 0.5°
Toluene	91° ± 1°	77° ± 1.5°
3121:1 POLY-**S**		
$THF_{3\,°C}$	38° ± 1.5°	16° ± 1.5°
$THF_{22\,°C}$	37° ± 1°	13° ± 1°
THF_{RTOL}	92° ± 0.5°	83° ± 1°

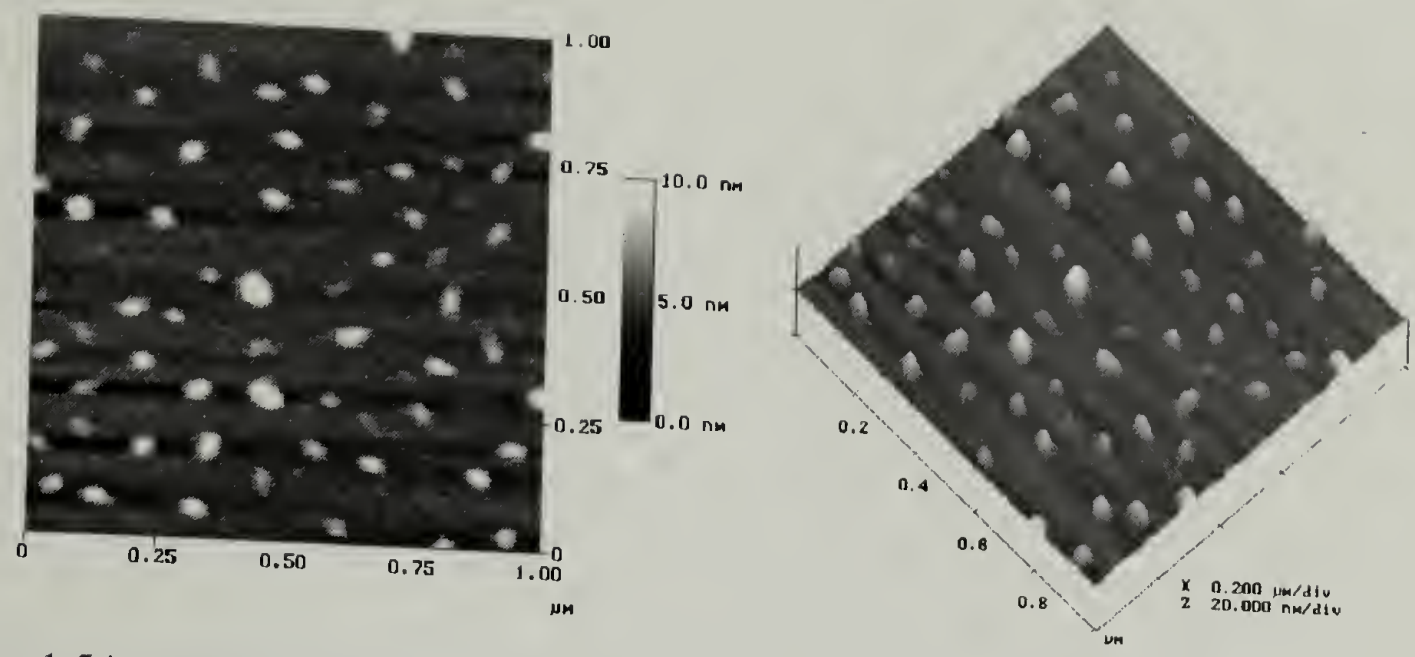

Figure 1.54. Tapping mode AFM height (left) and surface (right) image of adsorbed 312:1 poly–**R/S** from THF to native silicon oxide for 72 hours followed by rinsing in cold (3 °C) THF.

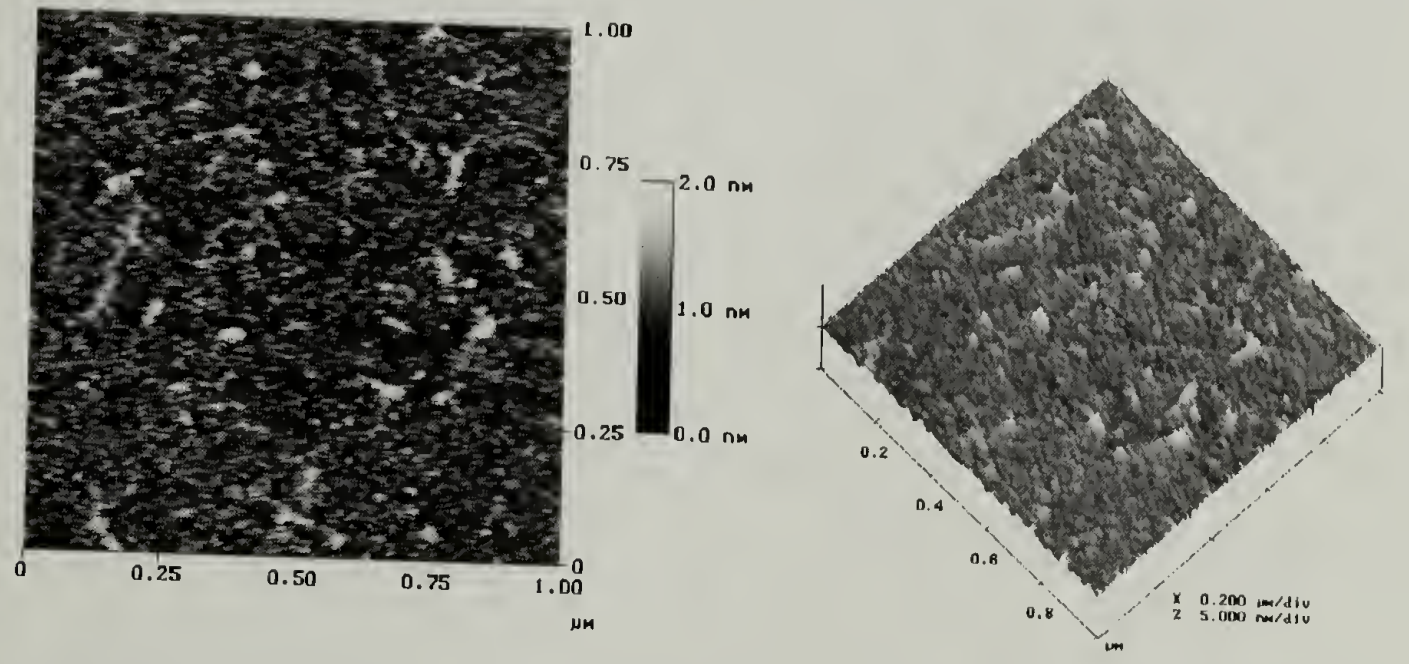

Figure 1.55. Tapping mode AFM height (left) and surface (right) image of an adsorbed thin film of 312:1 poly–**R/S** adsorbed from toluene to native silicon oxide for 72 hours followed by rinsing in room temperature (22 °C) THF.

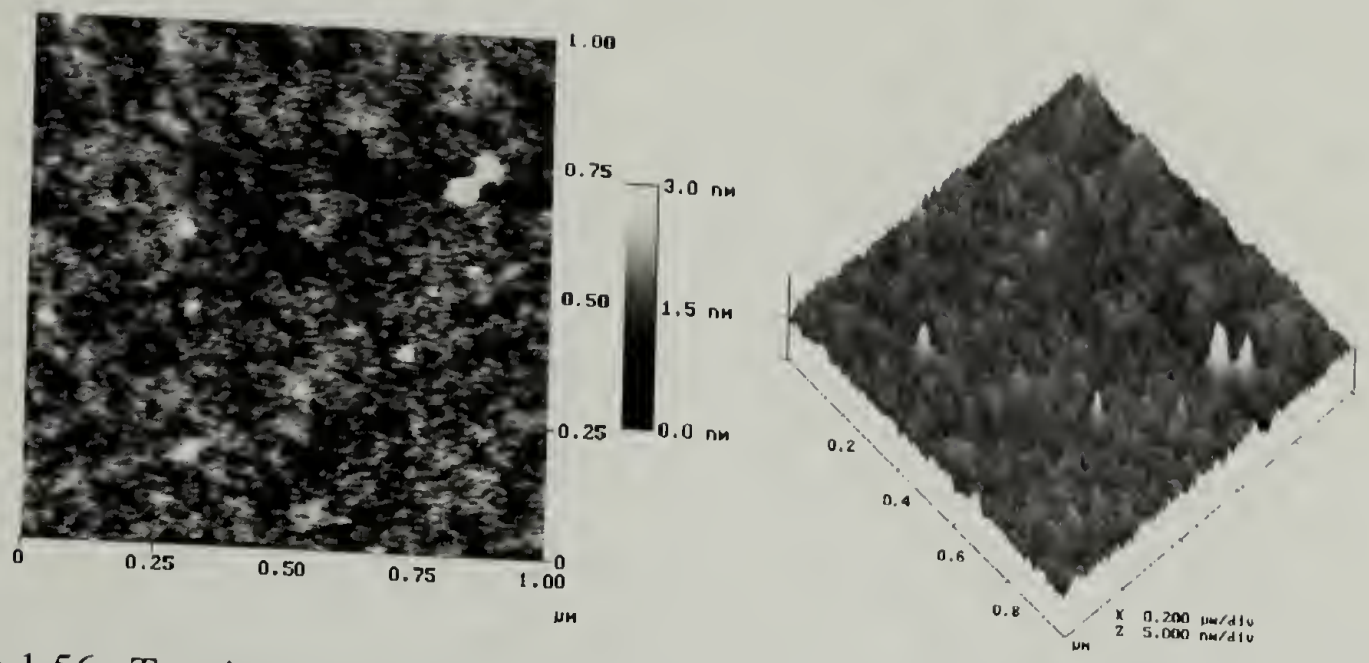

Figure 1.56. Tapping mode AFM height (left) and surface (right) image of an adsorbed thin film of 312:1 poly–**R/S** adsorbed from THF to native silicon oxide for 72 hours followed by rinsing in toluene.

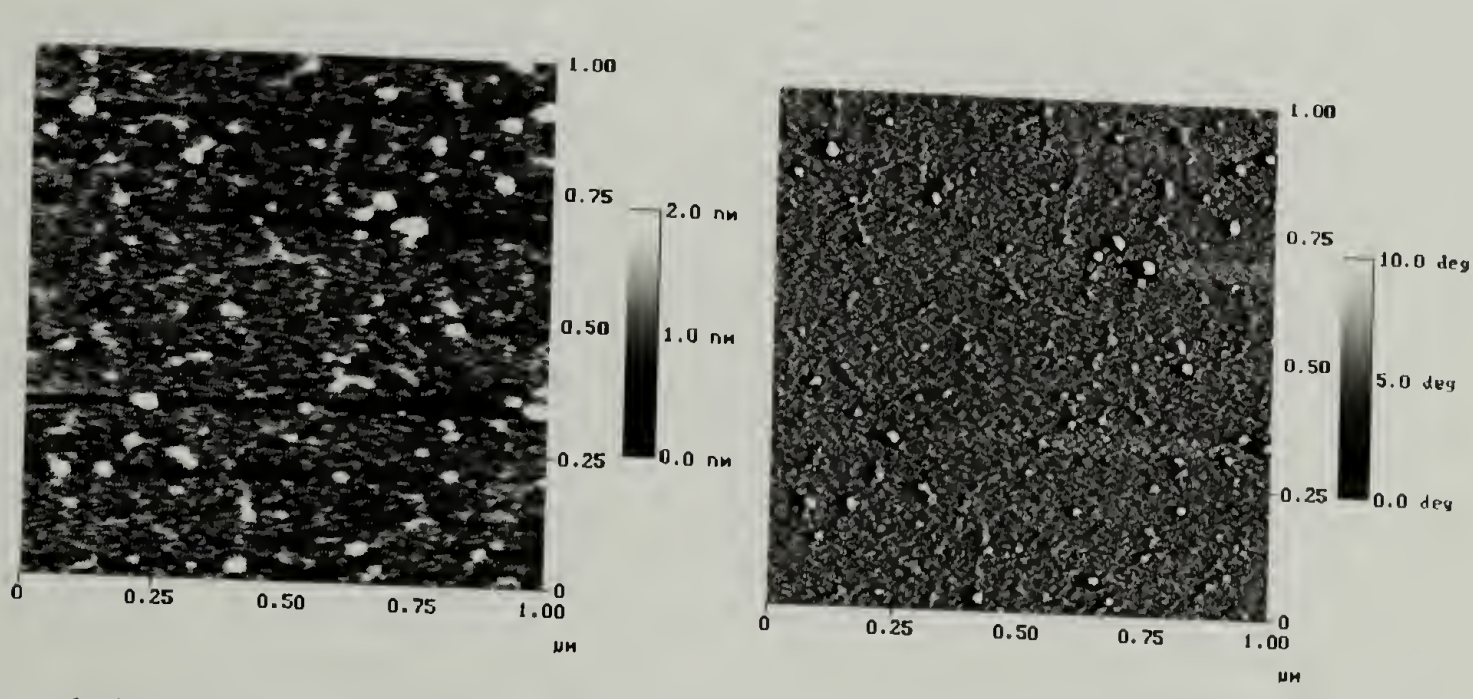

Figure 1.57. Tapping mode AFM height (left) and surface (right) image of adsorbed 312:1 poly–**R/S** from toluene to native silicon oxide from for 72 hours followed by rinsing in room temperature toluene.

Tapping mode AFM images for the adsorption of 312:1 poly-**S** are shown in Figures 1.58 and 1.59. Late stages of dewetting are indicated (Figure 1.58) for the adsorption from THF followed by THF rinse at 3 °C as shown by the formation of

droplets and small remnants of ribbons. The AFM height and surface images (Figure 1.59) of the adsorption from THF followed by toluene rinsing is consistent with previous observations (refer to Figure 1.56).

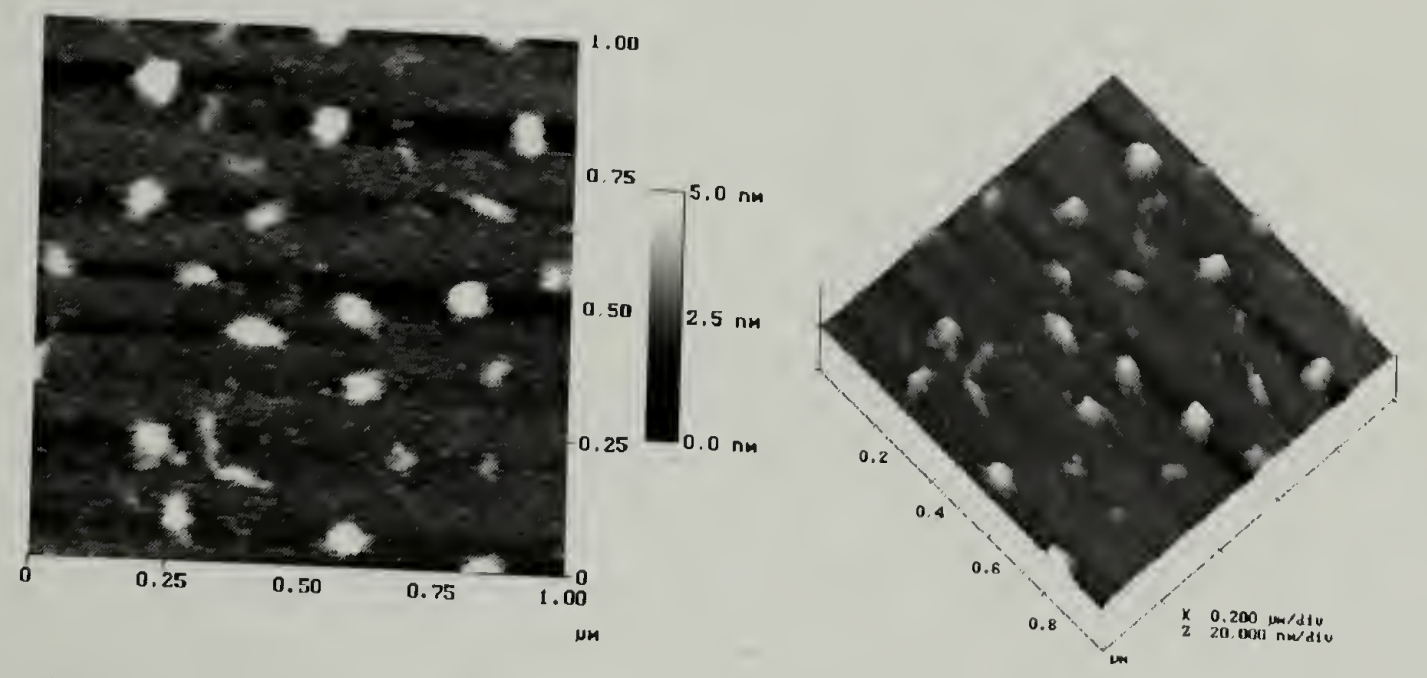

Figure 1.58. Tapping mode AFM height (left) and surface (right) image of adsorbed 312:1 poly–**S** from THF to native silicon oxide for 72 hours followed by rinsing in cold (3 °C) THF.

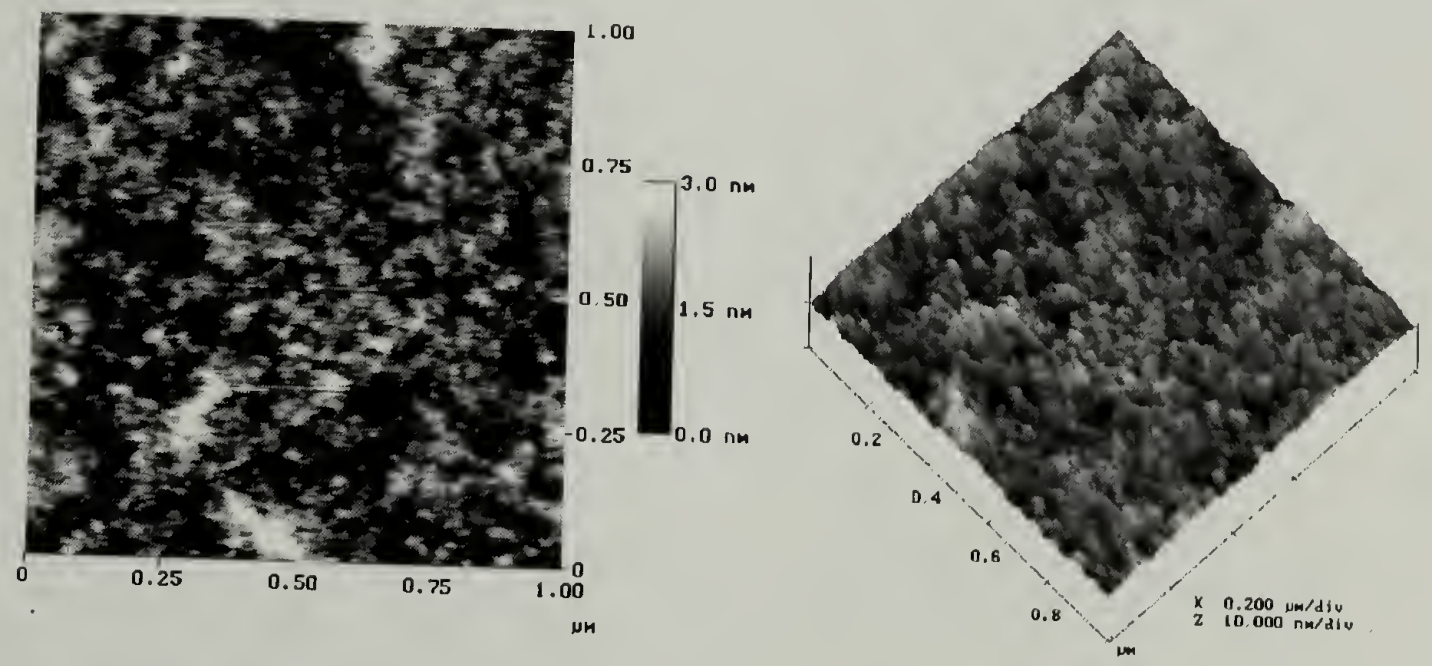

Figure 1.59. Tapping mode AFM height (left) and surface (right) image of an adsorbed thin film of 312:1 poly–**S** from THF to native silicon oxide for 72 hours followed by rinsing in room temperature toluene.

The tapping mode AFM images (see Fig. 1.60) for the adsorption of 3121:1 poly-**R/S** from THF followed by rinsing in 3 °C THF were similar to those described for 312:1 poly-**R/S** adsorbed under the same conditions. However, upon dewetting, a larger distribution of droplet sizes was observed with some much larger than observed with 312:1 poly-**R/S**. Intuitively, this would be expected since there is an order of magnitude difference in molecular weight. For the adsorption of both 3121:1 poly-**R/S** and 3121:1 poly-**S** from THF followed by rinsing in toluene, the AFM images (Figures 1.61 and 1.62) are similar to those observed for adsorbed films of 312:1 poly-**R/S** and poly-**S** (Figures 1.56 and 1.59 respectively) prepared under the same conditions. Furthermore, this similarity is supported by the contact angle data from Table 1.31.

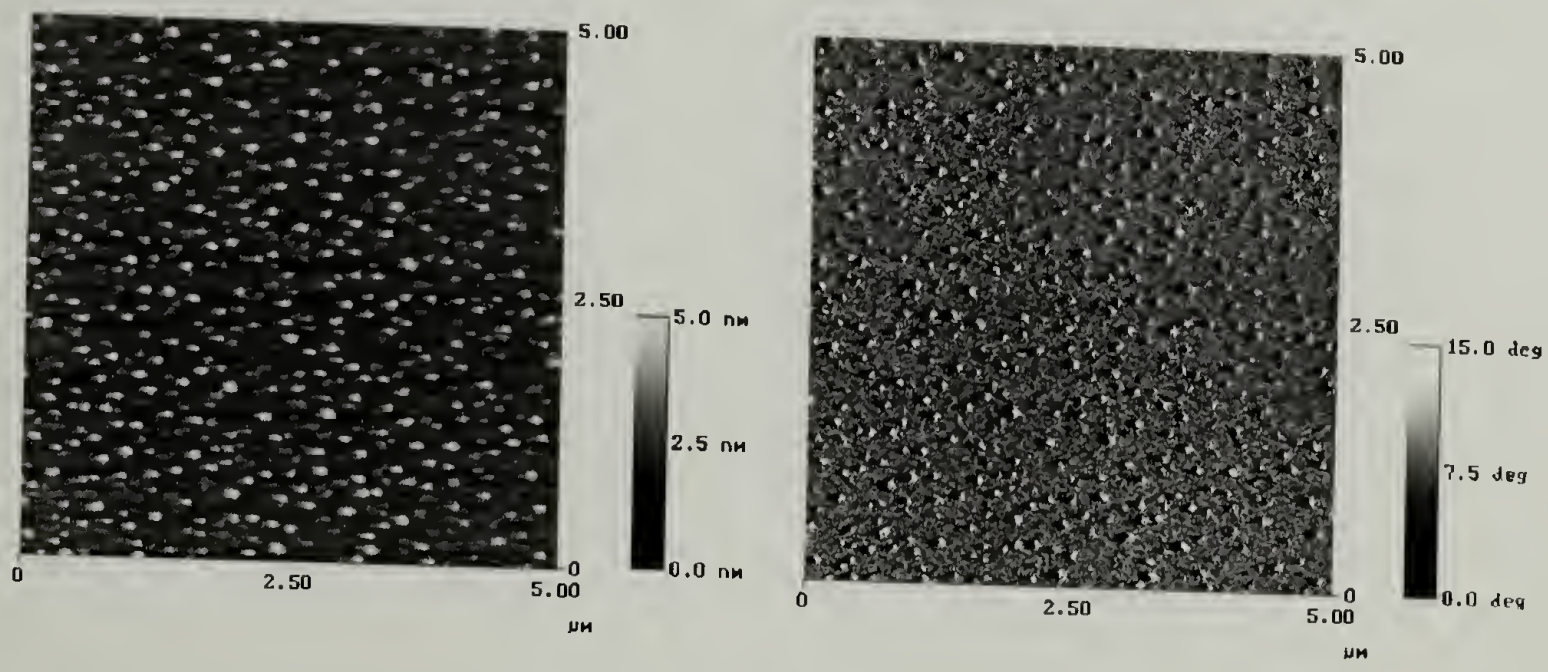

Figure 1.60. Tapping mode AFM height (left) and phase (right) image of adsorbed 3121:1 poly–**R/S** from THF to native silicon oxide for 72 hours followed by rinsing in room temperature (3 °C) THF.

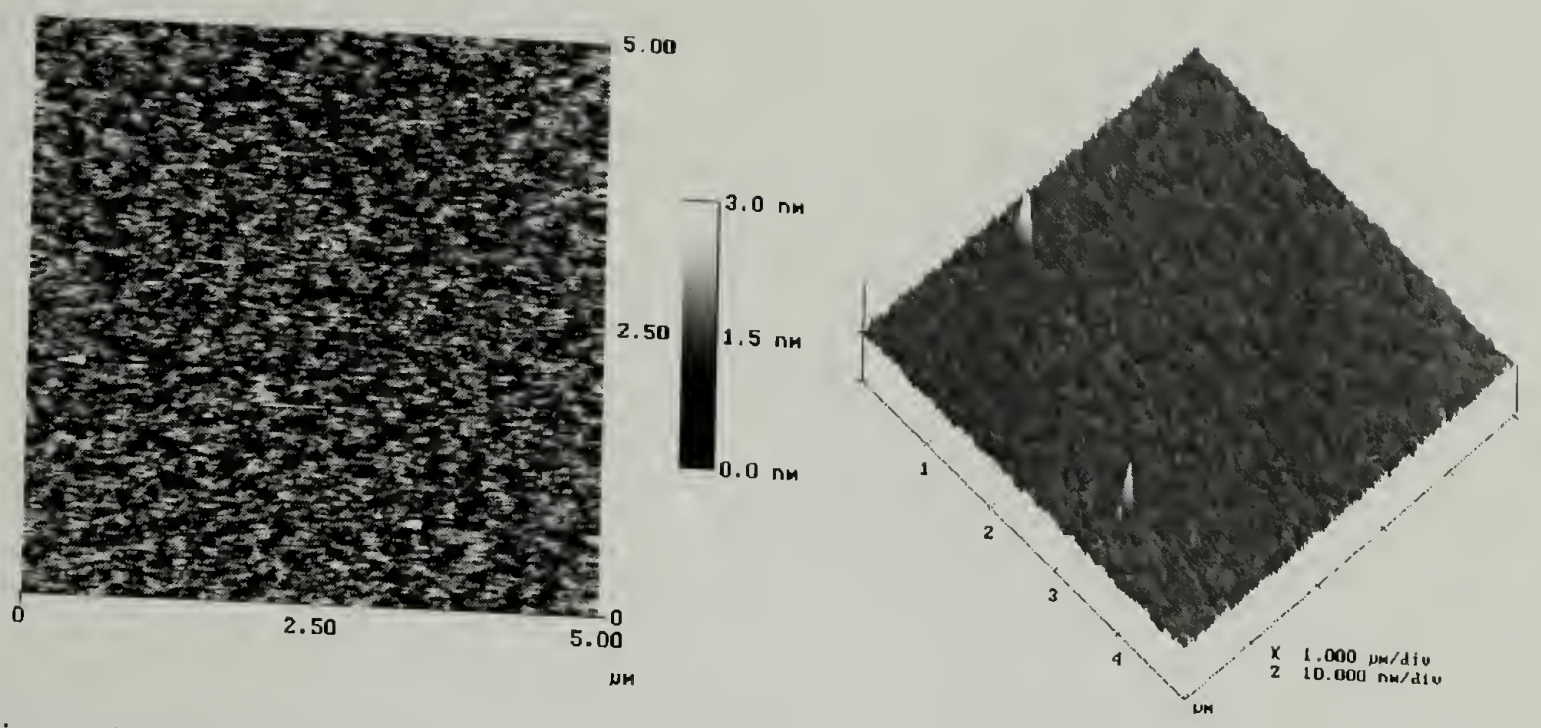

Figure 1.61. Tapping mode AFM height (left) and surface (right) image of an adsorbed thin film of 3121:1 poly–**R/S** adsorbed from THF to native silicon oxide for 72 hours followed by rinsing in room temperature toluene

Height and surface images measured by tapping mode AFM for the adsorption of 3121:1 poly-**S** from THF followed by rinsing in THF are shown in Figures 1.63 and 1.64. The difference between the two conditions was the rinse temperature. Figure 1.63 shows the AFM images for the 3 °C rinse and indicates two different degrees of dewetting. The image shows that a large hole formed with numerous finger instabilities, which continued to dewet, resulting in the formation of droplets and ribbons within the growing hole. The region to the left of the hole indicates the formation of much smaller holes surrounded by rims that due to kinetics of solvent evaporation were viscously frozen and unable to degrade to droplets. The images in Figure 1.64 show the surface topography for 22 °C rinse conditions. At higher temperatures, the solvent evaporation is faster therefore, the kinetics of dewetting intuitively would be reduced. This is supported by the resulting image indicating early stages of dewetting where small holes can be seen between the growing ribbons and droplets. In addition, these results concur with previous results on the affect of the rinse solvent temperature on the extent of dewetting.

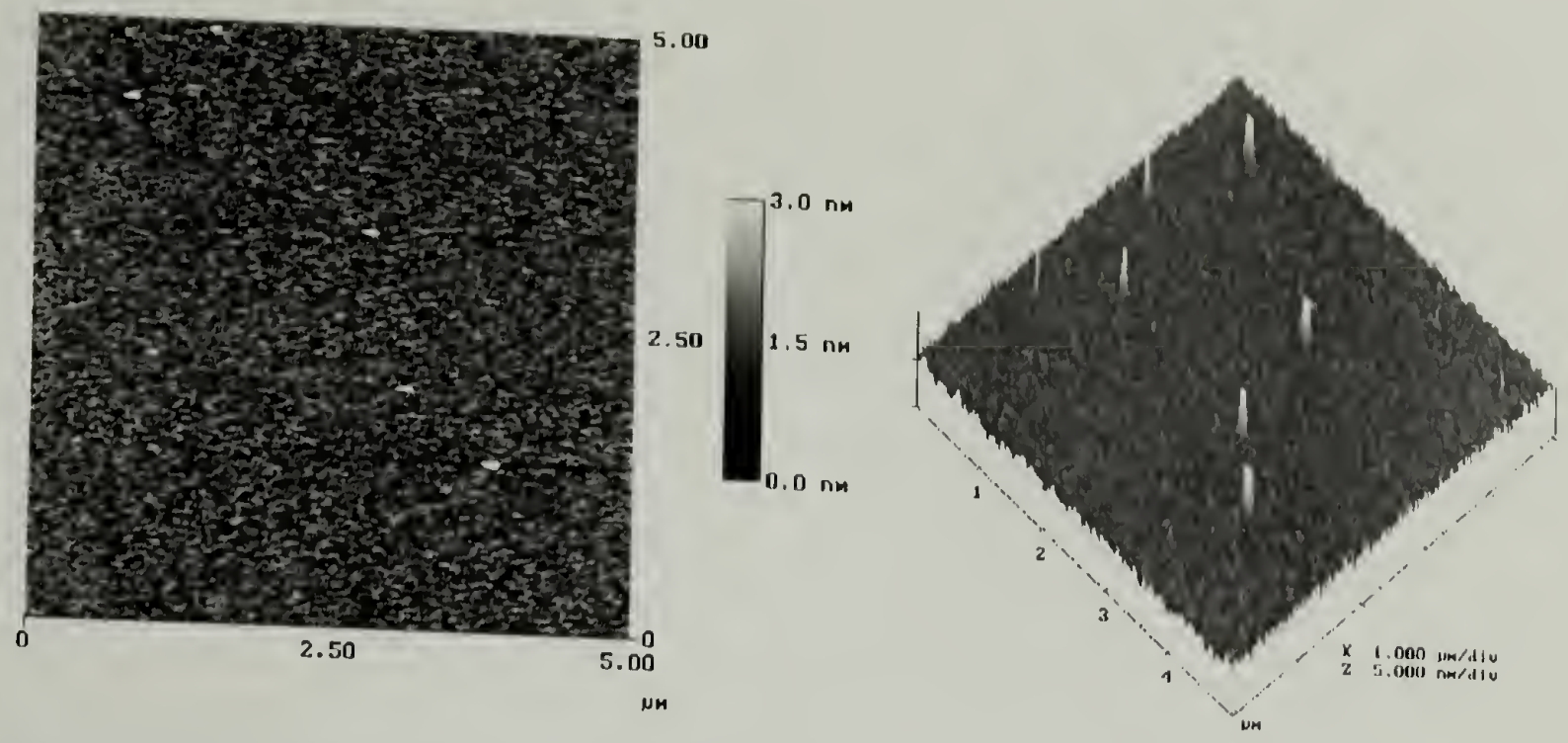

Figure 1.62. Tapping mode AFM height (left) and surface (right) image of an adsorbed thin film of 3121:1 poly–**S** adsorbed from THF to native silicon oxide for 72 hours followed by rinsing in room temperature toluene.

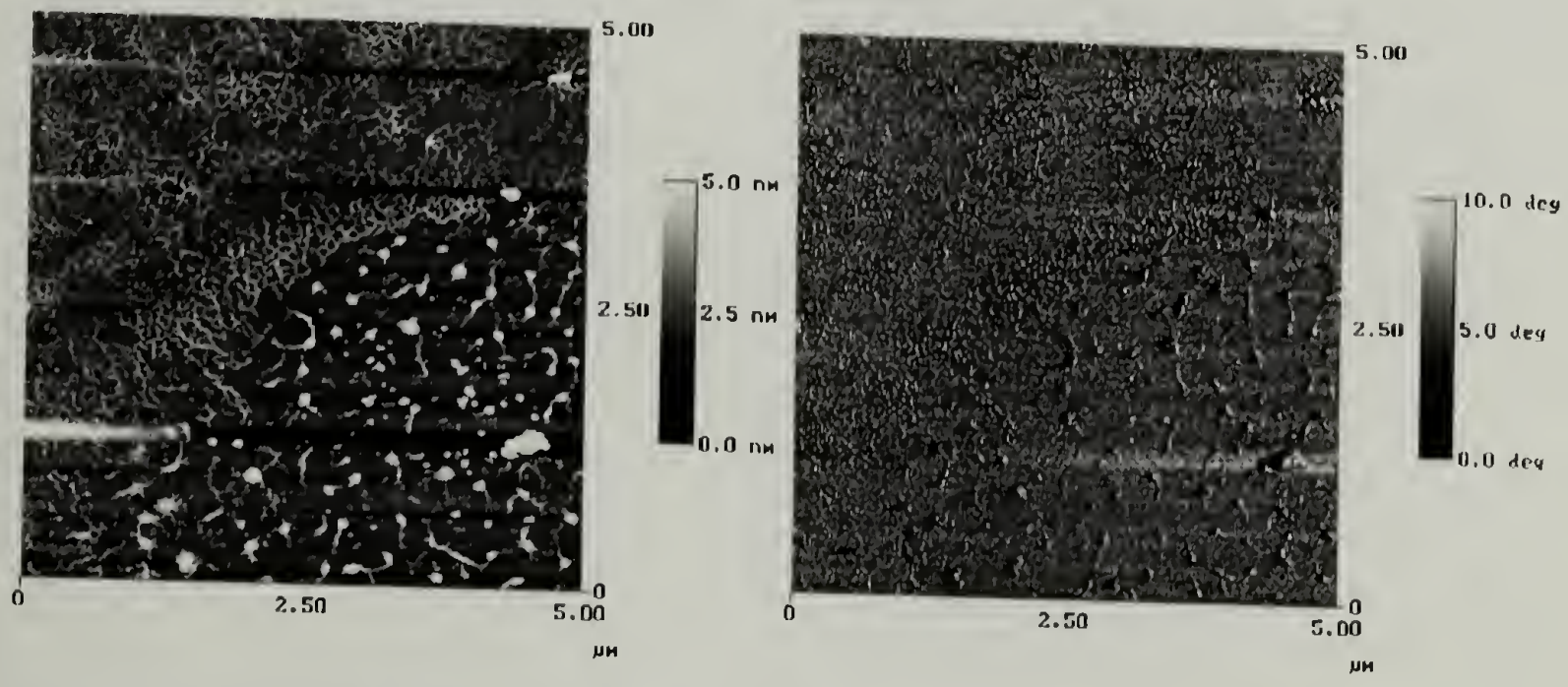

Figure 1.63. Tapping mode AFM height (left) and surface (right) image of adsorbed 3121:1 poly–S from THF to native silicon oxide for 72 hours followed by rinsing in cold (3 °C) THF.

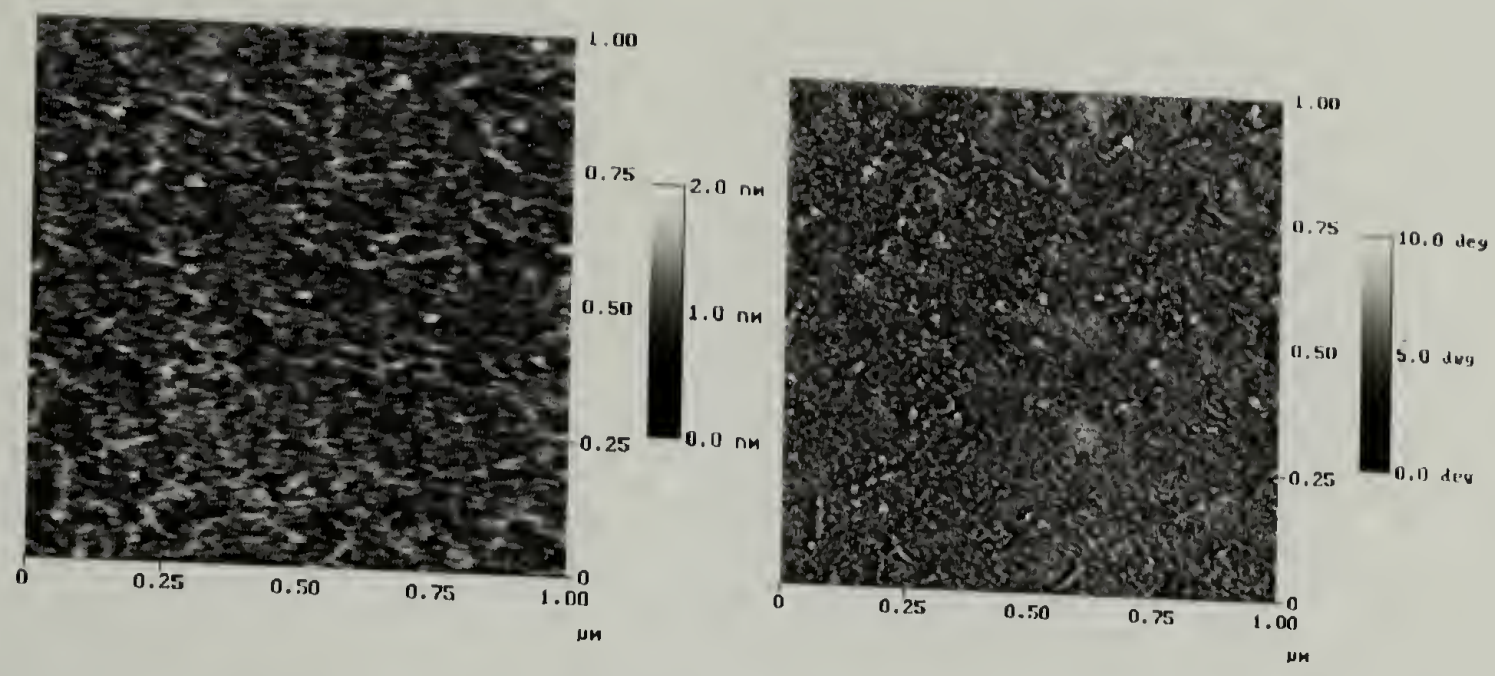

Figure 1.64. Tapping mode AFM height (left) and surface (right) image of adsorbed 3121:1 poly–**S** from THF to native silicon oxide for 72 hours followed by rinsing in room temperature (22 °C) THF.

Conclusions

We assessed the tendency for the wormlike poly-**R/S** and rodlike poly-**S** to adsorb to native silicon oxide. These polymers with well-defined architectures and extended conformations in solution were shown to adsorb to native silicon oxide. We studied the adsorption characteristics of both polymers as a function of molecular weight, solution conformation, solvent quality, kinetics, temperature, and rinse conditions. The adsorbed thin films were characterized by XPS, water contact angle, and TappingMode™ atomic force microscopy. High affinity adsorption isotherms were measured for 312:1 and 4681:1 poly-**R/S** from toluene to native silicon oxide. Atomic concentration data and water contact angle measurements indicated that for poly-**R/S**, the adsorbed (from toluene) film thickness increased with molecular weight. However, the adsorption of poly-**S** from toluene was not performed due to very slow solvation kinetics. Therefore, the adsorption of both polymers to native silicon oxide was performed from tetrahydrofuran (THF).

For adsorptions performed from THF followed by THF rinsing, the adsorbed amount, for equal molecular weights, of poly-**S** was greater than poly-**R/S**. Furthermore, for both polymers, as the molecular weight increased the adsorbed amount decreased. Thus, we concluded that the solution conformation affected the adsorbed amount. In addition, the XPS and water contact angle data indicated that for adsorptions from THF a much different adsorbed film structure formed compared to adsorptions from toluene. The data indicated that for poly-**R/S** the adsorbed amount was larger for adsorption from toluene than THF. We performed adsorption kinetic experiments on both polymers from THF and determined the minimum time (~ 50 hours) for the maximum adsorbed amount. When the XPS data from the kinetic experiments were plotted it showed a large amount of scatter. The scatter was found by AFM to be the result of the adsorbed film dewetting during the evaporation of the rinse solvent. The extent of dewetting was a function of solvent quality, temperature, and rinse condition. Analysis by AFM showed that for both polymers, the size of the surface structures increased with molecular weight. In addition, we demonstrated that the different stages of dewetting could be kinetically trapped by controlling the rinse condition and/or the evaporation rate of the rinse solvent by changes in temperature. An important conclusion from the above work is that caution should be exercised when analyzing adsorbed thin films by only XPS. We recommend using in concert with XPS a surface imaging technique such as AFM.

We also demonstrated that size-exclusion chromatography of polycarbodiimides can be performed by conditioning Polymer Labs mixed-B columns with acetonitrile and utilizing evaporative light scattering detection.

Notes and References

1. Fleer, G. J.; Stuart, M. A. c.; Scheutjens, J. M. H. M.; Cosgrove, T.; Vincent, B. *Polymers at Interfaces*; 1st ed.; Kluwer Academic Publishers: The Netherlands, 1993.

2. Chen, W.; McCarthy, T. J. *Macromolecules* **1998**, *31*, 3648-3655.

3. 3)Ward, W. J.; McCarthy, T. J. *Surface Modification*; 2nd ed.; Mark, H. F., Bikales, N. M., Overberger, N. M. and Menges, C. G., Ed.; John Wiley & Sons, Inc.: New York, 1989, pp 674-689.

4. Chen, W.; Fadeev, A. Y.; Hsieh, M. C.; Öner, D.; Youngblood, J.; McCarthy, T. J. *Langmuir* **1999**, *15*, 3395-3399.

5. Fadeev, A. Y.; McCarthy, T. J. *Langmuir* **1999**, *15*, 3759-3766.

6. Iyengar, D. R.; McCarthy, T. J. *Macromolecules* **1990**, *23*, 4344-4346.

7. Kolb, B. U. *Ph.D. Dissertation*; University of Massachusetts at Amherst: Amherst, Massachusetts, 1993, pp 198-213.

8. de Vincenzi, R. H.; Kolb, B. U.; McCarthy, T. J. *Synthesis of Functionalized Block Copolymers for Adsorption Studies*; 2 ed.; Culbertson, B. M., Ed.; The Division of Polymer Chemistry, Inc.: Washington, D.C., 1994; Vol. 35, pp 697.

9. Chen, W.; McCarthy, T. J. *Macromolecules* **1997**, *30*, 78-86.

10. Phuvanartnuruks, V.; McCarthy, T. J. *Macromolecules* **1998**, *31*, 1906-1914.

11. Masel, R. I. *Principles of Adsorption and Reaction on Solid Surfaces*; John Wiley & Sons, Inc.: New York, 1996.

12. Dijt, J. C.; Stuart, M. A. C.; Fleer, G. J. *Macromolecules* **1994**, *27*, 3229-3237.

13. Dorgan, J. R.; Stamm, M.; Toprakcioglu, C.; Jérôme, R.; Fetters, L. J. *Macromolecules* **1993**, *26*, 5321.

14. Dijt, J. C.; Stuart, M. A. c.; Hofman, J. E.; Fleer, G. J. *Colloids and Surfaces* **1990**, *51*, 141-158.

15. Dijt, J. C.; Stuart, M. A. C.; Fleer, G. J. *Macromolecules* **1994**, *27*, 3219-3228.

16. Krabi, A.; Stuart, M. A. C. *Macromolecules* **1998**, *31*, 1285-1291.

17. Santore, M.; Fu, Z. *Macromolecules* **1997**, *30*, 8516.

18. Scheutjens, J. M. H. M. *Mean-Field Lattice Models of Polymers at Interfaces*; Sanchez, I. C. and Fitzpatrick, L. E., Ed.; Butterworth-Heinemann: Boston, 1992, pp 117 - 137.

19. Dijt, J. C.; Stuart, M. A. C.; Fleer, G. J. *Macromolecules* **1994**, *27*, 3207-3218.

20. van Eijk, M. C. P.; Cohen Stuart, M. A. *Langmuir* **1997**, *13*, 5447-5450.

21. Jenkel, E.; Rumbach, B. *Z. Elektrochem.* **1951**, *55*, 612.

22. Tipton, D. L.; Russo, P. S. *Macromolecules* **1996**, *29*, 7402-7411.

23. Cohen Stuart, M. A.; Fleer, G. J.; Scheutjens, J. M. H. M. *Journal of Colloid and Interface Science* **1984**, *97*, 515 - 525.

24. Van der Beek, G. P.; Stuart, M. A. C.; Fleer, G. J.; Hofman, J. E. *Langmuir* **1989**, *5*, 1180-1186.

25. Cohen Staurt, M. A.; Fleer, G. J.; Scheutjens, J. M. H. M. *Journal of Colloid and Interface Science* **1984**, *97*, 526-535.

26. Van der Beek, G. P.; Cohen Stuart, M. A.; Fleer, G. J.; Hofman, J. E. *Macromolecules* **1991**, *24*, 6600-6611.

27. Kawaguchi, M.; Arai, T. *Macromolecules* **1991**, *24*, 889-892.

28. Roefs, S. P. F. M.; Scheutjens, J. M. H. M.; Leermakers, F. A. M. *Macromolecules* **1994**, *27*, 4810-4816.

29. Dimarzio, E. A.; Bishop, M. *Biopolymers* **1974**, *13*, 2331-2348.

30. Murakami, J. *J. Phys. Soc. Japan* **1976**, *41*, 633-639.

31. Khokhlov, A. R.; Ternovsky, F. F. *Makromol. Chem., Theory Simul.* **1993**, *2*, 151-168.

32. Kuznetsov, D. V.; Sung, W. *Macromolecules* **1998**, *31*, 2679 - 2682.

33. Reiter, G. *Macromolecules* **1994**, *27*, 3046-3052.

34. Henn, G.; Bucknall, D. G.; Stamm, M.; Vanhoorne, P.; Jérôme, R. *Macromolecules* **1996**, *29*, 4305-4313.

35. Reiter, G. *Langmuir* **1993**, *9*, 1344-1351.

36. Hall, D. B.; Underhill, P.; Torkelson, J. M. *Polymer Engineering and Science* **1998**, *38*, 2039-2045.

37. Müller-Buschbaum, P.; Stamm, M. *Macromolecules* **1998**, *31*, 3686-3692.

38. Reiter, G.; Sharma, A.; Casoli, A.; Marie-Odile, D.; Khanna, R.; Auroy, P. *Langmuir* **1999**, *15*, 2551-2558.

39. Karim, A.; Douglas, J. F.; Satija, S. K.; Han, C. C.; Goyette, R. J. *Macromolecules* **1999**, *32*, 1119-1127.

40. Ren, Y.; Shoichet, M. S.; McCarthy, T. J.; Stidham, H. D.; Hsu, S. L. *Macromolecules* **1995**, *28*, 358.

41. Rabolt, J. F. *Molecular Assembly on Surfaces*; Sanchez, I. C., Ed.; Butterworth-Heinemann: Boston, 1992, pp 304.

42. Fanton, X.; Cazabat, A. M. *Langmuir* **1998**, *14*, 2554-2561.

43. Fondecave, R.; Wyart, F. B. *Macromolecules* **1998**, *31*, 9305-9315.

44. Herminghaus, S.; Jocobs, K.; Mecke, K.; Bischof, J.; Fery, A.; Ibn-Elhaj, M.; Schlagowski, S. *Science* **1998**, *282*, 916-919.

45. Qu, S.; Clarke, C. J.; Liu, Y.; Rafailovich, M. H.; Sokolov, J.; Phelan, K. C.; G. Krausch *Macromolecules* **1997**, *30*, 3640.

46. Redon, C.; Brochard-Wyart, F.; Rondelez, F. *Physical Review Letters* **1991**, *66*, 715-718.

47. Redon, C.; Brzoska, J. B.; Brochard-Wyart, F. *Macromolecules* **1994**, *27*, 468-471.

48. Segalman, R. A.; Green, P. F. *Macromolecules* **1999**, *32*, 801-807.

49. Tomasetti, E.; Rouxhet, P. G.; Legras, R. *Langmuir* **1998**, *14*, 3435-3439.

50. Xie, R.; Karim, A.; Douglas, J. F.; Han, C. C.; Weiss, R. A. *Physical Review Letters* **1998**, *81*, 1251-1254.

51. Yuan, C.; Ouyang, M.; Koberstein, J. T. *Macromolecules* **1999**, *32*, 2329-2333.

52. de Genes, P.-G. *Rev. Mod. Phys.* **1985**, *57*, 827.

53. Brochard, F.; Redon, C.; Rondelez, F. *C. R. Acad. Sci., Ser 2* **1988**, *306*, 1143.

54. Israelachvili, J. N. *Intermolecular and Surface Forces*; Academic Press: London, 1985.

55. Dan, N. *Langmuir* **1996**, *12*, 1101.

56. Brochard-Wyart, F.; Martin, P.; Roden, C. *Langmuir* **1993**, *9*, 3682.

57. Brochard-Wyart, F.; Debregeas, G.; Martin, P. *Macromolecules* **1997**, *30*, 1211.

58. Martin, J. I.; Wang, Z. G. *Langmuir* **1996**, *12*, 4950.

59. Shull, K. R. *Macromolecules* **1996**, *29*, 8487.

60. Gay, C. *Macromolecules* **1997**, *30*, 5939.

61. Reiter, G. *Phys. Rev. Lett.* **1992**, *68*, 75.

62. Silberzan, P.; Leger, L. *Macromolecules* **1992**, *25*, 1267.

63. Zhao, W.; Rafailovich, M. H.; Sokolov, J. *J. Phys. Rev. Lett.* **1993**, *70*, 1453.

64. Genzer, J.; Kramer, E. J. *J. Phys. Rev. Lett.* **1997**, *78*.

65. Kerle, T.; Yerushalmi-Rozen, R.; Klein, J. *J. Europhys. Lett.* **1997**, *38*, 207.

66. Reiter, G.; Avroy, P.; Auray, L. *Macromolecules* **1996**, *29*, 2150.

67. Faldi, A.; Composto, R. J.; Winey, K. I. *Langmuir* **1997**, *13*, 1758.

68. Adamson, A. W.; Gast, A. P. *Physical Chemistry of Surfaces*; 6th ed.; Wiley-Interscience: New York, 1997.

69. Sperling, L. H. *Introduction to Physical Polymer Science*; 2nd ed.; John Wiley & Sons: New York, New York, 1992.

70. Ciferri, A. *Liquid Crystallinity in Polymers*; VCH Publishers: New York, 1991.

71. Zachariades, A. E.; Porter, R. S. *The Strength and Stiffness of Polymers*; Marcel Dekker: New York, 1983.

72. Allen, S. R.; Farris, R. J.; Thomas, E. L. *J. Mater. Sci.* **1985**, *20*, 2727-2734.

73. Allen, S. R.; Farris, R.; Thomas, E. L. *J. Mater. Sci.* **1985**, *20*, 4583-4592.

74. Sohn, D.; Yu, H.; Nakamatsu, J.; Russo, P. S.; Daly, W. H. *Journal of Polymer Science: Part B: Polymer Physics* **1996**, *34*, 3025.

75. Odian, G. *Principals of Polymerization*; 3rd ed.; John Wiley & Sons: New York, 1991.

76. Patten, T. E.; Novak, B. M. *J. Am. Chem. Soc.* **1996**, *118*, 1906-1916.

77. Goodwin, A.; Novak, B. M. *Macromolecules* **1994**, *27*, 5520-5522.

78. Novak, B. M. *Polymerization Through Hetero-Functional Groups*; Kobayashi, S., Ed.; John Wiley & Sons: New York, 1997, pp 113 - 133.

79. Shibayama, K.; Seidel, S. W.; Novak, B. M. *Macromolecules* **1997**, *30*, 3159.

80. Novak, B. M.; Goodwin, A.; Seery, T. *Polym. Prepr. (Am. Chem. Soc.: Div. Polym. Chem.)* **1994**, *35*, 678.

81. Novak, B. M.; Goodwin, A. A. *Polym. Prepr. (Am. Chem. Soc.: Div. Polym. Chem.)* **1995**; *36*, 611.

82. Goodwin, A. A. *Ph.D. Dissertation*; University of California at Berkeley: Berkeley, 1996, pp 310.

83. Deming, T. J.; Novak, B. M. *J. Am. Chem. Soc.* **1993**, *115*, 9101-9111.

84. Deming, T. J.; Novak, B. M. *Macromolecules* **1991**, *24*, 6043-6045.

85. Deming, T. J.; Novak, B. M. *Macromolecules* **1991**, *24*, 326-328.

86. Patten, T. E.; Novak, B. M. *Macromolecules* **1993**, *26*, 436-439.

87. Patten, T. E.; Novak, B. M. *J. Am. Chem. Soc.* **1991**, *113*, 5065-5066.

88. Hoff, S. M.; Novak, B. M. *Macromolecules* **1993**, *26*, 4067-4069.

89. van Beijnen, A. J. M.; Nolte, R. J. M.; Drenth, W.; Hezemans, A. M. F.; van de Coolwijk, P. J. F. M. *Macromolecules* **1980**, *13*, 1386-1391.

90. van Beijnen, A. J. M.; Nolte, R. J. M.; Naaktgeboren, A. J.; Zwikker, J. W.; Drenth, W.; Hezemans, A. M. F. *Macromolecules* **1983**, *16*, 1679-1689.

91. Kramer, P. C. J.; Cleij, M. C.; Nolte, R. J. M.; Harada, T.; Hezemans, A. M. F.; Drenth, W. *J. Am. Chem. Soc.* **1988**, *110*.

92. Kollmar, C.; Hoffman, R. J. *J. Am. Chem. Soc.* **1990**, *112*, 8230-8238.

93. Nolte, R. J. M. *Chem. Soc. Rev.* **1994**, 11-19.

94. Goodman, M.; Chen, S. *Macromolecules* **1970**, *3*, 398-402.

95. Green, M. M.; Gross, R. A.; Crosby III, C.; Schilling, F. C. *Macromolecules* **1987**, *20*, 992-999.

96. Green, M. M.; Andreola, C.; Munoz, B.; Reidy, M. P.; Zero, K. *J. Am. Chem. Soc.* **1988**, *110*, 4063-4065.

97. Deming, T. J.; Novak, B. M. *J. Am. Chem. Soc.* **1992**, *114*, 7926.

98. Green, M. M.; Peterson, N. C.; Sato, T.; Teramoto, A.; Cook, R.; Lifson, S. *Science* **1995**, *268*, 1860-1866.

99. Lifson, S.; Andreola, C.; Peterson, N. C.; Green, M. M. *J. Am. Chem. Soc.* **1989**, *111*, 8850-8858.

100. Green, M. M.; Gross, R. A.; Schilling, F. C.; Zero, K.; Crosby III, C. *Macromolecules* **1988**, *21*, 1839-1846.

101. Itou, T.; Chikiri, H.; Teramoto, A.; Aharoni, S. M. *Polym. J.* **1988**, *20*, 143-151.

102. Conio, G.; Bianchi, E.; Ciferri, A.; Krigbaum, W. R. *Macromolecules* **1984**, *17*, 856-861.

103. Kuwata, M.; Murakami, H.; Norisuye, T.; Fujita, H. *Macromolecules* **1984**, *17*, 2731-2734.

104. Murakami, H.; Norisuye, T.; Fujita, H. *Macromolecules* **1980**, *13*, 345-352.

105. Rubingh, D. H.; Yu, H. *Macromolecules* **1976**, *9*, 681-685.

106. Schneider, N. S.; Furusaki, S.; Lenz, R. W. *J. Polym. Sci.* **1965**, *3*, 933948.

107. Williams, A.; Ibrahim, I. T. *Chem. Rev.* **1981**, *81*, 589-636.

108. Lim, A. R.; Stewart, J. R.; Novak, B. M. *Solid State Communications* **1999**, *110*, 23-28.

109. Nieh, M. P.; Goodwin, A. A.; Stewart, J. R.; Novak, B. M.; Hoagland, D. A. *Macromolecules* **1998**, *31*, 3151 - 3154.

110. Clark, D. T.; Thomas, H. R. *J. of Polym. Sci.* **1977**, *15*, 2843-2867.

111. Andrade, J. D. *X-ray Photoelectron Spectroscopy*; Andrade, J. D., Ed.; Plenum Press: New York, 1985; Vol. 1, pp 105-195.

112. Chan, C.-M. *Polymer Surface Modification and Characterization*; Hanser Publishers: New York, 1993.

113. Wagner, C. D.; Riggs, W. M.; Davis, L. E.; Moulder, J. F. *Handbook of X-ray Photoelectron Spectroscopy*; Perkin-Elmer Corporation: Eden Prairie, Minnesota, 1979.

114. Ashley, J. C. *Journal of Electron Spectroscopy and Related Phenomena* **1982**, *28*, 177-194.

115. Binnig, G.; Quate, C. F.; Gerber, C. H. *Phys. Rev. Lett.* **1986**, *56*, 930.

116. Magonov, S. *Studies of Polymer Surfaces with Atomic Force Microscopy*; Digital Instruments, 1999; Vol. 1999.

117. *Dimension™ 3000 Reference Manual.*

118. McGhie, A. J.; Tang, S. L.; Li, S. F. Y. *Chemtech* **1995**, 20.

119. Zhong, Q.; Innis, D.; Kjoller, K.; Elings, V. B. *Surface Science Letters* **1993**, *290*, L688-692.

120. Porter, T. L.; Oden, P. I.; Caple, G. *Surface Science* **1991**, *259*, 221.

121. Meyers, G. F.; DeKoven, B. M.; Seitz, J. T. *Langmuir* **1992**, *8*, 2330-2335.

122. Magonov, S. N.; Bar, G.; Stocker, W.; Cantow, H. J. *Polym. Prepr. (Am. Chem. Soc.: Div. Polym. Chem.)* **1992**, *33*, 782.

123. Jing, J.; Henriksen, P. N.; Wang, H.; Marteny, P. *Journal of Materials Science* **1995**, *30*, 5700.

124. Krausch, G.; Hipp, M.; Böltau, M.; Marti, O.; Mlynek, J. *Macromolecules* **1995**, *28*, 260-263.

125. Tanaka, K.; Takahara, A.; Kajiyama, T. *Macromolecules* **1997**, *30*, 6626-6632.

126. Suzuki, A.; Yamazaki, M.; Kobiki, Y.; Suzuki, H. *Macromolecules* **1997**, *30*, 2350-2354.

127. Kajiyama, T.; Tanaka, K.; Takahara, A. *Macromolecules* **1997**, *30*, 280-285.

128. Feldman, K.; Tervoort, T.; Smith, P.; Spencer, N. D. *Langmuir* **1998**, *14*, 372-378.

129. Snétivy, D.; Rutledge, G. C.; Vancso, G. J. *Polym. Prepr. (Am. Chem. Soc.: Div. Polym. Chem.)* **1992**, *33*, 786.

130. van Dijk, M. A.; van den Berg, R. *Macromolecules* **1995**, *28*, 6773-6778.

131. van den Berg, R.; de Groot, H.; van Dijk, M. A.; Denley, D. R. *Polymer* **1994**, *35*, 5778-5781.

132. Leclère, P.; Lazzaroni, R.; Brédas, J. L.; Yu, J. M.; Dubois, P.; Jérôme, R. *Langmuir* **1996**, *12*, 4317.

133. Motomatsu, M.; Mizutani, W.; Tokumoto, H. *Polymer* **1997**, *38*, 1779-1785.

134. Meiners, J. C.; Quintel-Ritzi, A.; Mlynek, J.; Elbs, H.; Krausch, G. *Macromolecules* **1997**, *30*, 4945-4951.

135. Pientka, Z.; Oike, H.; Tezuka, Y. *Langmuir* **1999**, *15*, 3197-3201.

136. Walheim, S.; Ramstein, M.; Steiner, U. *Langmuir* **1999**, *15*, 4828-4836.

137. Koutsos, V.; Vegte, E. W. v. d.; Grim, P. C. M.; Hadziioannou, G. *Macromolecules* **1998**, *31*, 116-123.

138. Finot, M. O.; McDermontt, M. T. *Journal of the American Chemical Society* **1997**, *119*, 8564-8565.

139. Raposo, M.; Pontes, R. S.; Mattosos, L. H. C.; O. N. Oliveira, J. *Macromolecules* **1997**, *30*, 6095-6101.

140. Kelley, T. W.; Schorr, P. A.; Johnson, K. D.; Tirrell, M.; Frisbie, C. D. *Macromolecules* **1998**, *31*, 4297-4300.

141. Chi, L.; Li, H.; Zhang, X.; Fuchs, H.; Shen, J. *Polymer Bulletin* **1998**, *41*, 695-699.

142. Gerle, M.; Fischer, K.; Roos, S.; Müller, A. H. E.; Schmidt, M.; Sheiko, S. S.; Prokhorova, S.; Möller, M. *Macromolecules* **1999**, *32*, 2629-2637.

143. Sauer, B. B.; McLean, S. R.; Thomas, R. R. *Langmuir* **1998**, *14*, 3045-3051.

144. Lee, B.-w.; Clark, N. A. *Langmuir* **1998**, *14*, 5495-5501.

145. Bar, G.; Brandsch, R. *Langmuir* **1998**, *14*, 7343-7347.

146. Kajiyama, T.; Tanaka, K.; Ohki, I.; Ge, A.-R.; Yoon, J.-S.; Takahare, A. *Macromolecules* **1994**, *27*, 7932.

147. Gracias, D. H.; Somorjai, G. A. *Macromolecules* **1998**, *31*, 1269-1276.

148. Luckham, P. F.; Manimaaran, S. *Macromolecules* **1997**, *30*, 5025-5033.

149. Courvoisier, A.; Isel, F.; François, J.; Maaloum, M. *Langmuir* **1998**, *14*, 3727-3729.

150. Domke, J.; Radmacher, M. *Langmuir* **1998**, *14*, 3320-3325.

151. O'Shea, S. J.; Lantz, M. A.; Tokumoto, H. *Langmuir* **1999**, *15*, 922-925.

152. Ortiz, C.; Hadziioannou, G. *Macromolecules* **1999**, *32*, 780-787.

153. Miller, J. D.; Veeramasuneni, S.; Drelich, J.; Yalamanchili, M. R. *Polymer Engineering and Science* **1996**, *36*, 1849-1855.

154. Maman, M.; Ponsinet, V. *Langmuir* **1999**, *15*, 259-265.

155. DiNardo, N. J. *Nanoscale Characterization of Surfaces and Interfaces*; VCH: New York, 1994.

156. Kumaki, J.; Nishikawa, U.; Hashimoto, T. *J. Am. Chem. Soc.* **1996**, *118*, 3321.

157. Quist, A. P.; Björck, L. P.; Reimann, C. T.; Oscarsson, S. O.; Sundqvist, B. U. R. *Surface Science* **1995**, *325*, L406-L412.

158. Ebihara, K.; Koshihara, S.-y.; Yoshimoto, M.; Maeda, T.; Ohnishi, T.; Koinuma, H.; Fujiki, M. *Jpn. J. Appl. Phys.* **1997**, *36*, L 1211.

159. Kelley, S. O.; Barton, J. K.; Jackson, N. M.; McPherson, L. D.; Potter, A. B.; Spain, E. M.; Allen, M. J.; Hill, M. G. *Langmuir* **1998**, *24*, 6781-6784.

160. Cornelissen, J. J. L. M.; Hafkamp, R. J. H.; Sommerdijk, N. A. J. M.; Feiters, M. C.; Nolte, R. J. M. *Polym. Prepr. (Am. Chem. Soc.: Div. Polym. Chem.)* **1999**, 40, 517.

161. Karim, A.; Slawecki, T. M.; Kumar, S. K.; Douglas, J. F.; Satija, S. K.; Han, C. C.; Russell, T. P.; Liu, Y.; Overney, R.; Sokolov, J.; Rafailovich, M. H. *Macromolecules* **1998**, *31*, 857-862.

162. Affrossman, S.; Kiff, T.; O'Neill, S. A.; Pethrick, R. A.; Richards, R. W. *Macromolecules* **1999**, *32*, 2721-2730.

163. Ramirez-Aguilar, K. A.; Rowlen, K. L. *Langmuir* **1998**, *14*, 2562.

164. Keller, D. *Surface Science* **1991**, *253*, 353.

165. Pangborn, A. B.; Giardello, M. A.; Grubbs, R. H.; Rosen, R. K.; Timmers, F. J. *Organometallics* **1996**, *15*, 1518-1520.

166. Palomo, C.; Mestres, R. *Synthesis* **1981**, 373-374.

167. Rapi, G.; Sbrana, G. *Journal of the American Chemical Society* **1970**, *93*, 5213-5217.

168. King, S. T.; Strope, J. H. *Journal of Chemical Physics* **1971**, *54*, 1289-1295.

169. Mogul, P. H.; Kniseley, R. N.; Fassel, V. A. *Spectroscopy Letters* **1977**, *10*, 959-970.

170. Patten, T. E. *Ph.D. Dissertation*; University of California, Berkeley: Berkeley, 1994, pp 45-48.

171. Kratochvil, P. *Classical Light Scattering from Polymer Solutions*; Vlsevier: New York, 1987.

172. Lee, H. C.; Chang, T.; Harville, S.; Mays, J. W. *Macromolecules* **1998**, *31*, 690-694.

173. Ke, B. *Specific Refractive Index Increment*; Wiley: New York, 1964, pp 490-492.

174. Iyengar, D. R. *Ph.D. Dissertation*; University of Massachusetts: Amherst, Massachusetts, 1992, pp 350.

175. Fleer, G. J.; van Male, J.; Johner, A. *Macromolecules* **1999**, *32*, 845-862.

CHAPTER 2

THE ADSORPTION OF POLYCARBODIIMIDES ONTO CHEMICALLY SURFACE MODIFIED NATIVE SILICON OXIDE

Introduction

Organosilane coupling agents have long been used to bond organic polymers to inorganic substrates.[1] Without coupling agents, the bonds between polymer and metal oxides are susceptible to deterioration in humid or solvent-vapor conditions. The improved bonding in various environments comes from the stable chemical link (couple) of the silane between the polymer and the mineral. The applications and chemistry of silane coupling agents can be reviewed in texts by Plueddemann[1] and Leyden.[2] Our research interest is not in the adhesion promoting characters of organosilanes, but in their ability to form monolayers on metal oxides with controllable microstructures.

In the research presented here, we were interested in studying the adsorption behavior of polycarbodiimides to an inorganic substrate (silica) modified with organosilanes. The surface energy of the modified silica substrate can be controlled by the chemistry and the degree of heterogeneity within the organosilane layer(s).[3-8] Our objective is to adsorb polycarbodiimides to surfaces of known composition and surface energy, and study how molecular weight, chain architecture, surface energy, and surface chemistry affect the adsorbed polymer layer.

Organosilane Chemistry on Silica

Hydrophilic silica reacts with water resulting in the functionalization of the silica surface with silanol groups.[8] These silanol groups can then be reacted with chloro or alkoxy functionalized organosilanes to produce a chemisorbed monolayer (Fig. 2.1).

Figure 2.1. The reaction of silanol groups with an organosilane agent. (X = Cl or alkoxy group)

The formation of silanol groups on silica substrates can be accomplished by several mechanisms. Hair[9] used transmission infrared spectroscopy to monitor the dehydration of silica exposed to various heating conditions. It was discovered that physisorbed water on silica could be removed in vacuo at room temperature. At temperatures between 160 °C and approximately 450 °C (dry atmosphere), silanol groups condense and water is eliminated. However, the dehydration is completely reversible. As the temperature is increased above 450 °C, the dehydration process becomes progressively more irreversible. Upon heating above 800 °C, the dehydration was found irreversible and the surface became hydrophobic. Markham et al.[8] found that silica dehydrated at 1000 °C was readily rehydrated in water or high-ambient relative humidity to an extent necessary for the deposition of a octadecyltrichlorosilane (OTS) monolayer. There may exist some ambiguity in the extent of irreversibility of the dehydration process. From the literature,[3,4,6,8,10] most silica surfaces prepared for silane treatment are cleaned by strong oxidizers, washed in ultra-pure water, and dried in conditions which remove the physisorbed water.

Organosilane Surface Heterogeneity

Organosilane surface modification effectively changes the interaction of silica with respect to water. These changes are qualitatively monitored by measuring the advancing and receding contact angles using various probe fluids, such as water, hexadecane, and methylene iodide.[11,12] Also reported, along with other contact angle

procedures,[4,6] are other techniques used to help elucidate the structure of organosilanes on mineral surfaces. These techniques include XPS,[3,4,13] SEM,[10] AFM,[10] reflection and transmission IR,[10] ellipsometry,[10] solid-state NMR,[14] FTIR-photoacoustic spectroscopy,[15] and attenuated total reflectance (ATR)-FTIR.[4] However, measurements of dynamic contact angle infer information on the heterogeneity of the surfaces, which is related to the chemical composition. The extent of the surface heterogeneity can be characterized through contact angle hysteresis.

Silane Modification of Silica

The surface modification of silica by silane coupling agents has been used by several research groups to study surface phenomena.[3,4,6-8,10,13-16] Herzberg et al.[7] emphasized the importance of receding contact angles in characterizing surface heterogeneity. Their investigations were performed on glass microscope slides treated with dichlorodimethylsilane (Me_2SiCl_2) and chlorotrimethylsilane (Me_3SiCl). Me_2SiCl_2 was found to hydrolyze at the glass surface to form polydimethylsiloxanes. Essentially no water contact angle hysteresis (θ_A=110° and θ_R=107.5°) was measured for Me_2SiCl_2 surfaces. From the lack of hysteresis, it was inferred that the glass surface was composed of a homogeneous surface of chemisorbed polysiloxanes. This surface would account for the wetting properties similar to those anticipated for a surface of closely packed methyl groups.

When contact angle hysteresis was measured on Me_3SiCl modified surfaces, Herzberg et al. experimentally found that less than a monolayer of Me_3SiCl chemisorbed to the glass surface and measured an advancing water contact angle of 85°. It was concluded that a microscopic form of heterogeneity existed because a surface composed of large domains of Me_3SiCl should have an advancing contact angle the same as those for Me_2SiCl_2. Additional contact angle experiments were performed on Me_3SiCl surfaces where the concentration of methyl groups was reduced by hydrolysis. They observed that

small decreases in the concentration of trimethylsilyl groups resulted in sharp decline in receding contact angles. The corresponding advancing angles did not change. Their data supported the importance of receding contact angles in characterizing surfaces. This has been further emphasized by recent work in the McCarthy group.[17-20]

Menawat et al.[6] modified the surface energy of glass plates with the following monchloroorganosilanes: triphenylchlorosilane, t-butyl diphenylchlorosilane, t-butyl dimethylchlorosilane, and pentafluorophenyldimethylchlorosilane. Their research required modified silica surfaces that were reproducible, stable, and homogeneous. This was accomplished using monochloroorganosilanes. Multifunctional silanes were not used because they have the tendency to oligomerize in the presence of trace amounts of water.[4] Also, the resulting surfaces are heterogeneous and potentially exhibit large contact angle hysteresis. Their choice of organic substituents on the monochloroorganosilanes required specific characteristics. First, the substituents should not interfere with the chemisorption of the silane to the surface. They should allow high packing densities at maximum surface coverage. Furthermore, the substituents should be large enough to resist rehydrolyzation.

The affects of reagent concentration on the measurements of dynamic water contact angle were studied for the various silanes on glass (see Fig. 2.4). For all the silane reagents, the advancing contact angle increased with increasing reagent concentration. Thus, higher reagent concentrations resulted in an increased hydrophobicity. However, the contact angle hysteresis followed the general trend of decreasing with increasing reagent concentration up to a critical concentration. At the critical point, further increases in concentration resulted in increased hysteresis. Menawat et al. concluded that at low reagent concentrations, the silica surface is partially covered by the chemisorbed alkylsilane with exposed silanol groups protruding up from the silica. This surface is heterogeneous and exhibits large hysteresis. Further increases in reagent concentration results in a decrease in hysteresis. Thus, the surface becomes

more homogeneous because of the alkylsilanes chemisorbing in a close packed monolayer. At concentrations above the critical point, the increase in hysteresis is associated with a multilayered surface. The multilayered surface is the result of alkylsilanes physisorbed to the chemisorbed layer.

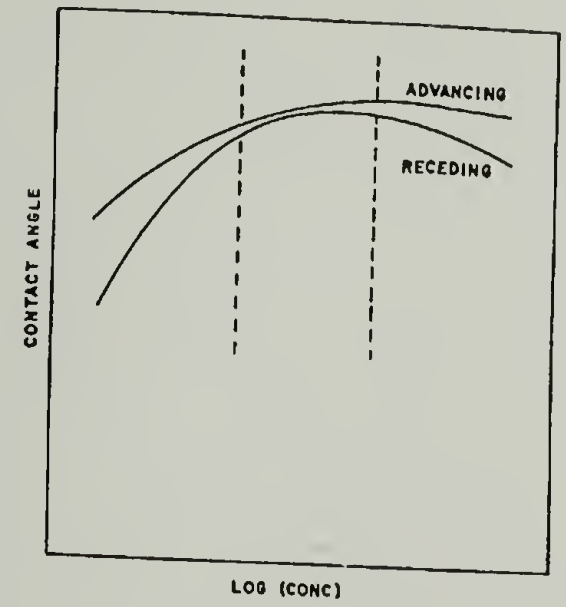

Figure 2.2 General trends in hysteresis observed for increasing reagent concentrations.[6] The area to the left of the dotted lines is associated with a heterogeneous surface due to chemisorbed and physisorbed alkylsilane reagent. In between the dotted lines, the surface is becoming more homogeneous as alkylsilane chemisorbs in a close packed monolayer. To the right of the dotted lines, the surface becomes heterogeneous due to physisorption of the alkylsilane results in a multilayered surface.

In Chapter 1, we characterized the trends in the adsorption of poly(*N*-methyl-*N'*-(α-phenylethyl)carbodiimide) onto native silicon oxide surfaces. That research focused on the effects of solvent, molecular weight, polymer stereochemistry, and temperature on the amount adsorbed. However, AFM images indicated dewetting of the adsorbed layer, and in addition, the aforementioned factors effected the extent of dewetting. The work presented here reports on the trends in the adsorption of poly(*N*-methyl-*N'*-(α–phenylethyl)carbodiimide) onto surfaces of varying surface energies and microstructures.

Characterization Techniques

Contact Angle Measurements

Contact angle measures the wettability of the outermost region of a surface.[21-26] Wettability is a macroscopic property influenced by the microstructure of the surface, and where the surface tension of the solid directly affects the amount of drop spreading. However, the contact angle is also a function of the liquid surface tension. The angle measured is shown in Figure 2.3.

Substrates with low surface energies (hydrophobic) are characterized by large water contact angles while the opposite is observed for high surface energy (hydrophilic) substrates. The contact angle (θ) is governed by the equilibrium between the surface tensions in the region of the solid/liquid/vapor three-phase boundary as described by Young's equation (Eq. 2.1).

$$\gamma_{lv}\cos\theta = \gamma_{sv} - \gamma_{sl} \qquad (2.1)$$

Where the variables are defined as (see Fig. 2.3): γ_{lv} is the surface tension of the liquid in equilibrium with its saturated vapor, γ_{sv} is the surface tension of the solid in equilibrium with the saturated vapor of the liquid, and γ_{sl} is the solid-liquid interfacial tension. This is

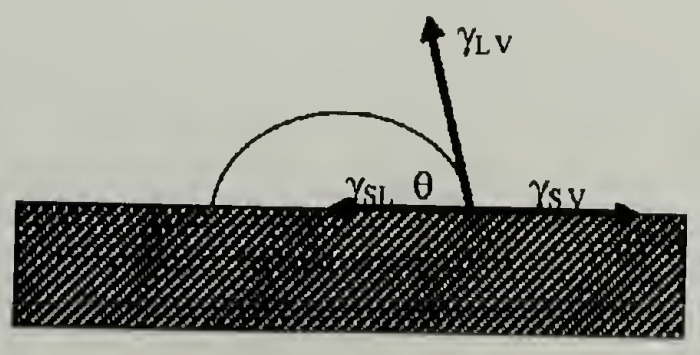

Figure 2.3. Equilibrium contact angle.

based on the following assumptions: the surface is rigid, immobile, nondeforming, and smooth; the composition is chemically homogeneous and the solid does not interact with the probe fluid. If all these conditions are met, then there is one equilibrium contact angle. However, in most practical systems, not all of the above criteria are met resulting in contact angle hysteresis.

There are two types of contact angle measurements: static and dynamic.[26] Static measures the contact angle of a stationary drop on a surface where the angle is governed by the equilibrium of the interfacial tensions (solid/liquid interface not in motion). Dynamic measures the contact angle of a moving drop on a surface where the angle is determined by the balance of the interfacial driving force and the viscous retarding force (solid/liquid interface in motion). For dynamic studies, two angles are of interest: the advancing contact angle, θ_A and the receding contact angle, θ_R. As probe fluid is added to a drop resting on a surface, the drop responds by advancing over the surface. The angle measured at the moment when the drop begins to spread is the advancing contact angle. The receding contact angle is the angle of the drop at the moment it begins to recede in response to the withdrawal of probe fluid. In addition, the rate at which probe fluid, is added or withdrawn can dramatically affect the measured angles. When the advancing and receding angles are equivalent, the interfacial tensions are in true thermodynamic equilibrium. Hysteresis is evident when there are differences between the advancing and receding angles. These differences can result from surface heterogeneity and surface roughness. Contact angle hysteresis due to surface heterogeneity is of great interest for this research (vide infra).

Contact Angle Hysteresis

Contact angle hysteresis can be classified as thermodynamic or kinetic.[21,26] A system exhibits thermodynamic hysteresis when multiple measurements of θ_A and θ_R are reproducible as well as being independent of time and frequency. Hysteresis under

kinetic control is dependent on time and frequency. When the advancing and receding contact angles are equivalent, then the thermodynamic hysteresis has reached a stable equilibrium state and the contact angle is referred to as the Cassie angle (vide infra).

A heterogeneous surface is shown in Figure 2.3.[21] Two-phases are present where region 1 is a discontinuous phase (represented as small domains), that is relatively hydrophobic and region 2 is the continuous phase, which is partially hydrophilic. As a liquid spreads across the continuous phase, it is exposed to the low-surface energy domains. These contact points (energy barriers) effectively pin the spreading liquid and prevent or retard its advancement. The result is an advancing contact angle that is higher

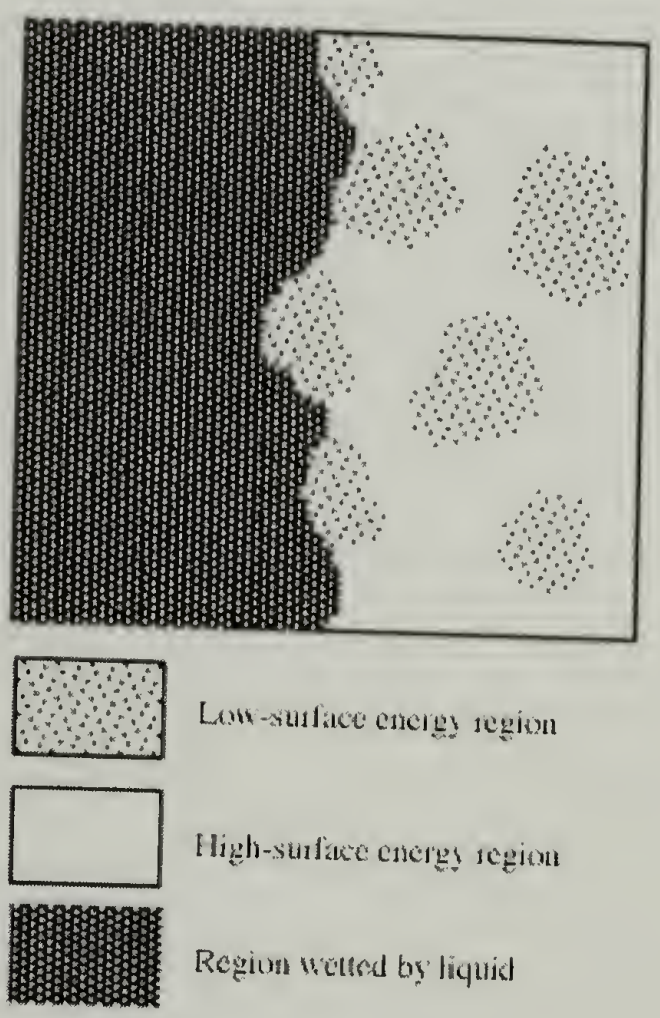

Figure 2.4. Schematic of a liquid spreading over a two-phase heterogeneous surface.

than expected. As the liquid is withdrawn, the hydrophilic phase prevents (or retards) the fluid from receding. This results in a lower-than-anticipated receding contact angle. The contact angle hysteresis is a result of the tendency for the advancing angles to be influenced by the low-surface energy regions, whereas the receding angles are influenced by the high-surface energy regions. Cassie and Baxter[27] derived an expression to describe the equilibrium contact angle (Cassie angle) θ_c for heterogeneous two-phase surfaces:

$$\cos\theta_c = f_1 \cos\theta_1 + f_2 \cos\theta_2 \qquad (2.2)$$

where f_1 and f_2 are the area fractions of each surface region such that $f_1 + f_2 = 1$ with equilibrium contact angles θ_1 and θ_2. This model is limited in that it does not take into account hysteresis effects because it was derived for a sessile drop in equilibrium with a surface.[21]

Cassie assumes the surface heterogeneity is in the form of discrete patches of either region 1 or 2. However, if the surface is heterogeneous at the atomic level, then intermolecular forces need to be considered. Israelachvili and Gee[5] modified the Cassie equation to account for the chemical heterogeneity at the molecular level:

$$(1+\cos\theta)^2 = f_1(1+\cos\theta_1)^2 + f_2(1+\cos\theta_2)^2 \qquad (2.3)$$

For example, this equation would be applied to silica surfaces with both siloxane and silanol groups present and to surfaces coated with mixed surfactant monolayers. This equation was not quantitatively studied due to the difficulties in determining f_1 and f_2. Generally, the differences in Equation 2.2 and 2.3 predict increasing hysteresis with increasing domain size of the discontinuous phase.

Experimental Section

Materials

Procedures for the synthesis and polymerization of poly(*N*-methyl-*N'*-(α-phenylethyl)carbodiimide) and poly(di-n-hexylcarbodiimide) are described in Chapter 1. All solvents (HPLC grade), sulfuric acid, hydrogen peroxide, and sodium dichromate were obtained from Fisher and used as received. Organosilanes were obtained from Gelest Inc. and used as received. House-purified water (reverse osmosis) was further purified using a Millipore Milli-Q_{UF} system that involves reverse osmosis, ion–exchange and filtration steps (18 MΩ/cm).

Pretreatment of Native Silicon Oxide Substrate

Silicon wafers were obtained from International Wafer Service (1" diameter, 500-550 μm thick, N-doped, single side polished, Part # 01549). Pretreatment of the silica surface was performed following procedures outlined by Fadeev et al.[12] Silanization reactions were carried out immediately after treating the silicon wafers.

Reaction of Silicon Wafers with Oraganosilanes in the Vapor Phase

The procedure followed was outlined by Fadeev et al.[12] Pretreated silicon wafers were suspended using a glass block in the bottom of a Schlenk flask containing approximately 1 mL of chloroorganosilane. There was no direct contact between the silicon wafers and the silane. The flask was submerged in a 65 °C hot oil bath and then completely covered with aluminum foil which acted as insulation, maintaining an environment of 60-70° C. The reaction was allowed to proceed for 72 hours at which time the wafers were rinsed (in this order) with 1 quick rinse toluene, 2 x 20 mL of toluene, 3 x 20 mL of ethanol, 2 x 20 mL of ethanol-water (1:1), 2 x 20 mL water, 2 x 20 mL ethanol, 2 x 20 mL water. Each rinse step was ten minutes and after rinsing, the

samples were transferred to a 120° C oven for ten minutes and then stored in sealed wafer holders.

Preparation of Binary Mixed Monolayers

Binary mixed monolayers of organosilanes were prepared using a two-step process. Native silicon oxide surface was pretreated as previously described followed by vapor phase chemisorption of tris(trimethylsiloxy)chlorosilane. After rinsing and drying, the modified silica was further modified by vapor phase chemisorption of the second organosilane, 10–(carbomethoxy)decyldimethylchlorosilane. The extent of modification was monitored by dynamic contact angle measurements.

Polymer Adsorption

Adsorption experiments with the modified silica substrates were performed from THF following the procedures outlined in Chapter 1. Both 321:1 and 3121:1 samples of poly-**R/S** and poly-**S** were studied. All adsorptions were performed between 72-96 hours unless otherwise stated.

Characterization

The adsorbed layers on modified silica substrates were characterized by the same techniques used to characterize adsorbed films on native silicon oxide. These characterization techniques were described in Chapter 1. They include dynamic contact angle, XPS, and tapping mode AFM.

Results and Discussion

Summary of Research

The work reported here studies the trends in the adsorption of polycarbodiimides onto organosilane modified silica. The chemistry and physics of trialkylsilane monolayers covalently attached to silicon surfaces has been described by Fadeev et al.[12] In addition, the affects on wettability of organosilyl monolayers covalently attached to silicon, as well as other chemical techniques has been reviewed.[17,18] The reader is referred to this literature for background information. However, the aforementioned research was used in this work to help prepare surfaces of known chemistry.

We first studied the trends in the adsorption of polycarbodiimides onto a lyophobic surface. This was accomplished by performing adsorptions onto single side silicon surfaces (Si wafers) modified with a dense monolayer of tris(trimethylsiloxy)chlorosilane (tris(TMS)). Fadeev et al.[19] characterized silicon surfaces modified with tris(TMS) and they reported water advancing/receding contact angles of 96°/87° and hexadecane contact angles of 33°/31°. In addition, they described a process for preparing mixed monolayers using tris(TMS). The procedure involves preparing complete monolayers of bulky organosilanes that are well packed, but contain "holes" in the array of grafted groups that can be "filled" by further reaction with organosilanes of dimensions smaller than that of the cross-sectional area of these holes.[20] Scheme 2.1 graphically describes this process and shows the chemistry followed in the researched reported here.

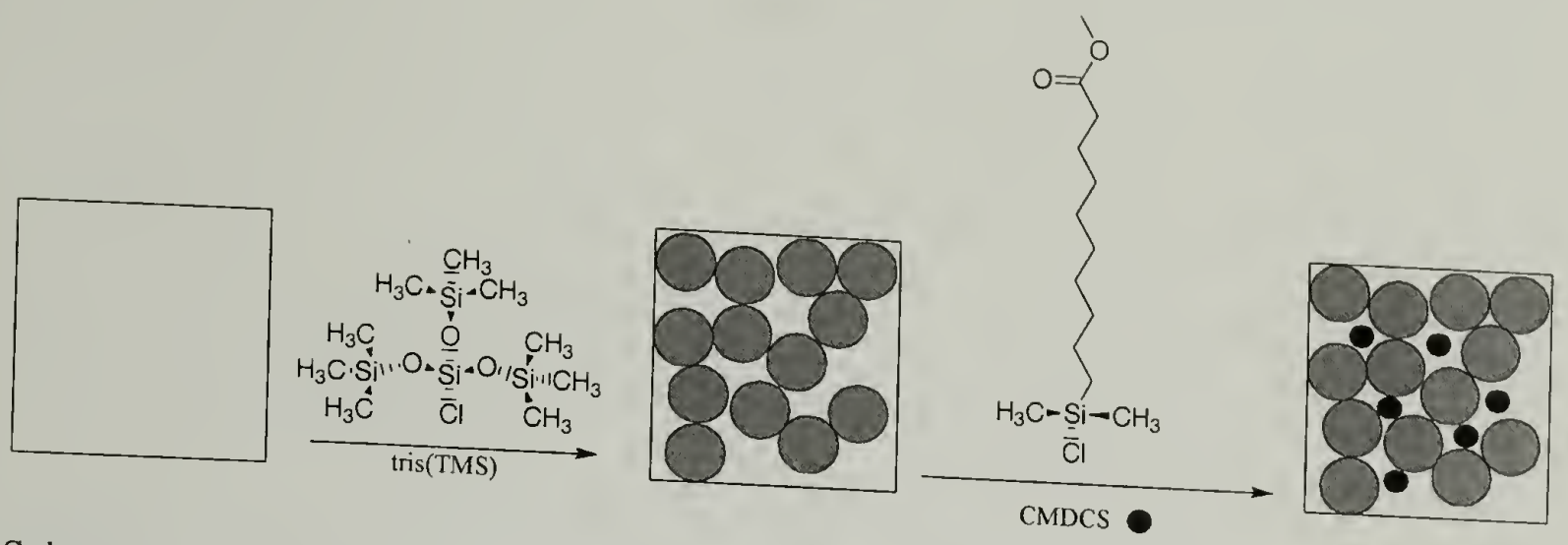

Scheme 2.1. Formation of uniform binary mixed monolayers through the two-step silanization procedure.

To study the adsorption behavior of poly-**R/S** and poly-**S** on surfaces that vary in hydrophobicity and lyophobicity, we proposed to use mixed monolayers. In addition, we wanted to study the adsorption behavior of polycarbodiimides to carboxylic acids. Since the basicity of the guanidine unit along the poly-**R/S** and poly-**S** backbone is equivalent, the surface structure of the adsorbed films would be a function of the solution chain architecture (stereochemistry). To study affects of carboxylic acid groups on the adsorption of polycarbodiimides, we proposed to modify silica surfaces with 10–(carbomethoxy)decyldimethylchlorosilane ($(Me_2SiCl)C_9H_{18}COOCH_3$ = CMDCS), then hydrolyze the methyl ester under dilute acid conditions. In addition, the CMDCS would be used to prepare mixed monolayers because it offered the capability to control the concentration of surface carboxylic acid groups through varying its ratio with tris(TMS).

Characterization of tris(TMS) and CMDCS-modified Silica

Contact angle data for the 5 day (67 °C) vapor phase chemisorption of tris(TMS) and CMDCS to silica (Si wafer) is listed in Table 2.1. Both surfaces are hydrophobic, however, the tris(TMS) sample is more lyophobic than the silica surface modified with

CMDCS. This difference in lyophobicity was expected because hexadecane will readily wet the methylene groups along the long alkyl-ester chain of the CMDCS. Hexadecane does not wet the tris(TMS)–modified silica sample because the surface is high in methyl group concentration. In addition, though the amount of hysteresis is large, the data does suggest the monolayers are dense and uniform.[19] Fadeev et al.[12] characterized the high hysteresis as an affect of molecular roughness and rigidity.

Table 2.1. Contact angle analysis of a monolayer of chemisorbed tris(TMS) and CMDCS on native silicon oxide from the vapor phase for 5 days at 67 ± 3 °C.

Coupling Agent	θ_A H_2O	θ_R H_2O	θ_A Hexadecane	θ_R Hexadecane
tris(TMS)	92° ± 1°	81° ± 1°	34° ± 2°	27° ± 2°
CMDCS	82° ± 2°	77° ± 2°	8° ± 1°	0°

Table 2.2. XPS atomic concentration results of adsorbed thin films of poly-**R/S** and poly–**S** adsorbed to tris(TMS)–modified (dense monolayer) native silicon oxide at 25 °C for 72 hours. Solvent refers to the solution solvent the polymer was adsorbed from.

Polymer/Solvent	$C_{15°}$	$N_{15°}$	$O_{15°}$	$Si_{15°}$	$C_{15°}$: $N_{15°}$	$Si_{15°}$: $N_{15°}$
Control tris(TMS) 312:1	30.62	-	39.88	29.50	-	-
RS/THF	25.64	0.11	46.25	28.00	233 : 1	255 : 1
S/THF	22.60	0.12	48.43	28.84	188 : 1	240 : 1
3121:1						
RS/THF	30.92	2.09	44.19	22.81	14.8 : 1	11 : 1
S/THF	23.80	0.24	47.59	28.37	99.2 : 1	118 : 1
RS/toluene	72.88	10.56	9.02	7.55	6.9 : 1	0.7 : 1

Polymer/Solvent	$C_{75°}$	$N_{75°}$	$O_{75°}$	$Si_{75°}$	$C_{75°}$: $N_{75°}$	$Si_{75°}$: $N_{75°}$
Control tris(TMS) 312:1	9.47	-	41.51	49.02	-	-
RS/THF	9.83	0.07	35.68	54.43	140 : 1	778 : 1
S/THF	8.91	0	37.99	53.09	-	-
3121:1						
RS/THF	13.46	1.06	33.69	51.79	12.7 : 1	49 : 1
S/THF	9.75	0.17	42.14	47.94	57.4 : 1	282 : 1
RS/toluene	35.95	5.03	23.99	35.02	7.1 : 1	7.0 : 1

Adsorptions of poly(*N*-methyl-*N'*-(α-phenylethyl)carbodiimide) onto tris(TMS) and CMDCS-modified silica were performed for 72 hours at 25 °C. Both 312:1 and 3121:1 molecular weights of poly-**R/S** and poly-**S** were adsorbed. The atomic concentration results from XPS analysis of adsorbed films on tris(TMS)–modified silica are listed in Table 2.2. The control surface data show an increase in carbon concentration along with an increase in contact angles (Table 2.3), therefore indicating modification of the silica surface.

Atomic concentration data for the adsorption of 312:1 poly-**R/S** and poly-**S** (Table 2.2) suggest that a small amount of both polymers adsorb to tris(TMS). In addition, the carbon to nitrogen ratio data for the 15° take-off angle suggest that a smaller amount of poly-**R/S** adsorbed than poly-**S**. However, the 75° take-off angle data for both ratios of carbon to nitrogen, as well as silicon to nitrogen indicate thicker films of poly-**R/S** adsorbed. The results only indicate that both polymers adsorb and the films are thin. Greater disparity is shown in the XPS and contact angle data for adsorbed films of 3121:1 polymers. In this case, a larger amount of poly-**R/S** adsorbed than poly-**S**. This result is opposite the trend shown in Chapter 1 for adsorptions on native silicon oxide surfaces. Therefore, it could be concluded that the higher adsorbed amount of 3121:1 poly-**R/S** than 3121:1 poly–**S** on a tris(TMS) surface is a function of chain architecture. In other words, the poly-**R/S** can adopt chain conformations that allow chain segments to penetrate "holes" in the monolayer resulting in chain segments adsorbing to the silica surface. For poly-**S**, chain rigidity restricts conformational changes near the surface, thereby limiting adsorption. For the 312:1 polymers, there is little difference in their chain rigidity because of fewer defects (i.e. kinks along the polymer chain) in the lower molecular weight poly-**R/S**. However, care must be taken interpreting the XPS data because surface roughness (a result of dewetting) may affect the results. This was demonstrated in Chapter 1, where dewetting of adsorbed films of poly-**R/S** and poly-**S** from native silicon oxide was indicated by tapping mode AFM. Nevertheless, the data

does indicate some obvious trends such as much larger amounts of 3121:1 poly-**R/S** adsorbed from toluene than THF. This is consistent with the results of similar adsorptions on native silicon oxide as shown in Chapter 1.

Contact angle data from Table 2.3 indicate similar trends as discussed from the XPS results. The contact angle results for the adsorptions of 312:1 poly-**R/S** and poly-**S** on tris(TMS) suggest very little (if any) polymer adsorbed because the advancing and receding angles are equal to those for the control surface. In addition, the water contact angles for an adsorbed layer of poly-**R/S** from toluene onto native silicon oxide were shown in Chapter 1 to be 94° advancing and 73° receding. Therefore, interpreting contact angle data between adsorbed polymer and tris(TMS)–modified surface is difficult. However, the increased hysteresis for adsorptions of 3121:1 polymers does indicate that polymer had adsorbed. Only using XPS and contact angle data to characterize the structure of adsorbed films may result in flawed interpretations of the data. As a result, techniques that map the surface topography, such as AFM, should be used in concert with XPS and contact angle.

Table 2.3. Water contact angle results of adsorbed thin films of poly-**R/S** and poly--**S** adsorbed to tris(TMS)–modified (dense monolayer) native silicon oxide at 25 °C for 72 hours. Solvent refers to the solution solvent the polymer was adsorbed from.

Polymer/Solvent	θ_A H_2O	θ_R H_2O
312:1		
RS/THF	94° ± 2°	80° ± 2°
S/THF	92° ± 1°	81° ± 1°
3121:1		
RS/THF	91° ± 1°	70° ± 2°
S/THF	91° ± 1°	77° ± 2°
RS/toluene	93° ± 1°	78° ± 1°

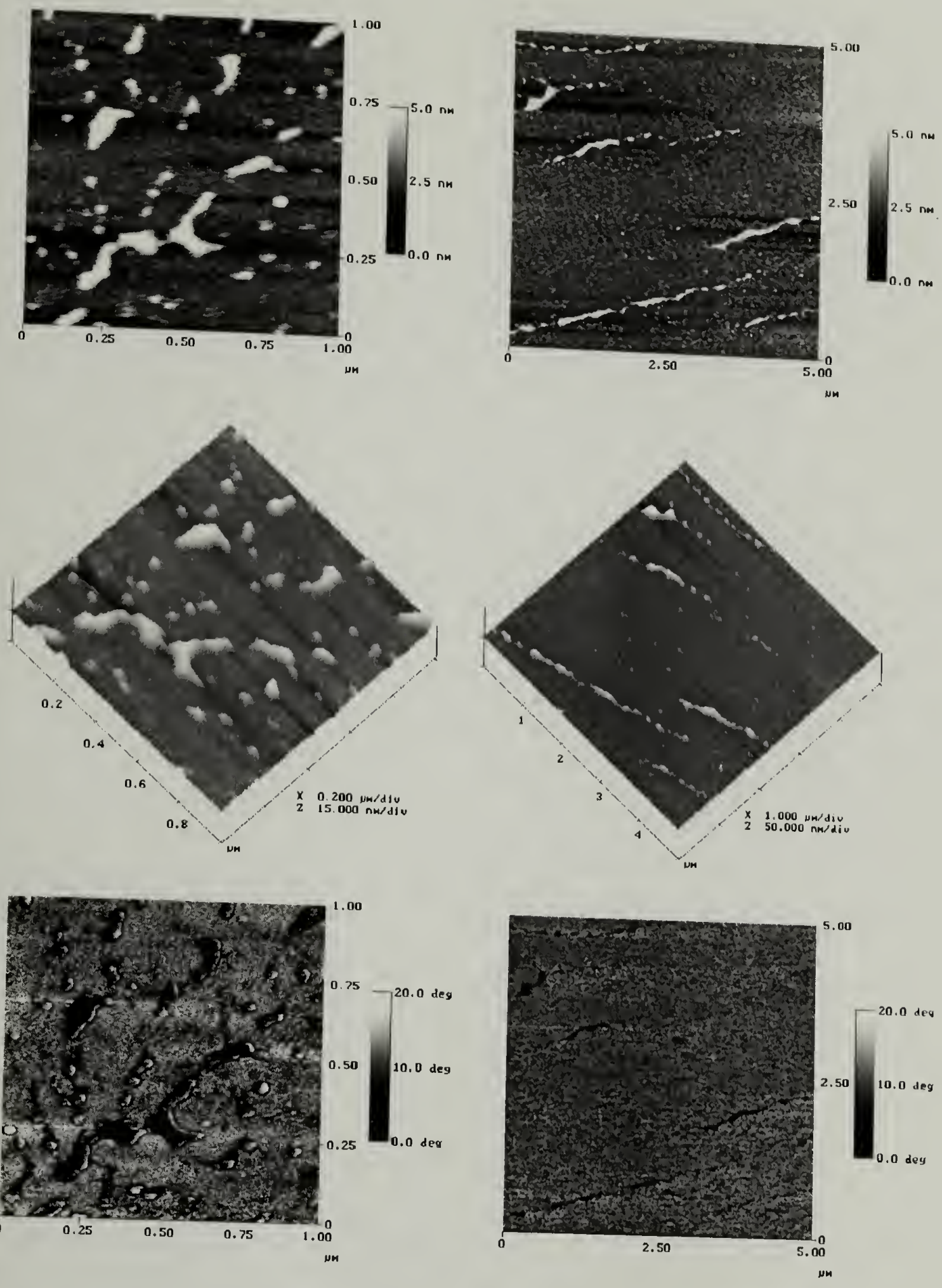

Figure 2.5. AFM tapping mode analysis of adsorbed 312:1 poly-**R/S** from THF to dense tris(TMS)–modified native silicon oxide for 72 hours at 25 °C. The pictures are height (top), surface (middle), and phase (bottom) images of a 1 μm^2 sampling area (left column) and a 25 μm^2 sampling area (right column).

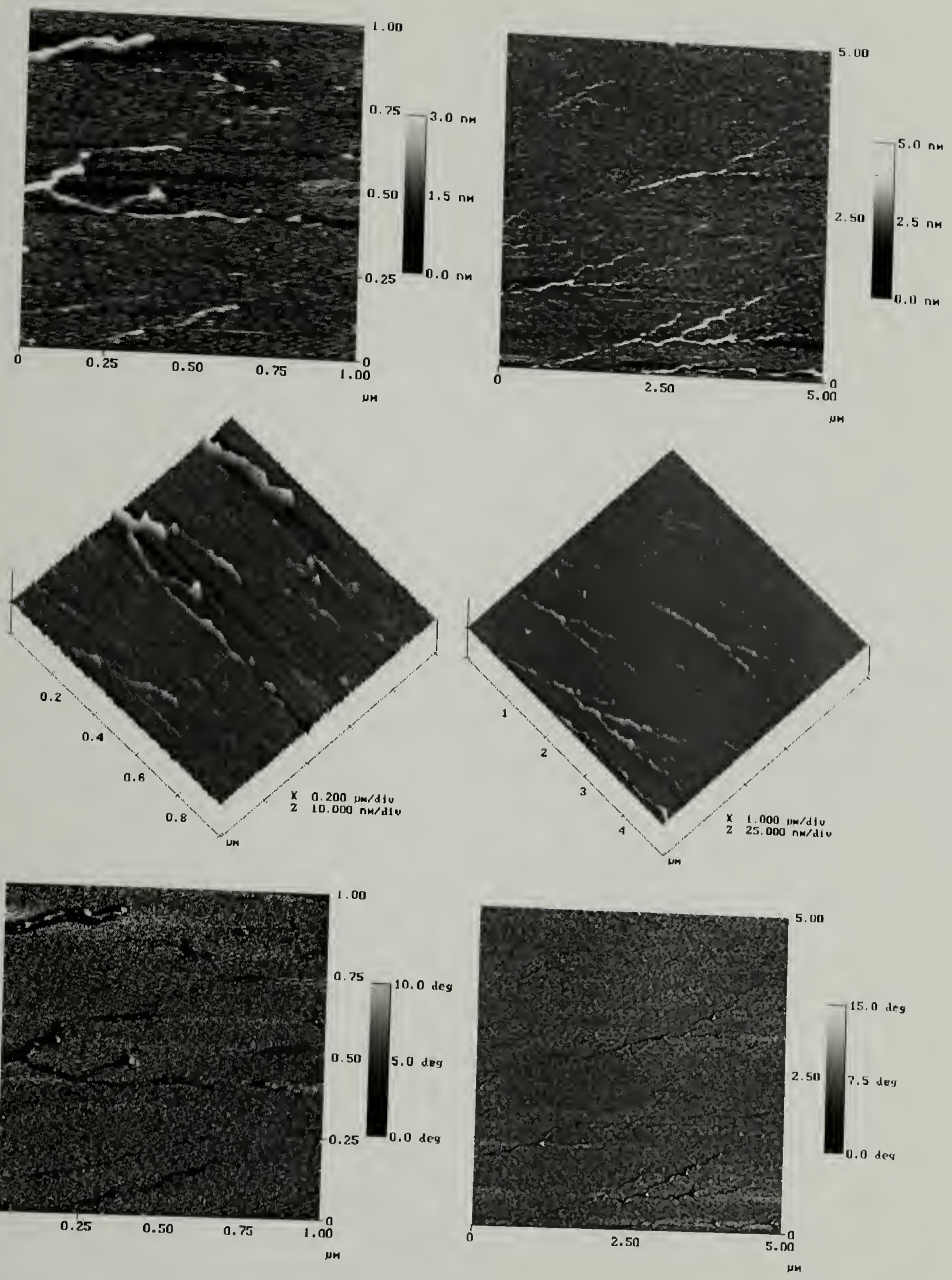

Figure 2.6. AFM tapping mode analysis of adsorbed 312:1 poly-**S** adsorbed from THF to dense tris(TMS)–modified native silicon oxide for 72 hours at 25 °C. The pictures are height (top), surface (middle), and phase (bottom) images of a 1 μm^2 sampling area (left column) and a 25 μm^2 sampling area (right column)

Tapping mode AFM was performed on samples prepared under the same conditions as described in Tables 2.2 and 2.3. For each sample shown in Figures 2.5-2.9, height, surface, and phase imaging were analyzed over areas of 1 μm^2 and 25 μm^2. In addition, each sample was analyzed in several areas around the center of the wafer, and the images show the most representative structures within that region. Figures 2.5 and 2.6 are respectively, AFM images of adsorbed films of 312:1 poly-**R/S** and 312:1 poly-**S** onto tris(TMS). Recalling that the XPS and contact angle data indicated that little (if any) 312:1 polymer adsorbed, AFM images do show adsorbed polymer. From the AFM images, it is difficult to conclude whether poly-**R/S** or poly-**S** adsorbed more, which concurs with the results from XPS and contact angle measurements. When compared to adsorptions of poly-**R/S** and poly-**S** onto native silicon oxide, far less polymer appears to have adsorbed. This suggests that independent of chain architecture, poly(*N*-methyl-*N'*-(α–phenylethyl)carbodiimide) has a low adsorption affinity for tris(TMS)–modified silica.

The 1 μm^2 images shown in Figure 2.5 were acquired within the long ribbons shown in the 25 μm^2 images. For the 312:1 poly-**R/S,** the 1 μm^2 images indicate late stages of dewetting where ribbons have almost completely spread into droplets. However, over the larger area, the dewetting does not appear to have classical shapes, i.e. holes, ribbons, and droplets forming Voronoi structures. Similar results are shown for 312:1 poly-**S** (see Figure 2.6),with the exception of very few droplets being evident in the 1 μm^2 images and much finer as well as more numerous ribbons are indicated.

It is difficult to generate conclusions about the differences in the adsorption behavior of 312:1 poly-**R/S** and poly-**S** based on the AFM results. Since the objective is to study the differences in the adsorption behavior of polycarbodiimides on surfaces that vary in surface energy, the data suggests that dewetting kinetics may be much faster on tris(TMS)–modified silica than on native silicon oxide. Intuitively, this is expected

because of the lyophobic nature of the tris(TMS) surface, and we originally anticipated that these polymers would not adsorb to a lyophobic surface.

As previously described, the disparity in the XPS and contact angle data between 3121:1 poly-**R/S** and 3121:1 poly-**S** is also indicated by the differences in their AFM images. The larger contact angle hysteresis for poly-**R/S** compared to poly-**S** indicated differences in the surface structure. The 14° difference between advancing and receding contact angles for poly-**S,** suggests the surface has less heterogeneity than the surface for poly-**R/S** which had a 21° difference between θ_A/θ_R contact angles. This was confirmed by AFM analysis.

More classical type dewetting was indicated (Figure 2.7) by AFM for the 3121:1 poly-**R/S** adsorbed to tris(TMS). The image shows late stages of dewetting as evidenced by the deterioration of holes into ribbons and droplets. Shown in Figure 2.8 are the AFM images for an adsorbed film of 3121:1 poly-**S** onto tris(TMS)–modified silica. This result shows a very different surface architecture than measured for poly-**R/S** where a combination of large and small ribbons formed. Though difficult to differentiate between adsorbed films of 312:1 poly-**R/S** and poly-**S**, both polymers generated similar adsorbed films because the extent of chain rigidity is relatively equivalent due to the low molecular weight. For the 3121:1 poly-**R/S,** the higher molecular weight would have more defects along the polymer chain thereby resulting in a more flexible conformation. Goodwin et al. confirmed this by light scattering. As previously described for the 3121:1 polymers, the flexibility of the poly-**R/S** would allow chain segments to "fit" into defects within the tris(TMS) layer, thereby allowing the polymer segments to interact with the substrate resulting in adsorption. For the poly-**S**, chain rigidity restricts chain segments from "fitting" into defects, thereby limiting adsorption.

Differences between the surface architecture of adsorbed films of poly-**R/S** and poly-**S** may be the result of chain rigidity. However, the differences could also be a result of the effects of liquid crystallinity. Goodwin et al.[28] performed intrinsic viscosity

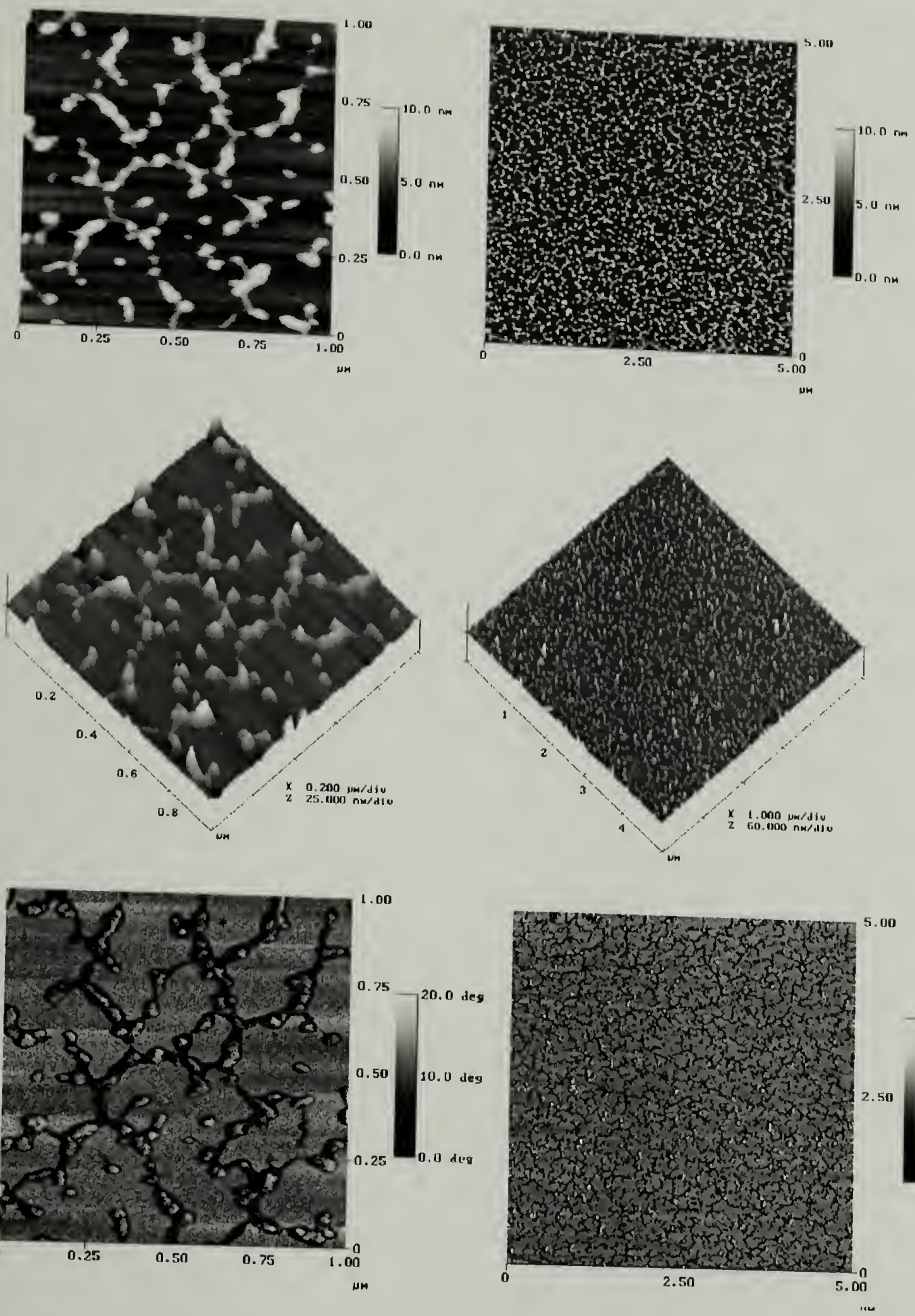

Figure 2.7. AFM tapping mode analysis of adsorbed 3121:1 poly-**R/S** adsorbed from THF to dense tris(TMS)–modified native silicon oxide for 72 hours at 25 °C. The pictures are height (top), surface (middle), and phase (bottom) images of a 1 μm^2 sampling area (left column) and a 25 μm^2 sampling area (right column).

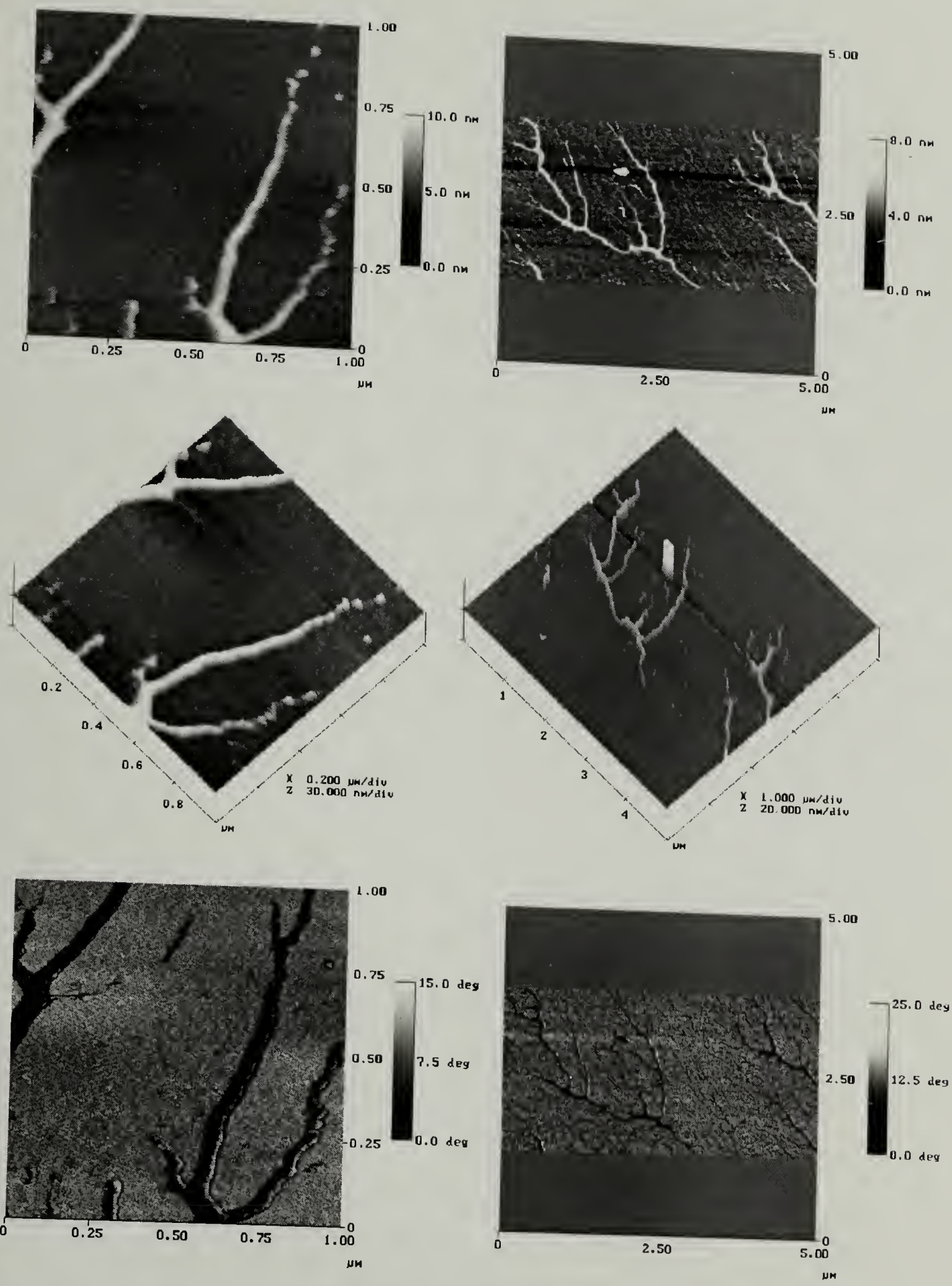

Figure 2.8. AFM tapping mode analysis of adsorbed 3121:1 poly-S from THF to dense tris(TMS)–modified native silicon oxide for 72 hours at 25 °C. The pictures are height (top), surface (middle), and phase (bottom) images of a 1 μm^2 sampling area (left column) and a 25 μm^2 sampling area (right column).

measurements and reported on the LCP nature of poly-**R/S** and poly-**S**. Qualitatively, toluene solutions containing a few percent of polycarbodiimide formed viscous solutions, while solutions approaching 10 weight percent behaved like a gel. Reduced viscosity measurements showed decreasing shear rate dependence with successive runs of a particular solution, and would asymptotically approach a reproducible value. Furthermore, after 0.5 hour during which time the polymer solution remained undisturbed, the value that was first measured would be measured again, and upon reanalysis, the gradual decrease to a reproducible value would be measured. Goodwin explained that these results were consistent with the behavior of liquid crystalline, rigid rod polymer undergoing chain alignment by the shearing forces, a result of the solution flowing through the capillary. Additional research in the Novak group has shown that polycarbodiimides are lytropic liquid crystalline polymers.

Rod-shaped polymer chains are used to make strong fibers because of the ease to orient the chains in the fiber direction without folding.[29] This ability to order the chains is demonstrated during the intrinsic viscosity measurements, where viscosity increases with solution concentration, and then shows an abrupt decrease. The increase in viscosity with concentration occurs while the liquid crystalline polymers are isotropic, and the sudden decrease is a result of increasing anisotropy. These concepts can be applied to the observation of ribbon formation on the tris(TMS)–modified substrate. When the solvent evaporates from the adsorbed film, the polymer solution concentration increases. Concurrently, there is the transition from an isotropic to an anisotropic condition. This lytropic liquid crystalline effect may result in the formation of ribbon like structures, as long as the segmental attachment energy can be overcome by the energies associated with ordering. Since the affinities for poly-**R/S** and poly-**S** on tris(TMS) have been shown to be low, and the more rigid polymers have shown adsorbed film architectures composed mostly of long ribbons, it should be noted these observations support that liquid crystallinity effects may contribute to the final surface structure.

Solvent quality has been shown to have an affect on the adsorption of poly-**R/S** onto native silicon oxide. Observed was dewetting of an adsorbed film of poly–**R/S** prepared from adsorptions performed from the better solvent THF, and more uniform films were observed for adsorptions performed from the poorer solvent toluene. In addition, similar results were observed for adsorbed films of poly-**S** adsorbed from THF followed by toluene rinse. Images from tapping mode AFM for the adsorption of 3121:1 poly–**R/S** from toluene onto tris(TMS)–modified silica are shown in Figure 2.9. The images appear to show a continuous film composed of tiny holes on the order of 10 – 30 nm in diameter. These holes may be the initiation of dewetting, but due to the fast evaporation of solvent, the dewetting process was frustrated, a result of increasing viscosity resulting in limited polymer drainage. Atomic concentration data from XPS analysis (see Table 2.2) indicated more poly-**R/S** adsorbed from toluene than THF. However, compared to adsorptions performed onto native silicon oxide, the XPS results suggest a thinner adsorbed film formed on tris(TMS). The AFM images indicate that the total surface area coverage by poly-**R/S** is less than observed for adsorptions on native silica. The data further support the necessity to combine surface analysis techniques such as contact angle, XPS, and AFM.

The adsorption experiments on tris(TMS) studied the adsorption behavior of polycarbodiimides onto a dense methyl surface. Further study on the affect of surface energy on the adsorption behavior of poly–**R/S** and poly-**S** was performed on silica substrates modified with CMDCS. These surfaces would be dense in methylene groups. Atomic concentration data for adsorbed films of polycarbodiimide onto CMDCS–modified silica are listed in Table 2.4. The data indicate that relative to previously tested substrates, very little poly-**R/S** adsorbs from THF or toluene to CMDCS-modified substrates. For poly-**S**, the XPS results indicate no adsorption occurred because nitrogen was not detected. However, the contact angle data in Table 2.5 suggests that polymer did adsorb to the CMDCS-modified surfaces due to the

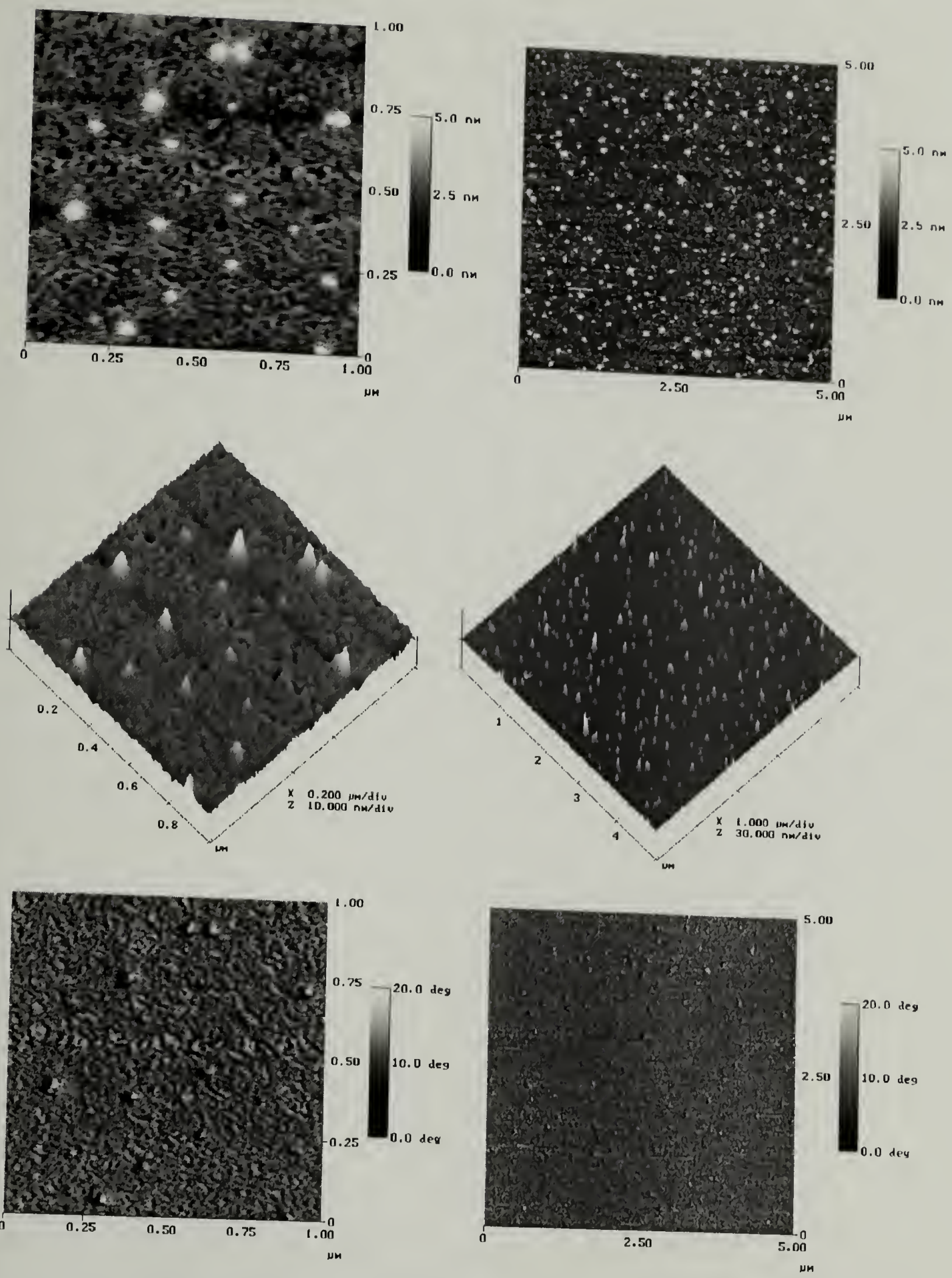

Figure 2.9. AFM tapping mode analysis of an adsorbed thin film of 3121:1 poly-**R/S** adsorbed from toluene to dense tris(TMS)–modified native silicon oxide for 72 hours at 25 °C. The pictures are height (top), surface (middle), and phase (bottom) images of a 1 μm^2 sampling area (left column) and a 25 μm^2 sampling area (right column).

increase in advancing and receding contact angles, in addition to the increase in hysteresis. The contact angle data for the adsorption of poly-**R/S** from toluene suggests that some amount of polymer adsorbed. Furthermore, the advancing angle was 5° less than observed for similar adsorptions on native silica, thereby indicating a difference in the surface structure of the adsorbed film on CMDCS-modified substrate.

The topography of adsorbed films of poly-**R/S** and poly-**S** on CMDCS-modified silica was studied by tapping mode AFM. The adsorbed films of 312:1 poly-**R/S** and 312:1 poly-**S** from THF (Figures 2.10 and 2.11) show little difference in surface structure between the two polymers. In addition, the AFM results indicate that a very small

Table 2.4. XPS atomic concentration results of adsorbed thin films of poly-**R/S** and poly–**S** on CMDCS-modified (dense monolayer) native silicon oxide at 25 °C for 72 hours. Solvent refers to the solution solvent the polymer was adsorbed from.

Polymer/Solvent	$C_{15°}$	$N_{15°}$	$O_{15°}$	$Si_{15°}$	$C_{15°} : N_{15°}$	$Si_{15°} : N_{15°}$
Control	50.13	-	32.13	17.73	-	-
312:1						
RS/THF	37.78	0.25	45.08	16.89	151 : 1	68 : 1
S/THF	35.62	-	46.46	17.93	-	-
3121:1						
RS/THF	38.42	0.73	44.11	16.74	53 : 1	23 : 1
S/THF	43.36	-	40.76	15.89	-	-
RS/toluene	53.63	3.51	30.66	12.20	15 : 1	3.5 : 1

Polymer/Solvent	$C_{75°}$	$N_{75°}$	$O_{75°}$	$Si_{75°}$	$C_{75°} : N_{75°}$	$Si_{75°} : N_{75°}$
Control	23.29	-	31.08	45.63	-	-
312:1						
RS/THF	13.07	0.24	33.58	53.11	54 : 1	221 : 1
S/THF	12.59	-	27.93	59.48	-	-
3121:1						
RS/THF	14.19	0.45	25.47	59.90	32 : 1	133 : 1
S/THF	14.13	-	30.33	55.53	-	-
RS/toluene	25.58	2.20	25.34	46.87	12 : 1	21 : 1

amount of polymer adsorbed as evidenced by the few droplets on the surface. For each adsorbed polymer, the volume for a few of the droplets was calculated using the

Nanoscope software's Bearing algorithm. The calculated volumes ranged between 1093 nm^3 to 2246 nm^3 for the 312:1 poly–**R/S** (see Fig. 2.10) and for 312:1 poly–**S** (see Fig. 2.11), the volumes ranged between 428 nm^3 to 1136 nm^3. These volumes were used to calculate the number of molecules in each droplet. For 312:1 poly-**R/S** (Fig. 2.10) and 312:1 poly-**S** (Fig. 2.11), the number of molecules ranged 13.2 to 27.1 molecules and from 5.2 to 13.7 molecules respectively. These droplets may or may not be indicative of a dewetting process. For example, in solution, the adsorbed chain may have few localized segment-surface attachment points (i.e. brush-like structure) where upon rinsing and drying the solvent evaporation resulted in a collapse of the chain onto the substrate, thereby forming a droplet-like structure.

Table 2.5. Water contact angle results of adsorbed thin films of poly-**R/S** and poly-**S** on CMDCS-modified (dense monolayer) native silicon oxide at 25 °C for 72 hours. . Solvent refers to the solution solvent the polymer was adsorbed from.

Polymer/Solvent	θ_A H_2O	θ_R H_2O
Control	82° ± 2°	77° ± 2°
312:1		
RS/THF	86° ± 1°	80° ± 2°
S/THF	86° ± 2°	79° ± 1°
3121:1		
RS/THF	85° ± 1°	78° ± 1°
S/THF	84° ± 2°	77° ± 1°
RS/toluene	92° ± 1°	76° ± 1°

Adsorbed films of 3121:1 poly-**R/S** and poly-**S** from THF were analyzed by AFM and the results are shown in Figures 2.12 and 2.13, respectively. When comparing all the samples adsorbed to CMDCS-modified silica from THF, a relatively more complex surface structure was observed for the higher molecular weight poly-**R/S** than the other polymers. The images in Figure 2.12 suggest that dewetting occurred because of the presence of ribbons and droplets. A few of the droplets ranged in volume from 575 nm^3

to 8209 nm^3 which calculates to 0.7 to 9.9 molecules per droplet respectively. For 3121:1 poly-**S**, AFM results for a 1 μm^2 area indicated little if any polymer adsorbed. However, AFM analysis of a 100 μm^2 area (Figure 2.13) confirmed polymer adsorption resulting in droplet formation of >10 nm in height on the surface. A few of these droplets for the 3121:1 poly-**R/S** ranged in volume from 1542 nm^3 to 116817 nm^3 which calculates to 1.9 to 141 molecules per volume respectively. Similar area measurements by AFM for 312:1 polymers showed the same droplet formation, but the droplets were fewer and smaller in height.

The surface topography for an adsorbed film of 3121:1 poly-**R/S** from toluene onto CMDCS-modified silica was measured by tapping mode AFM and is shown in Figure 2.14. The images show dewetting, indicated by the polygonal formation of holes, ribbons, and the early development of droplets.

The strong effect of solvent on the surface structure of the adsorbed film becomes very evident when comparing the AFM results between THF and toluene. The data support that when compared to native silicon oxide, poly-S and poly-**R/S** have a low affinity for the CMDCS surface. In good solvent, very little polymer adsorbed, yet there was an increase in the adsorbed amount with increasing molecular weight. The adsorption performed from toluene (a poorer solvent) indicates that solvent quality does affect the adsorbed amount, and in addition, gives qualitative information on χ parameters. In toluene, a more favorable segment-surface interaction overcomes the solvent-surface and solvent-segment interactions, thereby resulting in adsorption. A smaller amount of polymer adsorbs from THF because the solvent-surface interaction is less favorable than solvent-segment interactions. The segment-surface interaction also has limited affect because it is the same for both polymers. However, this assumes the CMDCS layer has an equivalent solution architecture in the presence of THF or toluene. In toluene, the CMDCS layer may strongly interact with solvent molecules in the adsorbed layer thereby extending away from the silica surface. This brush-like extension

away from the interface may allow more polymer segments to interact with the silica substrate.

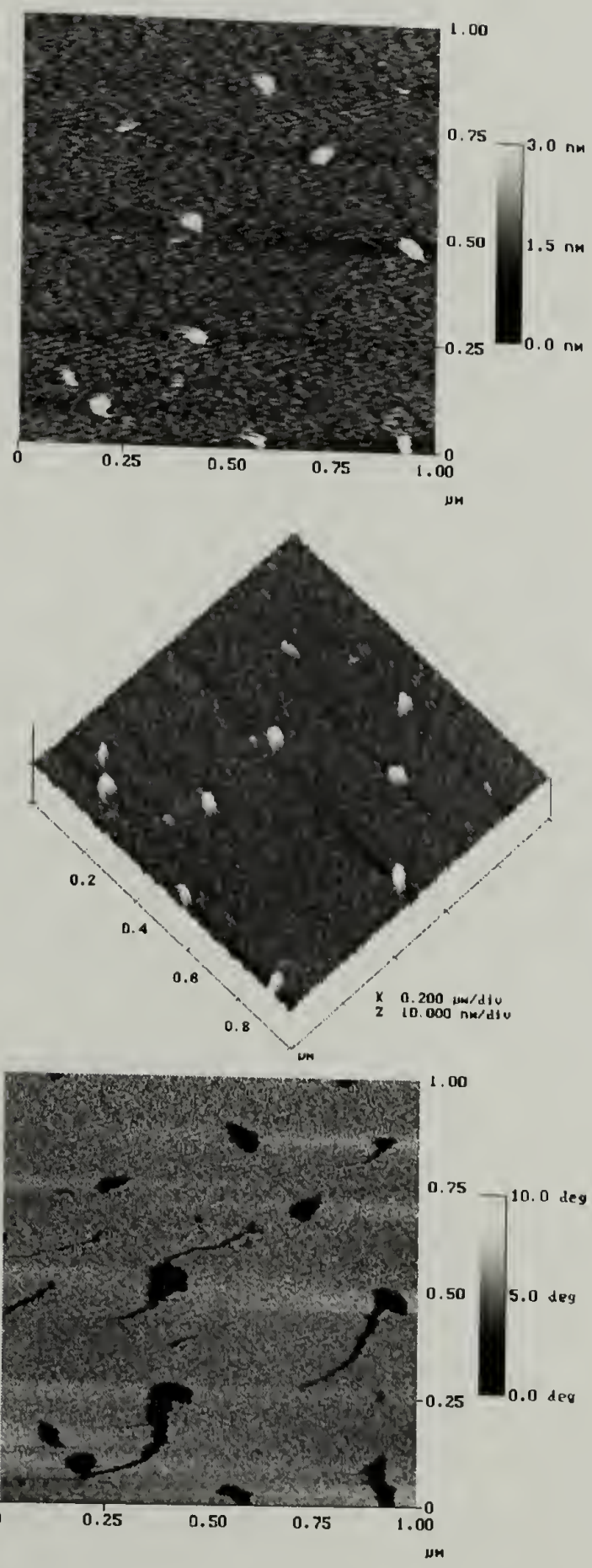

Figure 2.10. AFM tapping mode analysis of adsorbed 312:1 poly-**R/S** from THF to dense CMDCS-modified native silicon oxide for 72 hours at 25 °C. The pictures are height (top), surface (middle), and phase (bottom) images of a 1 μm^2 sampling area.

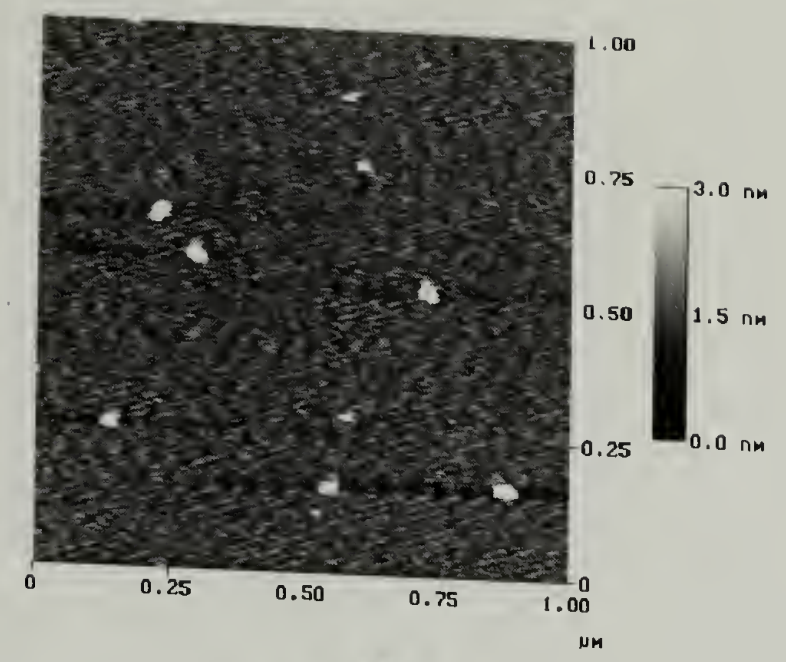

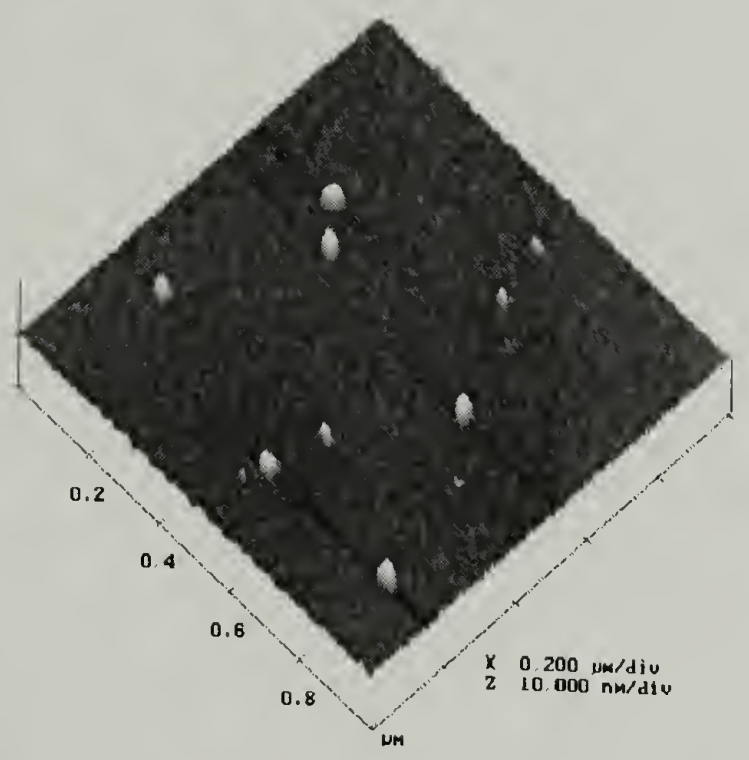

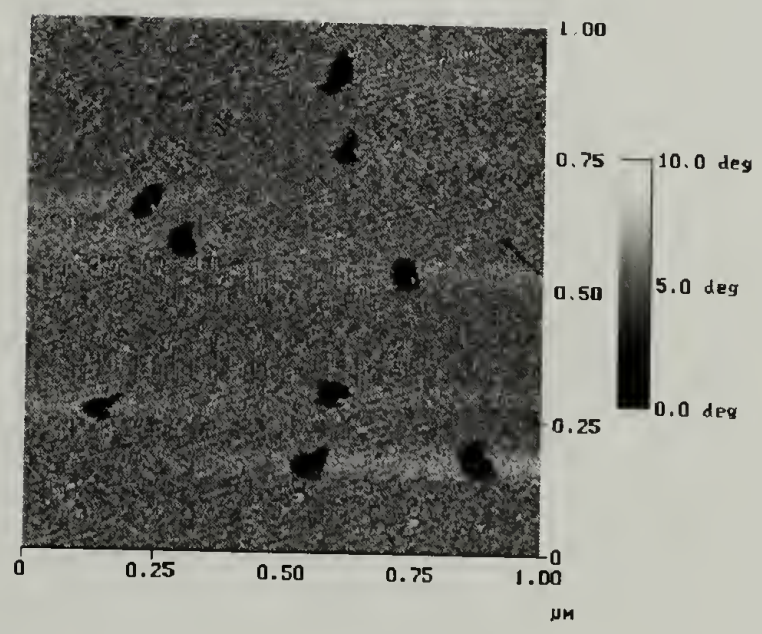

Figure 2.11. AFM tapping mode analysis of adsorbed 312:1 poly-**S** from THF to dense CMDCS-modified native silicon oxide for 72 hours at 25 °C. The pictures are height (top), surface (middle), and phase (bottom) images of a 1 μm^2 sampling area

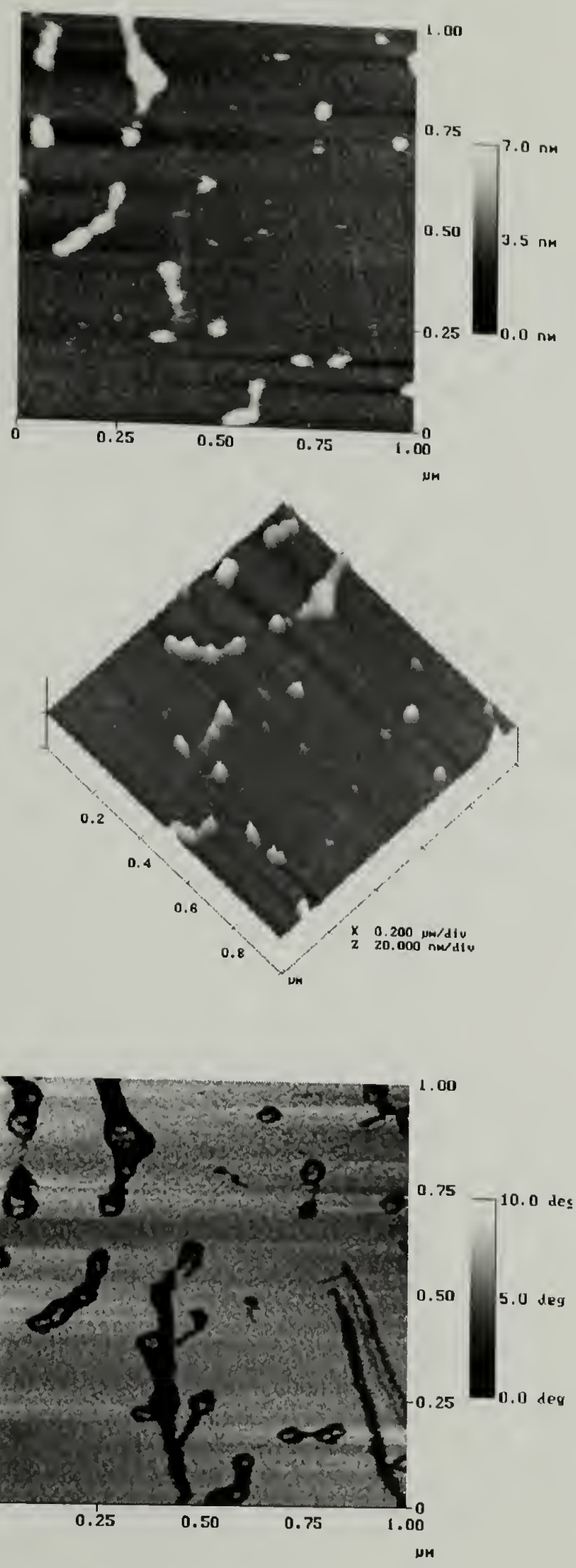

Figure 2.12. AFM tapping mode analysis of adsorbed 3121:1 poly-**R/S** from THF to dense CMDCS-modified native silicon oxide for 72 hours at 25 °C. The pictures are height (top), surface (middle), and phase (bottom) images of a 1 μm^2 sampling area.

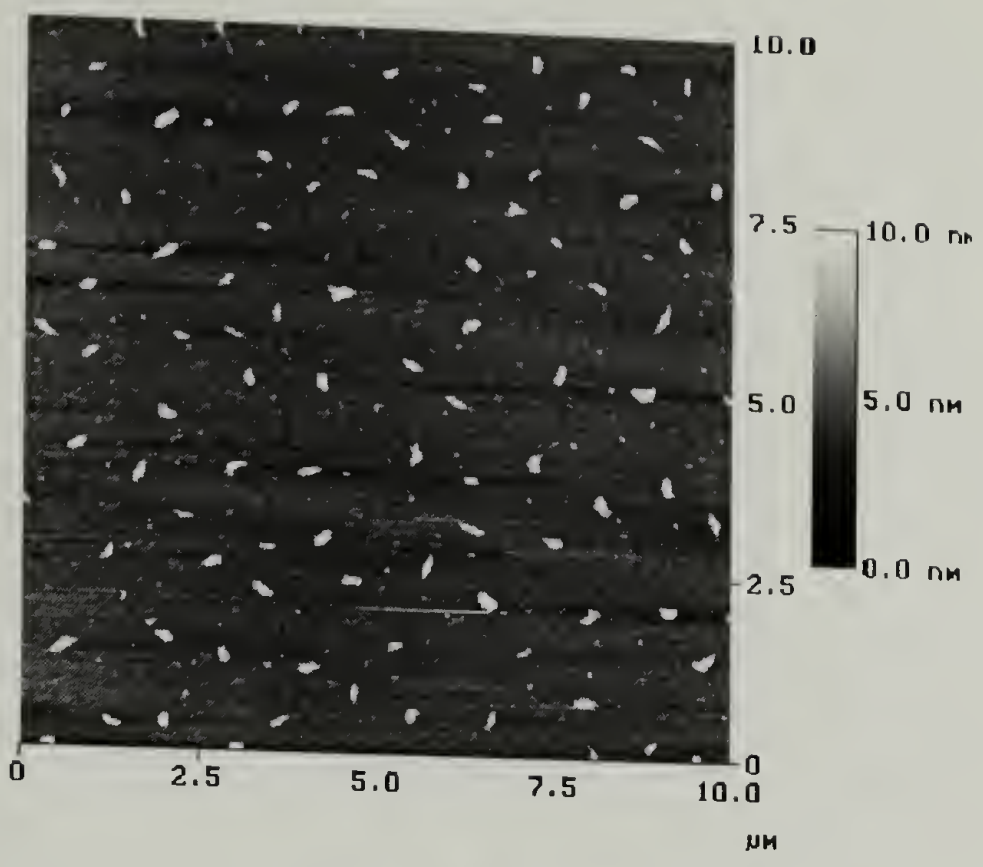

Figure 2.13. AFM tapping mode analysis of adsorbed 3121:1 poly-**S** from THF to dense CMDCS-modified native silicon oxide, from THF for 72 hours at 25 °C. The pictures are height (top) and surface (middle) images of a 100 μm^2 sampling area.

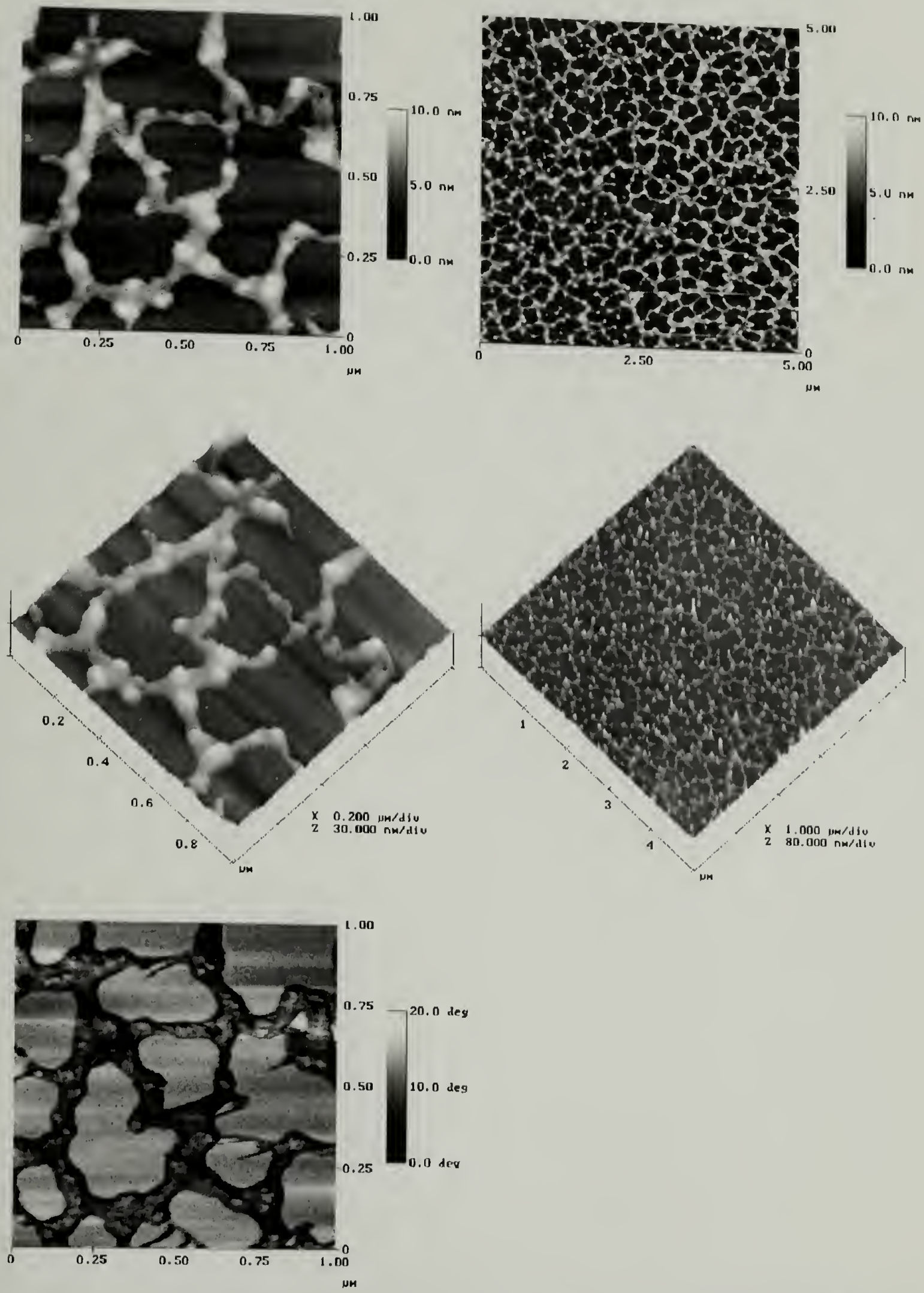

Figure 2.14. AFM tapping mode analysis of adsorbed 3121:1 poly-**R/S** adsorbed from toluene to dense CMDCS-modified native silicon oxide for 72 hours at 25 °C. The pictures are height (top), surface (middle), and phase (bottom) images of a 1 μm^2 sampling area (left column) and a 25 μm^2 sampling area (right column).

The chain architecture can affect the amount of polymer at the interface. In good solvents, the polymer is expanded and occupies more volume, whereas in poorer solvents, the chain is more collapsed, thus allowing a larger amount of polymer to occupy a similar volume. For adsorption to occur there must be defects in the CMDCS surface allowing the polymer segments to interact with the silica substrate. Therefore, under toluene conditions, a higher concentration of polymer can occupy the interface, as well as the more compact nature of chain in solution may allow more segments to interact with the silica surface via defects. In addition, as discussed on the previous page, the CMDCS monolayer in the presence of toluene may extend into the adsorbed layer allowing more polymer segments to interact with the substrate. Therefore, in the presence of THF the CMDCS monolayer may lay flat effectively shielding the substrate and limiting segment–surface interactions.

Surfaces composed of mostly methyl or methylene function have shown very little affinity for poly-**R/S** and poly-**S** to adsorb from THF, while a larger amount adsorbed for poly–**R/S** from toluene. By modifying a silica surface with phenyl groups, the adsorption behavior of poly-**R/S** and poly-**S** to aromatic groups could be studied. This was accomplished by preparing aromatic rich surfaces by chemisorption of diphenyldichlorosilane (DPDCS) onto native silicon oxide, followed by polymer adsorption using the same conditions described for tris(TMS) and CMDCS experiments.

Atomic concentration data for the samples prepared from the adsorption of polycarbodiimide from THF onto DPDCS–modified silica is shown in Table 2.6. The modification of silica with phenyl groups was indicated in the XPS multiplex spectrum for [C_{1s}], which showed the shake up peak associated with the π–π^* interaction of the phenyl groups. The XPS results for poly-**R/S** and poly-**S** suggest that very little polymer adsorbed. However, the contact angle results, shown in Table 2.7, indicate the polymer did adsorb because the advancing angle increased between 6° to 9°. Small changes in the

receding angle were measured but are not indications of polymer adsorption because films of polycarbodiimide have receding angles similar to the control.

Table 2.6. XPS atomic concentration results of adsorbed thin films of poly-**R/S** and poly–**S** on DPDCS–modified (dense monolayer) native silicon oxide at 25 °C for 72 hours. . Solvent refers to the solution solvent the polymer was adsorbed from.

Polymer/Solvent	$C_{15°}$	$N_{15°}$	$O_{15°}$	$Si_{15°}$	$C_{15°} : N_{15°}$	$Si_{15°} : N_{15°}$
Control 312:1	62.45	-	24.18	13.37	-	-
RS/THF	60.33	0.71	25.01	13.95	85 : 1	20 : 1
S/THF	56.18	0.17	27.91	15.74	330 : 1	93 : 1
3121:1						
RS/THF	56.50	0.80	27.54	15.16	71 : 1	19 : 1
S/THF	59.37	0.58	24.91	15.41	102 : 1	27 : 1

Polymer/Solvent	$C_{75°}$	$N_{75°}$	$O_{75°}$	$Si_{75°}$	$C_{75°} : N_{75°}$	$Si_{75°} : N_{75°}$
Control 312:1	25.77	-	25.91	48.32	-	-
RS/THF	27.36	0.27	33.50	38.87	101 : 1	144 : 1
S/THF	23.89	0.02	35.10	40.99	1195 : 1	2050 : 1
3121:1						
RS/THF	24.92	0.36	34.47	40.25	69 : 1	112 : 1
S/THF	27.47	-	32.18	40.35	-	-

Table 2.7. Water contact angle results of adsorbed thin films of poly-**R/S** and poly–**S** on DPDCS–modified (dense monolayer) native silicon oxide at 25 °C for 72 hours. . Solvent refers to the solution solvent the polymer was adsorbed from.

Polymer/Solvent	θ_A H_2O	θ_R H_2O
Control 312:1	84° ± 2°	74° ± 2°
RS/THF	93° ± 2°	71° ± 1°
S/THF	92° ± 2°	77° ± 2°
3121:1		
RS/THF	90°	79° ± 2°
S/THF	91° ± 1°	75° ± 2°

Topography analysis of the control surface and adsorbed layers was performed using tapping mode AFM. The control surface is shown in Figure 2.15 with the images

indicating a surface composed of islands. By Section analysis (Nanoscope software algorithm), the height of the islands was calculated to be on the order of 0.785 – 0.981 nm, and where the height of the large rim was measured to range between 1.569 – 1.867 nm.

Consider the surface modification of silica with a 0.001 M solution of octadecyltrichlorosilane (ODTS) in anhydrous toluene. The reaction occurs in a two-step process, where the first reactions maximize the covalent bonding to the surface at isolated sites followed by water-catalyzed polymerization to fill in between.[8,30] Rye et al.[30] showed that ODTS reacted with silica having a thin surface water layer and concluded that a major consideration in the reaction of silane coupling agents with silicon is the competition between reaction with surface hydroxyl groups and surface water. Though the reaction between DPDCS and silica was performed in the vapor phase, the patchy surface could be a result of similar events described for ODTS modification of silica. As DPDCS chemisorbs to surface hydroxyl groups, the adsorbed water layer begins to recede as the surface becomes more hydrophobic. Eventually, the water is displaced into ponds on the surface where dimerization and polymerization are catalyzed. In these regions, one or both of the chlorines of the silane can either chemisorb to the silica or polymerize with silane neighbors, thereby forming islands of polydiphenylsiloxane. Scheme 2.2 illustrates the paths of a molecule of DPDCS reacting with silica having a thin water layer. With multifunctional organosilanes, there is the potential for reactions other than those with surface silanol groups. For example, reaction A describes how the silane coupling agent can be hydrolyzed by water without reaction to surface silanols. This results in a molecule that can either hydrogen bond with the surface or form dimers with another chlorofunctional DPDCS followed by physisorption to the surface or condensation in the reaction vessel. Another possible reaction path is that the hydrolyzed DPDCS reacts with another chlorofunctional DPDCS followed by chemisorption to a

surface silanol group, thereby bonding dimer to the surface which can undergo further reactions producing polysiloxane.

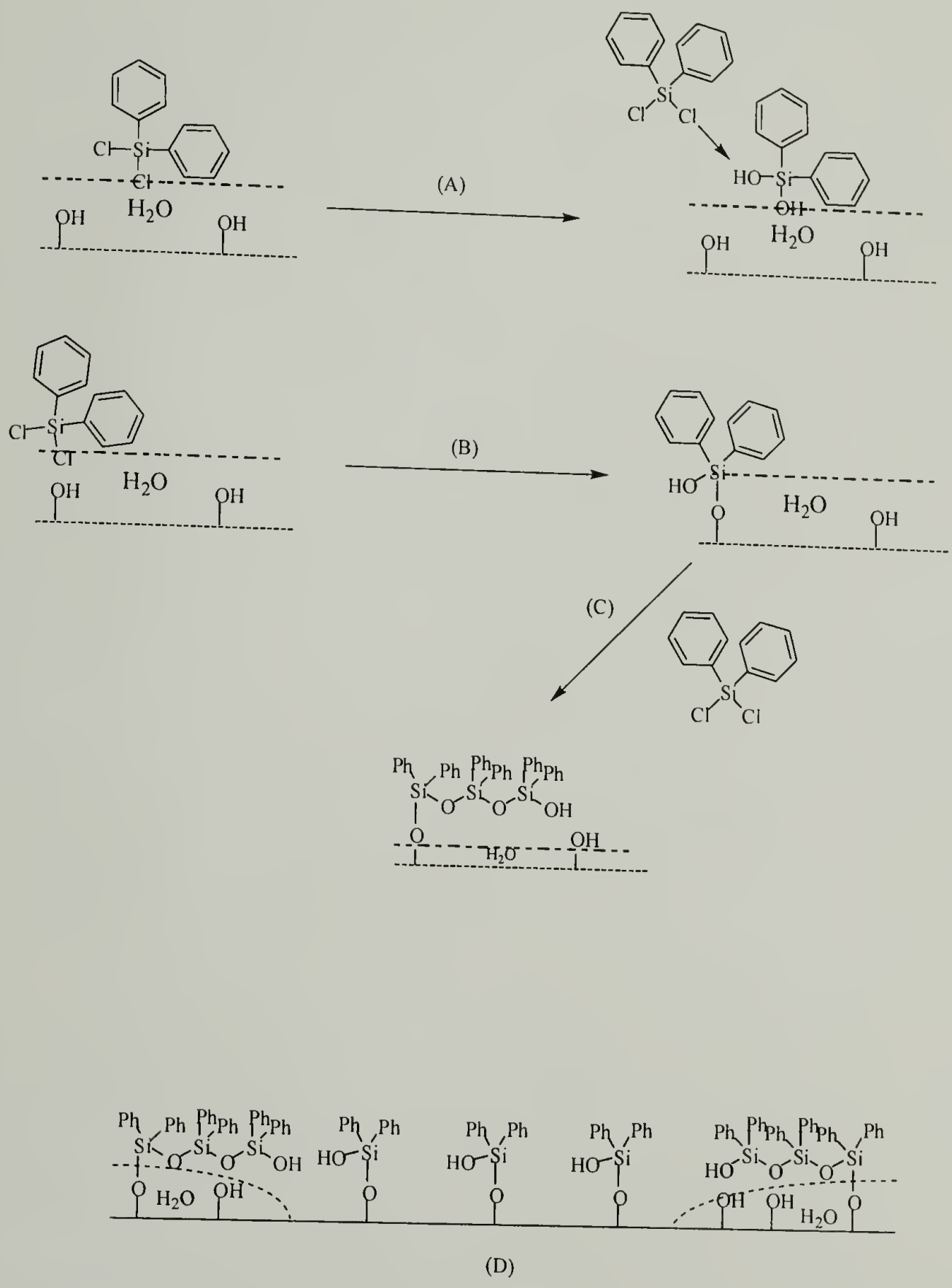

Scheme 2.2. Reaction paths for DPDCS modification of native silicon oxide.

The ideal condition step B, is where the DPDCS approaches the surface and reacts with a surface silanol followed by hydrolysis of the residual chlorine. As additional molecules of DPDCS come in the proximity of the covalently bound hydrolyzed DPDCS two reactions can occur. First, the DPDCS can react with another surface silanol or secondly, it can react with the hydroxyl group of the bound DPDCS resulting in dimerization. The island formation shown in Figure 2.15 suggest that as reaction B occurs the surface becomes more hydrophobic causing the thin water layer to dewet. These pools of water catalyze polymerization of the DPDCS generating islands of polysiloxane. This produces the surface shown as D in Scheme 2.2.

The effect of a patchy surface of DPDCS on polycarbodiimide adsorption and dewetting was studied by tapping mode AFM. Based on surface tensions, the amount of dewetting would be dependent on the surface region of the DPDCS–modified silica. Polysiloxanes have low surface tensions. For example, poly(oxymethylphenylsilylene) has a surface tension of 26.1 dyn/cm at 20° C.[31] Assuming the model for the patchy surface is correct, the area between the island is composed mostly of phenyl units. A dense layer of DPDCS results in a phenyl surface having a surface tension on the order of 45 dyn/cm.[31] Because of surface tensions, the phenyl surface would be more favorable to wetting relative to the islands of polysiloxane. For the 3121:1 poly-**R/S** and poly-**S**, the general trends shown by AFM suggest that rate of dewetting is faster on the island surface structures.

Tapping mode AFM images of adsorbed films of 312:1 poly-**R/S** and poly-**S** onto DPDCS–modified silica are shown in Figures 2.16 and 2.17. For both polymers the images suggest that very little polymer adsorbed on the islands. Adsorption of polymer is evident between the islands and qualitatively, it appears a higher amount of poly-**R/S** adsorbed compared to poly-**S**. Both polymers dewet the surface, and images indicate late stages of dewetting where ribbons are receding to droplets. Atomic concentration data

from XPS (Table 2.6) support this observation, however, due to roughness effects, caution should be exercised while interpreting the XPS results.

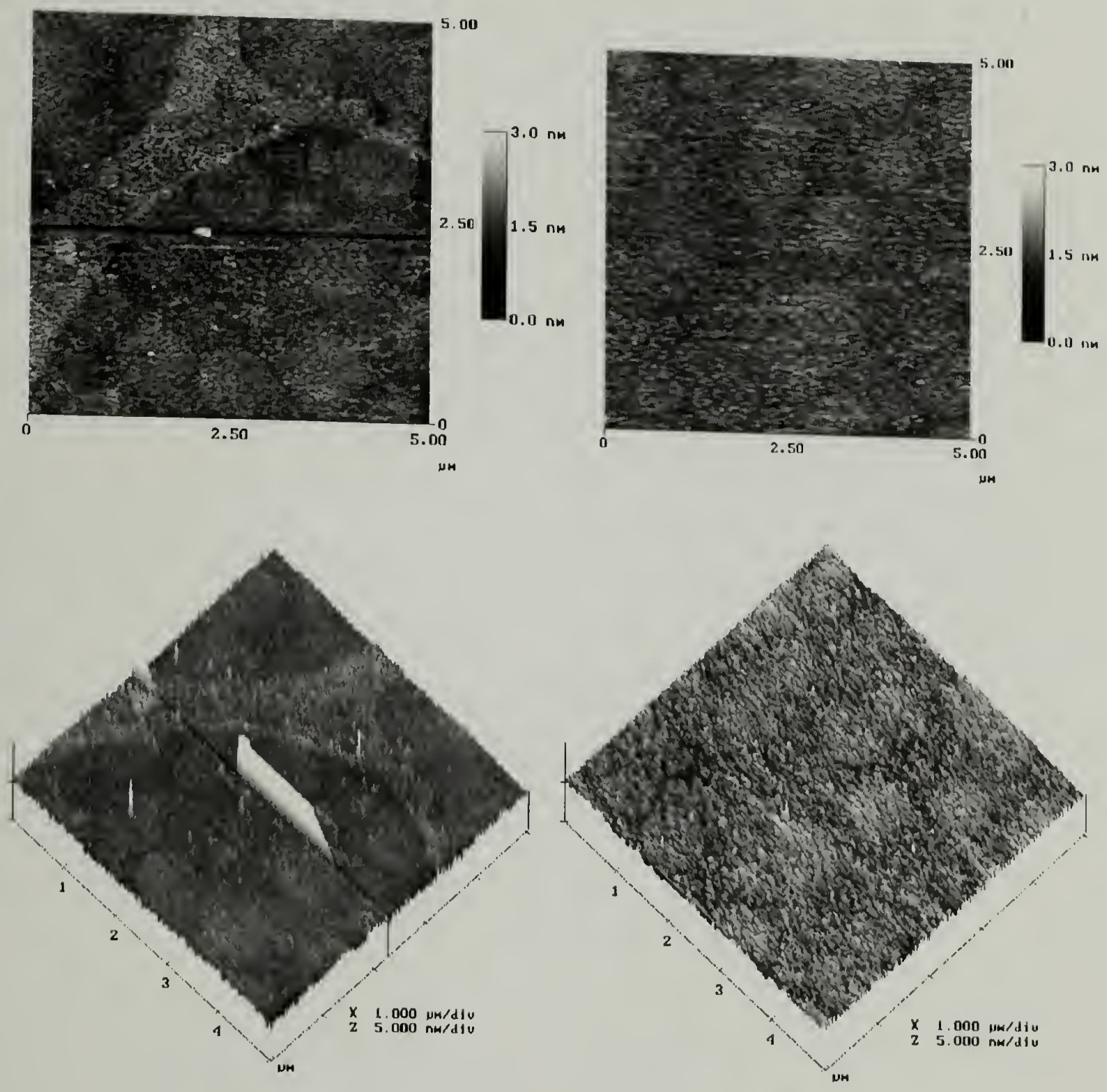

Figure 2.15. AFM tapping mode; height (top) and surface (bottom) images of a dense DPDCS monolayer chemisorbed (vapor phase, 5 days at 67 ± 3 °C) on native silicon oxide. The images on the left represent one area on the sample while the images on the right are of a second location on the same sample.

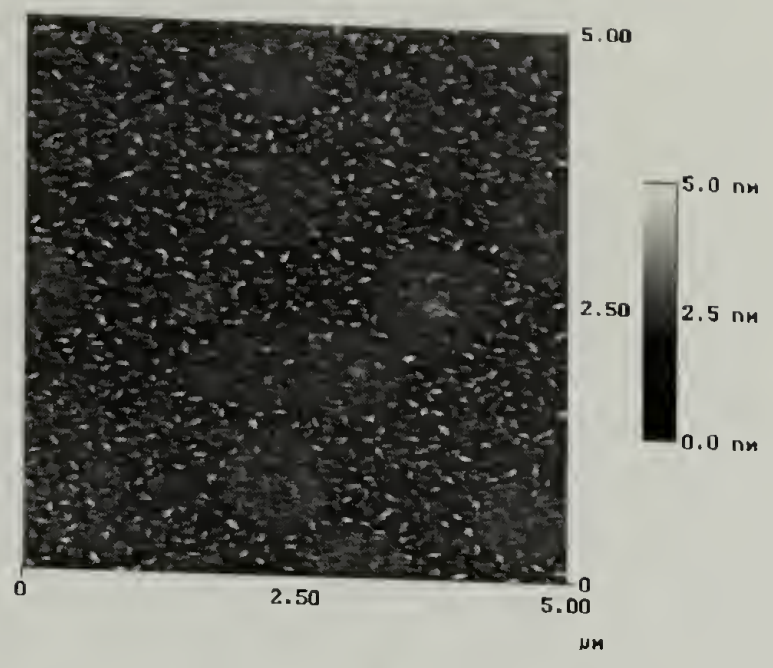

Figure 2.16. AFM tapping mode analysis of adsorbed 312:1 poly-**R/S** from THF to dense DPDCS–modified native silicon oxide for 72 hours at 25 °C. The pictures are height (top), surface (middle), and phase (bottom) images of a 25 μm^2 sampling area.

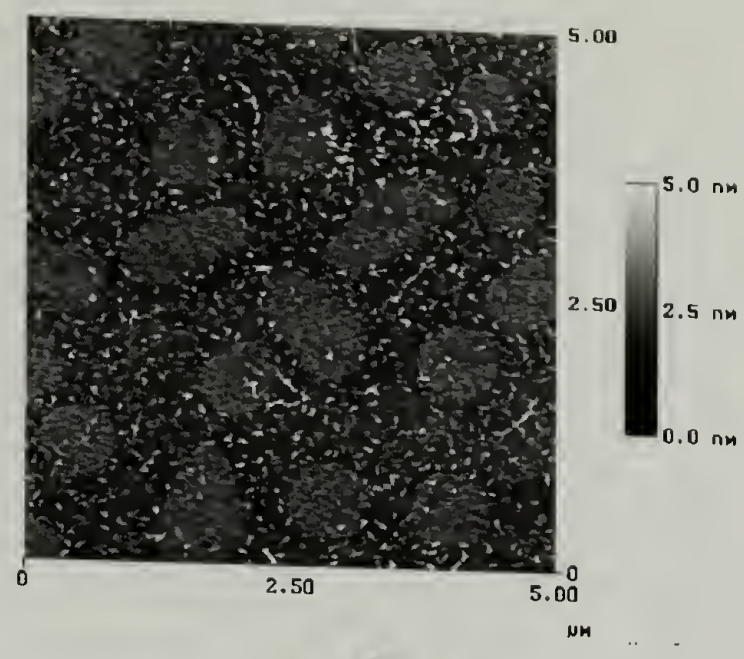

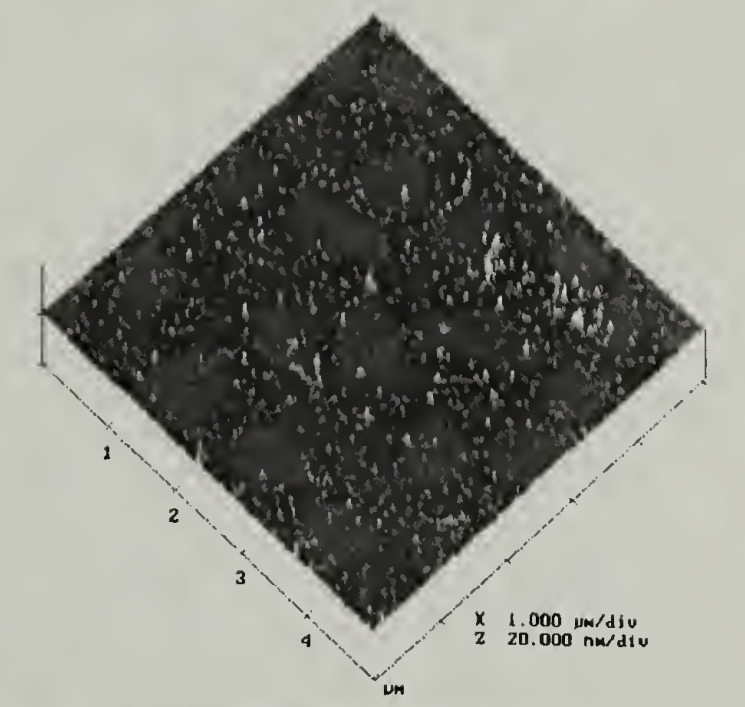

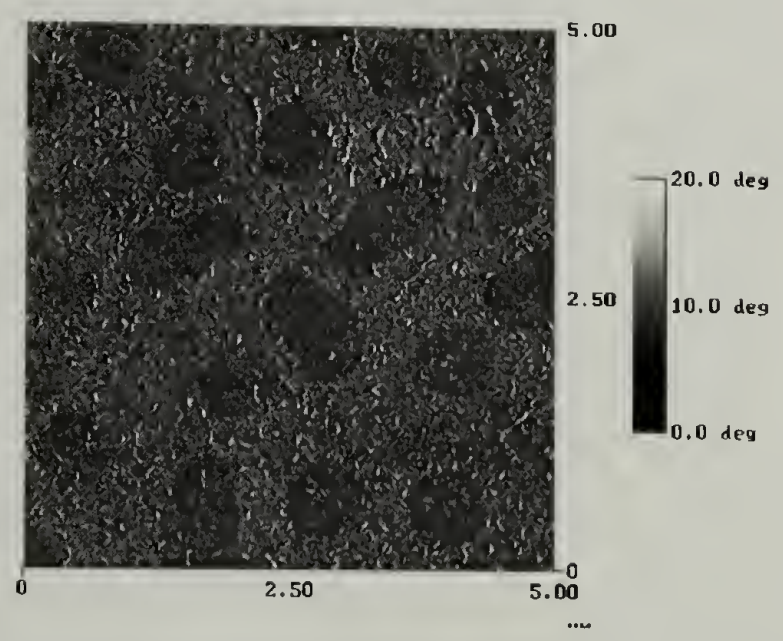

Figure 2.17. AFM tapping mode analysis of adsorbed 312:1 poly-**S** from THF to dense DPDCS–modified native silicon oxide for 72 hours at 25 °C. The pictures are height (top), surface (middle), and phase (bottom) images of a 25 μm^2 sampling area

For the higher molecular weight samples of poly-**R/S** and poly-**S,** the AFM images indicate that polymer adsorbed onto the islands. However, the degree of dewetting on the islands is different than observed between the islands. The image shown in Figure 2.18 is the resulting surface structure of a dewetted adsorbed film of 3121:1 poly-**R/S** where droplet formations on the islands indicate later stages of dewetting. Between the islands, the image shows earlier stages of dewetting as evident from the remnants of holes that have decomposed to ribbons and droplets. In comparison, the 3121:1 poly-**S** adsorbed film on DPDCS–modified silica is shown in Figure 2.19. The image indicates late stages of dewetting because the surface is composed of large droplets. Further, the islands appear much larger than those of the other samples. This may have an effect on the degree of dewetting because a larger surface area of polysiloxane exists. Generally, fewer polymer molecules appear to have adsorbed on the islands relative to the amount of polymer adsorbed between the islands.

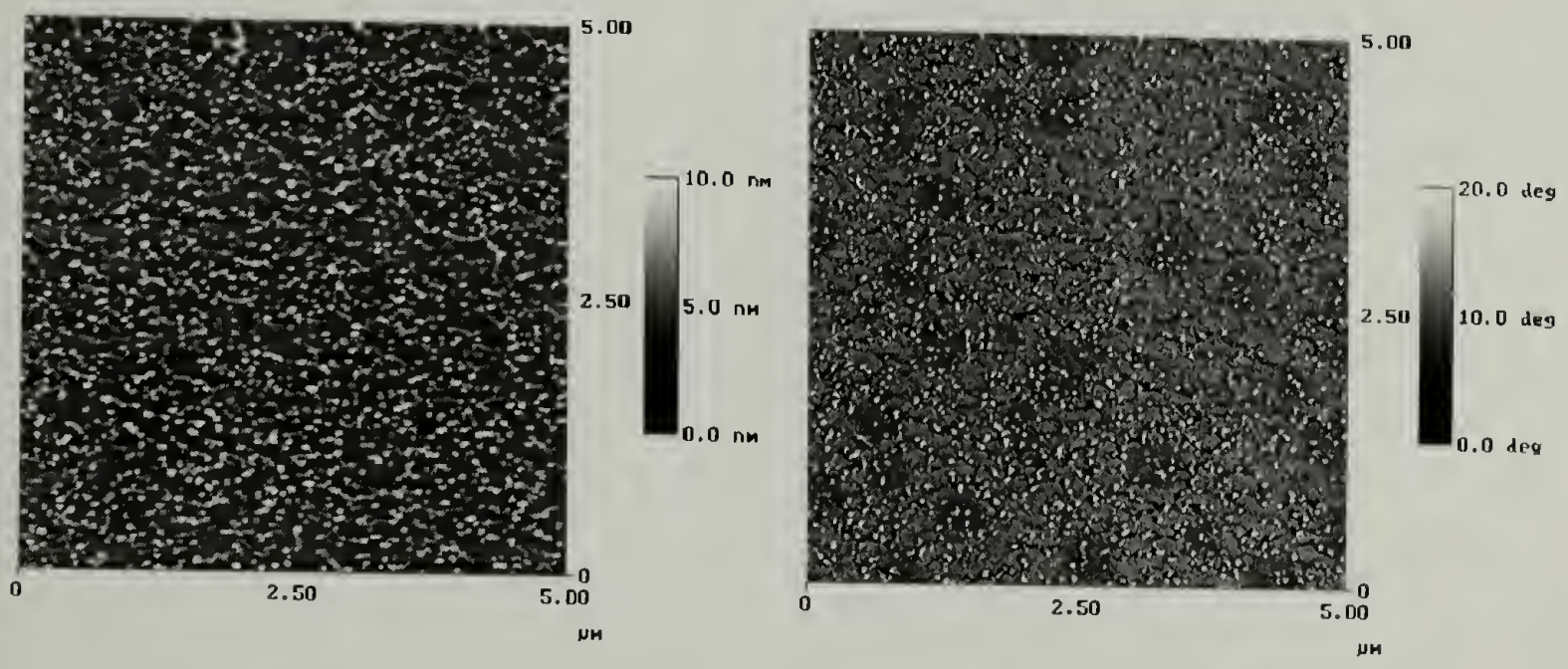

Figure 2.18. AFM tapping mode analysis of adsorbed 3121:1 poly-**R/S** from THF to dense DPDCS–modified native silicon oxide for 72 hours at 25 °C. The pictures are height (top) and phase (bottom) images of a 25 μm^2 sampling area.

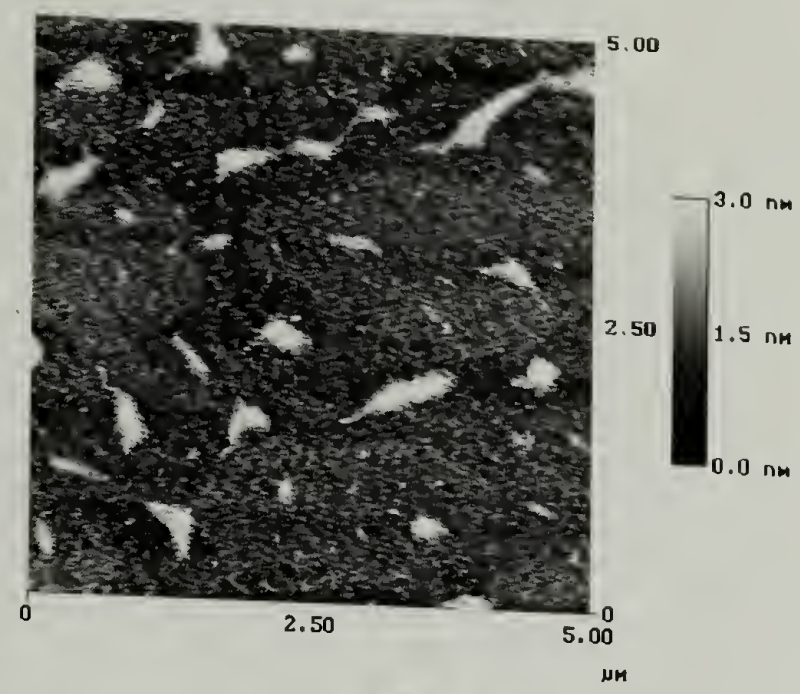

Figure 2.19. AFM tapping mode analysis of adsorbed thin film of 3121:1 poly-**S** from THF to dense DPDCS–modified native silicon oxide for 72 hours at 25 °C. The pictures are height (top), surface (middle), and phase (bottom) images of a 25 μm^2 sampling area.

Adsorption to Binary Monolayer Mixtures

Modification of surface properties by controlled dilution of surface functionality through a two step method has been described by Fadeev et al.[20] In their process, silica is first modified by a bulky organosilane such as tris(TMS), forming a dense monolayer comprised of nanosized "pores" between the covalent bound organosilane. The tris(TMS)–modified silica surface was further modified by the reaction of a smaller cross-sectional organosilane which "filled" the "pores".

With binary monolayer mixtures, surfaces can be prepared that are composed of lyophobic and hydrophilic functionality. In this work, the adsorption behavior of polycarbodiimides onto surfaces that vary in carboxylic acid functionality was accomplished by utilization of the techniques presented by Fadeev et al. Several binary monolayers of tris(TMS):CMDCS on silica were prepared that varied in the ratio of tris(TMS) to CMDCS. Following preparation of the mixed monolayers, hydrolysis of the methyl ester on CMDCS was performed using dilute sulfuric acid. Polycarbodiimides were then adsorbed to these surfaces and the adsorption behavior was studied by contact angle measurements and tapping mode AFM.

Hydrolysis of CMDCS: Kinetics

Prior to preparing binary mixed monolayers, the kinetics of methyl ester hydrolysis was measured. This was accomplished by first preparing a dense monolayer of CMDCS on silica by reaction of silicon wafers with CMDCS in the vapor phase. The CMDCS-modified silica was then transferred to a 100 mL beaker containing a magnetic stir bar and a 5% by weight solution of sulfuric acid diluted with house-purified water (reverse osmosis). The reaction was performed at room temperature and the extent of hydrolysis was monitored by contact angle analysis using water as the probe fluid. In five minute intervals, the sample was removed from the acid solution and rinsed in

flowing water, followed by drying the sample in a 120° C clean oven for ten minutes. The sample was then analyzed by water contact angle and returned to the acid solution for the next five minute interval. The extent of hydrolysis was determined by the amount of contact angle hysteresis. Reproducibility of the hydrolysis reaction was studied by performing the reaction on three different samples and these results are listed in Table 2.8.

Contact angle hysteresis was used to monitor the reaction because of the technique's sensitivity to surface changes. From Table 2.8, at time zero, the low hysteresis indicates the surface of the silicon wafer was composed of a dense monolayer of CMDCS. With increasing reaction time, the advancing and receding contact angles decreased as the surface became more hydrophilic. This is a result of methyl ester groups hydrolyzing to carboxylic acid. Concurrent with the decrease in contact angles is an increase in hysteresis indicating a larger degree of surface heterogeneity. After twenty-five minutes, the amount of hysteresis begins to increase suggesting hydrolysis of the silane-silica surface bond, resulting in an increase in the concentration of surface silanol groups. These surface silanol groups interact with the water probe fluid, and lower the receding contact angle thus leading to an increase in hysteresis. For these reasons, the maximum extent of CMDCS hydrolysis correlated with a reaction time of 25 minutes. This was the lowest obtained advancing contact angle prior to significant increases in hysteresis. All hydrolysis reactions for adsorption experiments were performed following the above procedures at a reaction time of 25 minutes. The hydrolyzed CMDCS is referred to as H-CMDCS.

Binary Monolayer Mixtures

Three binary monolayer mixed surfaces were prepared that varied in the concentration ratio of tris(TMS):CMDCS. Preparation of the surfaces followed the

procedures outlined by Fadeev et al.[20] First, silicon wafers were modified with tris(TMS) in the vapor phase, and to control the amount of modification the reaction time was varied. In Table 2.9 are shown the water and hexadecane contact angle results for the modification of the silica surface with tris(TMS). The amount of modification is designated by most dense, more dense, and least dense which is relative to the reaction time of 120 hours, 72 hours, and 1 hour respectively. Analysis of these surfaces by water and hexadecane contact angles show an increasing contact angle hysteresis with less reaction time, which is a result of decreased concentration of tris(TMS). However, reaction times less than 120 hours may result in non-uniform modification where the surface is comprised of patches of tris(TMS) separated by surface silanol groups. Such heterogeneity would be evident during contact angle analysis where a large variation in measurements would be observed over the surface. This was the case for the more dense surface where a larger variation in the contact angle of ± 4°-5° was measured. The variation in the contact angle measurements for the least dense tris(TMS) was ± 1° indicating a surface comprised mostly of surface silanol groups and some tris(TMS). A cartoon representation of these surfaces was shown previously in Scheme 2.1.

Table 2.8. Kinetics of hydrolysis measured by water contact angle. Hydrolysis of CMDCS (T = 23 °C) in 5% H_2SO_4.

Sample Rx time	1 θ_A / θ_R H_2O	2 θ_A / θ_R H_2O	3 θ_A / θ_R H_2O	1 Hyst.	2 Hyst.	3 Hyst.
0 min	84° ± 1° / 80° ± 2°	82° ± 1° / 78° ± 1°	84° ± 1° / 80° ± 1°	4	4	4
5 min	87° ± 2° / 79° ± 1°	87° ± 3° / 79° ± 1°	88° ± 2° / 78° ± 2°	8	8	10
10 min	83° ± 2° / 73° ± 2°	84° ± 2° / 75° ± 1°	86° ± 3° / 77° ± 3°	10	11	9
15 min	76° ± 1° / 69° ± 1°	78° ± 3° / 70° ± 2°	82° ± 4° / 70° ± 4°	7	8	12
20 min	73° ± 1° / 63° ± 4°	75° ± 2° / 65° ± 3°	78° ± 3° / 66° ± 4°	10	10	12
25 min	73° ± 2° / 62° ± 2°	72° ± 3° / 61° ± 2°	74° ± 2° / 62° ± 1°	11	11	12
30 min	67° ± 1° / 53° ± 4°	68° ± 3° / 54° ± 1°	68° ± 4° / 53° ± 3°	14	14	15
35 min	65° ± 2° / 52° ± 4°	67° ± 3° / 51° ± 3°	68° ± 4° / 52° ± 5°	13	16	16

Table 2.9. Contact angle results for mixed monolayers of tris(TMS) and CMDCS, chemisorbed on native silicon oxide from the vapor phase. The data was acquired prior to hydrolysis.

Sample	θ_A H_2O	θ_R H_2O	θ_A Hexadecane	θ_R Hexadecane
Dense tris(TMS)	92° ± 1°	81° ± 1°	34° ± 2°	27° ± 2°
Dense CMDCS	88° ± 1°	79° ± 1°	8° ± 1°	0°
Most dense tris(TMS)	91° ± 1°	82° ± 1°	33° ± 2°	26° ± 1°
Most dense tris(TMS) Mixed	85° ± 1°	79° ± 1°		
More dense tris(TMS)	85° ± 4°	58° ± 5°	33° ± 1°	21° ± 3°
More dense tris(TMS) Mixed	81° ± 1°	71° ± 3°		
Least dense tris(TMS)	57° ± 1°	44° ± 1°	30° ± 2°	11° ± 1°
Least dense tris(TMS) Mixed	82° ± 1°	77° ± 1°		

Further reaction of the most, more, and least tris(TMS)–modified silicon wafers with CMDCS was performed in the vapor phase for 120 hours. These surfaces were analyzed by water contact angle with the results listed in Table 2.9. For the most dense tris(TMS)–modified silica surface, the "filling" of "pores" with CMDCS lowered the advancing angle, while having less effect on the receding angle, suggesting that the modification resulted in a uniform binary monolayer. Increases in both advancing and receding contact angle for more dense and least dense tris(TMS) surfaces confirm that CMDCS modification occurred. The next step in preparing the mixed surfaces for the adsorption experiments involved hydrolysis of the methyl ester group of CMDCS.

Hydrolysis of tris(TMS):CMDCS Mixed Monolayers

Preparation of surfaces with varying concentration of carboxylic acid functionality was accomplished by hydrolysis of the methyl ester group in the silicon–supported binary monolayer mixture of tris(TMS) and CMDCS. The mixed monolayers surfaces used in the hydrolysis reaction are described in Table 2.9. The procedure developed during the measurements of hydrolysis kinetics called for the

samples to be dried at 120° C for 10 minutes in a clean oven. For comparison, two samples prepared under each condition were hydrolyzed followed by drying one by the oven method and the other by N_2 (g) flow over the surface until dried. There was concern that drying at elevated temperature could result in the carboxylic acid groups undergoing esterification with the surface or neighboring chemical groups. Contact angle analysis with probe fluid, water was used to study the effect of drying conditions. The results are listed in Table 2.10, showing that drying method had no difference in the resulting post-hydrolyzed surfaces.

The contact angle data for the hydrolyzed surfaces shown in Table 2.10 are all relatively equivalent to the contact angle measurements for a dense monolayer of H–CMDCS on silica. This equivalency in contact angle could be accounted for by ability of the H-CMDCS to undergo conformational changes that allow the molecule to "bend–over" and interact with the surface through hydrogen bonding with silanol groups. Under the most dense conditions, the carboxylic groups are shielded from the surface silanol groups by the tris(TMS) "umbrella". As the surface becomes less dense, more "holes" open allowing the hydrolyzed CMDCS groups to interact with the surface. Therefore, during water contact angle measurements, the water contacts tris(TMS) and methylene groups from the H-CMDCS resulting in contact angles indicating a somewhat hydrophobic surface. Furthermore, the non-uniformity of the more dense mixed monolayers surface is evident after hydrolysis as indicated by the large variation (± 5° for advancing and ± 6° for receding) in contact angle measurements.

Additional samples (from Table 2.10) of dense H-CMDCS and hydrolyzed samples of most, more, and least dense binary monolayer mixtures of tris(TMS):H–CMDCS were prepared. These samples were stored in water that was house purified (reverse osmosis) followed by further purification using a Millipore Milli-Q_{UF} system that involves reverse osmosis, ion exchange, and filtration steps (18 MΩ/cm). Prior to performing the adsorption experiments, the substrates were rinsed with THF. The adsorption of poly-

R/S and poly-**S** from THF onto the substrates was performed at room temperature for 72 hours. After adsorption, the samples were rinsed in THF, dried, and then analyzed by water contact angle and tapping mode AFM.

Table 2.10. Contact angle results for mixed monolayers of tris(TMS) and CMDCS, chemisorbed on native silicon oxide from the vapor phase. The data was acquire both prior and post hydrolysis.

Sample	θ_A H_2O	θ_R H_2O	θ_A Hexadecane	θ_R Hexadecane
Dense tris(TMS)	92° ± 1°	81° ± 1°	34° ± 2°	27° ± 2°
Dense CMDCS	88° ± 1°	79° ± 1°	8° ± 1°	0°
Dense H-CMDCS (N_2 dried)	75° ± 1°	70° ± 1°		
Dense H-CMDCS (Oven dried)	76° ± 3°	69° ± 2°		
Most dense tris(TMS)	91° ± 1°	82° ± 1°	33° ± 2°	26° ± 1°
Most dense tris(TMS) Mixed	85° ± 1°	79° ± 1°		
Post Hydrolysis (N_2 dried)	76° ± 1°	70° ± 1°		
Post Hydrolysis (Oven dried)	77° ± 1°	70° ± 2°		
More dense tris(TMS)	85° ± 4°	58° ± 5°	33° ± 1°	21° ± 3°
More dense tris(TMS) Mixed	81° ± 1°	71° ± 3°		
Post Hydrolysis (N_2 dried)	79° ± 5°	72° ± 6°		
Post Hydrolysis (Oven dried)	77° ± 2°	70° ± 2°		
Least dense tris(TMS)	57° ± 1°	44° ± 1°	30° ± 2°	11° ± 1°
Least dense tris(TMS) Mixed	82° ± 1°	77° ± 1°		
Post Hydrolysis (N_2 dried)	74° ± 1°	70° ± 1°		
Post Hydrolysis (Oven dried)	74° ± 1°	70° ± 1°		

The adsorption behavior of poly-**R/S** and poly-**S** onto the above substrates was analyzed by advancing and receding water contact angles with the data listed in Table 2.11. These results were compared with the contact angle data from Table 2.10, the substrate post hydrolysis. For the dense monolayer of H-CMDCS sample, 312:1 poly–**R/S** adsorbed as indicated by the increase in advancing (+10°) and receding (+6°)

contact angles. When compared with the results (Table 2.5) for the same polymer adsorbed to a dense monolayer of CMDCS (no hydrolysis), the data suggests that the polymer does have a higher affinity for the hydrolyzed surface. This result of higher adsorption affinity for H–CMDCS was also observed for 312:1 poly-**S** and 3121:1 poly–**R/S** and poly-**S**. This trend was expected because of the increase in potential surface-segment interaction, a result of acid-base interactions between the carboxylic acid group on the H-CMDCS and the basic guanidine unit along the polymer backbone. The contact angle data for the adsorption of 312:1 poly-**R/S** to the most dense surface

Table 2.11. Water contact angle results of adsorbed thin films of either poly-**R/S** or poly–**S** on native silicon oxide-supported mixed monolayers of tris(TMS) and H–CMDCS. Adsorptions were carried out from THF for 72 hours at 25 °C.

Polymer and Mixed Layer	$\theta_A H_2O$	$\theta_R H_2O$
312:1 poly-**R/S**		
Dense CMDCS	85° ± 2°	76° ± 2°
Most dense tris(TMS) Mixed	79° ± 1°	69° ± 1°
More dense tris(TMS) Mixed	83° ± 2°	71° ± 2°
Least dense tris(TMS) Mixed	83° ± 2°	73° ± 2°
312:1 poly-**S**		
Dense CMDCS	83° ± 2°	73° ± 2°
Most dense tris(TMS) Mixed	83° ± 2°	73° ± 2°
More dense tris(TMS) Mixed	82° ± 1°	73° ± 1°
Least dense tris(TMS) Mixed	88° ± 2°	73° ± 1°
3121:1 poly-**R/S**		
Dense CMDCS	86° ± 3°	70° ± 1°
Most dense tris(TMS) Mixed	84° ± 4°	64° ± 2°
More dense tris(TMS) Mixed	88° ± 3°	63° ± 3°
Least dense tris(TMS) Mixed	85° ± 2°	65° ± 2°
3121:1 poly-**S**		
Dense CMDCS	87° ± 1°	73° ± 1°
Most dense tris(TMS) Mixed	80° ± 2°	62° ± 2°
More dense tris(TMS) Mixed	86° ± 3°	70° ± 2°
Least dense tris(TMS) Mixed	85° ± 0°	73° ± 1°

(Table 2.11) indicate a small amount of polymer adsorbed, assuming (from Table 2.10) that a 2° increase in θ_A and 1° increase in θ_R are results of adsorbed polymer. With the substrate dense in tris(TMS), the carboxylic acid groups are shielded from surface silanol groups, thereby making them more available to interact with polymer. Nonetheless, because of the low concentration of H-CMDCS on the most dense substrate, it is intuitive that the adsorbed amount of polymer would be lowest compared to the other substrates. As the concentration of H-CMDCS increases in relation to tris (TMS), the adsorbed amount should increase. This trend is generally observed for adsorption of both molecular weights of poly-**R/S** and poly-**S** where the adsorbed amount increases from most dense to least dense hydrolyzed substrates. It should be emphasized that these trends are based on the comparison of water θ_A/θ_R from before (Table 2.10) and after (Table 2.11) polymer adsorption. Caution should be employed when making assumptions on adsorption behavior based on contact angle results. There is an assumption here that the surfaces are uniform and the amount of roughness is equivalent. Therefore, tapping mode AFM was used to study the topography and confirm the observation made from contact angle data.

To confirm the observations made from the contact angle data (Table 2.10 and 2.11), tapping mode AFM was performed which mapped the topography of the surface giving insight into the adsorption behavior. The AFM analyses of the 312:1 poly-**R/S** adsorbed onto the various substrates described in Table 2.11 are shown in Figures 2.20 through 2.23. Dewetting is evident for each of these samples, however for the hydrolyzed most dense surface (Figure 2.20) it is difficult to determine whether the apparent dewetting is in the early or late stages. Typically, the late stage of dewetting is associated with the surface comprised mostly of droplets. Nevertheless, the structures

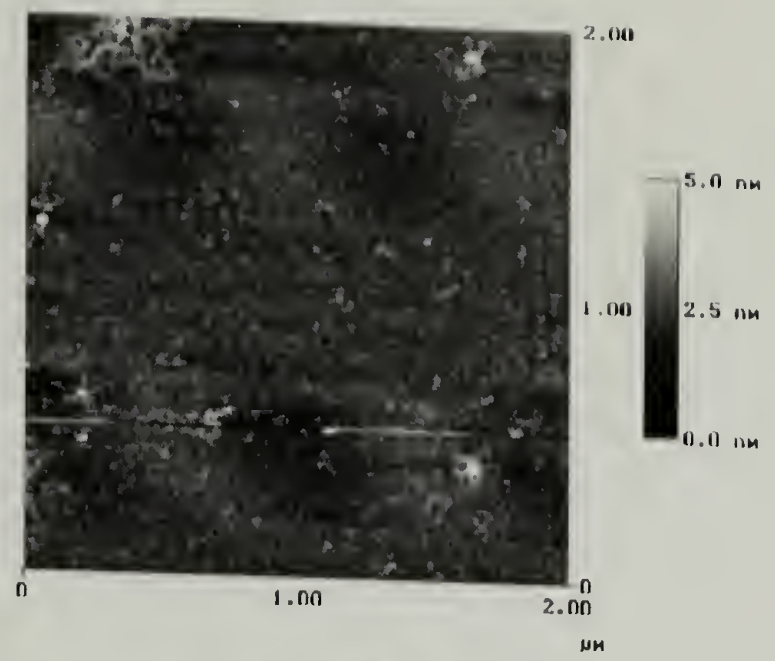

Figure 2.20. AFM tapping mode analysis of adsorbed 312:1 poly-**R/S** on native silicon oxide-supported mixed monolayers of most dense tris(TMS) and H-CMDCS. The adsorption was carried out for 72 hours at 25 °C. The pictures are height (top), surface (middle), and phase (bottom) images of a 4 μm^2 sampling area.

shown in Figure 2.20 resemble clusters of polymer with ribbons of polymer projected from the cluster, as well as ribbons of polymer dispersed throughout the imaged surface area. These clusters where observed previously for the dewetted adsorbed films of both 312:1 and 3121:1 poly-**S** onto native silicon oxide (Chapter 1, Figures 1.58,1.60, and 1.63). These structures became more prevalent with 312:1 poly-**S** adsorption to binary monolayer mixtures of tris(TMS) and H-CMDCS (vide infra).

Compared with the contact angle data, the AFM images indicate a similar trend where the adsorbed amount increases with concentration of H-CMDCS. This is only evident when comparing the most dense surface to the other three surfaces. However, the AFM results for the least dense surface (Figure 2.22) indicated that fewer polymer chains adsorbed relative to the most dense and more dense tris(TMS):H-CMDCS surfaces. It is difficult to compare the three samples because the least dense mixed monolayers sample shows more droplets indicating late stages of dewetting, whereas holes, ribbons, and droplets are observed for the most dense and more dense tris(TMS):H-CMDCS surfaces indicating earlier stages of dewetting. From the images, it appears the largest amount of adsorbed 312:1 poly-**R/S** occurred on the dense monolayer of H-CMDCS as shown in Figure 2.23. Intuitively, this was expected because this surface would be comprised of the highest concentration of carboxylic acid functionality.

Analysis of the adsorbed films of poly-**S** onto binary monolayer mixtures of tris(TMS):H-CMDCS by tapping mode AFM are shown in Figures 2.24 through 2.26. The AFM images indicate that the amount of adsorbed poly-**S** increased with the amount of carboxylic acid groups on the surface. A similar trend was previously shown for 312:1 poly-**R/S** adsorbed onto the same substrates. For 312:1 poly-**S** (Figure 2.24), very few polymer molecules adsorbed onto the most dense tris(TMS):H-CMDCS mixed monolayers. Upon solvent evaporation, the small amount of adsorbed polymer dewetted leaving a surface composed of a few droplets. The most dense tris(TMS):H-CMDCS

mixed monolayers had the least amount of carboxylic acid functionality, relative to the other surfaces. Therefore, it was expected to have the least amount of adsorbed polymer.

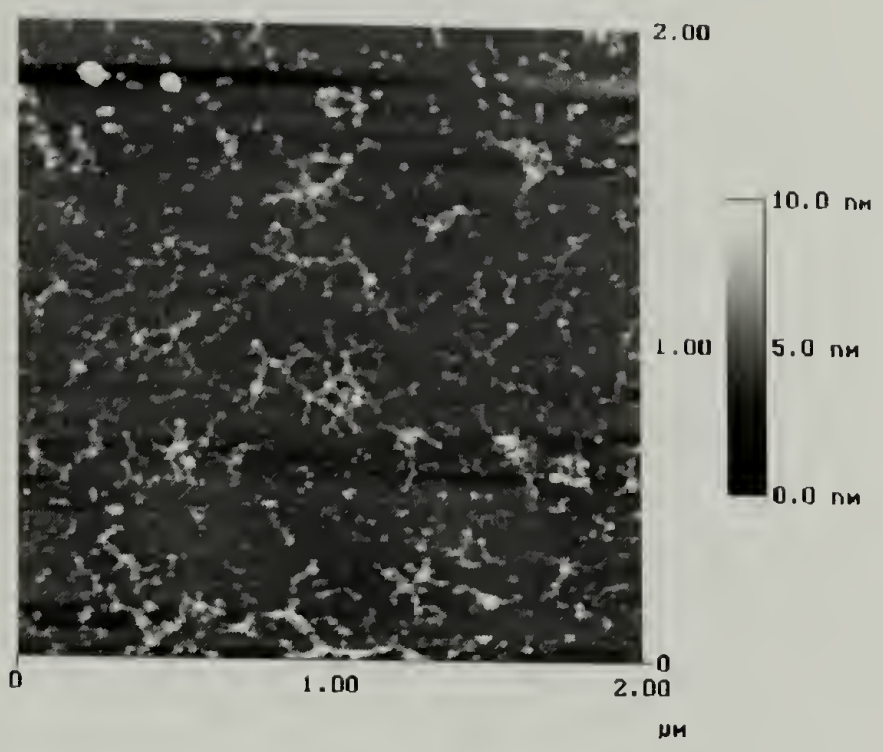

Figure 2.21. AFM tapping mode analysis of adsorbed 312:1 poly-**R/S** from THF to native silicon oxide-supported mixed monolayers of more dense tris(TMS):H–CMDCS. The adsorption was carried out for 72 hours at 25 °C. The pictures are height (top) and surface (bottom) images of a 4 μm^2 sampling area

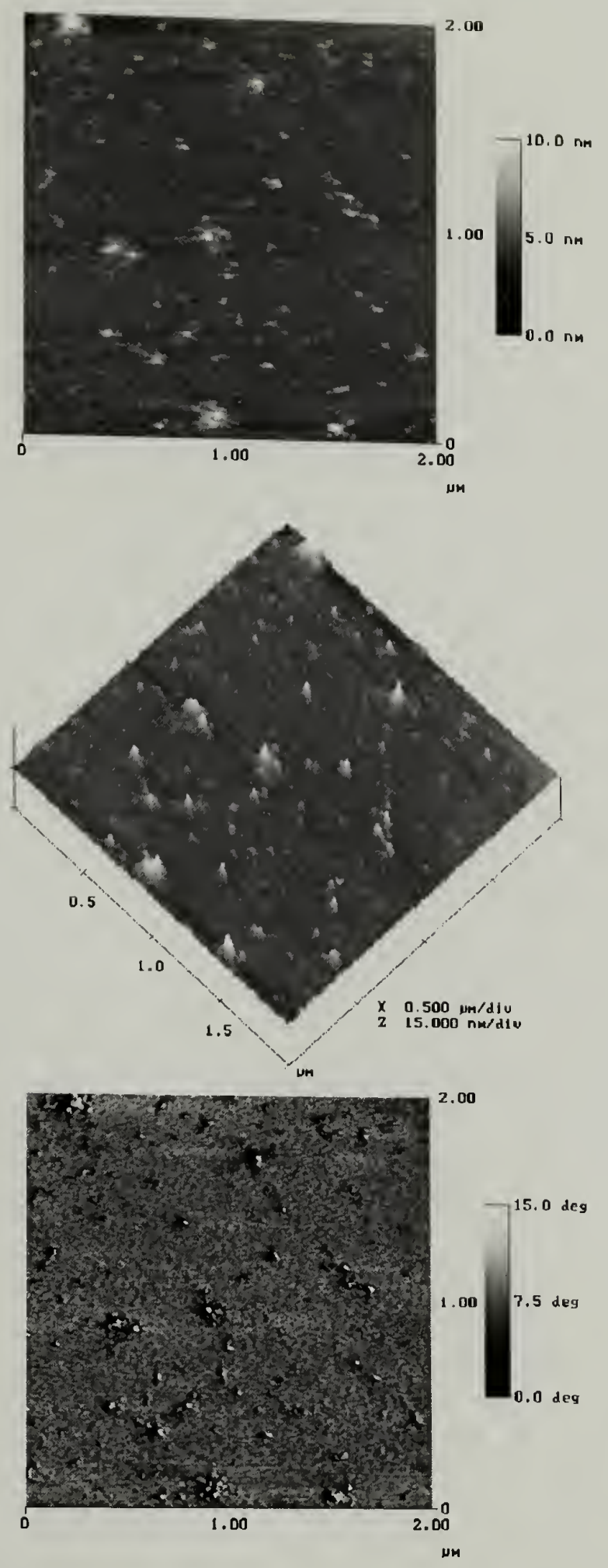

Figure 2.22. AFM tapping mode analysis of adsorbed 312:1 poly-**R/S** from THF to native silicon oxide-supported mixed monolayers of least dense tris(TMS):H-CMDCS The adsorption was carried out for 72 hours at 25 °C. The pictures are height (top), surface (middle), and phase (bottom) images of a 4 μm^2 sampling area.

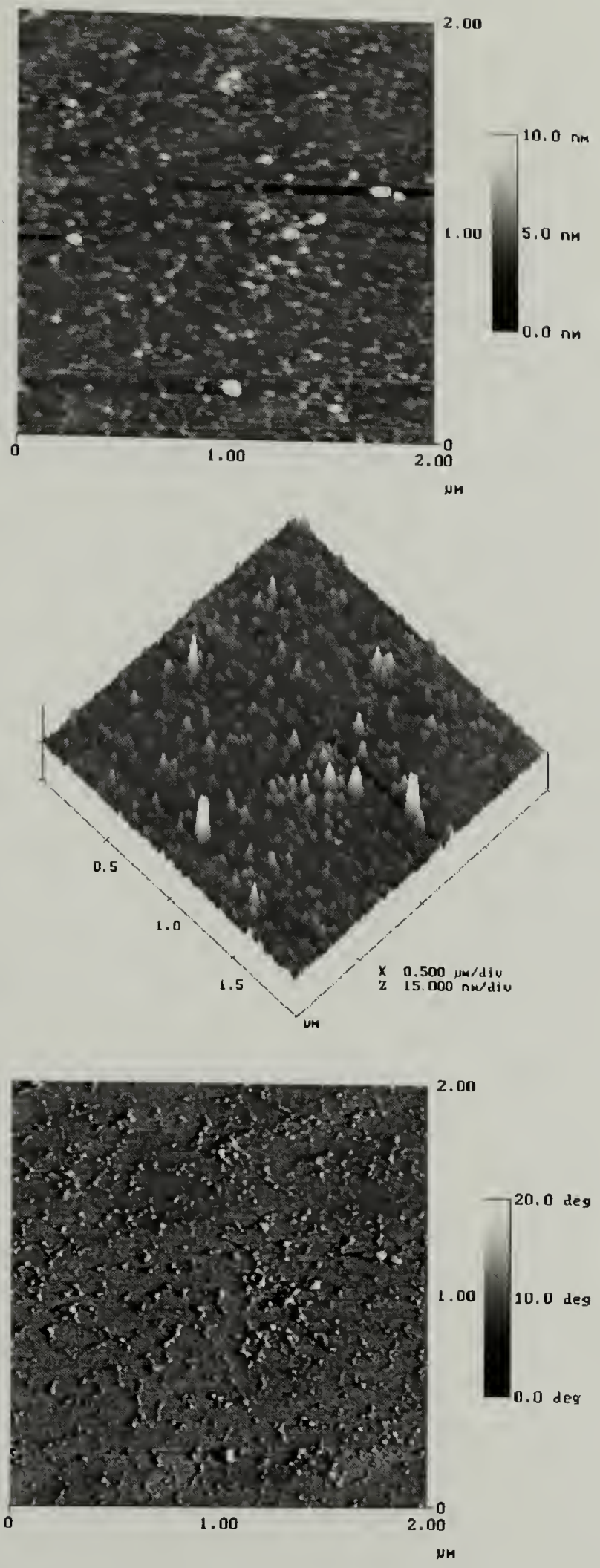

Figure 2.23. AFM tapping mode analysis of adsorbed 312:1 poly-**R/S** from THF to native silicon oxide-supported monolayers of dense H-CMDCS. The adsorption was carried out for 72 hours at 25 °C. The pictures are height (top), surface (middle), and phase (bottom) images of a 2 μm^2 sampling area.

With increasing surface density of H-CMDCS, additional surface structures appeared as shown in Figures 2.25 and 2.26. In Figure 2.26, which is a tapping mode AFM image of 312:1 poly-**S** adsorbed to the least dense tris(TMS):H-CMDCS mixed monolayers, the formation of not only droplets but also ribbons indicates dewetting. The larger droplets in both Figures 2.25 and 2.26 resemble a cluster of polymer molecules. Similar clusters were observed for 312:1 poly-**R/S** (Figures 2.20–2.23) adsorbed onto the same surfaces and clusters were also observed for both 312:1 and 3121:1 poly-**S** adsorbed onto native silicon oxide (Chapter 1; Figures 1.58, 1.60, and 1.63). From the AFM data, a model for the formation of clusters could be proposed based on solvent evaporation kinetics and the effect the rate has on the extent of dewetting. As solvent evaporates, the adsorbed film becomes unstable and begins to dewet. Holes form in the adsorbed film which continue to recede until they impinge forming walls between the holes. These walls are referred to as ribbons. Depending on the size of the intersections between several adjacent holes, the number of ribbons projecting from the intersection could be many. As the ribbons continue to dewet, the polymer chains aggregate at the intersection forming a cluster like structure. With continued dewetting, the aggregates begin to coalesce forming droplets.

Adsorption of 312:1 poly-**S** onto a silicon-supported dense monolayer of tris(TMS):H-CMDCS was analyzed by tapping mode AFM and the results are shown in Figure 2.27. The image shows late stages of dewetting because the adsorbed polymer is in the form of droplets. Previously, it was shown in Figure 2.11 that a small amount of 312:1 poly-**S** adsorbed onto dense CMDCS (not hydrolyzed) and upon solvent evaporation, the film rapidly dewetted forming droplet like structures.

The following questions arise: why does more 312:1 poly-**R/S** adsorb to the same dense H-CMDCS surface than 312:1 poly-**S,** and further, why does the poly-**R/S** adsorbed film structure indicate earlier stages of dewetting than poly-**S**? Though both polymers are chemically equivalent, the segment-surface interaction parameter is

influenced by the conformation and stereochemistry of adjacent segments along the polymer chain. Since both polymers are of equivalent molecular weight, then differences in the adsorption must be due to their conformation at the interface. Earlier, it was commented that the chain rigidity of the lower molecular weight poly-**R/S** and poly-**S** is more likely to be equivalent than higher molecular weight polymer. This was based on the probability of kinks along the polymer backbone, which are the result of enantiomeric monomers adding to the propagating chain, for example, in a -RSR- addition. For poly-**R/S**, these kinks may allow the polymer to "fit" into the H-CMDCS monolayer whereby the chain segments can interact with surface silanols or with carboxylic acid groups that are hydrogen bonded with the surface.

Differences in chain rigidity and conformation between 312:1 poly-**R/S** and poly–**S** became apparent when the adsorption behavior of the two polymers onto binary monolayer mixtures of tris(TMS):H-CMDCS were compared. Since more kinks are likely along the poly-**R/S** backbone relative to the poly-**S**, the number of potential locations of segment-surface interactions is greater for the poly-**R/S**. In addition, with poly–**S**, the extent of dewetting on all substrates was greater than poly–**R/S** suggesting that for poly-**S** the interaction between chain segments and the surface were fewer and/or weaker relative to poly-**R/S**. These weaker interactions may result from the polymer segments of poly-**S** not "fitting" into the monolayer as well as the chain segments of poly-**R/S,** resulting in long-range interactions. Therefore, during dewetting, the larger amount of segment-surface attachment points for poly-**R/S** (compared to poly-**S**) may effectively "pin" the polymer, thereby restricting the polymer mobility across the surface in the time frame of solvent evaporation. Furthermore, the more chain rigidity in poly–**S** relative to poly-**R/S** would result in larger ordering effect with solvent loss, a result of the lytropic liquid crystallinity of these polymers. This ordering difference may also effect the extent of dewetting due to viscosity effects. For lytropic LCP's, as the concentration of polymer increases, the viscosity rises until a critical concentration regime is

established which results in the isotropic phase changing to an anisotropic phase. Associated with the anisotropic phase is a rapid decrease in solution viscosity. The change from isotropy to anisotropy may occur at a lower solution concentration for poly–**S** relative to poly-**R/S** resulting in a less viscous solution which may allow a higher extent of dewetting. For the poly-**R/S**, the kinks limit ordering effects and in the time frame of solvent evaporation the viscosity remains high, limiting the extent of dewetting.

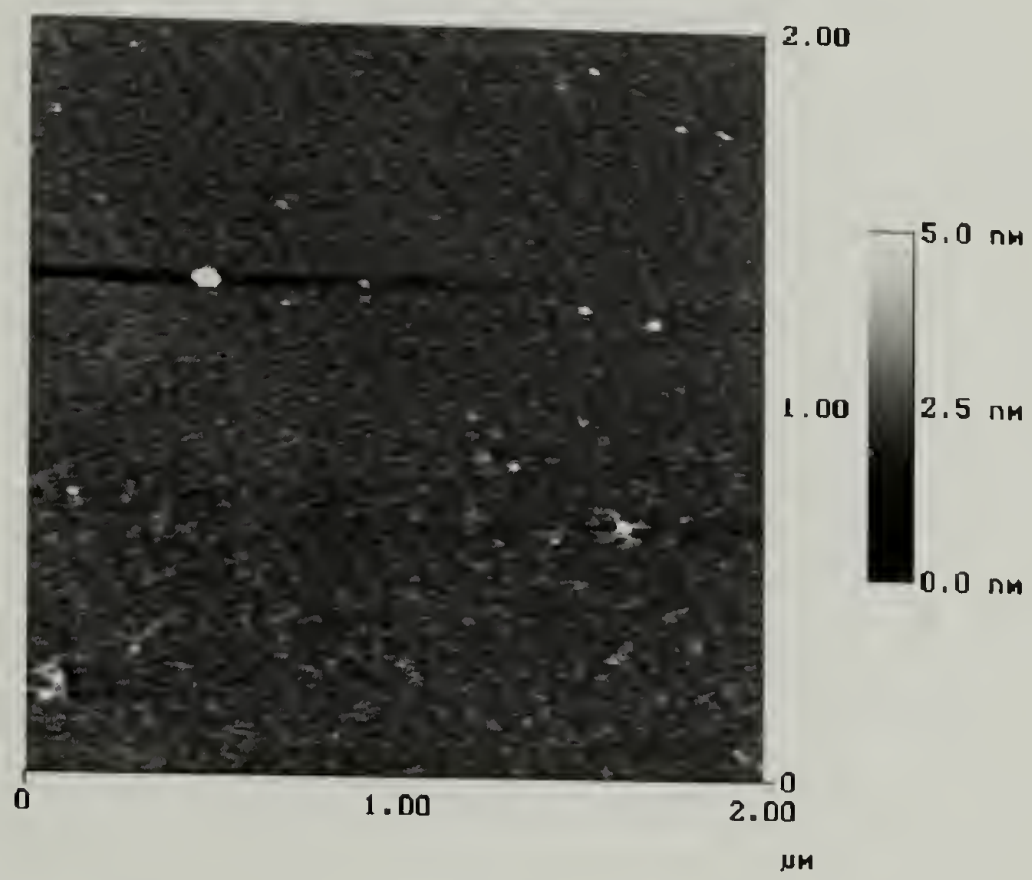

Figure 2.24. Height image from AFM tapping mode analysis of adsorbed 312:1 poly-**S** from THF to native silicon oxide-supported mixed monolayers of most dense tris(TMS):H-CMDCS. The adsorptions was carried out for 72 hours at 25 °C

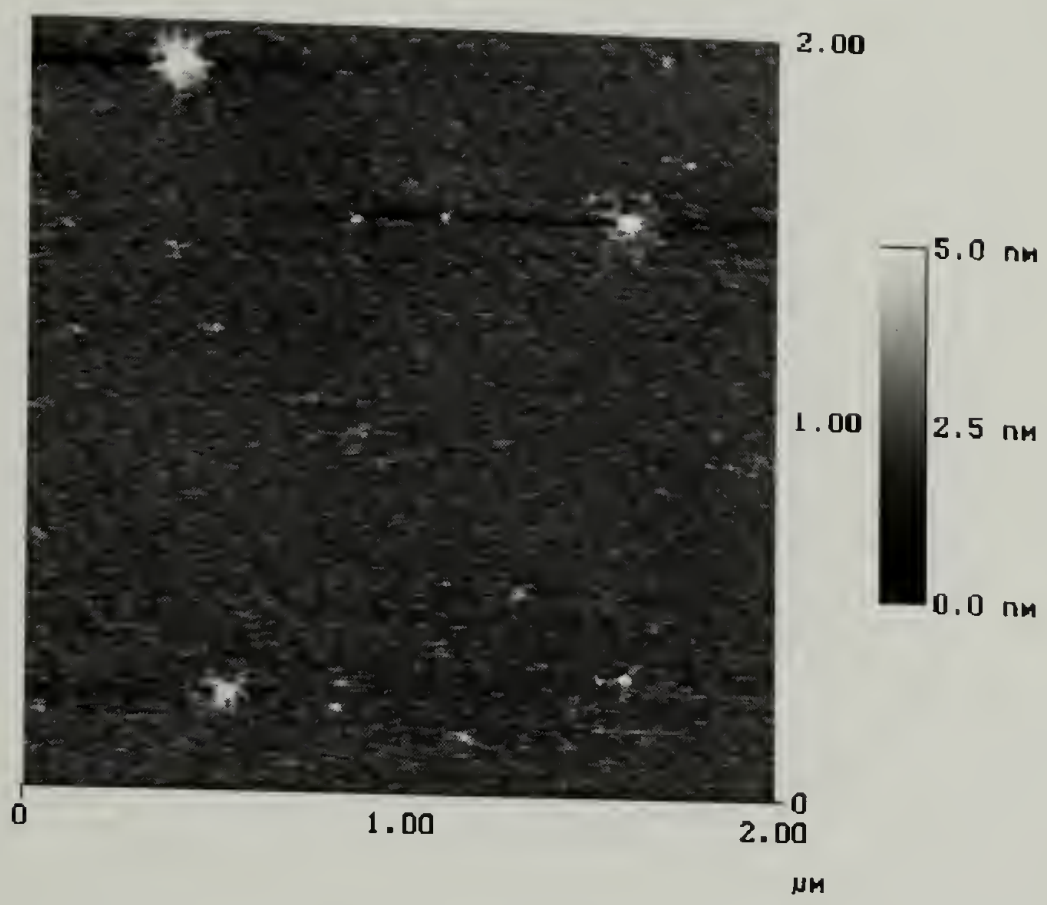

Figure 2.25. Height image from AFM tapping mode analysis of adsorbed 312:1 poly-**S** from THF to native silicon oxide-supported mixed monolayers of more dense tris(TMS):H-CMDCS. The adsorptions was carried out for 72 hours at 25 °C.

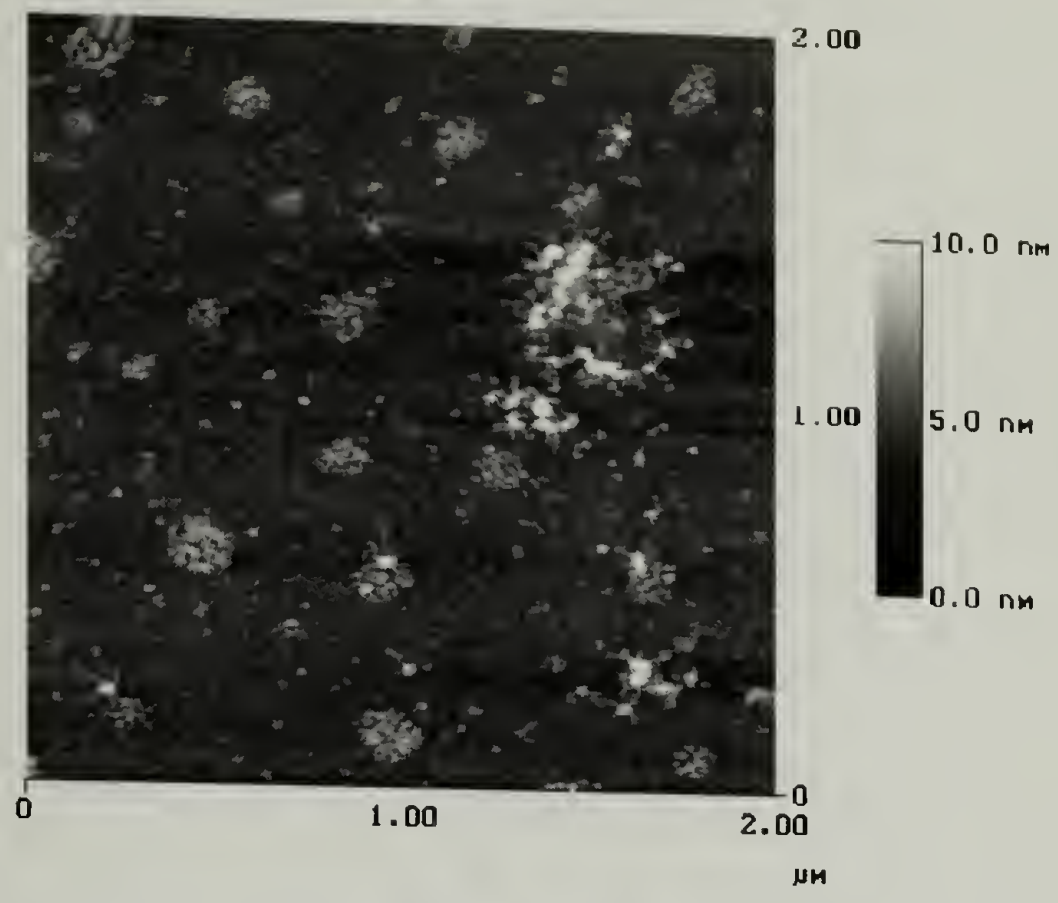

Figure 2.26. Height image (top) and surface image (bottom) from AFM tapping mode analysis of adsorbed 312:1 poly-**S** from THF to native silicon oxide-supported mixed monolayers of least dense tris(TMS):H-CMDCS. The Adsorption was carried out for 72 hours at 25 °C.

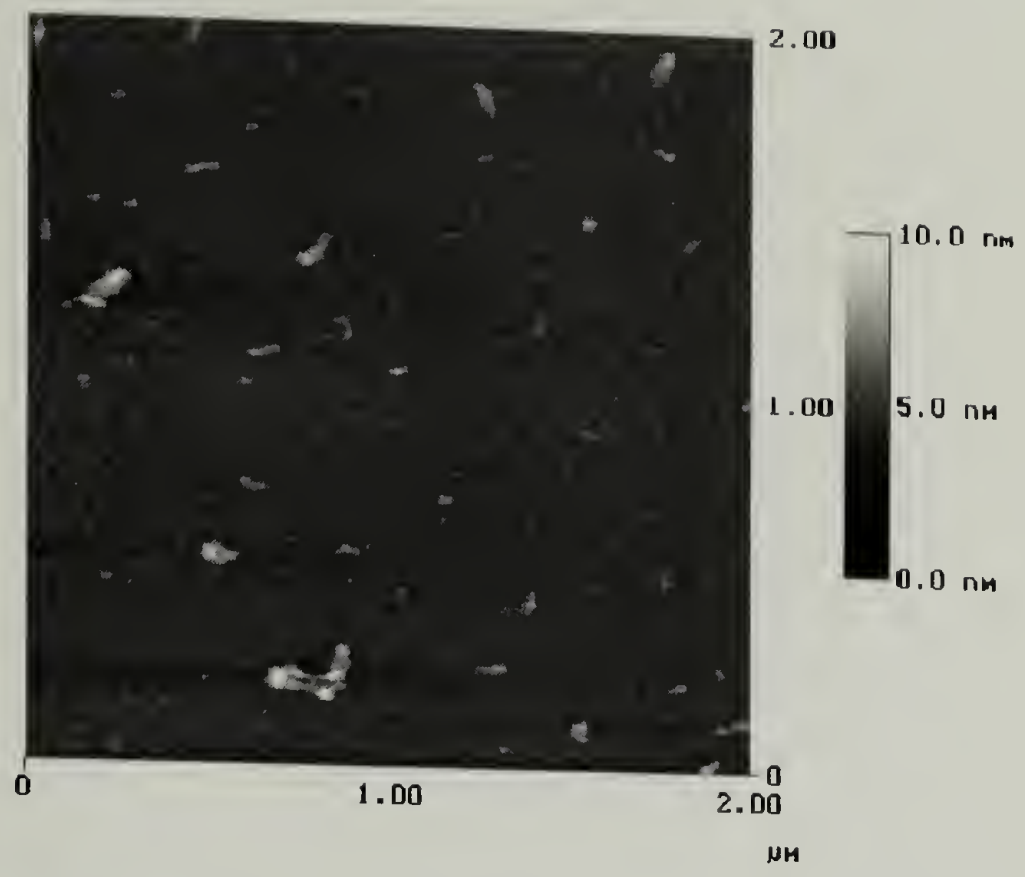

Figure 2.27. Height image from AFM tapping mode analysis of adsorbed 312:1 poly-**S** from THF to native silicon oxide-supported monolayers of dense H-CMDCS. The adsorption was carried out for 72 hours at 25 °C.

If there existed an ordering effect on the degree of dewetting, it would become more evident with the adsorption of the higher (3121:1) molecular weight polycarbodiimides onto the silicon-supported binary monolayer mixtures discussed previously. With increasing molecular weight, it would be expected that statistically the number of chain defects (e.g. kinks) would increase. Therefore, the amount of chain rigidity between poly-**R/S** and poly-**S** would be greater for poly-**S**. In addition, with increasing molecular weight, the statistical chance of chain defects along the poly–**S** backbone would increase. These defects result from monomer inserting into the growing polymer chain in a non-regiospecific manner. Thus, for a reason other than increased molecular weight, a larger amount of 3121:1 poly-**S** would be expected to adsorb relative to 312:1 poly-**S**. Further, the viscosity of the adsorbed film in solvent would be higher due to the higher molecular weight of the polymer. This suggests that during the solvent evaporation the adsorbed films of higher molecular weight polymer would show an

earlier degree of dewetting compared to the extent of dewetting for the lower molecular weight samples. This was indeed observed for the adsorption of 3121:1 poly-**R/S** and 3121:1 poly-**S** onto silicon-supported mixed monolayers of tris(TMS):H-CMDCS, as well as onto silicon-supported dense monolayer of H-CMDCS.

For 3121:1 poly-**R/S** adsorbed onto silicon-supported binary monolayers of tris(TMS):H-CMDCS, the trend in the adsorption behavior appears to suggest that the extent of dewetting is a function of the amount of H-CMDCS, yet the size scale of the surface structures associated with dewetting decreased respectively. These observations were drawn from the analysis of images generated by tapping mode AFM (see Figures 2.28-2.30). The adsorption of 3121:1 poly-**R/S** onto the most dense tris(TMS):H–CMDCS condition is shown in Figure 2.28 with the image indicating dewetting as evident by the large holes, numerous droplets, and developing ribbons. With an increase in the amount of H-CMDCS (Figure 2.29) dewetting appears more localized, with small holes and single ribbons receding into numerous droplets. Further increase in H-CMDCS (least dense tris(TMS):H-CMDCS surface) as shown in Figure 2.30, indicates highly localized dewetting with the surface composed mostly of small droplets. However, close examination of the surface by AFM showed small ribbons connecting the droplets, thereby indicating late stages of dewetting.

The adsorption behavior of 3121:1 poly-**R/S** onto the silicon-supported dense monolayer of H-CMDCS (see Figure 2.31) is similar to the adsorption of the same polymer onto the more dense tris(TMS):H-CMDCS mixed monolayers surface as shown in Figure 2.28. Under both conditions, the polymer dewetted during the evaporation of solvent leaving a surface structure composed of holes, ribbons, and droplets. Previously it was shown (see Figure 2.7) that 3121:1 poly-**R/S** adsorbed to a surface of silicon-supported dense tris(TMS), and the adsorbed film dewetted forming holes, ribbons, and droplets. In addition, a small amount of 3121:1 poly-**R/S** was shown in Figure 2.12 to adsorb to a silicon-supported dense monolayer of CMDCS, and where the polymer film

dewetted, localized ribbons with droplets formed along the ribbons. Thus, the large increase in adsorbed polymer onto hydrolyzed CMDCS surfaces is directly related to the presence of carboxylic acid groups.

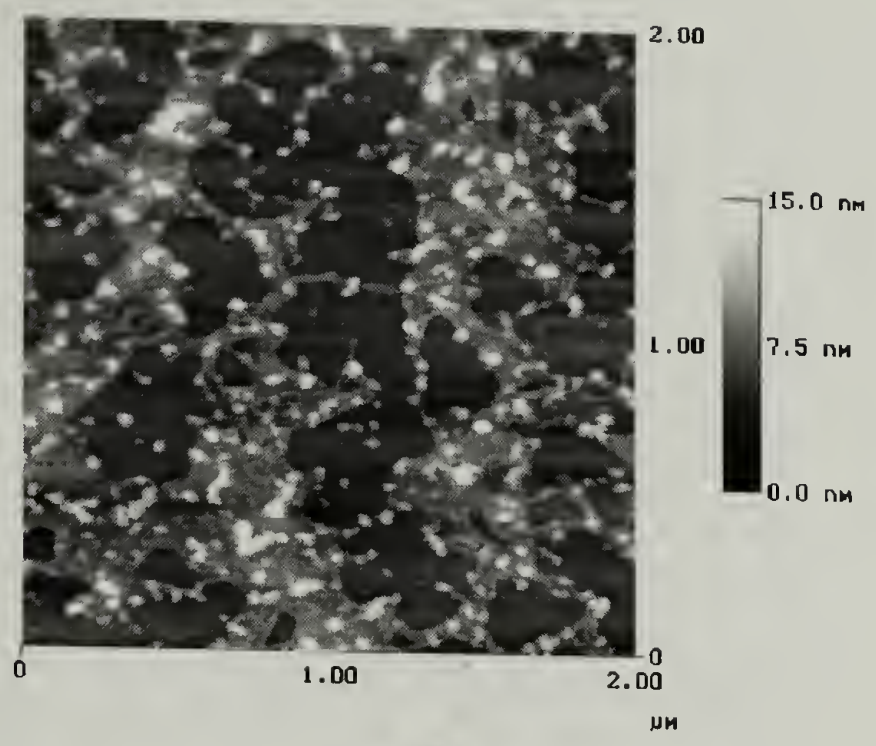

Figure 2.28. AFM tapping mode analysis of adsorbed 3121:1 poly-**R/S** from THF to native silicon oxide-supported mixed monolayers of most dense tris(TMS):H-CMDCS. The adsorption was carried out for 72 hours at 25 °C. The pictures are height (top) and surface (bottom) images of a 4 μm^2 sampling area.

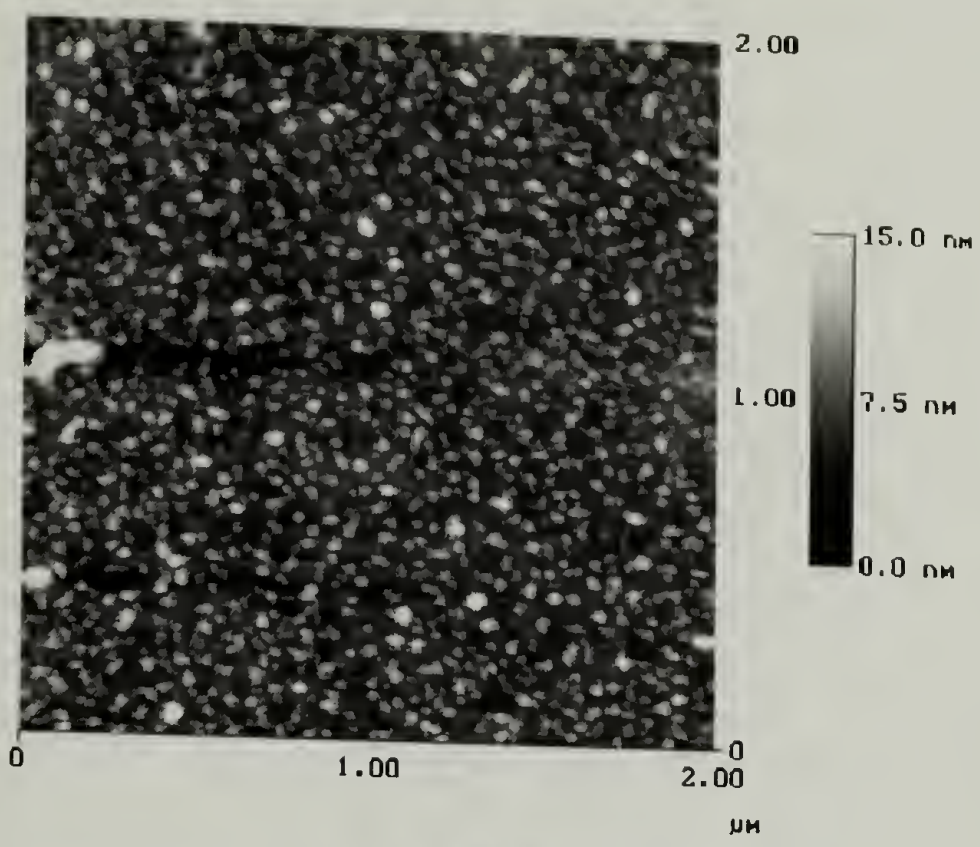

Figure 2.29. AFM tapping mode analysis of adsorbed 3121:1 poly-**R/S** from THF to native silicon oxide-supported mixed monolayers of more dense tris(TMS):H-CMDCS. The adsorption was carried out for 72 hours at 25 °C. The pictures are height (top) and surface (bottom) images of a 4 μm^2 sampling area.

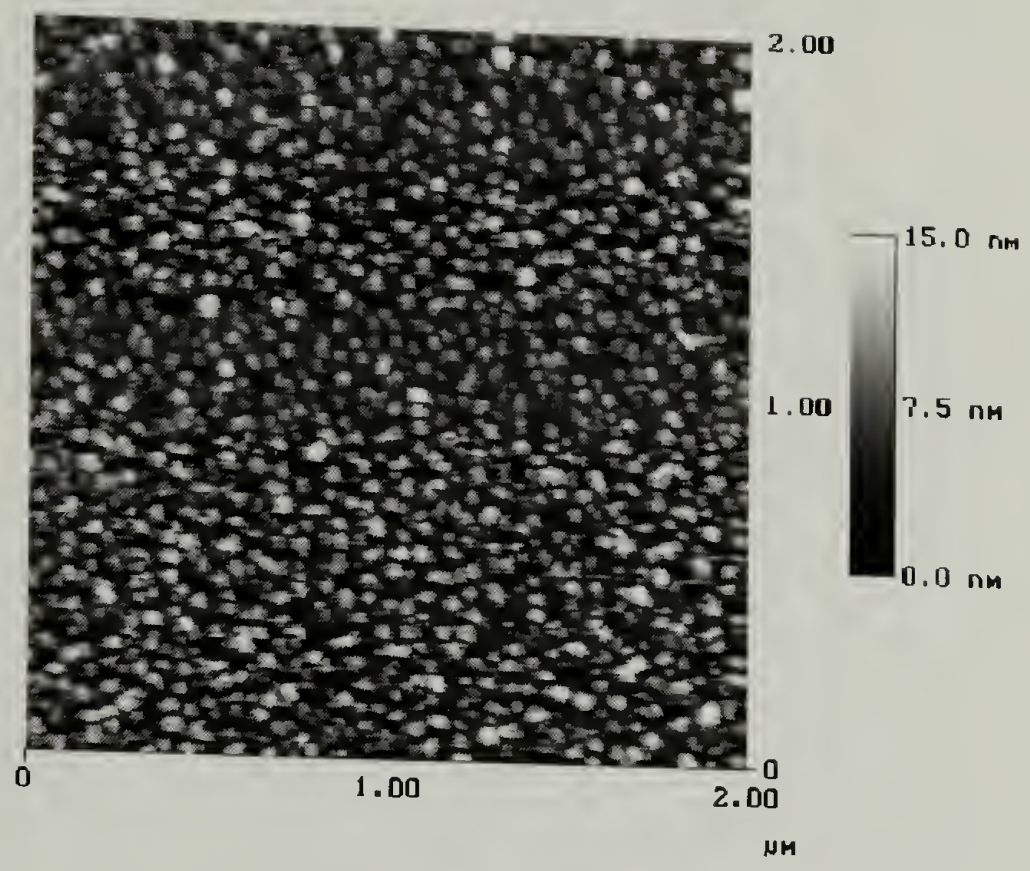

Figure 2.30. AFM tapping mode analysis of adsorbed 3121:1 poly-**R/S** from THF to native silicon oxide-supported mixed monolayers of least dense tris(TMS):H-CMDCS. The adsorption was carried out for 72 hours at 25 °C. The pictures are height (top) and surface (bottom) images of a 4 μm^2 sampling area.

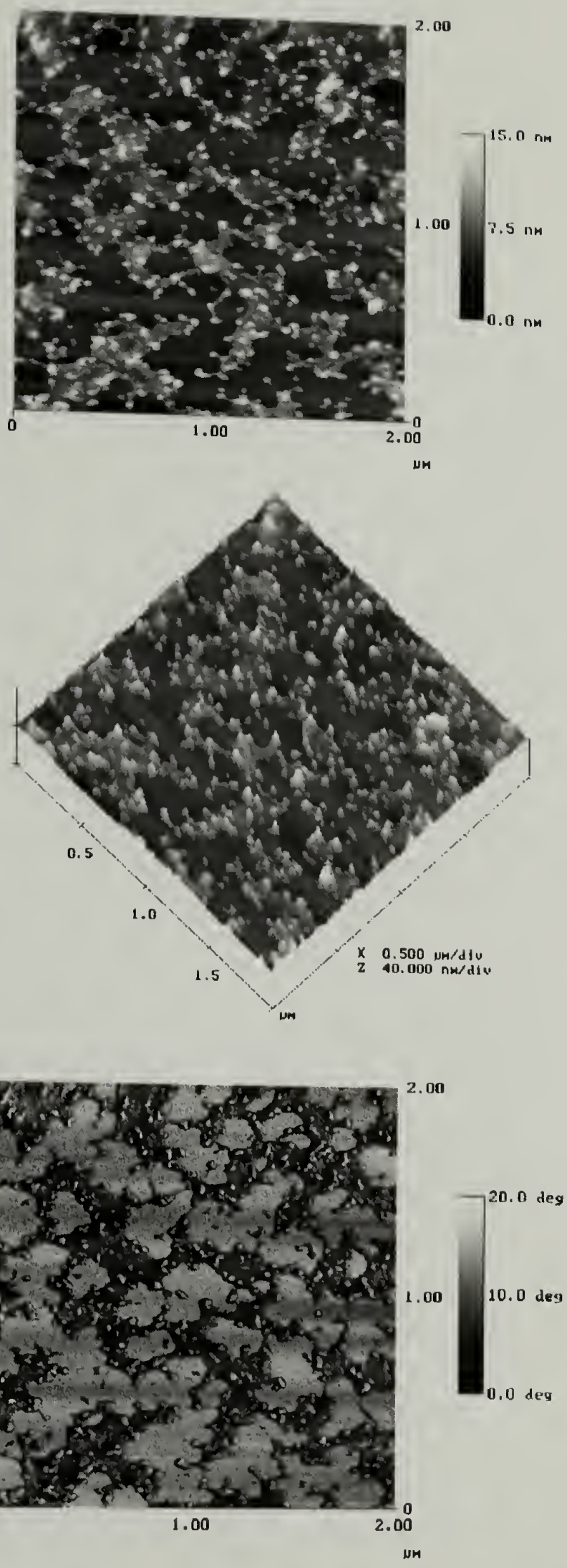

Figure 2.31. AFM tapping mode analysis of adsorbed 3121:1 poly-**R/S** from THF to native silicon oxide-supported monolayers of dense H-CMDCS. The adsorption was carried out for 72 hours at 25 °C. The pictures are height (top), surface (middle), and phase (bottom) images of a 4 μm^2 sampling area.

Tapping mode AFM was performed on a silicon-supported binary monolayer mixture of tris(TMS):H-CMDCS, where the surface was exposed to a 1 mg/mL THF solution of 3121:1 poly-**S** for 72 hours. The AFM images of the adsorbed films after solvent evaporation are shown in Figures 2.32-2.34. In addition, the adsorption of 3121:1 poly-**S** was performed on a dense monolayer of H-CMDCS as shown in Figure 2.35. For all conditions, the polymer adsorbed to the surface. However, the amount adsorbed to each surface appears equivalent. The surface did have an affect on the resulting surface structures, which for all samples, showed evidence of dewetting.

As previously described, the three surfaces which polymer was adsorbed to differ in the ratio of tris(TMS):H-CMDCS, with the most dense tris(TMS) surface (Figure 2.32) comprised of the largest amount of tris(TMS), and smallest amount of H-CMDCS. The AFM images for the adsorbed film of 3121:1 poly-**S** onto the most dense tris(TMS):H–CMDCS surface indicate dewetting, however the surface structures show a high degree of order. Though holes, ribbons, and droplets are evident, what stands out is the "logs in the river" appearance. Envision a river with logs floating in it, at a certain concentration of logs, interactions between logs begin to occur, resulting in the two dimensional spatial reorganization of the logs into a parallel orientation with its nearest neighbors. This orientation allows the rigid logs to maximize their surface coverage within a small area. The "logs in the river" analogy could be applied to describe the formation of the surface structures shown in Figure 2.32, where during dewetting, the rigid lytropic polymers orient as they become more concentrated due to the loss of solvent from evaporation.

The orientation observed in the dewetted film of adsorbed 3121:1 poly-**S** onto the most dense tris(TMS):H-CMDCS mixed monolayers was unique to that surface. For the same polymer adsorbed onto the more dense tris(TMS):H-CMDCS surface (see Figure 2.33), the polymer film dewetted. It should be noted that less, if any ordering was observed with the increasing amount of H-CMDCS. Dewetting was also observed for an

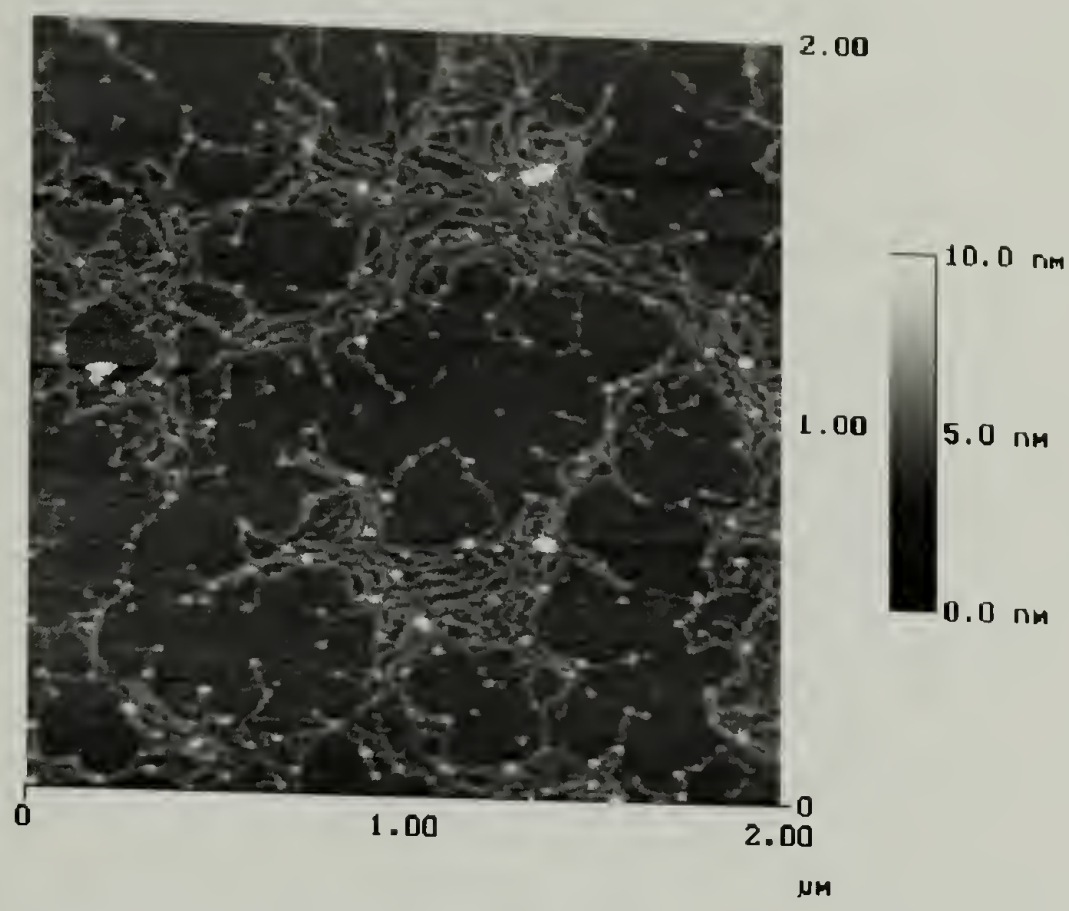

Figure 2.32. AFM tapping mode analysis of adsorbed 3121:1 poly-**S** from THF to native silicon oxide-supported mixed monolayers of most dense tris(TMS):H-CMDCS. The adsorption was carried out for 72 hours at 25 °C. The pictures are height (top) and surface (bottom) images of a 4 μm^2 sampling area.

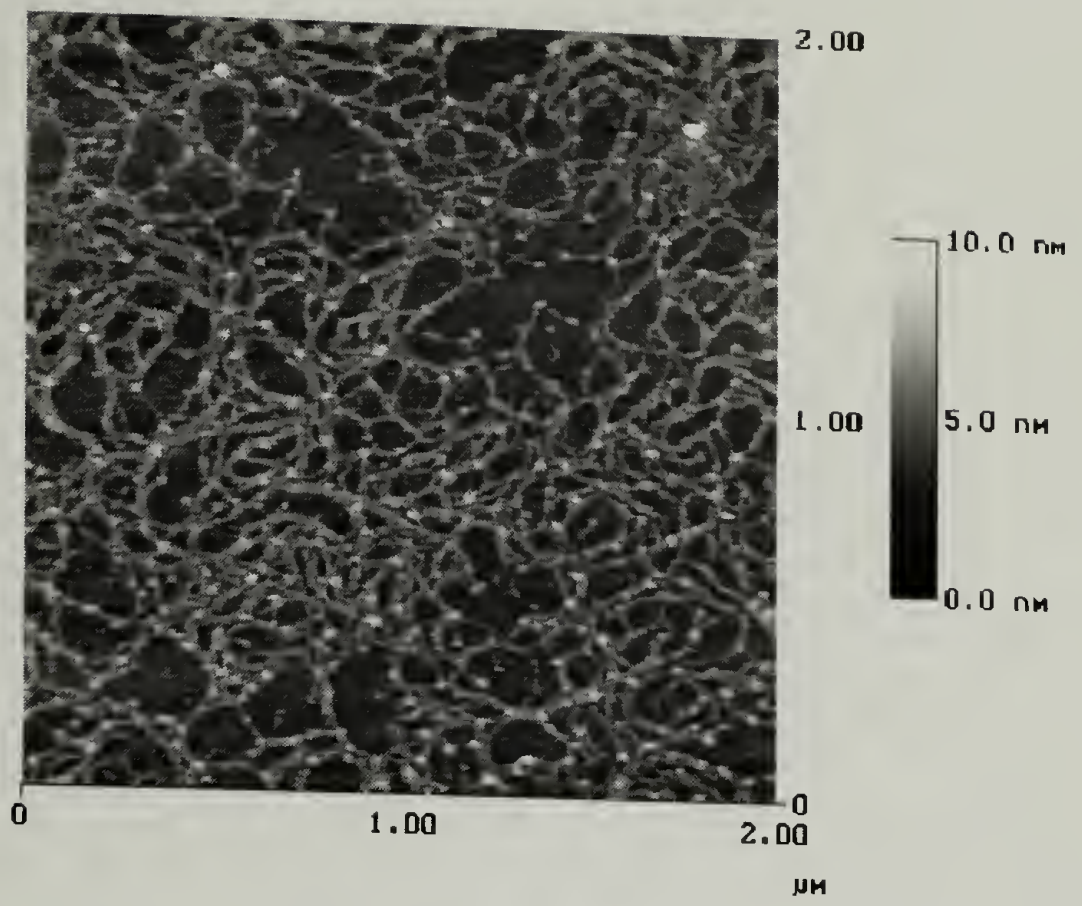

Figure 2.33. AFM tapping mode analysis of adsorbed 3121:1 poly-**S** from THF to native silicon oxide-supported mixed monolayers of more dense tris(TMS):H-CMDCS. The adsorption was carried out for 72 hours at 25 °C. The pictures are height (top) and surface (bottom) images of a 2 μm^2 sampling area.

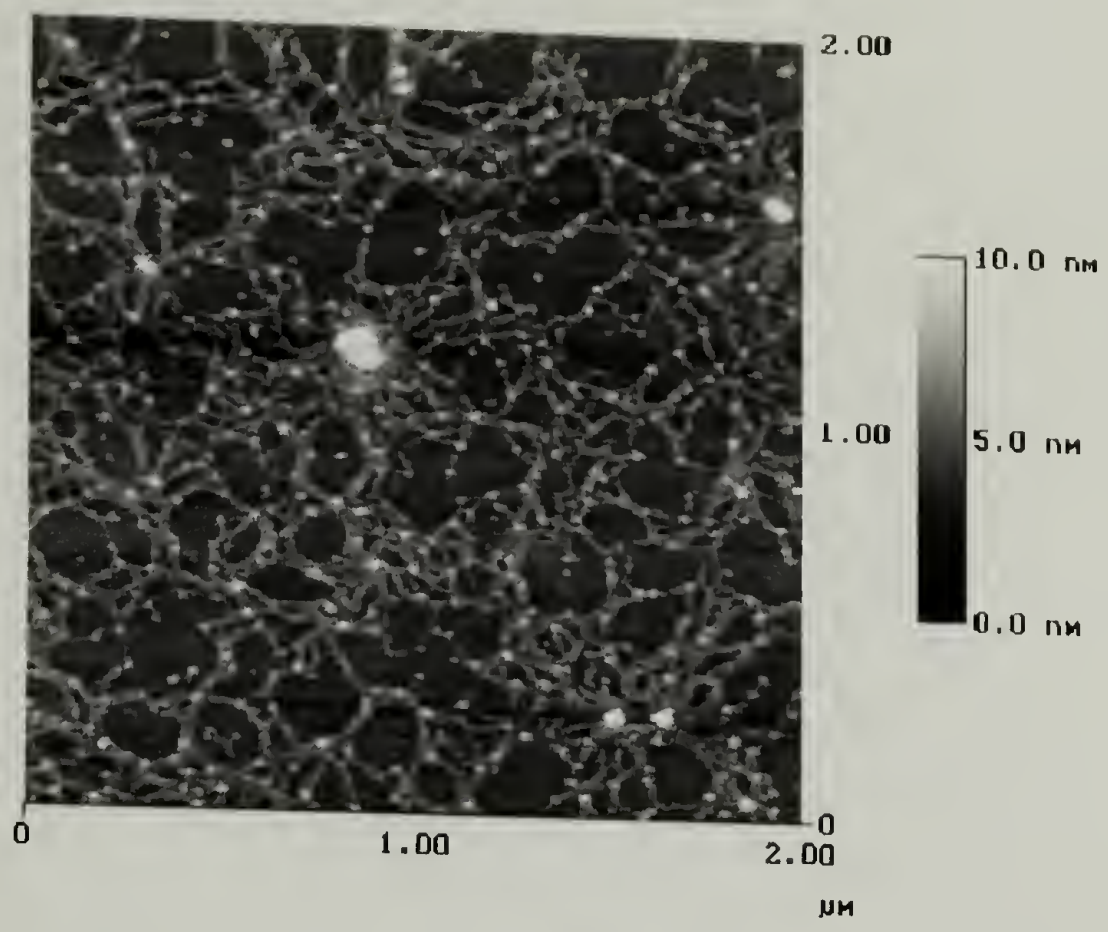

Figure 2.34. AFM tapping mode analysis of adsorbed 3121:1 poly-**R/S** from THF to native silicon oxide-supported mixed monolayers of least dense tris(TMS):H-CMDCS. The adsorption was carried out for 72 hours at 25 °C. The pictures are height (top) and surface (bottom) images of a 4 μm^2 sampling area.

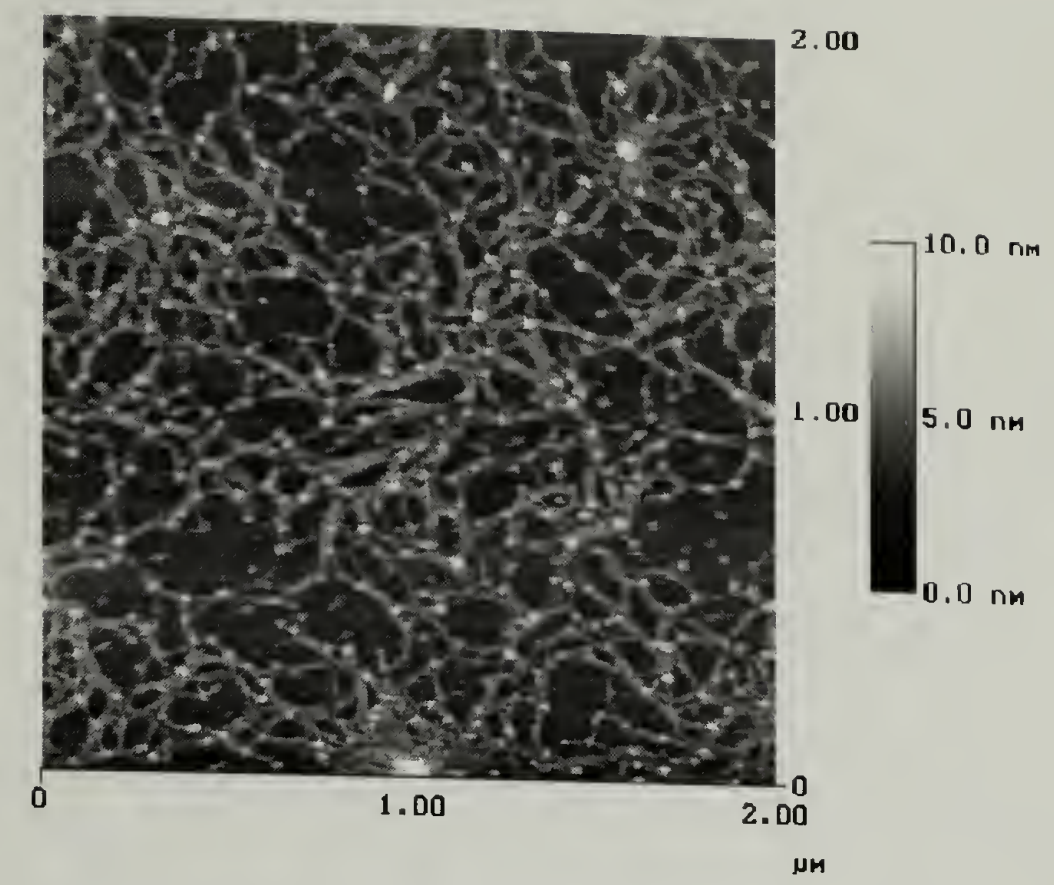

Figure 2.35. AFM tapping mode analysis of adsorbed 3121:1 poly-S from THF to native silicon oxide-supported mixed monolayers of dense H-CMDCS. The adsorption was carried out for 72 hours at 25 °C. The pictures are height (top) and surface (bottom) images of a 4 μm^2 sampling area.

adsorbed film of 3121:1 poly–**S** on both the least dense tris(TMS):H-CMDCS surface (see Figure 2.34) and dense monolayer of H-CMDCS surface (see Figure 2.35). Between these two surfaces, little difference was observed in the surface structure of the dewetted polymer film. From the AFM data for adsorbed 3121:1 poly-**S** on a silicon-supported binary monolayer mixture of tris(TMS):H-CMDCS, there may exist a critical amount of H-CMDCS which limits the polymers ability to orient and/or completely dewet. Previously it was shown that 3121:1 poly-**S** adsorbed to silicon-supported dense monolayer of tris(TMS) (see Figure 2.8) and proceeded to dewet as solvent evaporated. The resulting surface structure was composed of long thick ribbons resembling branches with thin ribbons of polymer chains dispersed between the branches. In addition, all the structures appear to be directional and ordered which may be a result of the lytropic nature of the polymer. The same polymer adsorbed on a dense monolayer of CMDCS (not hydrolyzed) (see Figure 2.13) rapidly dewetted upon solvent evaporation leaving a surface of polymer droplets. Therefore, on both tris(TMS) and CMDCS surfaces, 3121:1 poly-**S** dewetted to a far greater extent than observed when the same polymer is adsorbed onto silicon-supported binary monolayer mixtures of tris(TMS):H-CMDCS. Thus, the addition of carboxylic acid functionality has a very strong effect on the dewetting behavior of poly-**S.** Otherwise, similar surface structures as observed in Figures 2.8 and 2.13 should have been observed.

Conclusions

Using organosilane chemistry, we prepared lyophobic silicon-supported monolayers of tris(TMS), CMDCS, and DPDCS and then studied the adsorption behavior of poly-**R/S** and poly-**S** to the monolayers. Using XPS, contact angle, and AFM we researched how molecular weight, chain architecture, surface energy, and surface chemistry affect the adsorbed polymer layer. For both polymers there is little affinity to

adsorb, relative to native silicon oxide, to a silicon-supported dense monolayer of tris(TMS) and silicon-supported dense monolayer of CMDCS. Furthermore, both polymers were observed by AFM to have dewetted from the tris(TMS) and CMDCS silicon-supported monolayers. In addition, for poly-**R/S**, more polymer adsorbed from poorer solvent (toluene) than good solvent (THF). This trend concurs with observations from Chapter 1. In addition, the adsorbed amount increased with molecular weight but decreased with chain rigidity.

We also showed by AFM that the vapor phase modification of native silicon oxide by DPDCS results in a patchy surface. We postulated that patches of polydiphenylsiloxane are the result of polycondensation reactions of the DPDCS in regions were the adsorbed water concentration increased due to the surface progressively becoming more hydrophobic with increasing surface modification. Furthermore, it was shown that poly-**R/S** and poly-**S** preferentially adsorbed between the surface patches and the AFM images indicated surface structures associated with dewetting. Both polymers were shown to have a higher affinity for the DPDCS modified surfaces compared to adsorptions performed on silicon-supported monolayers of tris(TMS) and CMDCS.

In our last study, we wanted to see if the amount of adsorbed polymer could be controlled by adjusting the concentration of surface groups that would have a high affinity for poly-**R/S** and poly-**S**. To accomplish this we prepared binary mixed monolayers of tris(TMS) and CMDCS followed by hydrolysis of the methyl ester on CMDCS forming carboxylic acid groups. Adsorption experiments with poly-**R/S** and poly-**S** showed an increase in the adsorbed amount of polymer with increasing carboxylic acid functionality. In addition, when solvent evaporated from the adsorbed films, the films dewetted. The surface structures of the dewetted adsorbed films were dependent on the molecular weight of the polymer, the amount of H-CMDCS present and the stereochemistry (i.e. rigidity) of the polymer.

Notes and References

1. Plueddemann, E. P. *Silane Coupling Agents*; 2nd ed.; Plenum Press: New York, 1991.

2. Leyden, D. E. *Silanes, Surfaces, and Interfaces*; Gordon and Breach Science Publishers: New York, 1986.

3. Horr, T. J.; Ralston, J.; Smart, R. S. C. *Colloids and Surfaces A: Physiochemical and Engineering Aspects 97* **1995**, 183-186.

4. Park, J. M.; Andrade, J. D. *Dynamic Contact Angle Studies of n-Alkyl Derivatized Boro-silicate Glass Surfaces*; Andrade, J. D., Ed., 1988, pp 67-88.

5. Israelachvili, J. N.; Gee, L. G. *Langmuir* **1989**, *5*, 288-289.

6. Menawat, A.; Henry Jr., J.; Siriwardane, R. *Journal of Colloid and Interface Science* **1984**, *101*, 110-119.

7. Herzberg, W. J.; Marian, J. E.; Vermeulen, T. *J. Coll. Int. Sci.* **1970**, *33*, 164-171.

8. Markham, J. L.; LeGrange, J. D.; Kurkjian, C. R. *Plastic Engineering* **1993**, *49*, 27.

9. Hair, M. L. *Silica Surfaces*; Leyden, D. E., Ed.; Gordon and Breach Science Publishers: New York, 1986, pp 25-41.

10. Vandenberg, E. T.; Bertilsson, L.; Liedberg, B.; Uvdal, K.; Erlandsson, R.; Elwing, H.; Lundström, I. *Journal of Colloid and Interface Science* **1991**, *147*, 103.

11. Fadeev, A. Y.; McCarthy, T. J. *Langmuir* **1998**, *14*, 5586-5593.

12. Fadeev, A. Y.; McCarthy, T. J. *Langmuir* **1999**, *15*, 3759-3766.

13. Kallury, K. M. R.; Krull, U. J.; Thompson, M. *Anal. Chem.* **1988**, *60*, 169-172.

14. Bohlen, D. S.; Blum, F. D. *Dynamics of Coupling Agents on Metal Oxides Surfaces*; ACS, Ed.; ACS: San Francisco, 1992; Vol. 66, pp 310.

15. Urban, M.; Koenig, J. L. *Applied Spectroscopy* **1986**, *40*, 13.

16. Tsubokawa, N.; Kimoto, T.; Koyama, K. *Colloid Polym. Sci.* **1993**, *271*, 940.

17. Chen, W.; Fadeev, A. Y.; Hsieh, M. C.; Öner, D.; Youngblood, J.; McCarthy, T. J. *Langmuir* **1999**, *15*, 3395-3399.

18. Fadeev, A. Y.; McCarthy, T. J. *Polym. Prepr. (Am. Chem. Soc.: Div. Polym. Chem.)* **1999**, *40*, 725.

19. Fadeev, A. Y.; Stafford, C. M.; Russell, T. P.; McCarthy, T. J. *Polym. Prepr. (Am. Chem. Soc.: Div. Polym. Chem.)* **1999,** *40*, 603.

20. Fadeev, A. Y.; McCarthy, T. J. *Langmuir* **1999**, *15*, 7238 - 7243.

21. Andrade, J. D.; Smith, L. M.; Gregonis, D. E. *The Contact Angle and Interface Energetics*; Andrade, J. D., Ed.; Plenum Press: New York, 1985; Vol. 1, pp 249-292.

22. Lee, L.-H. *Roles of Molecular Interactions in Adhesion, Adsorption, Contact Angle, and Wettability*; Mittal, K. L., Ed.; VSP, 1993, pp 45 - 96.

23. Padday, J. F. *Spreading, Wetting, and Contact Angles*; Mittal, K. L., Ed.; VSP, 1993, pp 97-108.

24. Good, R. J. *Contact Angle, Wetting, and Adhesion: A Critical Review*; Mittal, K. L., Ed.; VSP, 1993, pp 3 - 36.

25. Thompson, P. A.; Brinckerhoff, W. B.; Robbins, M. O. *Microscopic Studies of Static and Dynamic Contact Angles*; Mittal, K. L., Ed.; VSP, 1993, pp 139 - 158.

26. Chan, C.-M. *Polymer Surface Modification and Characterization*; Hanser Publishers: New York, 1993.

27. Cassie, A. B. D.; Baxter, S. *Trans. Faraday Soc.* **1944**, *40*, 546-551.

28. Goodwin, A. A. *Ph.D. Dissertation*; University of California at Berkeley: Berkeley, 1996, pp 310.

29. Sperling, L. H. *Introduction to Physical Polymer Science*; 2nd ed.; John Wiley & Sons: New York, New York, 1992.

30. Rye, R. R.; Nelson, G. C.; Dugger, M. T. *Langmuir* **1997**, *13*, 2965-2972.

31. Wu, S. *Surface and Interfacial Tensions of Polymers, Oligomers, Plasticizers, and Organic Pigments*; 3rd ed.; Brandrup, J. and Immergut, E. H., Ed.; John Wiley & Sons: New York, 1989, pp 423.

CHAPTER 3

THERMAL DECOMPOSITON OF ADSORBED THIN FILMS OF POLYCARBODIIMIDES

Introduction

Though polymers have excellent bulk physical and chemical properties, they usually lack the surface properties necessary for applications such as adhesives, biomaterials, protective coatings, friction and wear, composites, microelectronics, and thin-film technologies.[1] These applications require surface properties with specific chemical composition, hydrophilicity, roughness, crystallinity, conductivity, lubricity, and crosslinking density. Being able to control the interfacial properties of polymers through surface modification, is an important subject of research which is actively being studied in the McCarthy group, as well as others.[2-12] The success of many of the previously mentioned applications requires easy and cost effective surface treatment techniques. Several popular surface techniques include corona, flame, plasma, vapor deposition, photon irradiation, and chemical etchants.[1,13] Some of these techniques, however, may give rise to unfavorable changes in the bulk properties of the polymer. Therefore, limiting the surface modification to the outermost surface layer is advantageous in many applications.

The goal of this research project was to study whether the concentration and structure of adsorbed thin films of polycarbodiimide on silica can be modified by thermal decomposition. Polycarbodiimides have the ability to thermally decompose back to monomer in near quantitative fashion.[14,15] Therefore, by measuring the rate of thermal decomposition, reaction conditions can be determined that allow the controlled decomposition of an adsorbed thin film of polymer on native silicon oxide. Our objective was to study how variables such as molecular weight, stereochemistry, and how the rate

of decomposition would all factor in both the ability to control thermal depolymerization at a surface, and the effects on polymer surface structure.

Thermal Decomposition of Polycarbodiimides

Overview: Thermal Depolymerization

The tendency of polymers to depolymerize is due to the inherent thermodynamic instabilities that occur above a critical temperature. For example, during some polymerization reactions there is a temperature at which the equilibrium (Eq. 3.1[16,17])

$$Mn^{\bullet} + M \underset{k_{dp}}{\overset{k_p}{\rightleftharpoons}} M_{n+1}^{\bullet} \qquad (3.1)$$

shifts to favor depolymerization. This is called the ceiling temperature, T_c.[18] The rate constant of the reverse reaction k_{dp} is termed depolymerization or depropagation.

Temperature plays an antagonistic role in these polymerizations, where an increase in temperature results in the increase of k_p, while also increasing k_{dp}. Eventually, a temperature (T_c) is reached were k_p is equal to k_{dp} resulting in the cessation of the polymerization. However, the measured critical temperature for an equilibrium reaction is dependent on the concentration of monomer present in the system. Using free energy relationships, it can be shown that polymerization-depolymerization equilibria is a function of the equilibrium monomer concentration $[M]_c$ (Eq. 3.2).[18]

$$\ln[M]c = \frac{\Delta H^{\circ}}{RTc} - \frac{\Delta S^{\circ}}{R} \qquad (3.2)$$

Since for most chain polymerizations, the enthalpic contribution (ΔH°) is exothermic (negative), increasing the temperature shifts the equilibrium to favor increasing monomer

concentration over polymer formation. This is graphically represented by plotting $\ln[M]_c$ versus 1/T which results in a negative linear slope of $\Delta H°/R$ and an intercept of $-\Delta S°/R$. This means that for every monomer concentration there is an associated ceiling temperature at which $[M] = [M]_c$. Reports of a single ceiling temperature are usually for pure monomer systems.

The above discussion focused on the effects that monomer concentration and temperature have on the active chain end of the growing polymer. Dead polymer chains, in which the active site is quenched, are stable and usually require high temperatures to initiate decomposition. Some polymers upon thermal decomposition produce active chain ends that favor depolymerization to monomer in near 100% yield. Examples of common polymers with this property are polymethylmethacrylate, polyα-methylstyrene, polytetrafluoroethylene, polyvinylidene cyanide, and polymethacrylonitrile.[19,20]

Whether a vinyl polymer completely depropagates to monomer depends essentially on the chemistry of the substituents.[19] Referring to scheme 3.1, polymers where the X and Y substituents are hydrogen, do not depolymerize to monomer due to extensive chain transfer by hydrogen extraction (e.g. polyethylene). In the case where X is a proton, the nature of Y is responsible for the amount of monomer formed upon depolymerization (e.g. polypropylene, polystyrene, and polymethylacrylate). For this case also, extensive chain transfer by hydrogen extraction limits the amount of monomer formation. It is the cases where X and Y are not protons, depolymerization can result in high yields of monomer. For this situation, the extent of hydrogen transfer is controlled by the nature of X and Y.

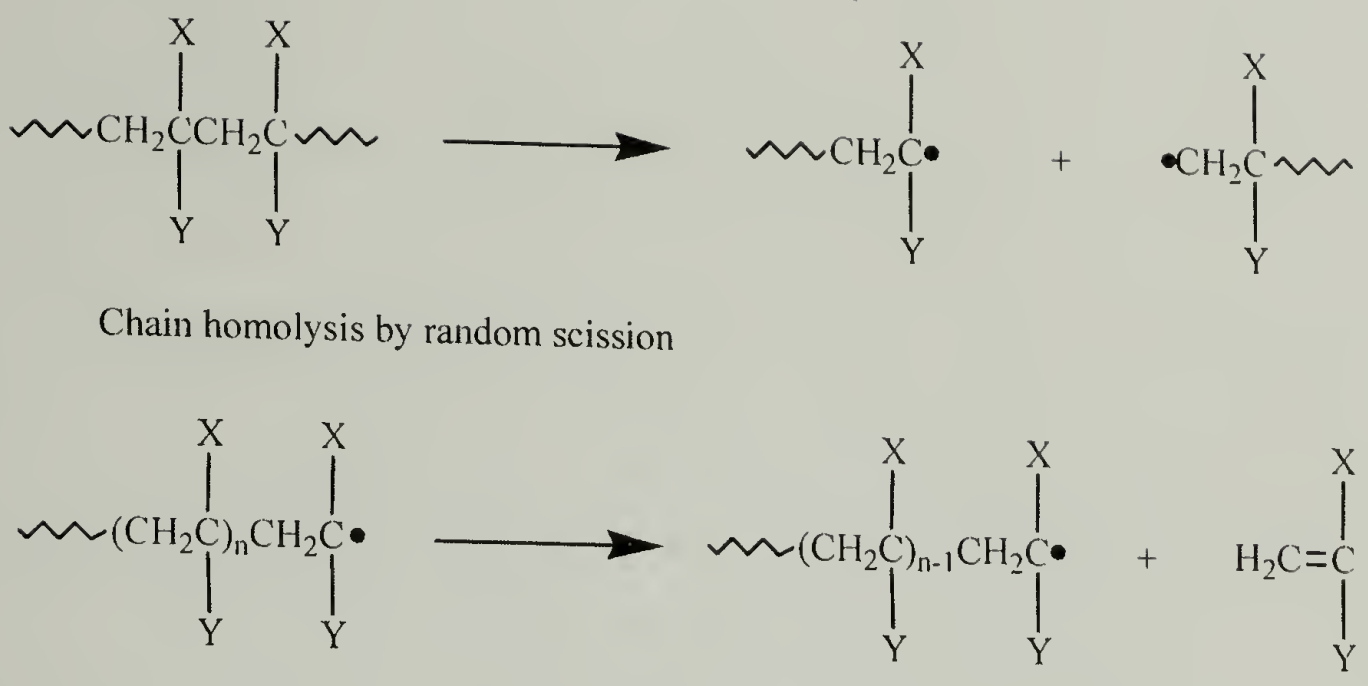

Scheme 3.1. Thermal depolymerization pathway for vinyl polymers.

Depolymerization of Polycarbodiimides

One of the salient features of polycarbodiimides is their ability to thermally depolymerize to monomer. Robinson,[21] was, to the best of our knowledge, the first to explore the polymerization of carbodiimides. Polymerization by cationic and radical techniques proved unsuccessful, but anionic techniques were successful in polymerizing aliphatic carbodiimides in good yields (60-96%). Side reactions of chain transfer and termination limited the polymers to very low molecular weights. One interesting observation was that these polymers would thermally depropagate to the original monomer.

The Novak group showed that the controlled polymerization of carbodiimide monomer is possible using transition metal initiators which attenuate the activity of the anionic growing chain end.[22-24] These reversible reactions have ceiling temperatures ranging between 60-160 °C. Generally, it was found that primary-primary, primary-secondary, and aromatic carbodiimides could be polymerized. However, either monomers with a tertiary center or two secondary centers were found not to polymerize.

Also found not to polymerize is carbodiimides with β-branches on both substituents (e.g. 1,3-di-(2-ethyl-n-hexyl)carbodiimide). The thermal degradation characteristic of polycarbodiimide, polymerized by the Novak group methodology, was found consistent with Robinson's observations. Utilizing this thermal decomposition property, Goodwin[14,15] was able to elucidate some of the finer polymerization issues associated with the regiochemistry of monomer addition and the copolymerization behavior.

Polycarbodiimides are believed to thermally depolymerize by a radical chain scission mechanism.[14,15] Differential scanning calorimetry measurements were used to help elucidate the mechanism. Three samples of poly(*N*-methyl-*N'*-(-(R)-(+)-α-phenylethyl)carbodiimide) (poly-**R**) were prepared where sample B contained the radical initiator AIBN (2,2'-azobisisobutyronitrile), sample C contained the radical scavenger BHT (2,6-di-tert-butyl-4-methylphenol), and sample A was neat poly-**R**. The resulting thermograms are shown in figure 3.1.[15]

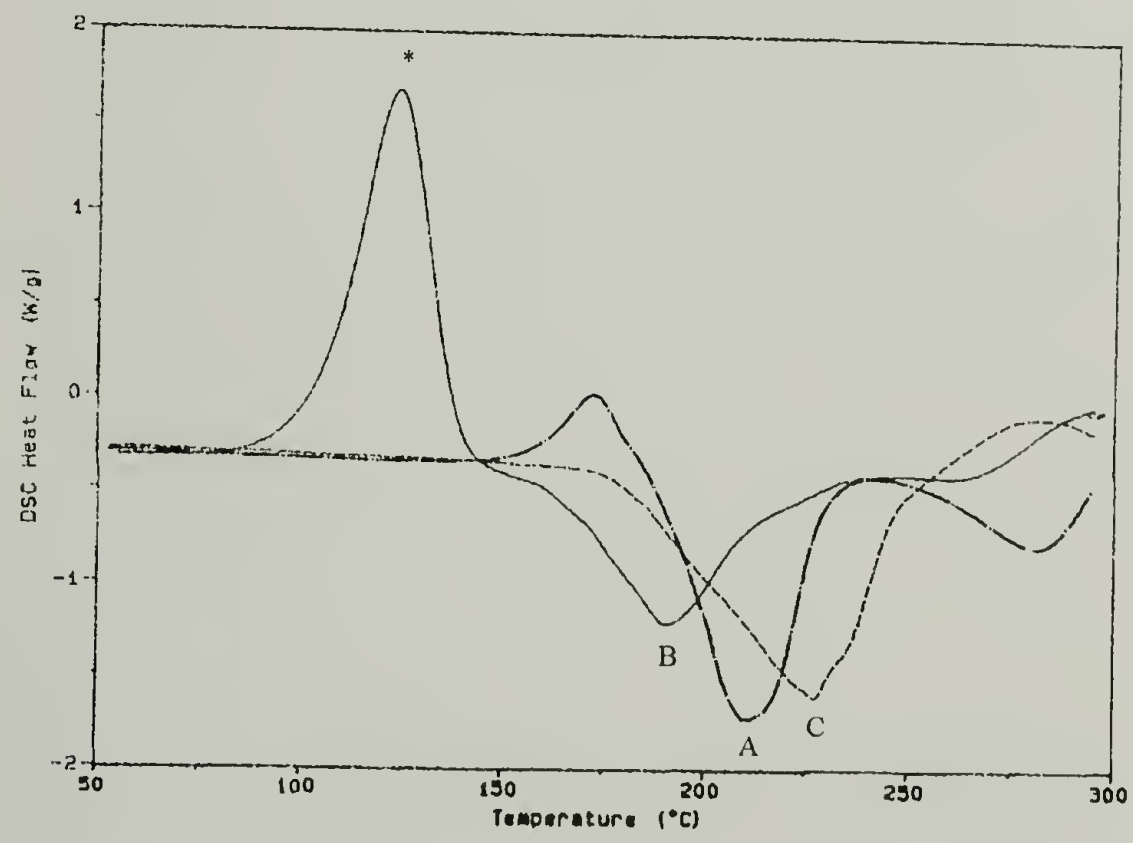

Figure 3.1. DSC thermograms of poly-**R** (A), poly-**R** + AIBN (B), and poly-**R** + BHT (C). (The exothermic peak (*) associated with the decomposition of AIBN)[15]

The thermograms support the radical mechanism because the onset of thermal depolymerization is lowered by the addition of a radical source (AIBN), whereas the addition of a radical scavenger (BHT) resulted in an increase of the onset temperature. Homolytic chain scission along the polycarbodiimide backbone would result in the formation of amidinate[25] and imidoyl[26-28] radicals. The formation of these active chain ends most likely initiates the depropagation along the backbone (Fig. 3.2).

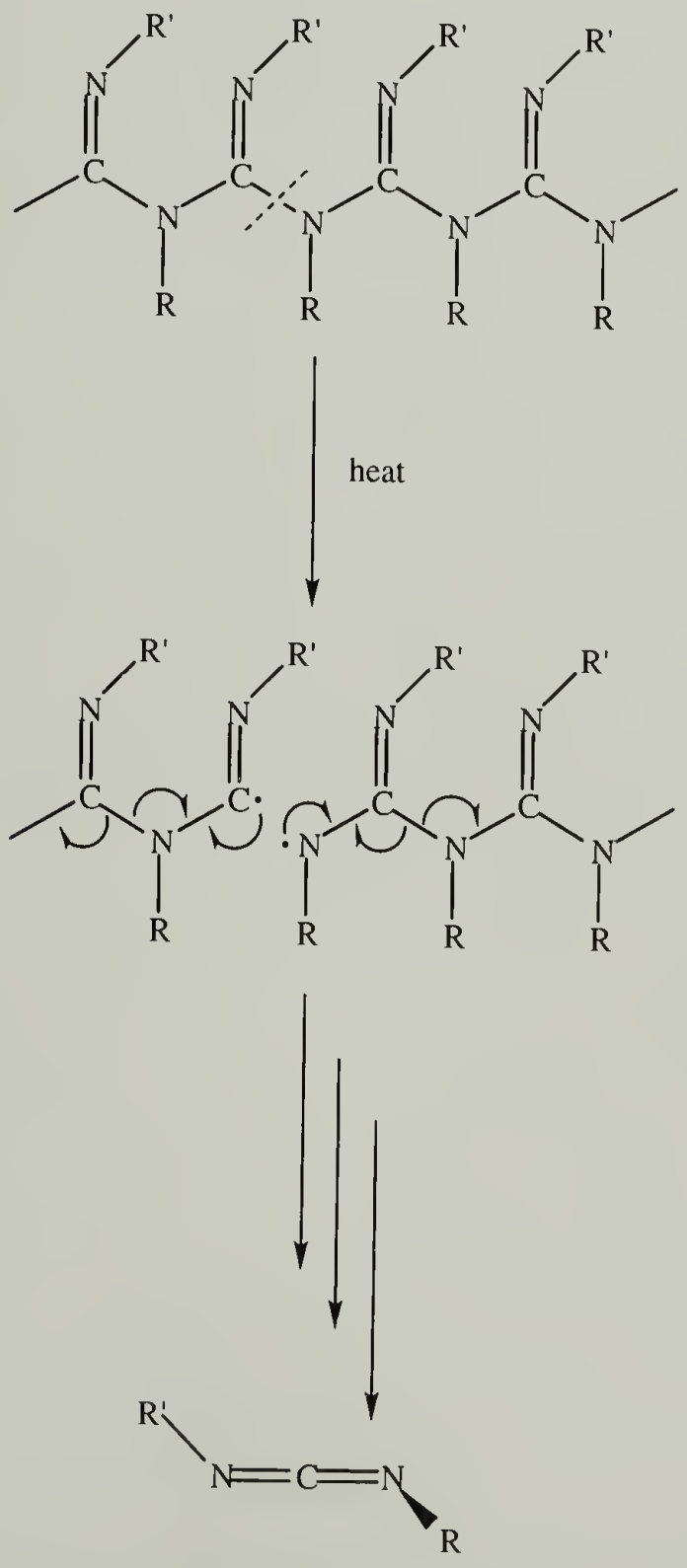

Figure 3.2. Thermal depolymerization mechanism for polycarbodiimides.

Thermal degradation kinetics

The thermal degradation of polymers is often a complex process involving several stages of reactions.[19] Attempts have been made to correlate polymer degradation processes by reference to bond energies and the pyrolysis behavior of related structures in small molecules. The conclusions made from these correlations can be incorrect because they lack consideration of how the long chain character of polymers can provide possibilities for several decomposition reactions which can proceed along the chain or between adjacent monomer units in the chain. Another important consideration is that polymers may contain many structural irregularities which are often the initiation points of the degradation process. With the potential for numerous reactions during the thermal decomposition of a polymer, measuring the kinetics can be a difficult task. For example, the analysis of degradation kinetics is usually obscured by the competition between kinetic processes.[29]

There are a number of variables that can bring about the deterioration of polymers. Most of these variables are associated with the environmental conditions of the experiment and sample preparation.[30,31] Examples of variables include: temperature, pressure, radiant flux, partial pressures of contiguous gases and vapors such as oxygen and water, both internal and external catalyst, mechanical stress, and others.[29] Careful interpretation of experimental results requires recognition and control of the variables which affect the degradation process.

Methods of Study

There are several analytical methods that are applicable to measuring thermal degradation events and comprehensive reviews can be found in texts by Turi[32] and Wendlandt.[30] The thermal decomposition of a polymer generally involves four main products. These are (a) permanent gases (H_2, CH_4, and CO); (b) condensable gases and liquids; (c) low volatility materials (e.g. dimer, trimer, etc.); and (d) the solid nonvolatile

residues such as char.[19] The choice of analytical method depends on which product(s) need to be measured. Examples of techniques used to measure the kinetics of thermal decomposition are gel permeation chromatography,[33-35] differential scanning calorimetry,[36] mass spectroscopy[36] and thermogravimetry.[29,35-38] For the purpose of the research proposed here, only thermogravimetry (TGA) and FTIR were used to analyze the depolymerization of polycarbodiimides.

Thermogravimetric Analysis (TGA)

Thermogravimetric analysis measures the mass change (mass-loss or gain) of a sample as a function of temperature or time. The three modes of thermogravimetry commonly used are: (a) isothermal (mass change as a function of time at constant temperature); (b) quasi-isothermal (sample is heated to constant mass at each of a series of increasing temperatures); (c) non-isothermal or dynamic (mass change as a function of temperature).[30] The major disadvantage in TGA experiments is that the measured data is mostly of an empirical nature. Only the change in mass is quantitative, whereas the mass-change versus temperature (or time) curves are dependent on instrumental and sample parameters. Therefore, care should be taken not to interpret the TGA curve as fundamental to the polymeric material.

Environmental Conditions

The two most widely studied environmental variables for TGA experiments are atmosphere and heating rate.[30] Atmospheric conditions can be either static or dynamic. Static atmospheres (fixed) are not favored for reactions where the gaseous degradation products are reversible. The concentrations of these products surrounding the sample increase with temperature and shift the equilibrium resulting in a reaction rate decrease. To improve accuracy in measuring the rate of degradation of reversible reactions, dynamic atmospheres (flowing) are used to limit the gaseous degradation products near

the sample. Care must be employed in choosing an atmosphere for thermal studies. The chemistry of the atmosphere can be inert (N_2 (g)) or reactive with the sample (e.g. air). Therefore, the choice of an atmosphere requires knowledge about the degradation mechanism for the material being studied.

The heating rate also has an effect on the extent of decomposition.[19,29,30] Generally, decomposition is greater at a low rate of heating than for a similar sample heated at a faster rate. Therefore, it is important to perform non-isothermal experiments at different heating rates. For example, early in the degradation process a polymer may undergo side group elimination reactions resulting in a modified polymer that fragments as the temperature is increased. This behavior may be influenced by the rate of heating.

McNeill,[19] summarized the optimum experimental conditions for kinetic measurements of polymeric materials as involving a very thinly distributed sample, rapid temperature equilibration, mild isothermal conditions in which the product composition remains constant, dynamic atmosphere, and monitoring of a degradation product as a means of establishing the initial rate at each temperature. The choice of degradation product to monitor should ideally, only be generated by a single mechanism. If more than one mechanism is possible, the measured kinetics may be misleading. For the purpose of the research presented here, only the rate of decomposition was measured. With this rate data, relative amounts of polymer were decomposed and the effects on surface structure were analyzed.

Experimental Section

Polymers

Polycarbodiimides used in this study were prepared following procedures as previously described in Chapter 1 of this dissertation. The three polycarbodiimides evaluated here were poly-**HC** (poly(di-*n*-hexylcarbodiimide)), poly-**R/S**

(poly(*N*–methyl–*N'*–((±)-α-phenylethyl)carbodiimide)), and poly-**S** (poly(*N*–methyl–*N'*–((-)-α-phenylethyl)carbodiimide)). The molecular weight of each polymer is represented by the monomer:catalyst ratio and reported for example, as 496:1. For polycarbodiimides, the difficulties in determining the molecular weight and polydispersity were detailed in Chapter 1 of this dissertation.

Rate of Decomposition by Thermal Real-time Reflective-absorbance Infrared Spectroscopy

Determination of the rate of decomposition by FTIR was performed using a custom designed horizontal thermal stage inserted into a Matson Polaris FTIR. The thermal stage was designed and manufactured at Markem Corporation in Keene, New Hampshire, and a general layout diagram of the laser path is shown in Figure 3.3. Sample preparation was performed by casting 5%-10% solutions of polymer dissolved in THF onto brass 360 (Cu = 61.5%, Zn = 35.4%, Pb = 3.1%) shims. Prior to casting, the brass shims were cleaned by sonication in acetone followed by submersion in both MEK and hexane. After casting, the films were dried under vacuum in a bell jar desiccator. The dried films were approximately 5 microns thick at a minimum coverage of 1.5 square inches. The sampling rate of the FTIR was set at 4 scans per second at 4 cm^{-1} resolution and each data point represents the average of 50 scans. Temperature was computer controlled (isothermal or dynamic) by adjusting the voltage applied to the heater. The precision in temperature control at 3 °C/min heating rate is shown in Figure 3.4 which is a plot of temperature with time. The curvature seen from t = 0 seconds (25 °C) to t = 500 seconds (50 °C) was believed to be a result of a voltage surge when the analysis was initiated. However, in all cases the temperature stabilized at 50 °C at 3 °C/min heating rate. Once stabilized the heating profile is linear where in Figure 3.4 the profile ended at 190 °C.

Decomposition experiments were performed by placing the coated brass shim onto the thermal stage followed by entering the temperature profile data into the

computer. It should be noted that the software controlling the temperature and data collection was written by Markem software engineers. For all cases using the FT-IR thermal stage, during decomposition the polymer was exposed to ambient environmental conditions, therefore water (3250 cm^{-1} and 1596 cm^{-1}) appeared in all spectra. An interesting observation was the amount of water that remained during experiments especially when the samples exceeded 100° C. It was found that at ambient conditions water vapor condensed on the zinc selenide lenses in the hot cell and as the sample was heated, these lenses would become warm yet never reach temperatures exceeding 100° C. Thus, for each experiment performed using the FT-IR thermal stage there was a reduction, but not elimination, in water during the entire run cycle. An attempt to nitrogen purge the hot cell resulted in large temperature fluctuations, thus this technique was abandon.

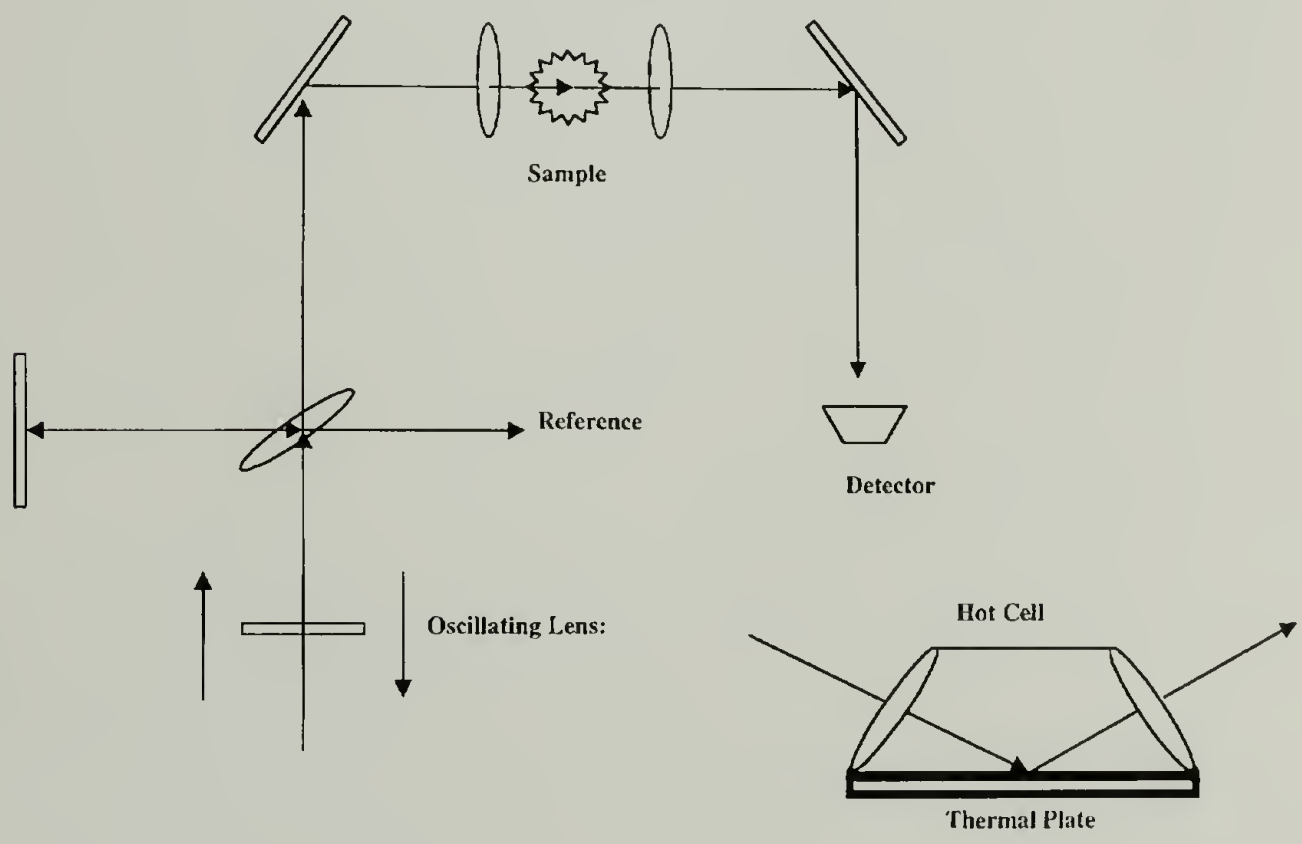

Figure 3.3. General layout diagram of the thermal real-time reflective-absorbance FTIR Hot Cell stage used to determine the rate of decomposition for polycarbodiimides.

Measuring the decomposition rates was accomplished by monitoring the loss with time or temperature, in guanidine intensity between 1625 cm^{-1} and 1645 cm^{-1}. In addition to the loss in guanidine vibrations, there was an increase in carbodiimide vibrations around 2130 cm^{-1}. The loss of guanidine and gain in carbodiimide are shown in Figure 3.5 which is the before and after spectra of 496:1 poly-**HC** heated from 25 °C to 223 °C. Associated with Figure 3.5 is both the graph in Figure 3.6 showing the loss of guanidine intensity with heating and the graph in Figure 3.7 showing the gain in carbodiimide vibrations with heating.

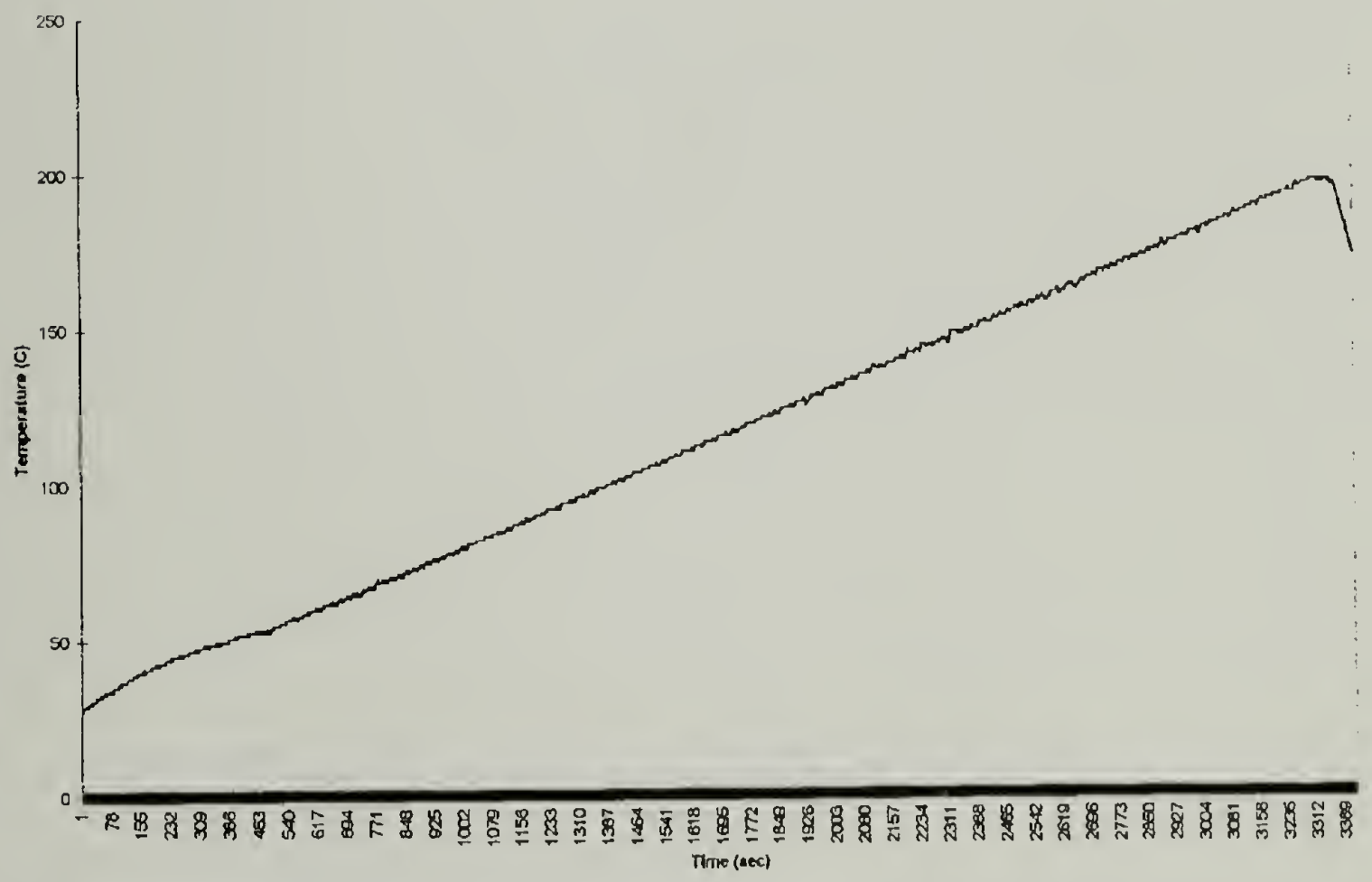

Figure 3.4. Real-time thermal FT-IR temperature profile at 3 °C/min.

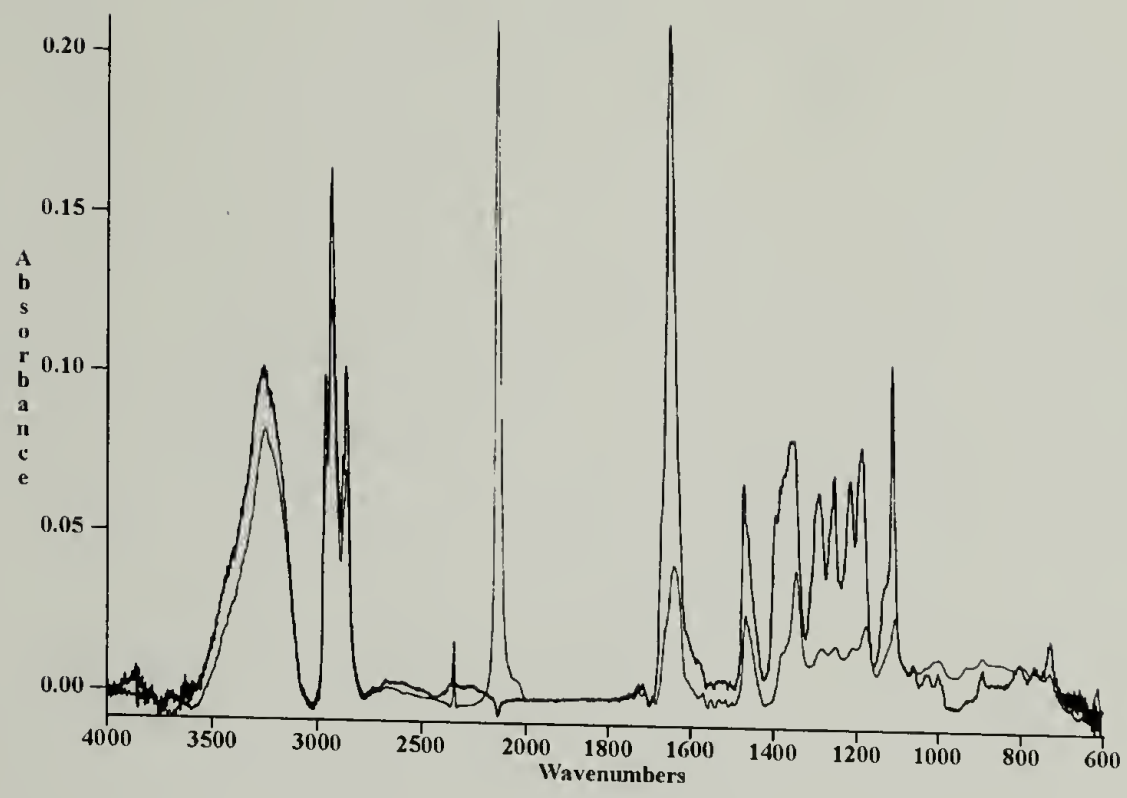

Figure 3.5. Example spectra from real-time thermal cell decomposition of 469:1 poly-**HC** at 3 °C/min. heating rate; bold spectrum at time 0 min. and the light spectrum taken at time 58 min. (T ~ 200 °C)

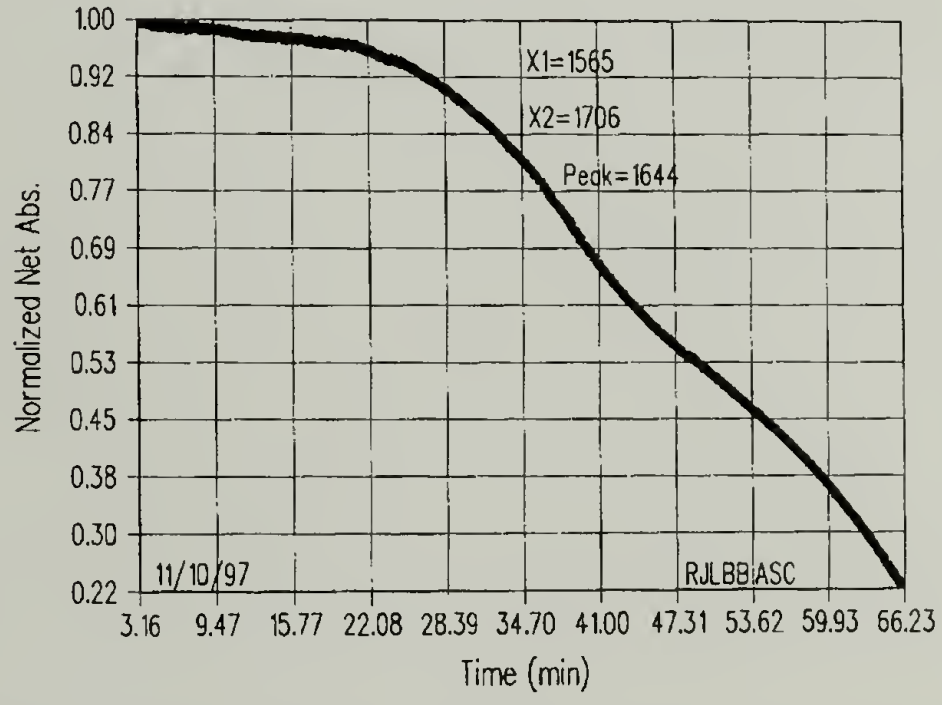

Figure 3.6. Loss of guanidine absorbance (1644 cm^{-1}) during the thermal decomposition of (monomer:catalyst) = 469:1 poly-**HC** as measured by real-time thermal FT-IR, rate 3 °C/min.

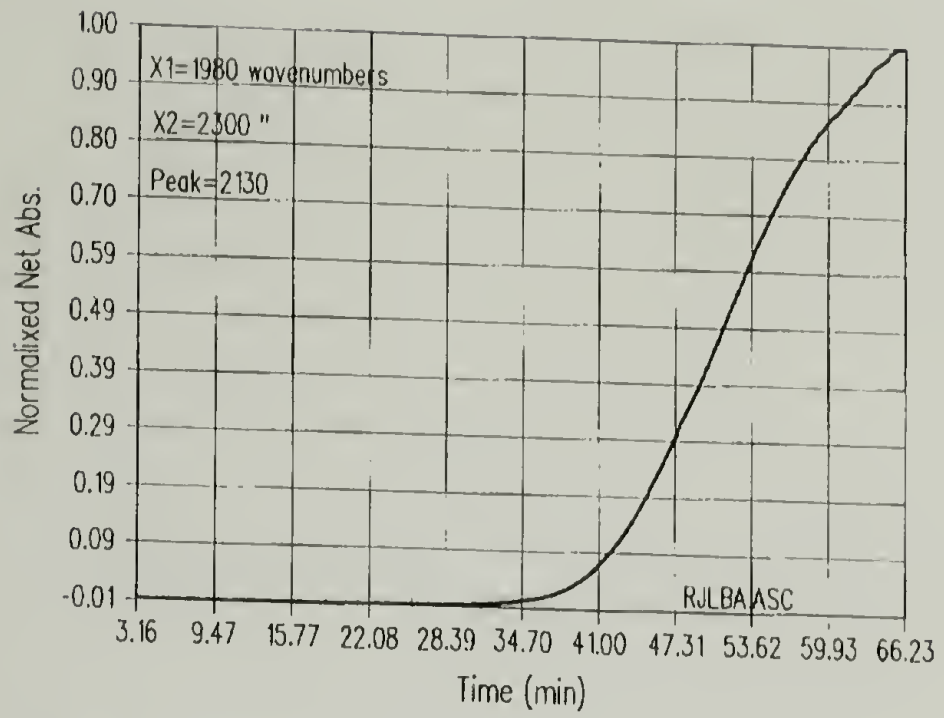

Figure 3.7. Gain in carbodiimide absorbance (2130 cm^{-1}) during the thermal decomposition of 469:1 poly-**HC** as measured by real-time thermal FT-IR, rate 3 °C/min.

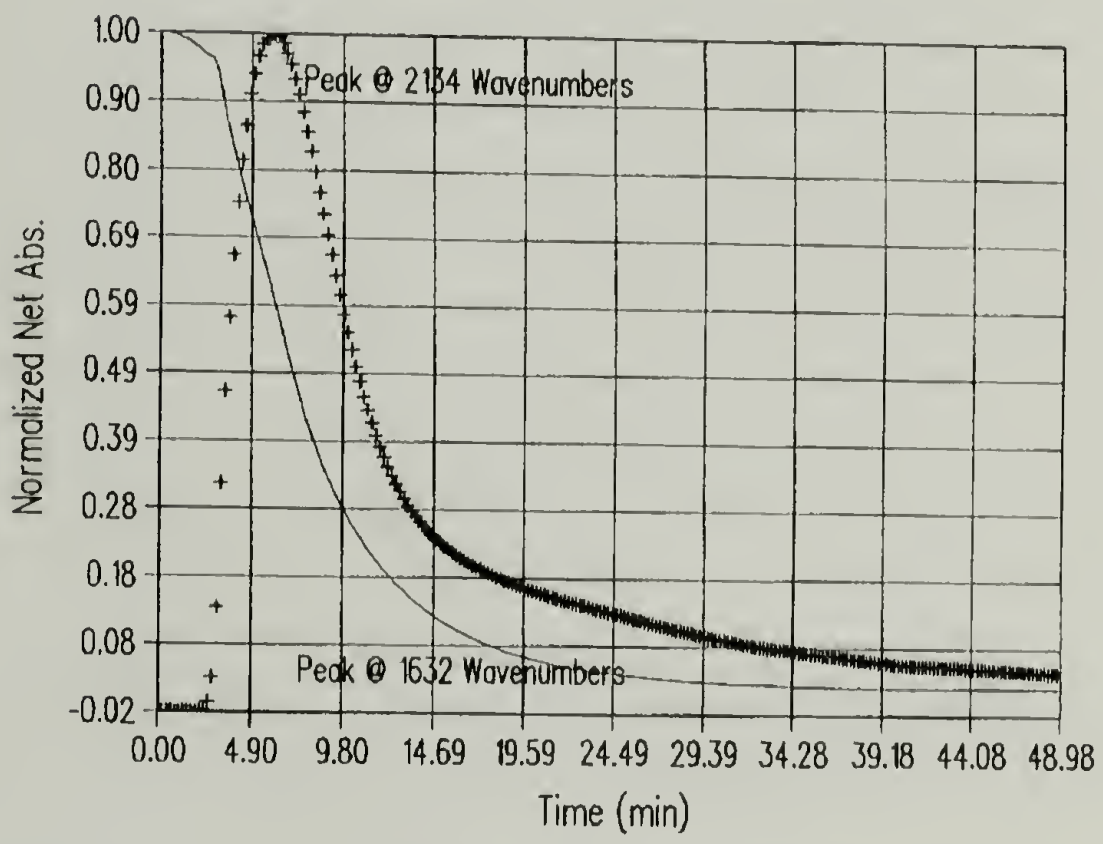

Figure 3.8. Loss of guanidine absorbance (1644 cm^{-1}) and gain in carbodiimide absorbance (2134 cm^{-1}) during the thermal decomposition 1560:1 poly-**R/S** as measured by real-time thermal FT-IR, rate 3 °C/min.

Rate of Decomposition by Thermal Gravimetric Analysis (TGA)

Rates of thermal decomposition for the polycarbodiimides studied here were also measured by TGA using a Perkin-Elmer System 7 TGA controlled by Perkin-Elmer Pyris software. Loading the polymer into the TGA pan was very difficult for two reasons. First, the lyophilized polymer was very light and fluffy, therefore making it difficult to load the pan. In addition, the second issue, static charging of the polymer in the pan would result in the partial loss of sample due to electrostatic interactions. This became more of a problem when the nitrogen purge turned on in the TGA analysis chamber. To overcome these issues, the samples were allowed to stabilize (measured weight) in an air purge, followed by switching the purge gas to nitrogen. After the nitrogen was turned on, the sample was again allowed to stabilize and at that point, the weight of the sample was recorded. The decomposition onset temperature for each polymer was measured by heating samples at 10 °C/min followed by calculating the trigger temperature (T_d) by using an algorithm in the Pyris software. Measurement of the decomposition rates was calculated from data generated during isothermal decompositions.

Decomposition of an Adsorbed Film of Polycarbodiimide

Adsorbed films of polycarbodiimide on a silicon wafers were decomposed by placing the wafer on a glass dish resting on a clean heating element. The test temperature was measured with a pyrometer using a J-type thermocouple. After placing the test wafers on the glass, the whole dish was covered with a funnel connected to a Tygon hose, connected to an argon source. The Ar (g) was allowed to flow at very low rate over the surface of the wafer. This was done to ensure an inert atmosphere around the surface of the wafer as well as to provide a mechanism for carrying away the volatiles from the interfacial region of the sample. In addition, the temperature of the glass surface that the wafers rested on was monitored, and no effect of Ar (g) purge on temperature was observed.

Results and Discussions

Decomposition by Real-time Thermal FT-IR

Measurements of the decomposition rates for the polycarbodiimides were first performed by real-time FT-IR thermal analysis. Plots of the data collected are shown in Figures 3.9-3.11 for 496:1 poly-**HC**, 1560:1 poly-**R/S**, and 4681:1 poly-**R/S**, respectively. These graphs were generated by plotting the normalized absorbance against time. For all conditions, the data indicates a temperature dependent rate of decomposition suggesting that the amount of decomposition could be controlled. However, in calculating the rate of decomposition from the IR data, some issues with the real-time IR technique became evident. In Table 3.1 are listed the rates of decomposition at isothermal conditions generated from the plots in Figures 3.9-3.11. These rates represent the largest loss rate of guanidine absorbance at each isothermal condition because the plots generally showed varying amounts of curvature where different loss rates could be calculated. For each run, there was an initial fast loss of guanidine absorbance that may be associated with annealing and thickness changes in the adsorbed film. Moreover, this initial loss rate was more apparent at lower temperature conditions, where at higher temperature conditions the changes in film thickness probably occurred during the heating of the sample. Since the amount of absorbance is a function of path length i.e. thickness (Beer's law), then during the decomposition the adsorbed film thickness lessens. This decrease in film thickness with time may be responsible for the curvature seen in the plots.

Besides thickness changes during the analysis, there were other events that may have affected the results. For example, volatile decomposition products trapped within the hot cell. As previously mentioned, an attempt to purge the volatile materials from the hot cell was not successful because large temperature fluctuations were observed as the nitrogen gas flowed across the sample thereby cooling the surface. Carbodiimide was the

most observed volatile in the hot cell, and after each run the zinc selenide lenses were coated with condensed carbodiimide. Another issue was the amount of water present in the hot cell environment that could react with carbodiimide forming urea solids on the surface of the sample. Moreover, carbodiimide could react with condensed water vapor on the zinc selenide lenses forming urea; but if formed, the amount was small because it was not observed in the IR spectra. Generally, to ensure the surface is not contaminated from decomposition products reacting with the environment (i.e. air and moisture), the experiment should be performed in an inert atmosphere. In addition, the effect of thickness changes upon decomposition potentially resulting in the curvature of the data suggested that a different technique be used to measure decomposition rates. Therefore, TGA was chosen to measure the weight loss of polycarbodiimide in an inert atmosphere from which the data was used to calculate the decomposition rate.

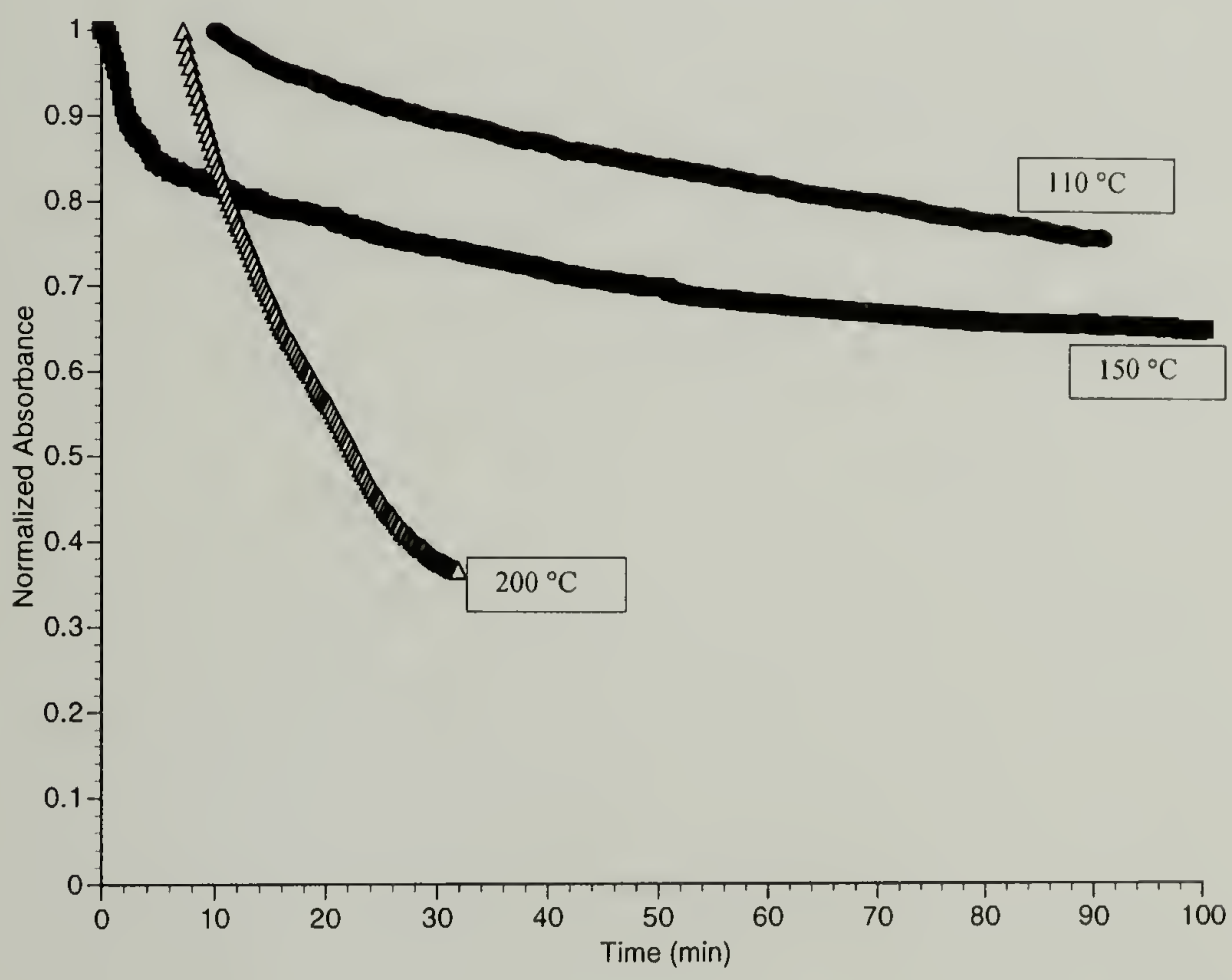

Figure 3.9. Loss of guanidine absorbance (1642 cm^{-1}) during the isothermal decomposition of 469:1 poly-**HC** as measured by real-time thermal FT-IR.

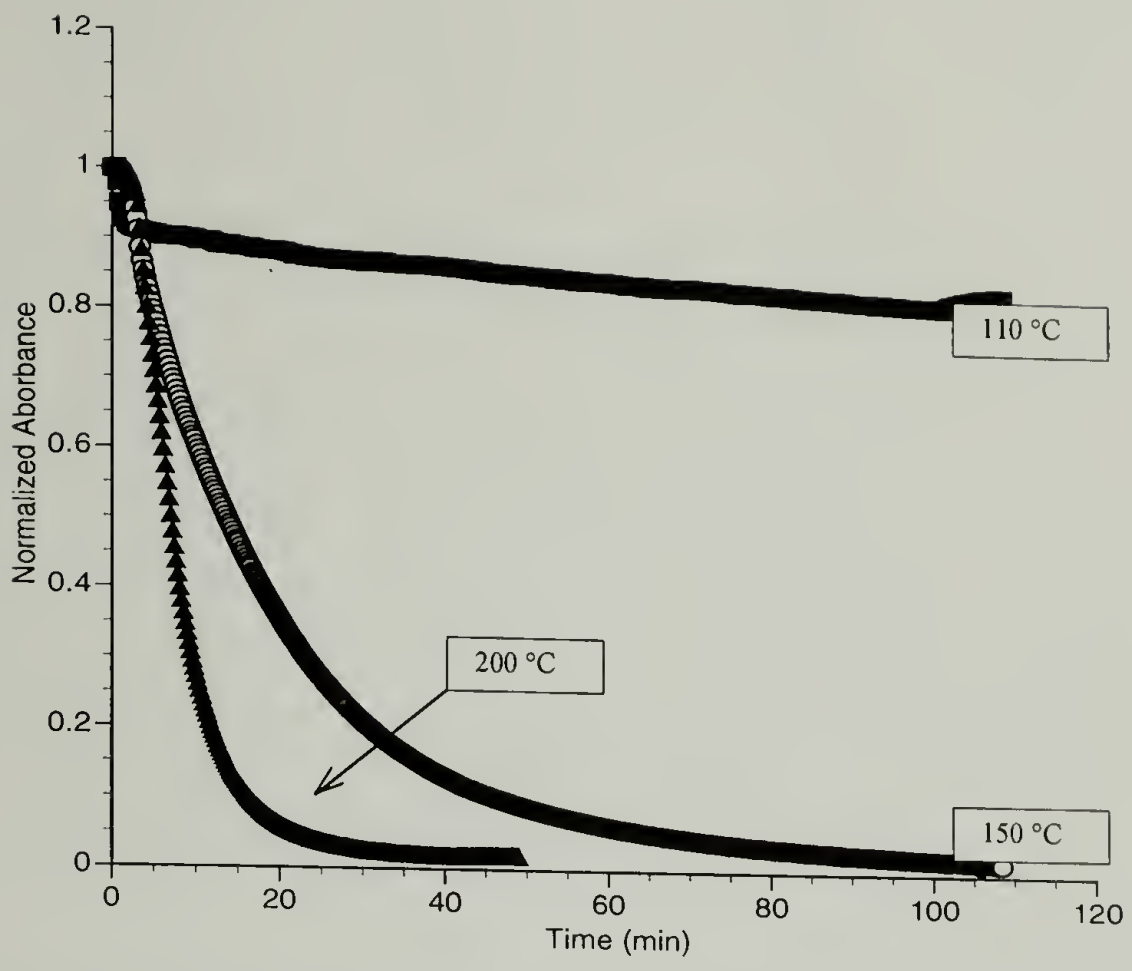

Figure 3.10. Loss of guanidine absorbance (1644 cm^{-1}) during the isothermal decomposition of 1560:1 poly-**R/S** as measured by real-time thermal FT–IR.

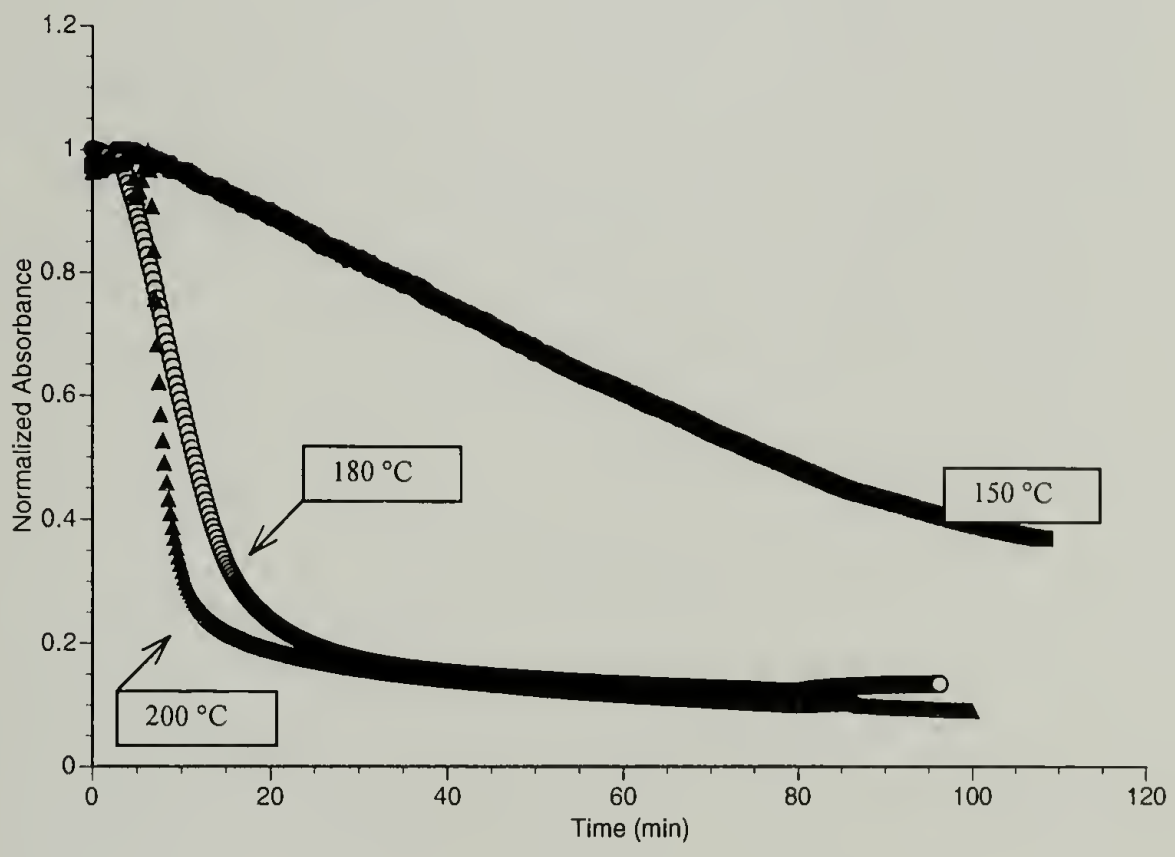

Figure 3.11. Loss of guanidine absorbance (1644 cm^{-1}) during isothermal decomposition of 4681:1 poly-**R/S** as measured by real-time thermal FT-IR.

Table 3.1. Highest decomposition rates for polycarbodiimides calculated from the normalized loss of guanidine absorbance over time during isothermal decomposition by real-time thermal FT-IR. Values are in loss in absorbance per minute.

Polymer	110 °C	115 °C	150 °C	180 °C	200 °C
496:1 poly-**HC**	0.1	-	0.3	-	5.2
1560:1 poly-**R/S**	-	0.1	-	3.2	11.0
4681:1 poly-**R/S**	-	-	0.7	6.2	26.0

Decomposition by Thermogravimetric Analysis

The majority of the adsorption work described in this dissertation focused on poly-**R/S** and poly-**S**. Since the results for adsorptions from THF showed dewetting, it became apparent that in order to study the thermal decomposition changes in a thin film of adsorbed polymer, it would be best if the initial surface was uniform. Thus, this limited the study to poly-**R/S** because adsorptions of this polymer from toluene resulted in structurally uniform adsorbed films. Goodwin[15] showed by TGA a 30° C difference in the onset of decomposition between poly-**R/S** and poly-**R**. For comparison, TGA was used to measure the difference between poly-**R/S** and poly-**S** and to study if molecular weight had an effect. The results of this study are listed in Table 3.2 with an example TGA thermogram shown in Figure 3.12. The data indicates an approximately 13 °C difference between poly-**R/S** and poly-**S** in the onset of decomposition (T_d). It should be noted that the method used in this study for determining the onset temperature was the trigger temperature algorithm used in the Pyris software. In the work by Goodwin, they do not discuss their method for determining T_d therefore, differences in T_d would be expected. Further, the data in Table 3.2 indicates no significant molecular weight effect on T_d.

Continuing with the work performed using the real-time thermal FT-IR, the decomposition rate for both 1560:1 and 4681:1 poly-**R/S** was calculated using TGA analysis. Graphs of the percent weight loss as a function of time (at isothermal

conditions) for 1560:1 and 4681:1 poly-**R/S** are shown in Figures 3.13 and 3.14 respectively. The calculated decomposition rate at each temperature is listed in Table 3.3 and the rates were acquired within the region of largest amount of weight loss.

As mentioned in the introduction, TGA analysis is mostly of an empirical nature therefore, care must be taken in interpreting the results as fundamental to the polymer. The results suggested that at temperatures below T_d the rate of decomposition was very slow and samples would take hours to prepare. Therefore, the temperature of 180 °C was chosen to decompose an adsorbed film of poly-**R/S** on silica. In addition, since no significant difference in T_d with molecular weight was shown, the polymer chosen to prepare the adsorbed layers was the 936:1 poly-**R/S**.

Table 3.2. Thermal decomposition temperature of both poly-**R/S** and poly-**S** as a function of molecular weight (monomer: catalyst), measured by thermogravimetric analysis at a heating rate of 10 °C/min.

Sample	Trigger Temperature
312:1 poly-**R/S**	159 °C
936:1 poly-**R/S**	158 °C
312:1 poly-**S**	172 °C
936:1 poly-**S**	170 °C
3121:1 poly-**S**	173 °C

Table 3.3. Decomposition rates for polycarbodiimides calculated from the percent weight loss over time during isothermal decomposition by TGA. Values are in percent weight loss per minute (%/min).

Polymer	115 °C	130 °C	150 °C	180 °C	200 °C
1560:1 poly-**R/S**	0.05	0.14	-	5.23	12.04
4681:1 poly-**R/S**	-	0.04	0.16	1.46	4.69

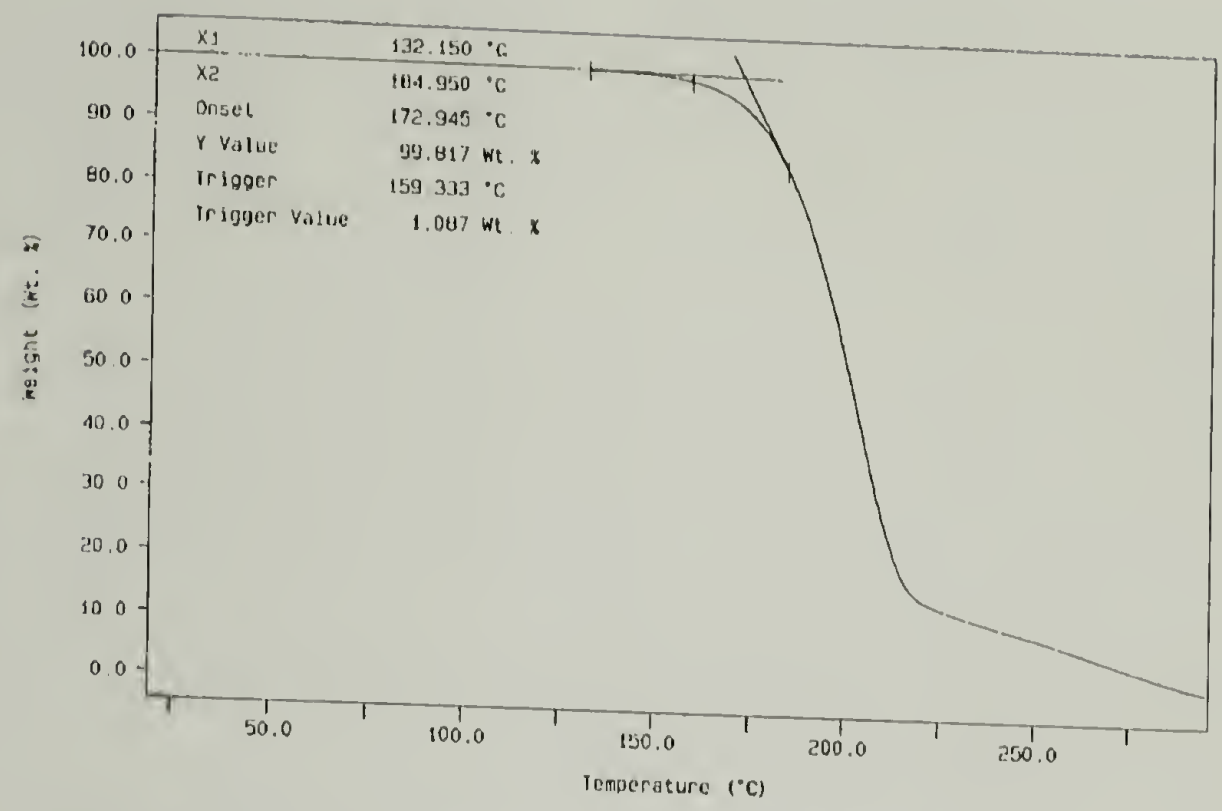

Figure 3.12. Plot of the loss of weight as a function of temperature of 312:1 poly-**R/S** heated at a rate of 10 °C/min in a TGA. An example of the trigger temperature, Td, used to acquire the data in Table 3.2.

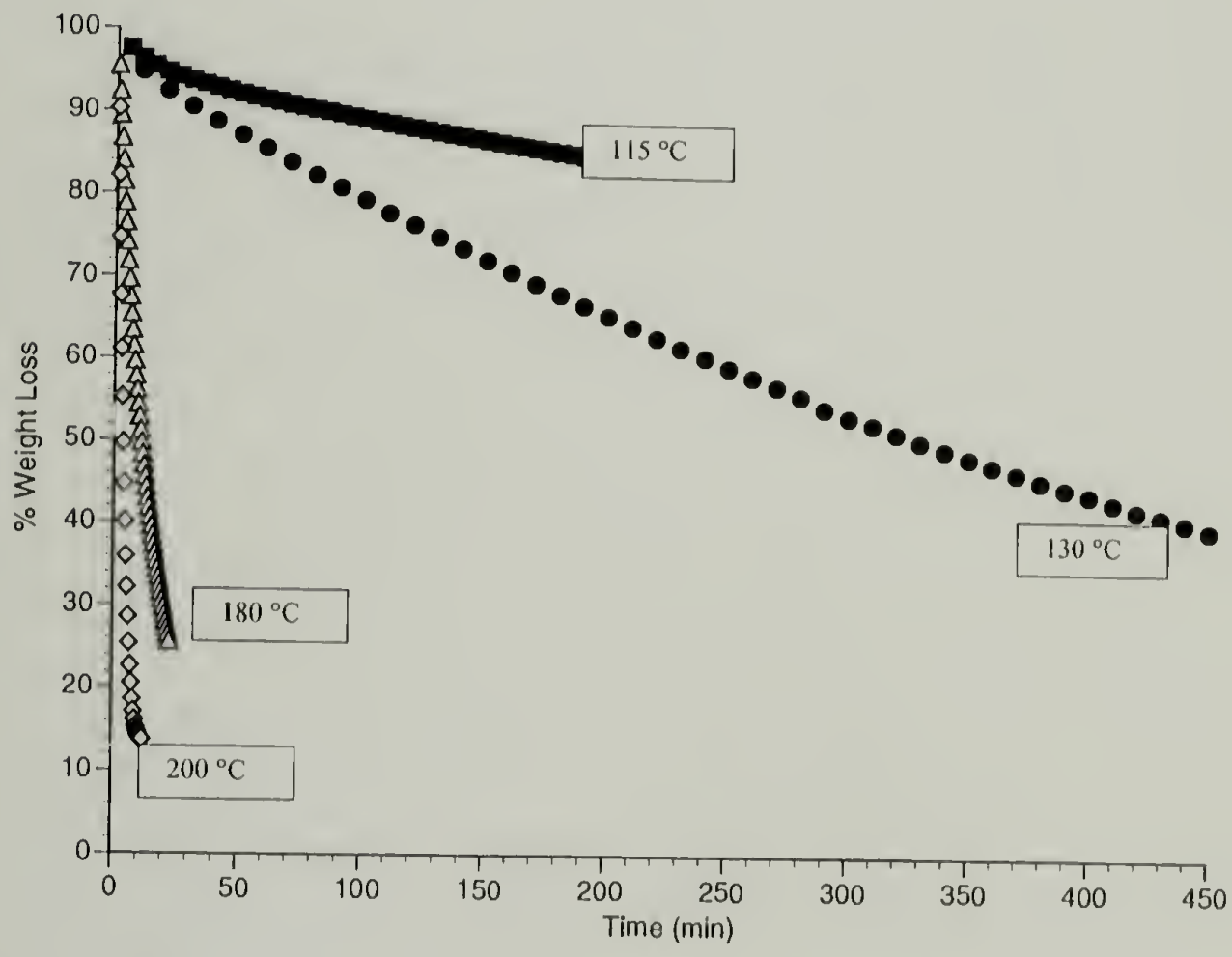

Figure 3.13. Plot of the loss in weight of 1560:1 poly-**R/S** over time as measured by isothermal thermogravimetric analysis.

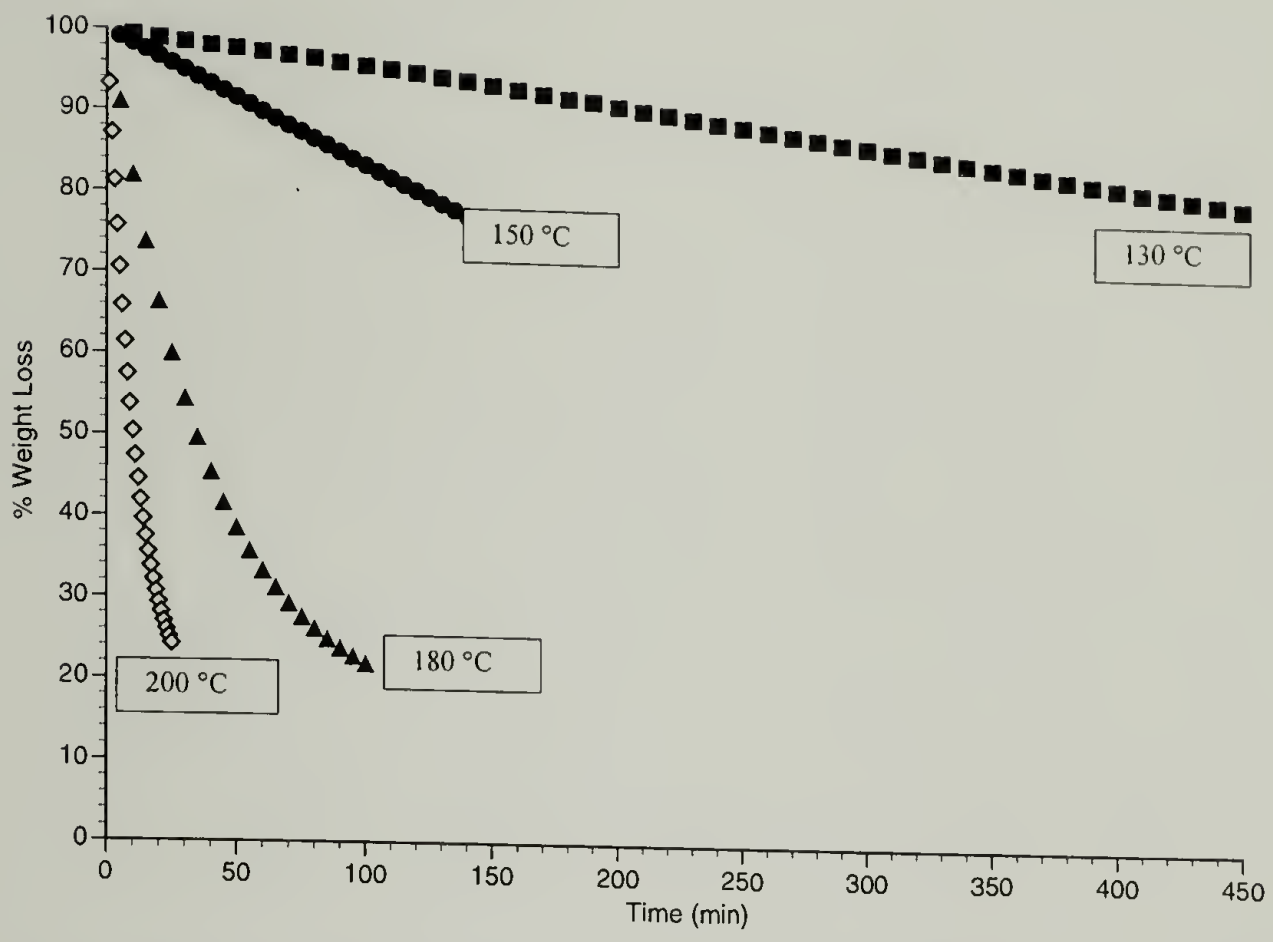

Figure 3.14. Plot of the percent weight loss of (monomer:catalyst) = 4681:1 poly-**R/S** over time as measured by isothermal thermogravimetric analysis.

Analysis of Decomposed Films

Two methods were studied for following poly-**R/S** decomposition. The first method followed the decomposition of the same adsorbed film as it was subjected to repeated exposures at temperature. The second method followed several different samples of adsorbed polymer where each sample was exposed for specific periods at temperature. After experimenting with both methods, the second method was chosen because the sample would only be analyzed once by water contact angle and AFM. Moreover, analysis of the decomposed adsorbed films was extremely difficult to perform because for both water contact angle and tapping mode AFM the results indicated that some of the decomposed films were loosely bound to the silica surface. Thus it became difficult to determine the advancing contact angle on decomposed surfaces that was loose

because the angle would change as surface material was absorbed or displaced by the water droplet. Further, the AFM analysis was plagued by artifacts in the images because of loose material collecting on the tip and to make matters worse, the buildup of material on the tip could only be resolved by changing the tip. This becomes very time consuming and potentially expensive.

Two sets of six wafers were prepared by adsorbing 936:1 poly-**R/S** in toluene onto silicon wafers following procedures outlined in Chapter 1 of this dissertation. The first six wafers were exposed to 180 °C where the first wafer was exposed for 4 minutes (n = 4 minutes) and the remaining wafers exposed for (n + 1) minute intervals. Water contact angle analysis for the wafer between 4 minutes and 9 minutes exposure at 180 °C showed little deviation in advancing contact angle compared to the control. However, the receding contact angles for all the samples between 4 minutes and 9 minutes exposure decreased from 80° for the control to 72° ± 3°. Thus, the reduction in receding contact angle was most likely the result of polymer decomposition and/or thermally induced surface restructuring of the adsorbed layer. In addition, AFM analysis of the first six wafers suggested some surface changes occurred with thermal exposure. This is shown in Figures 3.15 and 3.16 which respectively show the AFM image of the control surface prior to thermal exposure and a surface after six minutes of thermal exposure. The surface exposed for six minutes became rougher than the control suggesting decomposition occurred.

The second set of six wafers were exposed to 180 °C, where the first wafer was exposed for 10 minutes (n = 10 minutes), and the remaining wafers exposed for (n + 1) minute intervals. Some interesting results were observed between this exposure time where the samples exposed for the longest period of time showed partial decomposition and the shorter exposure time samples, between 11 minutes and 12 minutes, showed nearly complete decomposition.

Water contact angle results are listed in Table 3.4 where the control is 936:1 poly–**R/S** adsorbed from toluene onto native silicon oxide. Measurement of both the advancing and receding contact angle for samples from 10-12 minutes was difficult, because within seconds, the water droplet would spontaneously advance with the subsequent change in θ_A from approximately 93° to approximately 80°. This indicated that the adsorbed film was loose and dispersing into the water droplet. Therefore, the advancing contact angle measurements reported in Table 3.4 for 10 – 12 minutes represent the averaging of 5 angles with each angle taken within five seconds of the water droplet hitting the surface. The 12-minute sample had a higher advancing contact angle than the control, which indicate the 12 minutes sample surface was rougher. The 11 minute sample had a high static contact angle approaching 100° however, within a couple of seconds the drop would spontaneously advance thus making it very difficult to obtain the initial advancing angle. In addition, the 0° receding contact angle for the 10-12 minutes samples indicate the probe fluid strongly interacted with silica. This confirms that decomposition of the adsorbed polymer film was complete in certain areas or the adsorbed layer was completely dispersed into the water sessile drop. In the case of the 13–15 minute samples, there was no evidence of a loose surface because both advancing and receding contact angles were easy to obtain. In fact, the contact angle data for 13-15 minutes was very similar to the results obtained for the samples between 4-9 minutes. To fully characterize the resulting structure of the adsorbed film after thermal treatment required the use of tapping mode AFM.

Performing AFM analysis on the 10-12 minute samples was very difficult because the surface was loose and easily adhered to the tip, resulting in numerous artifacts in the images. Nonetheless, this was anticipated because water contact angle on these surfaces indicated the surface was loose. In addition, for the 13-15 minute samples, measurement of the water contact angle was easily acquired; therefore, the surface was not as mobile (if at all) as the 10-12 minute samples. Further, tapping mode AFM was significantly

easier to perform on the 13-15 minute samples, thereby suggesting that sessile drop analysis of the surface prior to AFM can be used to indicate potential imaging problems, i.e. loose surface.

Table 3.4. Thermal decomposition of 936:1 poly-**R/S** adsorbed on native silicon oxide from toluene for 72 hours at 25 °C.

Exposure Time minutes (T° = 180 °C)	θ_A H_2O	θ_R H_2O
Control	93° ± 2°	80° ± 2°
10	88° ± 11°	0°
11	78° ± 2°	0°
12	99° ± 3°	0°
13	91° ± 1°	72° ± 1°
14	93° ± 1°	73° ± 2°
15	92° ± 1°	70° ± 4°

The AFM results for the 13-15 minutes samples are represented in the image shown in Figure 3.17, the 13 minutes sample at 180 °C. The roughness of the surface was comparable to that measured for the 4-9 minute samples. For the 14 minute and 15 minute samples, similar surface structures, as observed for the 13 minute sample, were observed by AFM. The most decomposition was observed in the 10-12 minute samples. However, for these samples, only two images for the 11 minute sample were successfully acquired and they are shown in Figures 3.18 and 3.19. The surface is composed of large droplet-like structures and possibly silica between the droplets. This surface would also explain the water contact angle data where the receding contact angle of 0° indicates that the water probe fluid was interacting with surface silanol groups on the silicon wafer.

From the water contact angle data and AFM images, the decomposition of an adsorbed film of 936:1 poly-**R/S** on silica can be accomplished by thermal treatment. However, controlling the amount of thermal decomposition was not attainable because the decomposition events that occur at the surface may vary due to the effects of

thickness, number of segmental contacts with the surface, initial structure of the adsorbed film, and the atmospheric environment at the interface with the surface. Moreover, the apparatus used to perform the decomposition experiments may have been inadequate. The objective of this project was to study whether the surface of an adsorbed film of polycarbodiimide could be modified by thermal decomposition and the results conclude that this does occur.

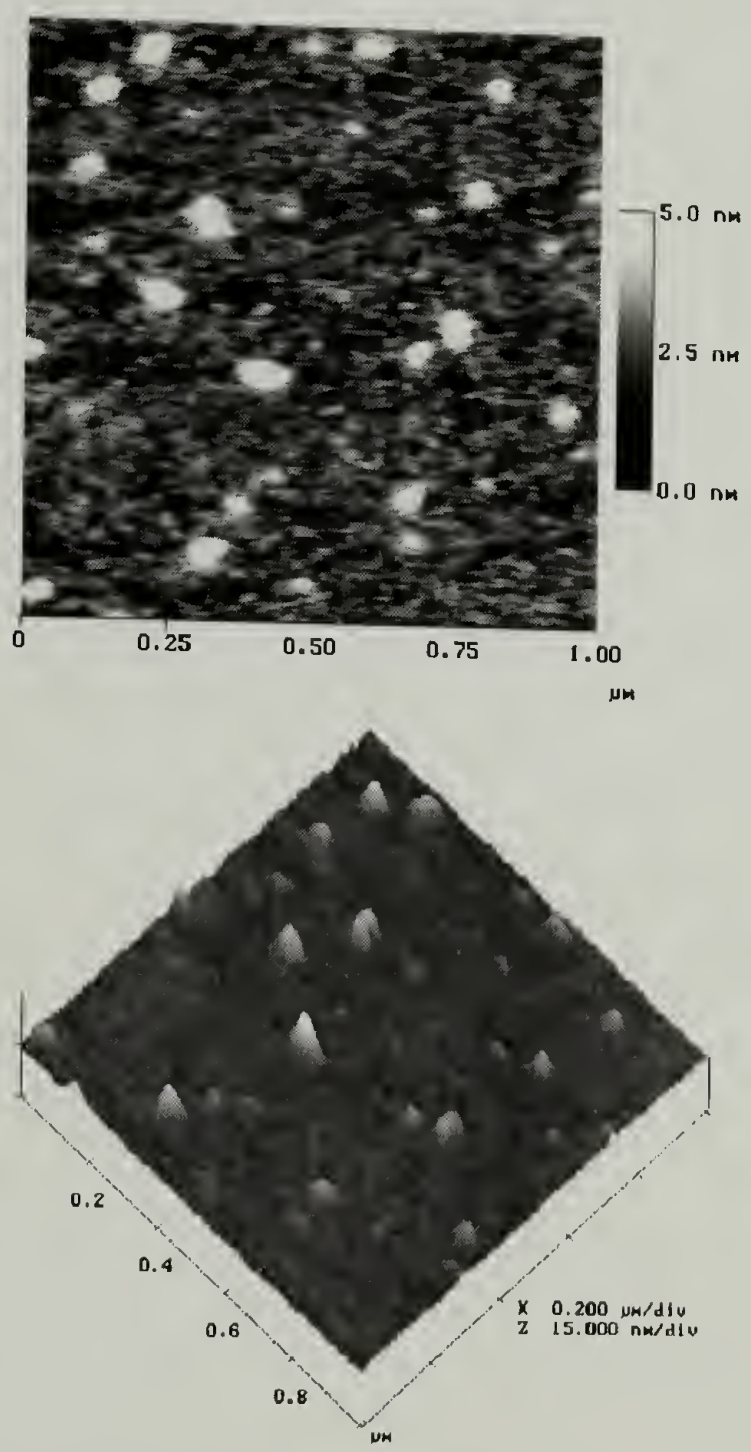

Figure 3.15. Tapping mode AFM height (top) and surface (bottom) image of the control sample prior to thermal exposure. The control was an adsorbed layer of 936:1 poly-**R/S** from toluene to native silicon oxide for 72 hours at 25 °C.

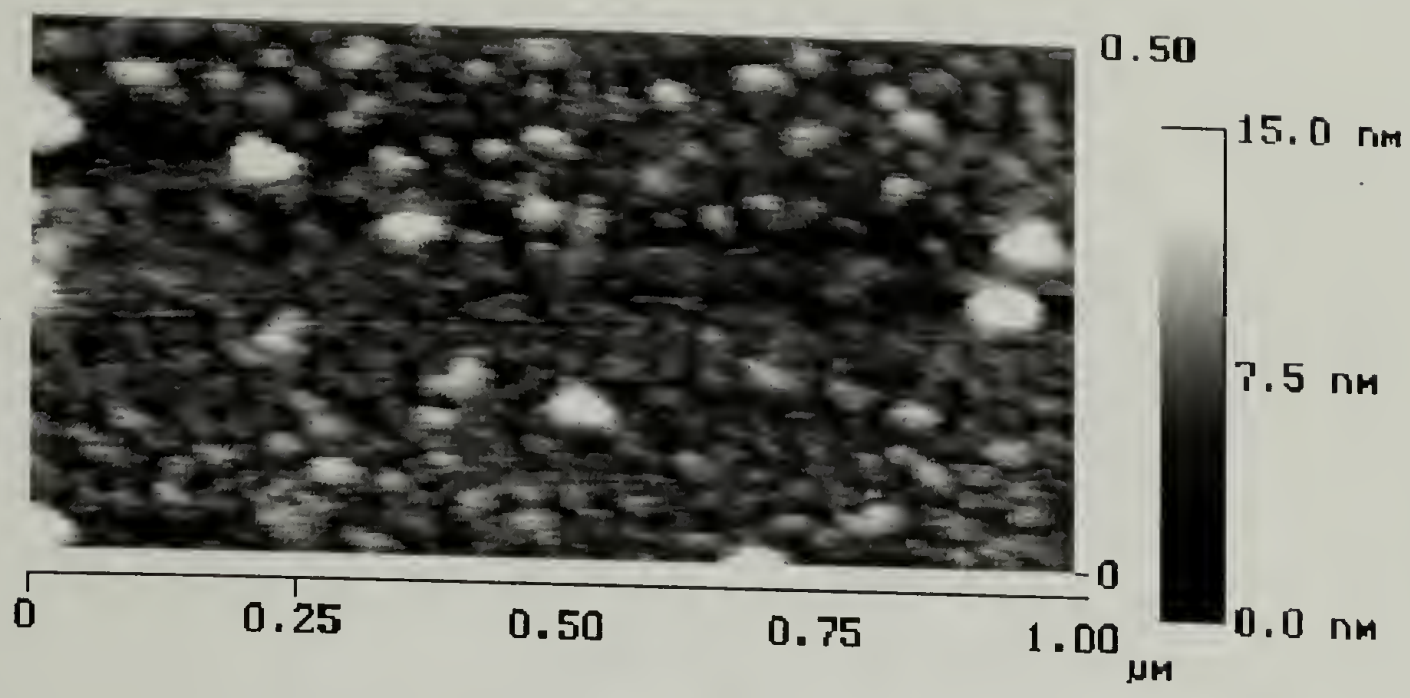

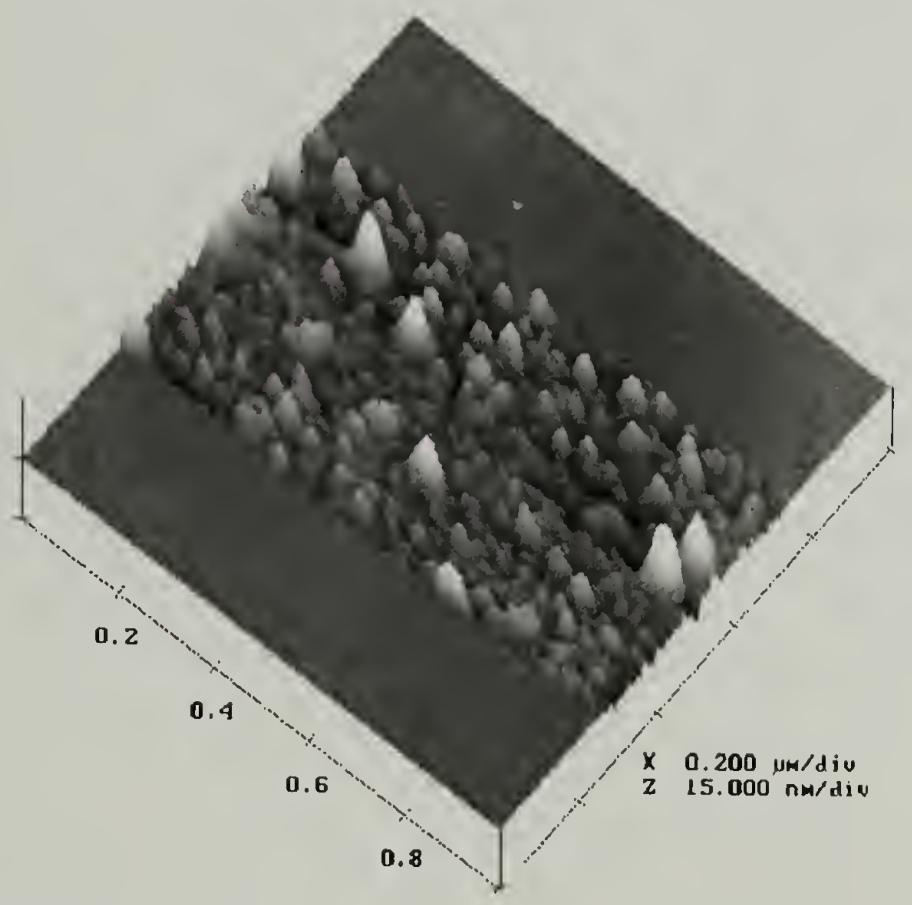

Figure 3.16. Tapping mode AFM height image (top) and surface image (bottom) of an adsorbed thin film of 936:1 poly-**R/S** on native silicon oxide from toluene (72 hours at 25 °C). The image shows the extent of decomposition, the result of thermally exposing the sample to 180 °C for 6 min.

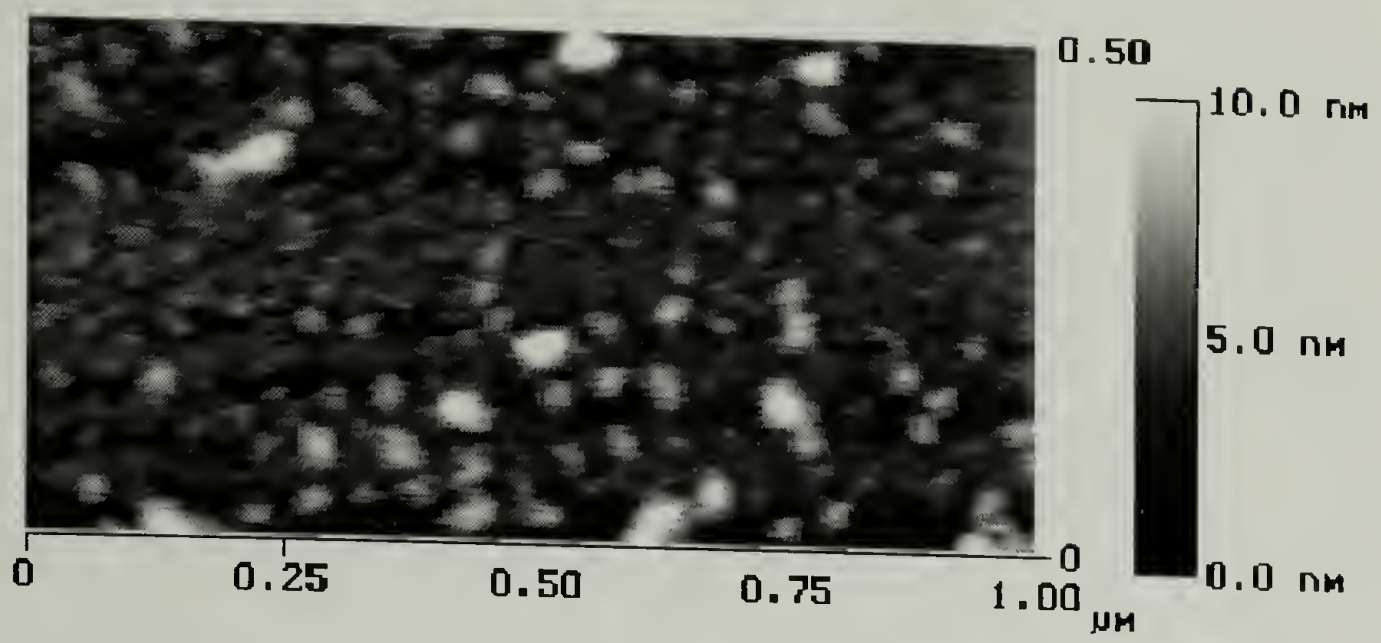

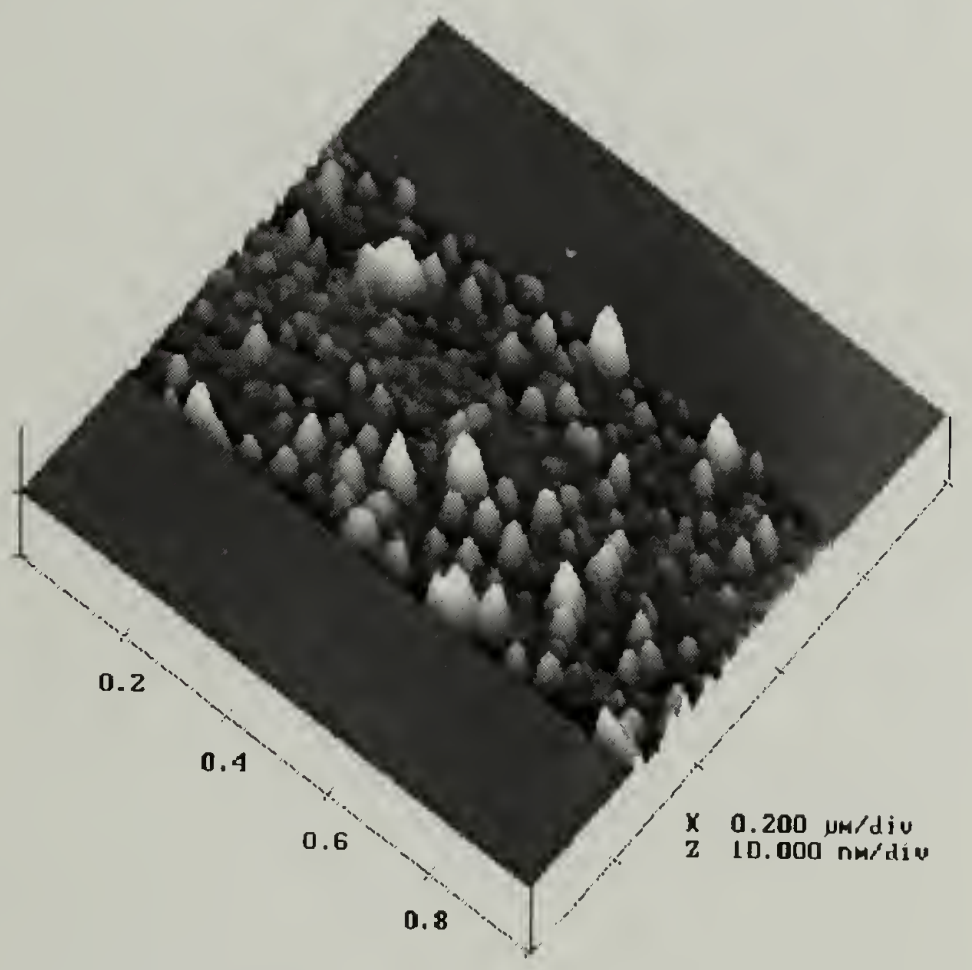

Figure 3.17. Tapping mode AFM height image (top) and surface image (bottom) of adsorbed 936:1 poly-**R/S** from toluene to native silicon oxide for 72 hours at 25 °C. The image shows the extent of decomposition, the result of thermally exposing the sample to 180 °C for 13 min.

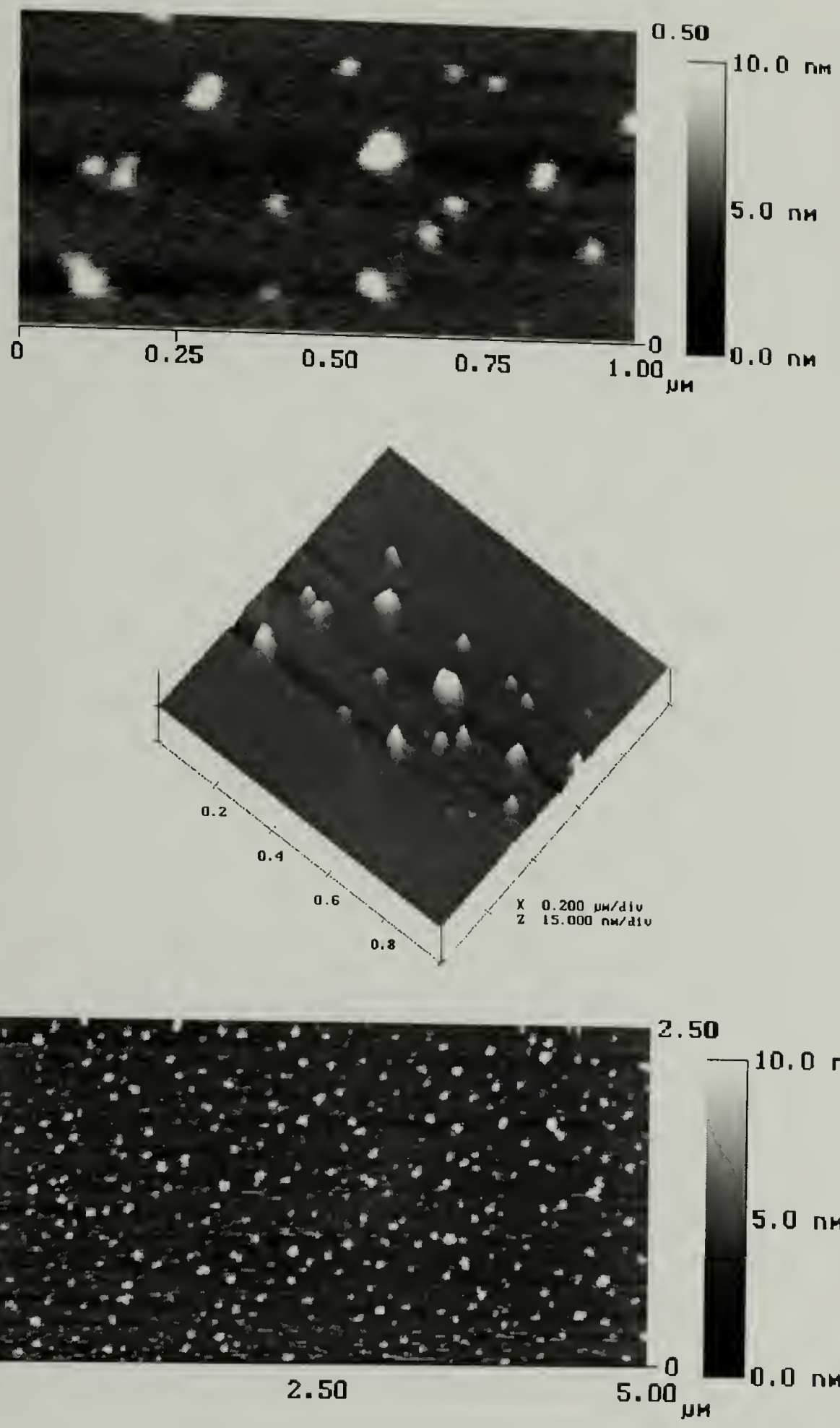

Figure 3.18. Tapping mode AFM, height image (top) and surface image (middle) of a 1 μm^2 area, and a height image (bottom) of a 12.5 μm^2 area of adsorbed 936:1 poly-**R/S** from toluene to native silicon oxide for 72 hours at 25 °C. The image shows the extent of decomposition, the result of thermally exposing the sample to 180 °C for 11 min.

Conclusions

We have studied the thermal decomposition of adsorbed thin films of different molecular weights of poly-**R/S** on native silicon oxide. Our first objective was to measure the decomposition rates of polycarbodiimides by real-time FT-IR spectroscopy but discovered the technique has limited applicability for these studies. This was due to instrumental design limitations, such as the environment around the sample could not be adequately controlled. Since the depolymerization reaction was radical based, and the atmosphere used was limited to air, concern about radical quenching and side reactions invalidated this technique for the purposes presented here. Therefore, the rate of decomposition for the polymer samples was performed using thermogravimetric analysis, TGA. In addition, during the measurements, this technique allowed the use of an inert atmosphere.

By TGA, it was shown that the onset temperature, T_d, for poly-**R/S** and poly-**S** is independent of molecular weight. However, higher T_d was measured for poly-**S** than poly-**R/S** indicating that stereochemistry has an effect on decomposition. For poly-**R/S**, the rate of decomposition was both temperature and molecular weight dependent, where higher decomposition rates were measured for the lower molecular weight polymer.

Adsorbed thin films of poly-**R/S** on native silicon oxide were thermally decomposed and studied by water contact angle and tapping mode AFM. During thermal decomposition, the film becomes loose on the surface making analyses very difficult. However, tapping mode AFM analyses showed structural changes in the adsorbed film with increasing thermal exposure. With heating, the film begins to decompose forming holes while also becoming rougher. Simultaneously, during decomposition, the film becomes mobile and with additional thermal exposure, the film decomposes to near completion. Our data suggests that surface modification can be achieved by thermal decomposition of and adsorbed film of polycarbodiimide on native silicon oxide.

Notes and References

1. Chan, C.-M. *Polymer Surface Modification and Characterization*; Hanser Publishers: New York, 1993.

2. Bee, T. G.; McCarthy, T. J. *Macromolecules* **1992**, *25*, 2093-2098.

3. Bee, T. G.; Cross, E. M.; Dias, A. J.; Lee, K. W.; Shoichet, M. S.; McCarthy, T. J. *Journal of Adhesion Science and Technology* **1992**, *6*, 719-731.

4. Chen, W.; McCarthy, T. J. *Macromolecules* **1997**, *30*, 78-86.

5. Chen, W.; McCarthy, T. J. *Macromolecules* **1998**, *31*, 3648-3655.

6. Franchina, N. L.; McCarthy, T. J. *Macromolecules* **1991**, *24*, 3045-3049.

7. Idage, S. B.; Badrinarayanan, S. *Langmuir* **1998**, *14*, 2780.

8. Lee, K. W.; McCarthy, T. J. *Macromolecules* **1988**, *21*, 2318-2330.

9. Levasalmi, J.-M.; McCarthy, T. J. *Macromolecules* **1995**, *28*.

10. Phuvanartnuruks, V.; McCarthy, T. J. *Macromolecules* **1998**, *31*, 1906-1914.

11. Prucker, O.; Rühe, J. *Macromolecules* **1998**, *31*, 592-601.

12. Wang, T.; Kang, E. T.; Neoh, K. G.; Tan, K. L.; Liaw, D. J. *Langmuir* **1998**, *14*, 921-927.

13. Ward, W. J.; McCarthy, T. J. *Surface Modification*; 2nd ed.; Mark, H. F., Bikales, N. M., Overberger, N. M. and Menges, C. G., Ed.; John Wiley & Sons, Inc.: New York, 1989, pp 674-689.

14. Novak, B. M.; Goodwin, A. A. *Polym. Prepr. (Am. Chem. Soc.: Div. Polym. Chem.)* **1995**, *36*, 611.

15. Goodwin, A. A. *Ph.D. Dissertation*; University of California at Berkeley: Berkeley, 1996, pp 310.

16. Joshi, R. M.; Zwolinski, B. J. *Heats of Polymerization and Their Structural and Mechanistic Implications*; Part 1 ed.; Ham, G. E., Ed.; Marcel Dekker: New York, 1967; Vol. 1, pp Chap. 8.

17. Sawada, H. *Thermodynamics of Polymerization*; Marcel Dekker: New York, 1976.

18. Odian, G. *Principals of Polymerization*; 3rd ed.; John Wiley & Sons: New York, 1991.

19. McNeill, I. C. *Thermal Degradation*; Allen, G. and Bevington, J., Ed.; Pergamon Press: New York, 1989; Vol. 6, pp 451-500.

20. Allen, N. S.; Edge, M. *Fundamentals of Polymer Degradation and Stabilization*; Elsevier Science Publishers, Inc.: New York, 1992.

21. Robinson, G. C. *J. Polym. Sci. Pt. A* **1964**, *2*, 3901-3908.

22. Goodwin, A.; Novak, B. M. *Macromolecules* **1994**, *27*, 5520-5522.

23. Novak, B. M. *Polymerization Through Hetero-Functional Groups*; Kobayashi, S., Ed.; John Wiley & Sons: New York, 1997, pp 113 - 133.

24. Shibayama, K.; Seidel, S. W.; Novak, B. M. *Macromolecules* **1997**, *30*, 3159.

25. Brunton, G.; Taylor, J. F.; Ingold, K. U. *Journal of the American Chemical Society* **1976**, *98*, 4879-4882.

26. Banks, R. E.; Haszeldine, R. N.; Stephens, C. W. *Tetrahedron Letters* **1972**, *35*, 3699-3701.

27. Kim, S. *Tetrahedron Letters* **1977**, *32*, 2741-2744.

28. Singer, L.; Kim, S. S. *Tetrahedron Letters* **1974**, 861-863.

29. Flynn, J. H. *Degradation Kinetics Applied to Lifetime Prediction of Polymers*; Shalaby, S. W., Ed.; The Franklin Institute Press: Philadelphia, 1978, pp 163-186.

30. Wendlandt, W. W. *Thermal Analysis*; 3rd ed.; Wiley-Interscience: New York, 1986; Vol. 19.

31. Mills, G. *Degradation and Stabilization of Polymeric Coating Materials*; Hamid, S. H., Amin, M. B. and Maadhah, A. G., Ed.; Marcel Dekker, Inc.: New York, 1992, pp 553-571.

32. Turi, E. A. *Thermal Characterization of Polymeric Materials*; Academic Press, Inc.: New York, 1981, pp 972.

33. Chan, J. H.; Blake, S. T. *Polymer Degradation and Stability* **1997**, *57*, 113.

34. Gatzonis, Y.; Siddiquee, S. K.; Egmond, J. W. v. *Macromolecules* **1997**, *30*, 7253-7262.

35. 3González-Velasco, J. R.; González-Marcos, J. A.; Delgado, J. A.; Elguea, C. G.-O. D.; Gutiérrez-Ortiz, J. I. *Chemical Engineering Science* **1996**, *51*, 1113.

36. Kishore, K.; Verneker, V. R. P.; Nair, M. N. R. *Journal of Applied Polymer Science* **1976**, *20*, 2355-2365.

37. Campbell, T. W.; Monagle, J. J.; Foldi, V. S. *Journal of the American Chemical Society* **1962**, *84*, 3673-3677.

38. Chan, J. H.; Blake, S. T. *Polymer Degradation and Stability* **1997**, *57*, 135.

APPENDIX

ABBREVIATIONS

poly-**R/S**	poly(*N*-methyl-*N'*-((±)-α-phenylethyl)carbodiimide)
poly-**S**	poly(*N*-methyl-*N'*-((-)-α-phenylethyl)carbodiimide)
poly-**R**	poly(*N*-methyl-*N'*-((+)-α-phenylethyl)carbodiimide)
Poly-**HC**	poly(1,3-di-*n*-hexylcarbodiimide)
tris(TMS)	tris(trimethylsiloxy)chlorosilane
CMDCS	10-(carbomethoxy)decyldimethylchlorosilane
H-CMDCS	Hydrolyzed 10-(carbomethoxy)decyldimethylchlorosilane
DPDCS	diphenyldichlorosilane
XPS	x-ray photoelectron spectroscopy
AFM	atomic force microscopy
FTIR	Fourier transform infrared spectroscopy

BIBLIOGRAPHY

Adamson, A. W. and Gast, A. P.; *Physical Chemistry of Surfaces*; Wiley-Interscience: New York, 1997; p784

Affrossman, S.; Kiff, T.; O'Neill, S. A.; Pethrick, R. A. and Richards, R. W.; *Macromolecules* **1999**, *32*, 2721

Allen, N. S. and Edge, M.; *Fundamentals of Polymer Degradation and Stabilisation*; Elsevier Science Publishers, Inc.: New York, 1992; p1

Allen, S. R.; Farris, R. and Thomas, E. L.; *J. Mater. Sci.* **1985**, *20*, 4583

Allen, S. R.; Farris, R. J. and Thomas, E. L.; *J. Mater. Sci.* **1985**, *20*, 2727

Andrade, J. D.; *Surface and Interfacial Aspects of Biomedical Polymers*, Andrade, J. D. ed.; Plenum Press: New York, 1985; 1, p105

Andrade, J. D.; Smith, L. M. and Gregonis, D. E.; *Surface and Interfacial Aspects of Biomedical Polymers*, Andrade, J. D. ed.; Plenum Press: New York, 1985; 1, p249

Ashley, J. C.; *Journal of Electron Spectroscopy and Related Phenomena* **1982**, *28*, 177

Banks, R. E.; Haszeldine, R. N. and Stephens, C. W.; *Tetrahedron Letters* **1972**, *35*, 3699

Bar, G. and Brandsch, R.; *Langmuir* **1998**, *14*, 7343

Bee, T. G.; Cross, E. M.; Dias, A. J.; Lee, K. W.; Shoichet, M. S. and McCarthy, T. J.; *Journal of Adhesion Science and Technology* **1992**, *6*, 719

Bee, T. G. and McCarthy, T. J.; *Macromolecules* **1992**, *25*, 2093

Binnig, G.; Quate, C. F. and Gerber, C. H.; *Phys. Rev. Lett.* **1986**, *56*, 930

Bohlen, D. S. and Blum, F. D.; Spring Meeting of The American Chemical Society (ACS), **1992**, *66*, 310.

Brochard, F.; Redon, C. and Rondelez, F.; *C. R. Acad. Sci., Ser 2* **1988**, *306*, 1143

Brochard-Wyart, F.; Debregeas, G. and Martin, P.; *Macromolecules* **1997**, *30*, 1211

Brochard-Wyart, F.; Martin, P. and Roden, C.; *Langmuir* **1993**, *9*, 3682

Brunton, G.; Taylor, J. F. and Ingold, K. U.; *Journal of the American Chemical Society* **1976**, *98*, 4879

Campbell, T. W.; Monagle, J. J. and Foldi, V. S.; *Journal of the American Chemical Society* **1962**, *84*, 3673

Cassie, A. B. D. and Baxter, S.; *Trans. Faraday Soc.* **1944**, *40*, 546

Chan, C.-M.; *Polymer Surface Modification and Characterization*; Hanser Publishers: New York, 1993; p285

Chan, J. H. and Blake, S. T.; *Polymer Degradation and Stability* **1997**, *57*, 113

Chan, J. H. and Blake, S. T.; *Polymer Degradation and Stability* **1997**, *57*, 135

Chen, W.; Fadeev, A. Y.; Hsieh, M. C.; Öner, D.; Youngblood, J. and McCarthy, T. J.; *Langmuir* **1999**, *15*, 3395

Chen, W. and McCarthy, T. J.; *Macromolecules* **1998**, *31*, 3648

Chen, W. and McCarthy, T. J.; *Macromolecules* **1997**, *30*, 78

Chi, L.; Li, H.; Zhang, X.; Fuchs, H. and Shen, J.; *Polymer Bulletin* **1998**, *41*, 695

Ciferri, A.; *Liquid Crystallinity in Polymers* **1991**,

Clark, D. T. and Thomas, H. R.; *J. of Polym. Sci.* **1977**, *15*, 2843

Cohen Staurt, M. A.; Fleer, G. J. and Scheutjens, J. M. H. M.; *Journal of Colloid and Interface Science* **1984**, *97*, 526

Cohen Stuart, M. A.; Fleer, G. J. and Scheutjens, J. M. H. M.; *Journal of Colloid and Interface Science* **1984**, *97*, 515

Conio, G.; Bianchi, E.; Ciferri, A. and Krigbaum, W. R.; *Macromolecules* **1984**, *17*, 856

Cornelissen, J. J. L. M.; Hafkamp, R. J. H.; Sommerdijk, N. A. J. M.; Feiters, M. C. and Nolte, R. J. M.; American Chemical Society National Meeting (The Division of Polymer Chemistry, Inc.), **1999**, *40*, 517.

Courvoisier, A.; Isel, F.; François, J. and Maaloum, M.; *Langmuir* **1998**, *14*, 3727

Dan, N.; *Langmuir* **1996**, *12*, 1101

de Genes, P.-G.; *Rev. Mod. Phys.* **1985**, *57*, 827

de Vincenzi, R. H.; Kolb, B. U. and McCarthy, T. J.; Polymer Preprints (Am. Chem. Soc. Div. Polym. Chem.) (The Division of Polymer Chemistry, Inc.), **1994**, *35*, 697.

Deming, T. J. and Novak, B. M.; *J. Am. Chem. Soc.* **1992**, *114*, 7926

Deming, T. J. and Novak, B. M.; *J. Am. Chem. Soc.* **1993**, *115*, 9101

Deming, T. J. and Novak, B. M.; *Macromolecules* **1991**, *24*, 326

Deming, T. J. and Novak, B. M.; *Macromolecules* **1991**, *24*, 6043

Dijt, J. C.; Stuart, M. A. C. and Fleer, G. J.; *Macromolecules* **1994**, *27*, 3219

Dijt, J. C.; Stuart, M. A. C. and Fleer, G. J.; *Macromolecules* **1994**, *27*, 3207

Dijt, J. C.; Stuart, M. A. C. and Fleer, G. J.; *Macromolecules* **1994**, *27*, 3229

Dijt, J. C.; Stuart, M. A. c.; Hofman, J. E. and Fleer, G. J.; *Colloids and Surfaces* **1990**, *51*, 141

Dimarzio, E. A. and Bishop, M.; *Biopolymers* **1974**, *13*, 2331

DiNardo, N. J.; *Nanoscale Characterization of Surfaces and Interfaces*; VCH: New York, 1994;

Domke, J. and Radmacher, M.; *Langmuir* **1998**, *14*, 3320

Dorgan, J. R.; Stamm, M.; Toprakcioglu, C.; Jérôme, R. and Fetters, L. J.; *Macromolecules* **1993**, *26*, 5321

Ebihara, K.; Koshihara, S.-Y.; Yoshimoto, M.; Maeda, T.; Ohnishi, T.; Koinuma, H. and Fujiki, M.; *Jpn. J. Appl. Phys.* **1997**, *36*, L 1211

Fadeev, A. Y. and McCarthy, T. J.; *Langmuir* **1999**, *15*, 7238

Fadeev, A. Y. and McCarthy, T. J.; American Chemical Society Meeting (The Division of Polymer Chemistry), **1999**, *40*, 725.

Fadeev, A. Y. and McCarthy, T. J.; *Langmuir* **1998**, *14*, 5586

Fadeev, A. Y. and McCarthy, T. J.; *Langmuir* **1999**, *15*, 3759

Fadeev, A. Y.; Stafford, C. M.; Russell, T. P. and McCarthy, T. J.; American Chemical Society Meeting (The Division of Polymer Chemistry), **1999**, *40*, 603.

Faldi, A.; Composto, R. J. and Winey, K. I.; *Langmuir* **1997**, *13*, 1758

Fanton, X. and Cazabat, A. M.; *Langmuir* **1998**, *14*, 2554

Feldman, K.; Tervoort, T.; Smith, P. and Spencer, N. D.; *Langmuir* **1998**, *14*, 372

Finot, M. O. and McDermontt, M. T.; *Journal of the American Chemical Society* **1997**, *119*, 8564

Fleer, G. J.; Stuart, M. A. c.; Scheutjens, J. M. H. M.; Cosgrove, T. and Vincent, B.; *Polymers at Interfaces*; Chapman & Hall: London, UF, 1993; p502

Fleer, G. J.; van Male, J. and Johner, A.; *Macromolecules* **1999**, *32*, 845

Flynn, J. H.; *Thermal Methods in Polymer Analysis*, Shalaby, S. W. ed.; The Franklin Institute Press: Philadelphia, 1978; p163

Fondecave, R. and Wyart, F. B.; *Macromolecules* **1998**, *31*, 9305

Franchina, N. L. and McCarthy, T. J.; *Macromolecules* **1991**, *24*, 3045

Gatzonis, Y.; Siddiquee, S. K. and Egmond, J. W. v.; *Macromolecules* **1997**, *30*, 7253

Gay, C.; *Macromolecules* **1997**, *30*, 5939

Genzer, J. and Kramer, E. J.; *J. Phys. Rev. Lett.* **1997**, *78*,

Gerle, M.; Fischer, K.; Roos, S.; Müller, A. H. E.; Schmidt, M.; Sheiko, S. S.; Prokhorova, S. and Möller, M.; *Macromolecules* **1999**, *32*, 2629

González-Velasco, J. R.; González-Marcos, J. A.; Delgado, J. A.; Elguea, C. G.-O. D. and Gutiérrez-Ortiz, J. I.; *Chemical Engineering Science* **1996**, *51*, 1113

Good, R. J.; *Contact Angle, Wettability and Adhesion*, Mittal, K. L. ed.; VSP: 1993; p3

Goodman, M. and Chen, S.; *Macromolecules* **1970**, *3*, 398

Goodwin, A. and Novak, B. M.; *Macromolecules* **1994**, *27*, 5520

Goodwin, A. A.; *Ph.D. Dissertation*, University of California at Berkeley, 1996.

Gracias, D. H. and Somorjai, G. A.; *Macromolecules* **1998**, *31*, 1269

Green, M. M.; Andreola, C.; Munoz, B.; Reidy, M. P. and Zero, K.; *J. Am. Chem. Soc.* **1988**, *110*, 4063

Green, M. M.; Gross, R. A.; Crosby III, C. and Schilling, F. C.; *Macromolecules* **1987**, *20*, 992

Green, M. M.; Gross, R. A.; Schilling, F. C.; Zero, K. and Crosby III, C.; *Macromolecules* **1988**, *21*, 1839

Green, M. M.; Peterson, N. C.; Sato, T.; Teramoto, A.; Cook, R. and Lifson, S.; *Science* **1995**, *268*, 1860

Hair, M. L.; *Silanes, Surfaces, and Interfaces*, Leyden, D. E. ed.; Gordon and Breach Science Publishers: New York, 1986; p25

Hall, D. B.; Underhill, P. and Torkelson, J. M.; *Polymer Engineering and Science* **1998**, *38*, 2039

Henn, G.; Bucknall, D. G.; Stamm, M.; Vanhoorne, P. and Jérôme, R.; *Macromolecules* **1996**, *29*, 4305

Herminghaus, S.; Jocobs, K.; Mecke, K.; Bischof, J.; Fery, A.; Ibn-Elhaj, M. and Schlagowski, S.; *Science* **1998**, *282*, 916

Herzberg, W. J.; Marian, J. E. and Vermeulen, T.; *J. Coll. Int. Sci.* **1970**, *33*, 164

Hoff, S. M. and Novak, B. M.; *Macromolecules* **1993**, *26*, 4067

Horr, T. J.; Ralston, J. and Smart, R. S. C.; *Colloids and Surfaces A: Physiochemical and Engineering Aspects 97* **1995**, 183

Idage, S. B. and Badrinarayanan, S.; *Langmuir* **1998**, *14*,2780

Israelachvili, J. N.; *Intermolecular and Surface Forces*; Academic Press: London, 1985;

Israelachvili, J. N. and Gee, L. G.; *Langmuir* **1989**, *5*, 288

Itou, T.; Chikiri, H.; Teramoto, A. and Aharoni, S. M.; *Polym. J.* **1988**, *20*, 143

Iyengar, D. R.; *Ph.D. Dissertation*, University of Massachusetts, 1992.

Iyengar, D. R. and McCarthy, T. J.; *Macromolecules* **1990**, *23*, 4344

Jenkel, E. and Rumbach, B.; *Z. Elektrochem.* **1951**, *55*, 612

Jing, J.; Henriksen, P. N.; Wang, H. and Marteny, P.; *Journal of Materials Science* **1995**, *30*, 5700

Joshi, R. M. and Zwolinski, B. J.; *Vinyl Polymerizations*, Part 1; Ham, G. E. ed.; Marcel Dekker: New York, 1967; 1, Chapter 8

Kajiyama, T.; Tanaka, K.; Ohki, I.; Ge, A.-R.; Yoon, J.-S. and Takahare, A.; *Macromolecules* **1994**, *27*, 7932

Kajiyama, T.; Tanaka, K. and Takahara, A.; *Macromolecules* **1997**, *30*, 280

Kallury, K. M. R.; Krull, U. J. and Thompson, M.; *Anal. Chem.* **1988**, *60*, 169

Karim, A.; Douglas, J. F.; Satija, S. K.; Han, C. C. and Goyette, R. J.; *Macromolecules* **1999**, *32*, 1119

Karim, A.; Slawecki, T. M.; Kumar, S. K.; Douglas, J. F.; Satija, S. K.; Han, C. C.; Russell, T. P.; Liu, Y.; Overney, R.; Sokolov, J. and Rafailovich, M. H.; *Macromolecules* **1998**, *31*, 857

Kawaguchi, M. and Arai, T.; *Macromolecules* **1991**, *24*, 889

Ke, B.; *Specific Refractive Index Increment* **1964**, 490

Keller, D.; *Surface Science* **1991**, *253*, 353

Kelley, S. O.; Barton, J. K.; Jackson, N. M.; McPherson, L. D.; Potter, A. B.; Spain, E. M.; Allen, M. J. and Hill, M. G.; *Langmuir* **1998**, *24*, 6781

Kelley, T. W.; Schorr, P. A.; Johnson, K. D.; Tirrell, M. and Frisbie, C. D.; *Macromolecules* **1998**, *31*, 4297

Kerle, T.; Yerushalmi-Rozen, R. and Klein, J.; *J. Europhys. Lett.* **1997**, *38*, 207

Khokhlov, A. R. and Ternovsky, F. F.; *Makromol. Chem., Theory Simul.* **1993**, *2*, 151

Kim, S.; *Tetrahedron Letters* **1977**, *32*, 2741

King, S. T. and Strope, J. H.; *Journal of Chemical Physics* **1971**, *54*, 1289

Kishore, K.; Verneker, V. R. P. and Nair, M. N. R.; *Journal of Applied Polymer Science* **1976**, *20*, 2355

Kolb, B. U.; *Ph.D. Dissertation*, University of Massachusetts at Amherst, 1993.

Kollmar, C. and Hoffman, R. J.; *J. Am. Chem. Soc.* **1990**, *112*, 8230

Koutsos, V.; Vegte, E. W. v. d.; Grim, P. C. M. and Hadziioannou, G.; *Macromolecules* **1998**, *31*, 116

Krabi, A. and Stuart, M. A. C.; *Macromolecules* **1998**, *31*, 1285

Kramer, P. C. J.; Cleij, M. C.; Nolte, R. J. M.; Harada, T.; Hezemans, A. M. F. and Drenth, W.; *J. Am. Chem. Soc.* **1988**, *110*,

Kratochvil, P.; *Classical Light Scattering from Polymer Solutions*; Vlsevier: New York, 1987;

Krausch, G.; Hipp, M.; Böltau, M.; Marti, O. and Mlynek, J.; *Macromolecules* **1995**, *28*, 260

Kumaki, J.; Nishikawa, U. and Hashimoto, T.; *J. Am. Chem. Soc.* **1996**, *118*, 3321

Kuwata, M.; Murakami, H.; Norisuye, T. and Fujita, H.; *Macromolecules* **1984**, *17*, 2731

Kuznetsov, D. V. and Sung, W.; *Macromolecules* **1998**, *31*, 2679

Leclère, P.; Lazzaroni, R.; Brédas, J. L.; Yu, J. M.; Dubois, P. and Jérôme, R.; *Langmuir* **1996**, *12*, 4317

Lee, B.-w. and Clark, N. A.; *Langmuir* **1998**, *14*, 5495

Lee, H. C.; Chang, T.; Harville, S. and Mays, J. W.; *Macromolecules* **1998**, *31*, 690

Lee, K. W. and McCarthy, T. J.; *Macromolecules* **1988**, *21*, 2318

Lee, L.-H.; *Contact Angle, Wettability and Adhesion*, Mittal, K. L. ed.; VSP: 1993; p45

Levasalmi, J.-M. and McCarthy, T. J.; *Macromolecules* **1995**, *28*,

Leyden, D. E.; *Silanes, Surfaces, and Interfaces* **1986**,

Lifson, S.; Andreola, C.; Peterson, N. C. and Green, M. M.; *J. Am. Chem. Soc.* **1989**, *111*, 8850

Lim, A. R.; Stewart, J. R. and Novak, B. M.; *Solid State Communications* **1999**, *110*, 23

Luckham, P. F. and Manimaaran, S.; *Macromolecules* **1997**, *30*, 5025

Magonov, S.; *Studies of Polymer Surfaces with Atomic Force Microscopy* **1999**, *1999*,

Magonov, S. N.; Bar, G.; Stocker, W. and Cantow, H. J.; Spring Meeting of The American Chemical Society (The Division of Polymer Chemistry, Inc.), **1992**, *33*, 782.

Maman, M. and Ponsinet, V.; *Langmuir* **1999**, *15*, 259

Markham, J. L.; LeGrange, J. D. and Kurkjian, C. R.; *Plastic Engineering* **1993**, *49*, 27

Martin, J. I. and Wang, Z. G.; *Langmuir* **1996**, *12*, 4950

Masel, R. I.; *Principles of Adsorption and Reaction on Solid Surfaces*; John Wiley & Sons, Inc.: New York, 1996; p804

McGhie, A. J.; Tang, S. L. and Li, S. F. Y.; *Chemtech* **1995**, 20

McNeill, I. C.; *Comprehensive Polymer Science*, Allen, G. and Bevington, J. ed.; Pergamon Press: New York, 1989; 6, p451

Meiners, J. C.; Quintel-Ritzi, A.; Mlynek, J.; Elbs, H. and Krausch, G.; *Macromolecules* **1997**, *30*, 4945

Menawat, A.; Henry Jr., J. and Siriwardane, R.; *Journal of Colloid and Interface Science* **1984**, *101*, 110

Meyers, G. F.; DeKoven, B. M. and Seitz, J. T.; *Langmuir* **1992**, *8*, 2330

Miller, J. D.; Veeramasuneni, S.; Drelich, J. and Yalamanchili, M. R.; *Polymer Engineering and Science* **1996**, *36*, 1849

Mills, G.; *Handbook of Polymer Degradation*, Hamid, S. H., Amin, M. B. and Maadhah, A. G. ed.; Marcel Dekker, Inc.: New York, 1992; p553

Mogul, P. H.; Kniseley, R. N. and Fassel, V. A.; *Spectroscopy Letters* **1977**, *10*, 959

Motomatsu, M.; Mizutani, W. and Tokumoto, H.; *Polymer* **1997**, *38*, 1779

Müller-Buschbaum, P. and Stamm, M.; *Macromolecules* **1998**, *31*, 3686

Murakami, H.; Norisuye, T. and Fujita, H.; *Macromolecules* **1980**, *13*, 345

Murakami, J.; *J. Phys. Soc. Japan* **1976**, *41*, 633

Nieh, M. P.; Goodwin, A. A.; Stewart, J. R.; Novak, B. M. and Hoagland, D. A.; *Macromolecules* **1998**, *31*, 3151

Nolte, R. J. M.; *Chem. Soc. Rev.* **1994**, 11

Novak, B. M.; *Catalysis in Precision Polymerization*, Kobayashi, S. ed.; John Wiley & Sons: New York, 1997; p113

Novak, B. M.; Goodwin, A. and Seery, T.; Polymer Preprints (Am. Chem. Soc. Div. Polym. Chem.) (The Division of Polymer Chemistry, Inc.), **1994**, *35*, 678.

Novak, B. M. and Goodwin, A. A.; Polymer Preprints (Am. Chem. Soc. Div. Polym. Chem.) (American Chemical Society), **1995**, *36*, 611.

O'Shea, S. J.; Lantz, M. A. and Tokumoto, H.; *Langmuir* **1999**, *15*, 922

Odian, G.; *Principals of Polymerization*; John Wiley & Sons: New York, 1991; p768

Ortiz, C. and Hadziioannou, G.; *Macromolecules* **1999**, *32*, 780

Padday, J. F.; *Contact Angle, Wettability, and Adhesion*, Mittal, K. L. ed.; VSP: 1993; p97

Palomo, C. and Mestres, R.; *Synthesis* **1981**, 373

Pangborn, A. B.; Giardello, M. A.; Grubbs, R. H.; Rosen, R. K. and Timmers, F. J.; *Organometallics* **1996**, *15*, 1518

Park, J. M. and Andrade, J. D.; *Polymer Surface Dynamics*, Andrade, J. D. ed.; 1988; p67

Patten, T. E.; *Ph.D. Dissertation*, University of California, Berkeley, 1994.

Patten, T. E. and Novak, B. M.; *J. Am. Chem. Soc.* **1996**, *118*, 1906

Patten, T. E. and Novak, B. M.; *J. Am. Chem. Soc.* **1991**, *113*, 5065

Patten, T. E. and Novak, B. M.; *Macromolecules* **1993**, *26*, 436

Phuvanartnuruks, V. and McCarthy, T. J.; *Macromolecules* **1998**, *31*, 1906

Pientka, Z.; Oike, H. and Tezuka, Y.; *Langmuir* **1999**, *15*, 3197

Plueddemann, E. P.; *Silane Coupling Agents*; Plenum Press: New York, 1991; p253

Porter, T. L.; Oden, P. I. and Caple, G.; *Surface Science* **1991**, *259*, 221

Prucker, O. and Rühe, J.; *Macromolecules* **1998**, *31*, 592

Qu, S.; Clarke, C. J.; Liu, Y.; Rafailovich, M. H.; Sokolov, J.; Phelan, K. C. and G. Krausch; *Macromolecules* **1997**, *30*, 3640

Quist, A. P.; Björck, L. P.; Reimann, C. T.; Oscarsson, S. O. and Sundqvist, B. U. R.; *Surface Science* **1995**, *325*, L406

Rabolt, J. F.; *Physics of Polymer Surfaces and Interfaces*, Sanchez, I. C. ed.; Butterworth-Heinemann: Boston, 1992; p304

Ramirez-Aguilar, K. A. and Rowlen, K. L.; *Langmuir* **1998**, *14*, 2562

Rapi, G. and Sbrana, G.; *Journal of the American Chemical Society* **1970**, *93*, 5213

Raposo, M.; Pontes, R. S.; Mattosos, L. H. C. and O. N. Oliveira, J.; *Macromolecules* **1997**, *30*, 6095

Redon, C.; Brochard-Wyart, F. and Rondelez, F.; *Physical Review Letters* **1991**, *66*, 715

Redon, C.; Brzoska, J. B. and Brochard-Wyart, F.; *Macromolecules* **1994**, *27*, 468

Reiter, G.; *Phys. Rev. Lett.* **1992**, *68*, 75

Reiter, G.; *Macromolecules* **1994**, *27*, 3046

Reiter, G.; *Langmuir* **1993**, *9*, 1344

Reiter, G.; Avroy, P. and Auray, L.; *Macromolecules* **1996**, *29*, 2150

Reiter, G.; Sharma, A.; Casoli, A.; Marie-Odile, D.; Khanna, R. and Auroy, P.; *Langmuir* **1999**, *15*, 2551

Ren, Y.; Shoichet, M. S.; McCarthy, T. J.; Stidham, H. D. and Hsu, S. L.; *Macromolecules* **1995**, *28*, 358

Robinson, G. C.; *J. Polym. Sci. Pt. A* **1964**, *2*, 3901

Roefs, S. P. F. M.; Scheutjens, J. M. H. M. and Leermakers, F. A. M.; *Macromolecules* **1994**, *27*, 4810

Rubingh, D. H. and Yu, H.; *Macromolecules* **1976**, *9*, 681

Rye, R. R.; Nelson, G. C. and Dugger, M. T.; *Langmuir* **1997**, *13*, 2965

Santore, M. and Fu, Z.; *Macromolecules* **1997**, *30*, 8516

Sauer, B. B.; McLean, S. R. and Thomas, R. R.; *Langmuir* **1998**, *14*, 3045

Sawada, H.; *Thermodynamics of Polymerization*; Marcel Dekker: New York, 1976; Chaps. 1

Scheutjens, J. M. H. M.; *Physics of Polymer Surfaces and Interfaces*, Sanchez, I. C. and Fitzpatrick, L. E. ed.; Butterworth-Heinemann: Boston, 1992; p117

Schneider, N. S.; Furusaki, S. and Lenz, R. W.; *J. Polym. Sci.* **1965**, *3*, 933948

Segalman, R. A. and Green, P. F.; *Macromolecules* **1999**, *32*, 801

Shibayama, K.;Seidel, S. W. and Novak, B. M.; *Macromolecules* **1997**, *30*, 3159

Shull, K. R.; *Macromolecules* **1996**, *29*, 8487

Silberzan, P. and Leger, L.; *Macromolecules* **1992**, *25*, 1267

Singer, L. and Kim, S. S.; *Tetrahedron Letters* **1974**, 861

Snétivy, D.; Rutledge, G. C. and Vancso, G. J.; Spring Meeting of The American Chemical Society (The Division of Polymer Chemistry, Inc.), **1992**, *33*, 786.

Sohn, D.; Yu, H.; Nakamatsu, J.; Russo, P. S. and Daly, W. H.; *Journal of Polymer Science: Part B: Polymer Physics* **1996**, *34*, 3025

Sperling, L. H.; *Introduction to Physical Polymer Science*; John Wiley & Sons: New York, New York, 1992; p594

Suzuki, A.; Yamazaki, M.; Kobiki, Y. and Suzuki, H.; *Macromolecules* **1997**, *30*, 2350

Tanaka, K.; Takahara, A. and Kajiyama, T.; *Macromolecules* **1997**, *30*, 6626

Thompson, P. A.; Brinckerhoff, W. B. and Robbins, M. O.; *Contact Angle, Wettability and Adhesion*, Mittal, K. L. ed.; VSP: 1993; p139

Tipton, D. L. and Russo, P. S.; *Macromolecules* **1996**, *29*, 7402

Tomasetti, E.; Rouxhet, P. G. and Legras, R.; *Langmuir* **1998**, *14*, 3435

Tsubokawa, N.; Kimoto, T. and Koyama, K.; *Colloid Polym. Sci.* **1993**, *271*, 940

Turi, E. A.; *Thermal Characterization of Polymeric Materials* **1981**, 972

Urban, M. and Koenig, J. L.; *Applied Spectroscopy* **1986**, *40*, 13

van Beijnen, A. J. M.; Nolte, R. J. M.; Drenth, W.; Hezemans, A. M. F. and van de Coolwijk, P. J. F. M.; *Macromolecules* **1980**, *13*, 1386

van Beijnen, A. J. M.; Nolte, R. J. M.; Naaktgeboren, A. J.; Zwikker, J. W.; Drenth, W. and Hezemans, A. M. F.; *Macromolecules* **1983**, *16*, 1679

van den Berg, R.; de Groot, H.; van Dijk, M. A. and Denley, D. R.; *Polymer* **1994**, *35*, 5778

Van der Beek, G. P.; Cohen Stuart, M. A.; Fleer, G. J. and Hofman, J. E.; *Macromolecules* **1991**, *24*, 6600

Van der Beek, G. P.; Stuart, M. A. C.; Fleer, G. J. and Hofman, J. E.; *Langmuir* **1989**, *5*, 1180

van Dijk, M. A. and van den Berg, R.; *Macromolecules* **1995**, *28*, 6773

van Eijk, M. C. P. and Cohen Stuart, M. A.; *Langmuir* **1997**, *13*, 5447

Vandenberg, E. T.; Bertilsson, L.; Liedberg, B.; Uvdal, K.; Erlandsson, R.; Elwing, H. and Lundström, I.; *Journal of Colloid and Interface Science* **1991**, *147*, 103

Wagner, C. D.; Riggs, W. M.; Davis, L. E. and Moulder, J. F.; *Handbook of X-ray Photoelectron Spectroscopy*; Muilenberg, G. E.; Perkin-Elmer Corporation: Eden Prairie, Minnesota, 1979; p28

Walheim, S.; Ramstein, M. and Steiner, U.; *Langmuir* **1999**, *15*, 4828

Wang, T.; Kang, E. T.; Neoh, K. G.; Tan, K. L. and Liaw, D. J.; *Langmuir* **1998**, *14*, 921

Ward, W. J. and McCarthy, T. J.; *Encyclopedia of Polymer Science and Engineering*, 2nd; Mark, H. F., Bikales, N. M., Overberger, N. M. and Menges, C. G. ed.; John Wiley & Sons, Inc.: New York, 1989; p674

Wendlandt, W. W.; *Thermal Analysis*; Wiley-Interscience: New York, 1986; p9

Williams, A. and Ibrahim, I. T.; *Chem. Rev.* **1981**, *81*, 589

Wu, S.; *Polymer Handbook*, 3rd; Brandrup, J. and Immergut, E. H. ed.; John Wiley & Sons: New York, 1989; p423

Xie, R.; Karim, A.; Douglas, J. F.; Han, C. C. and Weiss, R. A.; *Physical Review Letters* **1998**, *81*, 1251

Yuan, C.; Ouyang, M. and Koberstein, J. T.; *Macromolecules* **1999**, *32*, 2329

Zachariades, A. E. and Porter, R. S.; *The Strength and Stiffness of Polymers*; Marcel Dekker: New York, 1983;

Zhao, W.; Rafailovich, M. H. and Sokolov, J.; *J. Phys. Rev. Lett.* **1993**, *70*, 1453

Zhong, Q.; Innis, D.; Kjoller, K. and Elings, V. B.; *Surface Science Letters* **1993**, *290*, L688